A CASE STUDY: SITE-SPECIFIC SEISMIC RESPONSE ANALYSIS FOR BASE-ISOLATED BUILDING IN DÜZCE

A Thesis Submitted to
the Graduate School of Engineering and Sciences of
İzmir Institute of Technology
in Partial Fulfillment of the Requirements for the Degree of

MASTER OF SCIENCE

in Civil Engineering

by

Volkan Gökçe EREN

December 2020
İZMİR

ACKNOWLEDGMENTS

I would like to thank Assoc. Prof. Nurhan ECEMİŞ ZEREN for teaching me throughout my entire education life, for making the most significant contribution to my development, always being a guide, and providing light to the progress of my thesis and the facilitation of my studies.

I would like to thank Dr. Mustafa Koç, who always assisted in the preparation of this thesis and taught and guided all the information in my professional life.

I would like to thank my brothers Emre Korkmaz, Mustafa Doğuş Uğur, and Serkan Karalı to support all my studies for the thesis.

I would like to thank all the Destech and Ghafari staff for providing me with the use of all the data that constitutes the content of this study.

The biggest thanks are also to my dear family and Yasemin Kabakçı, who enlightened my way with their thoughts, for being by my side in every moment of my life and supporting me in every decision.

ABSTRACT

A CASE STUDY: SITE-SPECIFIC SEISMIC RESPONSE ANALYSIS FOR BASE-ISOLATED BUILDING IN DÜZCE

Under seismic loads, soil-structure interaction, and its effect on performance of pavements is more important today. Turkey is located in one of the most active seismic zones in the world. In the past, many destructive earthquakes happened in Turkey. The fact is that due to frequent earthquakes in the future, we may suffer a significant loss of life and property. Therefore, it has been necessary to minimize demolitions by conducting soil behavior analysis for each site.

To design buildings, bridges, and other structures with base-isolators according to performance, it is necessary to carefully evaluate the long-term ground motions, especially in determining the earthquake ground motion. In these evaluations, empirical and theoretical methods to predict the response spectrum, considering and analyzing the effects of the near-fault, scaling the spectrum for different damping ratios, and simulation of long-term ground motions time-history constitute an essential place. It is necessary to determine the principles required for modifying the design spectrum in the long-period boundaries. The regulations are required to simulate long-period ground motions in the time-history and the necessary rules for selecting and scaling the earthquake ground motion records by considering the long-period effect.

In this thesis, commonly used approaches in national and international regulations in defining the earthquake effect were evaluated, and the recommended earthquake levels for structures within the Düzce city in Turkey are explained. While evaluating the earthquake hazard in the study area, the general geology, tectonic features, ground conditions, and existing fault systems of the region were considered. For the study area, besides the classical hazard spectra, hazard curves for different spectral ordinates that allow the calculation of probabilistic seismic hazard maps and spectral coordinates for various periods are presented. Earthquake records were selected according to these spectra, and nonlinear analyses were made by simulating earthquake data for structural analysis. Turkey Earthquake Building Regulations (TBDY, 2018) to determine the seismic design spectrum is considered.

ÖZET

VAKA ANALİZİ: DÜZCE'DE BAZ-İZOLATÖRLÜ BİNADA SAHAYA ÖZEL SİSMİK TEHLİKE ANALİZİ

Günümüzde, sismik yükler altında, zemin-yapı etkileşimi ve üstyapının ne kadar etkilendiği önemli hale gelmiştir. Ülkemiz genel olarak incelendiğinde deprem ve hareketli tektonik bölgesinde yer almaktadır. Konumu itibari ile tarihten günümüze birçok depreme şahit olmuş ve bu depremler birçok can ve mal kaybına yol açmıştır. Bundan dolayı, her saha özelinde zemin davranış analizleri yapılarak yıkımları en aza indirmek mühendislik ve sosyal-ekonomik yapı açısından şart olmuştur.

İzolatörlü bina, köprü ve diğer yapıları performansa göre tasarlamak için özellikle deprem yer hareketinin belirlenmesinde uzun vadeli yer hareketlerinin dikkatlice değerlendirilmesi gerekmektedir. Bu değerlendirmelerde, tepki spektrumunu tahmin etmek için ampirik ve teorik yöntemler, yakın fay etkilerini hesaba katmak ve analiz etmek, farklı sönüm oranları için spektrumu ölçeklendirmek ve uzun vadeli yer hareketlerinin simülasyonu ve zaman tanım aralığı önemli bir yer oluşturmaktadır. Uzun dönem sınırlarında tasarım spektrumunu değiştirmek için gerekli ilkelerin belirlenmesi gerekmektedir. Yönetmeliklerin zaman tanım aralığında uzun dönem yer hareketlerini simüle etmesi ve deprem yer hareketi kayıtlarının uzun dönem etkisi dikkate alınarak seçilmesi ve ölçeklendirilmesi için bazı kurallar gerekmektedir. 2018 yılında yayımlanan Türkiye Bina Deprem Yönetmeliği bu kurallara gereken ışığı tutmaktadır.

Bu tez kapsamında, deprem etkisinin tanımlanmasında ulusal ve uluslararası düzenlemelerdeki genel yaklaşımlar incelenmiş ve Düzce'de yapılması planlanan fabrika yapıları için önerilen deprem düzeyleri açıklanmıştır. İnceleme alanındaki deprem tehlikesi değerlendirilirken bölgenin genel jeolojisi, tektonik özellikleri, zemin koşulları, mevcut fay sistemleri dikkate alınmıştır. İnceleme alanı için, klasik tehlike spektrumlarının yanı sıra, çeşitli tekrarlanma periyodu için olasılıksal sismik tehlike haritalarının ve spektral koordinatların hesaplanmasına olanak sağlayan farklı spektral ordinatlar için tehlike eğrileri sunulmuştur. Bu spektrumlara göre deprem kayıtları seçilmiş olup simülasyonu yapılarak lineer olmayan analizler yapılarak yapısal analizlerde kullanılmak üzere deprem verileri elde edilmiştir.

TABLE OF CONTENT

LIST OF TABLES

Table **Page**

LIST OF FIGURES

Figure **Page**

Figure **Page**

Figure **Page**

Figure **Page**

CHAPTER 1

INTRODUCTION

1.1. General

Earthquake is defined as the vibrations that occur suddenly due to the ruptures in the earth's crust spread in waves and shake the environment and the earth. Since the world's formation, it has been known that earthquakes have occurred sequentially in seismically active areas, and millions of people died, and shelters have been destroyed as a result. As it is well known, Turkey is in one of the most significant earthquake zones in the world. There were many destructive earthquakes happened in Turkey in the past. It is a fact that we may suffer a considerable loss of life and property due to earthquakes that will frequently occur in the future. According to the Earthquake Zones Map given in e-state of Turkey, it is known that 92% of Turkey is in earthquake zones, 95% of our population lives under earthquake danger, and 98% of large industrial centers and 93% of our dams are located in earthquake zones.

Turkey passed to history as the second-largest recording earthquakes with the 7.4 magnitude Kocaeli earthquake that occurred on 17 August 1999. The earthquake, whose epicenter was Gölcük, was felt throughout the Marmara Region. The earthquake that happened with the North Anatolian Fault Line's breaking caused the loss of life and property in Istanbul, Bolu, Bursa, Eskişehir, Kocaeli, Sakarya, and Yalova. About three months after the earthquake happened on 17 August 1999, another earthquake occurred on November 12, again on the North Anatolian Fault Line, with the epicenter of Düzce. The magnitude of the Düzce Earthquake was 7.2 magnitude and lasted 30 seconds. 845 people died. These two earthquakes have caused more discussion of measures to be taken against the expected break in Turkey. Figure 1.1 illustrates the extent of the destruction of the earthquake in Düzce.

Figure 1.1 Damages and Collapses in Düzce City, www.koeri.boun.edu.tr

This thesis aims to provide seismic hazard analysis and select and scale time history records for the factory structures planned in the Çilimli district, Düzce, Turkey. The facility was designed with base isolators where some necessary secondary units are with fixed-base design.

This thesis consists of following parts:

- Examination of soil condition and engineering geology of Düzce,
- Investigation of seismicity and seismotectonic units,
- Definition of earthquake effect on Turkish Earthquake Code for Buildings (TBDY 2018),
- Assessment of existing seismic hazard,
- Identification of near-fault effect,
- Determination of design spectrums and selecting Ground Motion Data
- Scaling and matching to the appropriate design spectrum
- 1D Site specific seismic response analysis

accordingly.

Initially, general, and international regulations were investigated for in the definition of earthquake effect and the earthquake levels recommended for Düzce. The case study area's assessment of current earthquake hazard was made by analyzing the

tectonic features, soil conditions, engineering geology of the region, seismotectonic units (existing fault systems), source of earthquakes and the area's seismicity with the recent earthquakes that occurred in the region. Turkish Earthquake Code (TBDY, 2018) is considered to determine earthquake design spectra and the earthquake ground motions spectrum. Some other issues that are not stated in the Turkish Code (near-fault effects, etc.) are studied using international research available in the literature.

1.2. Organization of Thesis

Within the scope of this thesis, first, the principles regarding the determination of design-based ground motion in earthquake specifications will be examined, and earthquake design criteria would develop for the case study. To determine the earthquake hazard under the light of these criteria does not appear to be modifying the subject of the tectonic units (fault systems). That may affect the study area, earthquakes affecting the region throughout history, and the region's seismicity in the last century. Considering this information, design spectra would constitute earthquake design at different performance levels.

The thesis consists of nine chapters. The first chapter is the introduction includes general information and organization of the thesis. The second chapter is background information comprises the definition of earthquake effect at the different code. The third chapter includes the investigation area, the geology of the case study area, and soil assessment at the site. The fourth chapter is an examination of seismicity and seismotectonic units. The fifth chapter is the result, and the discussion includes liquefaction analysis according to in-situ tests. The sixth chapter is the assessment of existing seismic hazards and identification of the near-fault effect. The seventh chapter provides a spectrum matching simulation of earthquake ground motion in the time domain. The eighth chapter is the scaled earthquake data will be transferred to the surface with the help of nonlinear models. The final chapter is conclusions and recommendations of site-specific seismic response analysis.

CHAPTER 2

DEFINITION OF EARTHQUAKE EFFECT AT DIFFERENT CODES

2.1. Introduction

The principles about obtaining design ground motions for the earthquake-resistant design of engineering structures are included in existing earthquake regulations. The most widely used and known standards in Turkey: Turkish Earthquake Code (TBDY, 2018), Minimum Design Loads and Associated Criteria for Buildings and Other Structures (American Society of Civil Engineers, ASCE 7-16), Eurocode8 TS EN-1998 (EC8, 2003), and International Building Code (IBC, 2006). This chapter includes (1) definition of earthquake effect at different codes, (2) code spectra-based assessment for selecting and scaling earthquake ground motion data, and (3) near fault effect on earthquake ground motion.

2.2. Existing Earthquake Regulations

2.2.1. ASCE 7-16 (2017)

ASCE 7-16 used in the United States defines a single level seismic effect. ASCE 7-16 describes the Maximum Considered Earthquake (MCE) effect with a 2% exceedance probability in 50 years and recommends taking 2/3 of this earthquake effect in new buildings. The performance target in the new buildings is "Life Safety." It also describes MCE, in which site class B ($V_{s,30}$>760 m/s- Little weathered medium-strong rocks) is taken as a reference by defining spectral acceleration (S_s) in the short period (0.2s) and 1.0s period spectral acceleration (S_1).

2.2.2. Eurocode8 (EC8, 2003)

Eurocode 8, which is commonly used in Europe, defines two different earthquake effects for construction. The effect of the first earthquake performance target with a 10% exceedance probability in 10 years (return period is 95 years) is specified as “Damage Limitation.” The performance target has been defined as "Collapse Prevention" for the second earthquake effect with a 10% exceedance probability in 50 years (return period is 475 years).

2.2.3. Turkish Earthquake Code for Buildings (TBDY, 2018)

Within the Turkish Earthquake Code (2018), earthquake ground motion spectrums are calculated for a 5% damping ratio based on reference soil conditions for a certain level of earthquake ground motion.

These calculations are defined as a standard form depending on the coefficients of dimensionless spectral acceleration and coefficients of local site effect or defined site-specific seismic hazard analyzes. The rules that must be applied for the selection and scaling of the earthquake ground motions required for one or two and three-dimensional earthquake calculation in the time domain of the structural system elements; are defined in the relevant sections of this Code (TBDY, Section-2.4 general data, Section 14 for Base isolators).

Within scope of code, four different earthquake ground motion levels are defined. These are DD-1, DD-2, DD-3, and DD-4. Site-specific earthquake ground motion data for varying earthquake ground motion levels are identified by Turkish Earthquake Hazard Maps, accessed through the website www.tdth.afad.gov.tr. (turkiye.gov.tr)

AFAD is the synonym of Disaster and Emergency Management Agency. The Agency is working, depending on the Republic of Turkey Ministry of Interior. The principal duty and purpose of the institution is to carry out the management and coordination of pre-disaster preparedness and mitigation, intervention during the disaster and recovery after the disaster.

(DD-1) Earthquake Ground Motion Level-1:

This level refers to the very infrequent earthquake ground motion, which has a 2% exceedance probability in 50 years, and the corresponding return period is 2475 years. This ground motion is also called the maximum earthquake ground motion.

(DD-2) Earthquake Ground Motion Level-2:

This level refers to the periodic earthquake ground motion, which has a 10% exceedance probability in 50 years, and the corresponding return period is 475 years. This ground motion is also called the standard design earthquake ground motion.

(DD-3) Earthquake Ground Motion Level-3:

This level refers to the frequent earthquake ground motion, which has a 50% exceedance probability in 50 years, and the corresponding return period is 72 years.

(DD-4) Earthquake Ground Motion Level-4:

This level refers to the continuous earthquake ground motion, which has a 68% exceedance probability in 50 years (50% exceedance probability in 30 years) and the corresponding return period is 43 years. This ground motion is also called the service earthquake ground motion.

2.3. Elastic Design Spectrum Based on TBDY (2018)

Horizontal elastic design spectral accelerations S_{ae} (T), which are ordinates of the horizontal elastic design acceleration spectrum for any earthquake ground motion level, are defined with the following set of equations in terms of acceleration (g) depending on the natural period (T). Representation of horizontal elastic design spectrum defined in TBDY 2018 is given in Figure 2.1.

$$S_{ae}(T) = \left(0.4 + 0.6\frac{T}{T_A}\right) S_{DS} \quad (0 \le T \le T_A) \tag{2.1}$$

$$S_{ae}(T) = S_{DS} \quad (T_A \le T \le T_B) \tag{2.2}$$

$$S_{ae}(T) = \frac{S_{D1}}{T} \quad (T_B \le T \le T_L) \tag{2.3}$$

$$S_{ae}(T) = \frac{S_{D1}T_L}{T^2} \quad (T_L \le T) \tag{2.4}$$

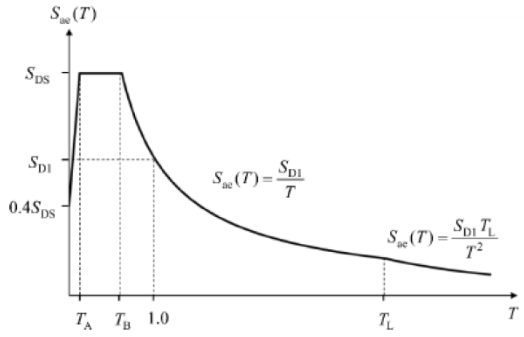

Figure 2.1 Horizontal Elastic Design Spectrum (TBDY 2018)

S_{DS} and S_{D1} are the design spectral acceleration coefficients. Horizontal design spectrum periods T_A and T_B are defined with the following equation depending on S_{DS} and S_{D1}.

$$T_A = 0.2\frac{S_{D1}}{S_{DS}} \qquad T_B = \frac{S_{D1}}{S_{DS}} \tag{2.5}$$

The transition period to the fixed displacement zone T_L is taken 6 s.

Vertical elastic design spectral accelerations S_{aeD} (T), which are ordinates of the vertical elastic design acceleration spectrum for any earthquake ground motion level, are defined in terms of gravitational acceleration (g) depending on the short-period design spectral acceleration coefficient and natural period specified for horizontal earthquake ground motion are determined by the following set of equations. Representation of vertical elastic design spectrum defined in TBDY 2018 is given in Figure 2.2.

$$S_{aeD}(T) = \left(0.32 + 0.48\frac{T}{T_{AD}}\right)S_{DS} \quad (0 \le T \le T_{AD}) \tag{2.6}$$

$$S_{aeD}(T) = 0.8S_{DS} \quad (T_{AD} \le T \le T_{BD}) \tag{2.7}$$

$$S_{aeD}(T) = 0.8S_{DS}\frac{T_{BD}}{T} \quad (T_{BD} \le T \le T_{LD}) \tag{2.8}$$

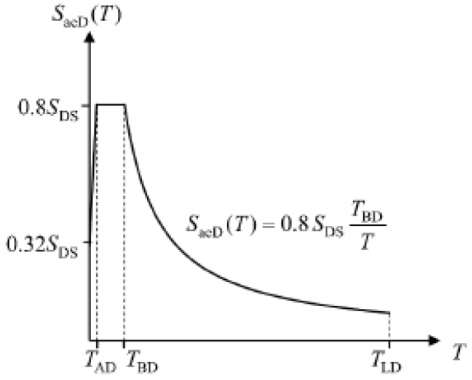

Figure 2.2 Vertical Elastic Design Spectrum (TBDY 2018)

T_{AD} and T_{BD} vertical spectrum corner periods and T_{LD} period are defined by the following equation.

$$T_{AD} = \frac{T_A}{3} \qquad T_{BD} = \frac{T_B}{3} \qquad T_{LD} = \frac{T_L}{3} \tag{2.9}$$

2.4. Code Spectra Based Assessment for Selecting and Scaling

Turkish Earthquake Code for Buildings (2018) is used to generalize and scale earthquake ground motion as an initial view. Afterward, the Uniform Hazard Assessment analysis is provided in chapter 7, and the results are given for comparison.

2.4.1. Definitions and Review of Code Provisions TBDY 2018

- **Site-Specific Elastic Spectrum**

Turkish Earthquake Code gives general information regarding the site-specific elastic spectrum preparation. It states in TBDY 2018 that "In some special conditions, site-specific earthquake hazard analysis and site-specific ground motion spectrums can be identified. This type of spectrums can be used for any cases with the preference of Design Engineer".

The site-specific ground motion spectrum's ordinates shall never be lower than the 90% of the design spectrum defined in TBDY 2018.

- **Selection of Ground Motions**

TBDY 2018 considers a method to select a viable ground motion data. It is identified that the ground motions to be used in time domain analysis in structural systems need to be selected from events of moment magnitudes, the distance of fault from source, and source mechanisms that are consistent with the design earthquake level. In case there are historical earthquake ground motion records compatible with design strong ground motions, these earthquake data can be used as a priority.

Disaggregation can define fault distances and magnitudes that shall be the main variables in hazard analysis. In case there is a lack of existing ground motion records, synthetic earthquake records that are simulated in the time domain can be used. The seismic source, wave propagation, and local soil effects need to be considered while using

these synthetic data. The simulation process must prove that the synthetic records are compatible with the real recorded motions.

The selection of ground motion data can be made using the website https://ngawest2.berkeley.edu/. NGA is one of the richest databases for ground motion data. Accurate earthquake ground motion records (EQGMs) are used for determining each ground motion compatible with the design spectra/uniform hazard spectrum for specified seismic levels corresponding to return periods of 2475 years and 475 years.

- **Scaling of Ground Motions (Basic Amplitude Scaling)**

TBDY 2018 is related to the scaling of time-domain records as time histories. Beyond Soil Behavior analysis, the (basic) scaling procedure for time history design can be done.

For one and two-dimensional analysis, the set of scaled records shall not be less than the design response spectrum over the period range from $0.2T_p$ to $1.5T_p$ (where T_p is the elastic first- "mode" vibration period of the structure) as described in TBDY 2018. The amplitude of the time histories can be scaled accordingly.

For three-dimensional analyses, each pair of horizontal components should be combined with the square root of the sum of the squares (SRSS) method. The average of the combined spectrums of all the selected records is then scaled. The scaled spectrum and design spectrum ratio should not fall below 1.3 times in the period range from $0.2T_p$ to $1.5T_p$. Each pair of ground motions will be scaled with the same scale factor.

For base-isolated structures, the SRSS spectra's average from all horizontal component pairs does not fall below the corresponding ordinate of the response spectrum used in the design between the periods $0.5T_D$ and $1.25T_M$, respectively, where T_D is the significant period of the isolated structure at design displacement. T_M is the considerable period of the isolated structure at maximum displacement.

The conditional mean spectrum related to the structure period can be used to prevent scattering in scaling if the site-specific ground motion spectrum is defined or structural properties necessitate the situation.

- **Spectral Matching**

TBDY 2018 states that; Spectral matching can be used for ground motions. These matched spectrums (matched ground motion data) be used in soil behavior analysis or any other calculation in the time domain. The mean of matched ground motion data shall be over the design spectrum ordinates.

2.5. Near-Fault Effects on Earthquake Ground Motion

Near-field ground motions differ from other ground motions because they usually include strong and dynamic long-term pulses and permanent displacements. Dynamic movements are determined by the long-period pulses of the movements on the horizontal component perpendicular to the fault slip caused by rupture directivity effects. Ground displacements that occur as a result of close field ground motions are caused by the resultant of the two-way movement on the fault where the earthquake occurred.

Near field ground motions, especially forward directional motions, have different characteristics from ground motions recorded at medium-long distances. These features raise the question of whether the current field response approach is directly applicable to near field ground movements.

It is considered that the near field region is typically limited to 10-15 km of the action triggering fault. The immediate benefit is the forward bias effect that matters. The forward bias conditions produce ground motions characterized by the strong pulse or pulse series observed in the velocity-time domain.

Forward-looking recordings have led to a number of studies addressing the prediction of such movements and their effect on structural response (eg. Somerville 1998, Krawinkler and Alavi 1998, Sasanian and Bertero 2000). In order to make a more realistic seismic risk assessment, it is necessary to understand the close field ground motions and the mechanisms controlling the interaction of close field ground motions with soil layers.

The main consequences of near-fault effect can be summarized as; (1) Directivity Effect, (2) Fling-step, (3) Velocity pulse, (4) Vertical Seismic Component and Hanging Wall (not for Strike-slip mechanism), (5) Rotational Seismic Component (Grimaz, 2014).

The effect of these items is briefly explained hereafter and shall be considered both in the Code Spectra method or Probabilistic Seismic Hazard Assessment (PSHA) method.

2.5.1. Rupture Directivity Effect

The directional effect is produced because the rupture velocity of the fault is less than the shear wave propagation velocity. While the forward direction (rupture front) radiates from the focal point, a shear wave front is formed with the accumulation of shear waves traveling along the forward direction. In the case where the field is located at one end of the fault, the wave that starts at the other end of the rupture and reaches towards the field can be seen at the beginning of the earthquake recording as a large slip movement (Somerville et al., 1997). This condition is known as forward-directivity and is illustrated in Figure 2.3.

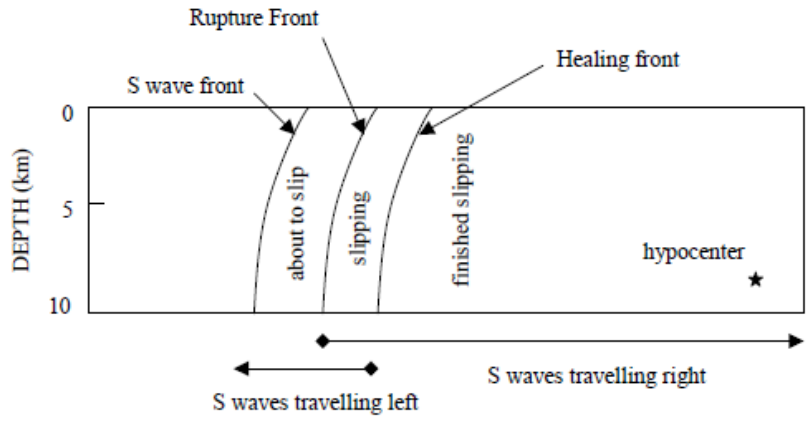

Figure 2.3 Schematic Diagram of the Directional Effect for a Strike-Slip Fault (Somerville et al. 1997)

Ground motion records in areas subject to forward bias are characterized by the fact that most of the seismic energy reaches a single large pulse motion at the beginning of the recording (Somerville, 1997). This large pulse of motion is located perpendicular to the direction of the fault. There is no clear definition of the orientation effect in TBDY 2018. Somerville (1998) stated that time history representation better captures the effects of near field ground motions on structures.

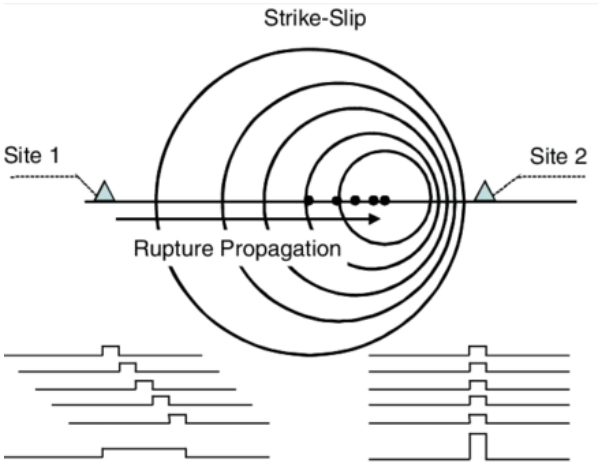

Figure 2.4 Schematic View of Forward and Backward Effect

The directional effect depends on the direction of forward bias in the event of an earthquake. If the rupture direction of the fault is in the direction approaching the field, this is defined as forward directivity. If the fault is in the direction away from the field to the rupture direction, this is defined as backward directivity (Figure 2.4).

Ground motion parameters created by taking the directional effects into account; the average horizontal response spectrum is the ratio of the fault normal response spectrum to the fault parallel response spectrum and the duration of ground motion. The model used to define geometric conditions for directivity is shown in Figure 2.5.

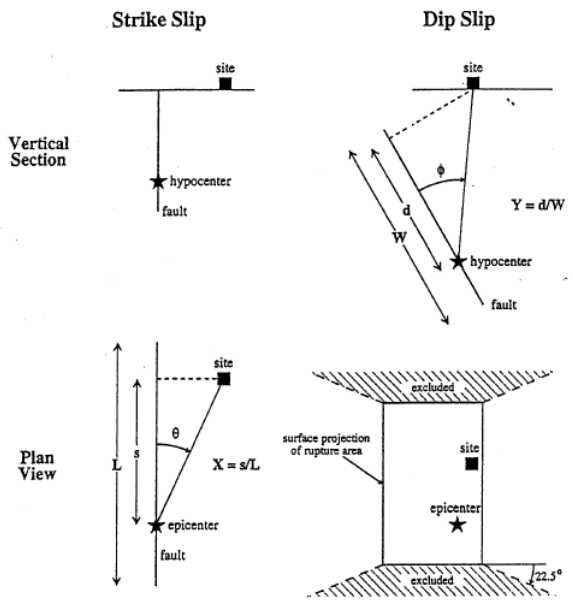

Figure 2.5 Representation of the Parameters Considered in the Effect of Directivity (Somerville et al. 1997)

Directionality effects depend on two main parameters; The angle between the rupture propagation direction (for strike-slip faults, φ for dip-slip faults) and the direction of the waves from the fault to the field, Second, the amount of the fault rupture surface located between the focal center and the field (X for strike-slip faults, Y for dip-slip faults)). The smaller the angle, the greater the orientation conditions encountered in the field which is shown in Figure 2.5.

Similarly, the effects of directionality are greater if a larger part of the fault is located between the field and the focal center. Somerville et al. (1997) tried to model the directional effects for strike-slip and oblique-slip faults using the Xcosθ and Ycosφ functions, respectively. Somerville et al. The equations developed by (1997) are presented in Table 2.1 and Table 2.2 and the effect of these equations on spectral amplification rates are shown in Figure 2.6 and Figure 2.7. The parameters defining forward directional conditions in the Somerville model can also be used to define areas with forward directional potential.

Table 2.1 Modification of Ground Motion Parameters Used to Explain Directional Effects (Somerville et al. 1997)

Ground Motion Parameter	Description	Equation	Range of Applicability
Amplitude Factor: Ratio of data/model	Bias in average horizontal response spectral acceleration (log) with respect to Abrahamson and Silva (1997)	Strike-Slip faults: $y = C_1+C_2 X\cos\theta$ Dip-Slip faults: $y = C_1+C_2 Y\cos\phi$	Moment Magnitude (M_w): 6.5 – 7.5 Distance (R): 0 – 50 km C_1, C_2 functions of period
Duration factor: Ratio of data/model ($D_{0.05-0.75}$)	Bias in duration of acceleration with respect to Abrahamson and Silva (1997)	Strike-Slip faults: $y = C_1+C_2 X\cos\theta$ Dip-Slip faults: $y = C_1+C_2 Y\cos\phi$	$6.5 \le Mw \le 7.5$ $0 \le R \le 20$ km
Strike Normal/Average Amplitude	Natural logarithm of the ratio of strike normal to average horizontal spectral acceleration	$y = \cos 2\xi\,[C_1 + C_2 \ln(R + 1) + C_3(M_w\text{-}6)]$	$6.0 \le Mw \le 7.5$ $0 \le R \le 50$ km $\xi = \theta$ for strike-slip, ϕ for dip-slip. $0 < \xi < 90°$ C_1, C_2, C_3 function of period. Given separately for cases in which dependence on ξ is included, and cases in which dependence on ξ is ignored.

Table 2.2 Parameters Used in Directivity Model (Somerville et al. 1997)

Parameter	Range of Applicability (Related to the ground motion parameters in Table 1)
M: Moment magnitude	6.0–7.5 (parameter 3); 6.5–7.5 (parameters 1, 2)
r_{rup}: Rupture distance	0–50km for amplitudes (parameters 1, 3) 0–20km for duration (parameter 2)
Style of faulting	Crustal Earthquakes (parameters 1 and 2): Strike-slip—no restriction on area covered Dip-slip—between ends of fault only (Figure 5)
Site classification	All models are independent of site classification. Models for parameters 1 and 2 are based on residuals from Abrahamson and Silva (1997a,b).
X: Length ratio (fraction of fault along strike that ruptures toward site)	0–1; used for strike-slip faults, parameters 1 and 2
Y: Width ratio (fraction of fault up dip that ruptures toward site)	0–1; used for dip-slip faults, parameters 1 and 2
θ: Azimuth angle between fault plane and ray path to site.	used for strike-slip faults: 0–90 degrees (parameters 1 and 2) 0–45 degrees (parameter 3)
ϕ: Zenith angle between fault plane and ray path to site	used for dip-slip faults: 0–90 degrees (parameters 1 and 2) 0–45 degrees (parameter 3)

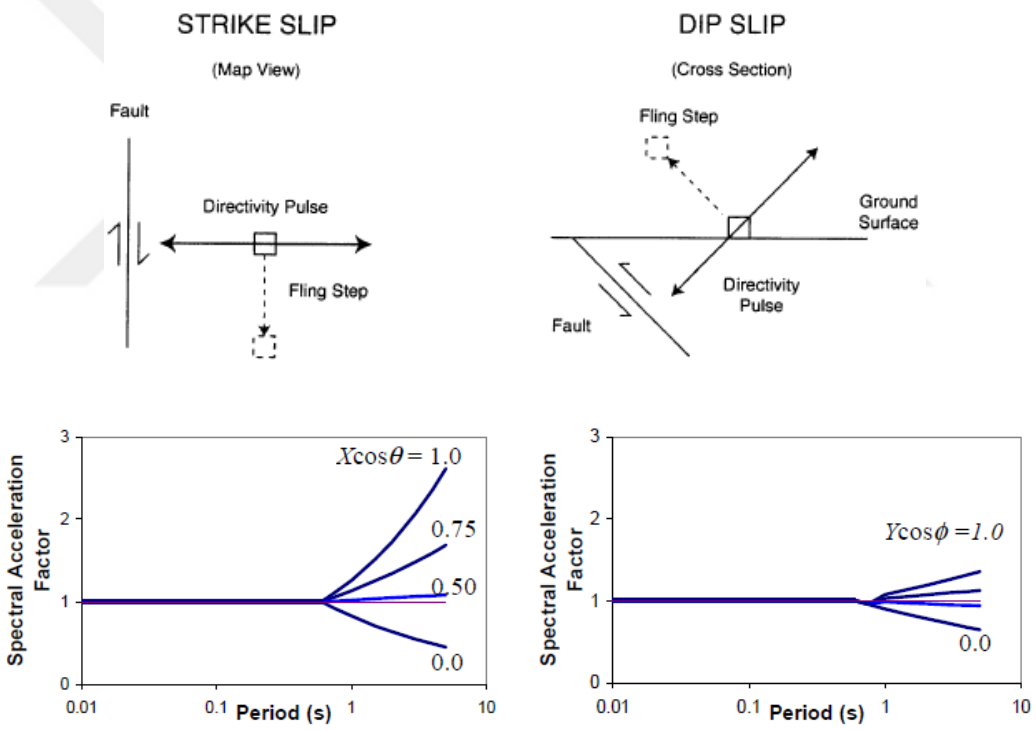

Figure 2.6 Relation of Average Spectral Accelerations with Period and Directional Effects (Somerville et al. (1997))

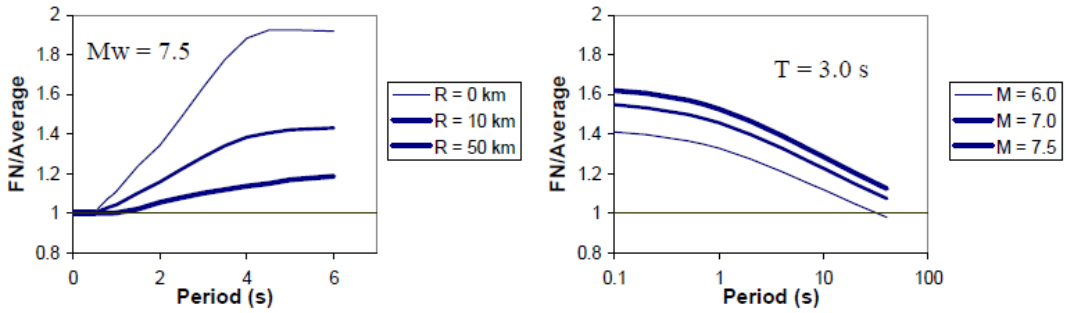

Figure 2.7 Average Horizontal Spectral Ratios for Maximum Forward-Directivity conditions (Xcosθ = 1) (Somerville et al. (1997))

The directional effect has different values for the fault normal and fault parallel directions (in particular, for strike-slip and oblique slip, the fault is maximum in the normal direction). In addition, in case of orientation, there may be an increase in the ground motion amplitudes in long periods. As move away from the field, there may be a decrease in the ground motion amplitudes in long periods.

2.5.2. Velocity Pulse

Grimaz (2014) stated that fling-step and directivity effects can cause long periods and high-value velocity (velocity pulses) effects. According to Moustafa and Takewaki (2010), pulses have high amplitude and long period, high Peak Ground Velocity/ Peak Ground Acceleration (PGV/PGA) and Peak Ground Displacement/ Peak Ground Acceleration (PGD/PGA) ratios, unexpected response spectrum shapes, and the amount of energy accumulated in one or more pulses. Ground motions, which show a throwing feature, are classified according to their periods (Usually called T_p). Baker (2007) made these classifications using different signal analysis.

Hayden et al. (2012) roughly estimated the number of ground motions showing the throw feature to be used in the design. The study proposes to use the design ground motion parameter epsilon (ε) and the closest distance from the field to the source (R in km) with the following equation. Figure 2.8 shows that the relationship between epsilon and proportion pulse.

$$Proportion\ of\ Pulse\ Motions = \frac{\exp(0.891 - 0.188R + 1.230\varepsilon)}{1 + \exp(0.891 - 0.188R + 1.230\varepsilon)} \quad (2.10)$$

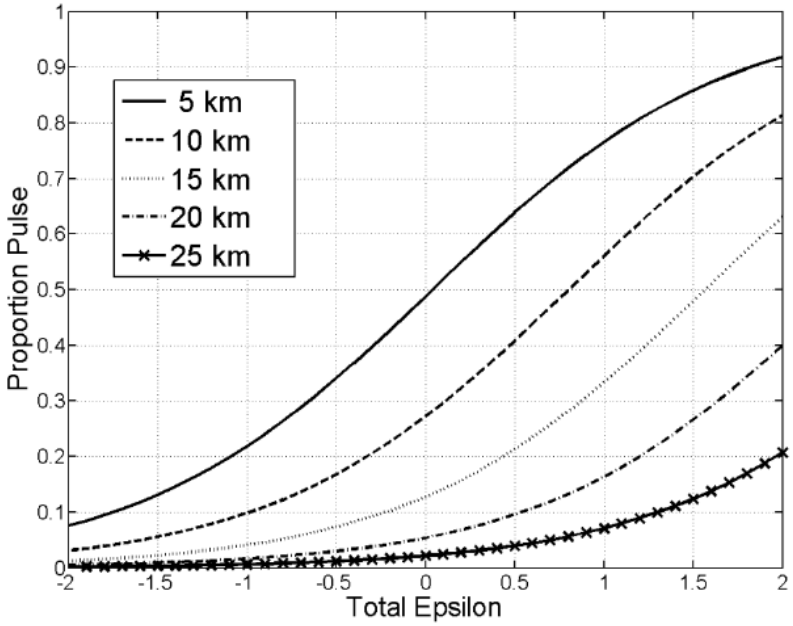

Figure 2.8 Relation of Pulse Rate to Epsilon and Distance (Hayden et al. 2012)

2.5.3. Fault Normal - Fault Parallel Components

In near field ground motions, the fault is larger than the normal component fault and is generally used as input data in structural response studies. The period of the normal component of the fault varies between 0.6 and 4.0 seconds. The lower value is Somerville et al. (1997) has also been used in empirical analysis of orientation effects in the studies. (Figure 2.9)

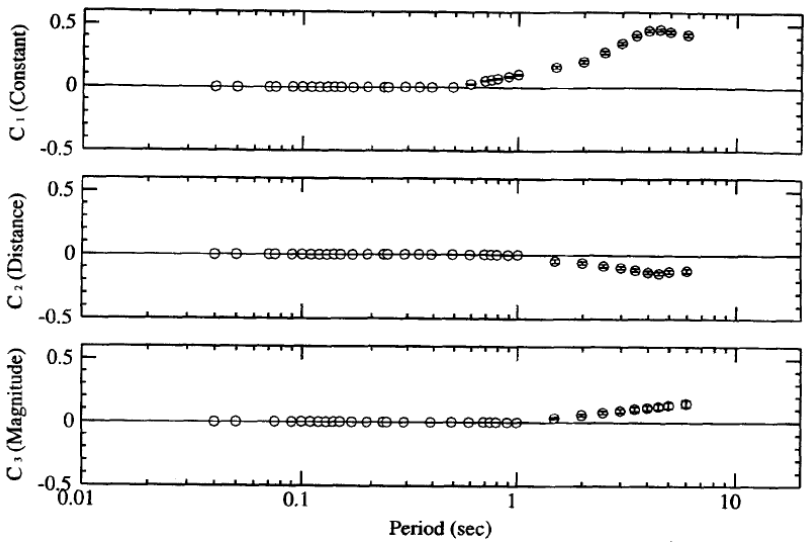

Figure 2.9 Coefficients of the Empirical Model for FN-FP Components

2.5.4. Fling-Step Effect

Ground motions in the form of throw are produced by the intensification of the sliding behavior. The slip originated beats, called "fling-step", have different characteristics from the forward beats. The displacement effect (fling-step) produces unilateral velocity pulses. The fling-step effect is associated with the permanent ground displacement and unidirectional large amplitude velocity pulse. This effect occurs in strike-slip faults in the parallel fault direction and dip-slip faults in the normal fault direction (Figure 2.10).

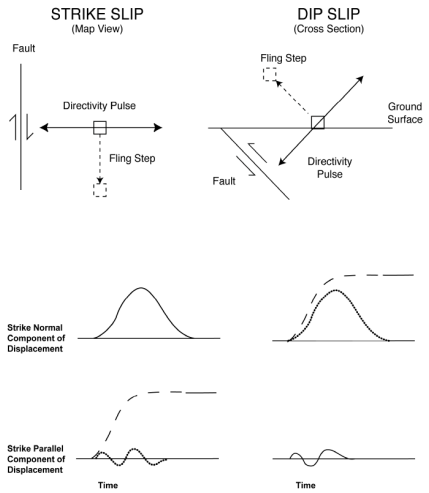

Figure 2.10 Schematic Representation of the Rupture Directivity Pulse and Displacement Effects (Somerville (2005))

2.5.5. Vertical Seismic Component

The vertical component effect has been studied by many researchers in the near field. The main features of the vertical component, as given in Grimaz, 2014, are as follows. The ratio between spectra of vertical and horizontal components depends on the period, and vertical ground acceleration generally has a higher frequency content than the horizontal component. Most of the energy of vertical ground motion occurs in a narrow high frequency band (Collier and Elnashai, 2001). The maximum value of the vertical component occurs earlier than the horizontal component; The lag time between two maximum points generally increases with the distance (Collier and Elnashai, 2001; Shreshta, 2009).

The ratios of vertical maximum ground acceleration values to horizontal maximum ground acceleration values (peak ground acceleration) in the near field situation are generally higher than the 2/3 value suggested by Newmark et al. (1973).

2.5.6. Hanging Wall Effect

The hanging wall effect is directly related to the fault mechanism and cannot be evaluated for strike-slip faults. Ground motions in the hanging-wall systematically show higher values than the foot-wall ground motion (46% to 50% higher than the estimated average in the 5 to 25 km near field range). Also, this effect causes larger short period ground movements in the hanging part compared to the footwall block part at the same distance. Figure 2.11 illustrates schematic view of hanging wall.

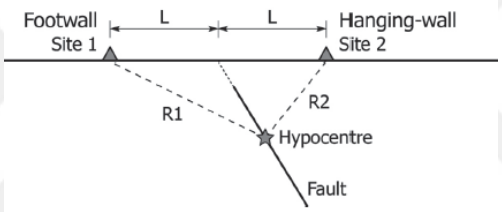

Figure 2.11 Illustration of Hanging-Wall and Footwall (from Li and Xie, 2007)

2.5.7. Maximum Rotated (Max Rot) Component

Selected ground motion records can be rotated 180 degrees counterclockwise at one-degree intervals. Based on Huang et al. (2008), the maximum rotation can be calculated using values given in Table 2.3.

Table 2.3 Coefficients of Max. Rotation (Huang et al. (2008))

	Bin 1 (All Earthquake Records)		Bin 2 (No Chi-Chi Earthquake Records)		Bin 3 (Forward-Directivity Earthquake Records)	
Period (Seconds)	Median	84th Percentile	Median	84th Percentile	Median	84th Percentile
0	1.0	1.8	1.2	2.1	1.3	2.2
0.05	1.0	1.8	1.2	2.2	1.3	2.3
0.1	0.9	1.7	1.1	2.0	1.2	2.1
0.2	0.9	1.7	1.2	2.1	1.2	2.2
0.3	1.0	1.9	1.3	2.4	1.3	2.5
0.5	1.2	2.1	1.3	2.6	1.4	2.8
1	1.3	2.3	1.3	2.5	1.5	2.9
2	1.3	2.5	1.3	2.7	1.6	2.9
3	1.4	2.6	1.3	2.9	1.7	3.1
4	1.4	2.7	1.3	2.7	1.7	3.0

CHAPTER 3

SITE INVESTIGATION IN DUZCE

3.1. Introduction

The aim of site investigation is to evaluate soil and foundation engineering (bearing capacity, settlement etc.) assessment based on boreholes, seismic risks including liquefaction risk. This chapter presents evaluation of the soil investigation and description of the general geology in Düzce. Location of case study area is given in Figure 3.1.

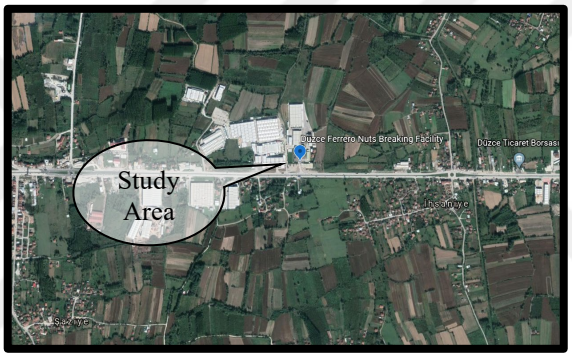

Figure 3.1 The Location of The Investigation Area

There are two previous geotechnical interpretation reports prepared by Zemin Etüd ve Tasarım A.Ş. published on 30.06.2017 and 10.11.2017, these reports are summarized in this chapter.

Destech Consulting Engineering and Project Inc. carried out fieldworks between 14.01.2020-21.02.2020. Besides, geophysical investigation studies are carried out in May 2020. For soil investigation purposes, twenty-three different boreholes with varying depths between 20 and 30 meters are drilled with a total depth of 491.45 meters. Laboratory tests were carried out on disturbed and undisturbed soil samples that are collected from the boreholes. Three hundred eighteen Standard Penetration Tests (SPT) and seven Cone Penetration Tests (CPT) were performed in the investigation area. Besides several geophysical investigation tests were performed on the investigation area covering (1) five Wenner electrical resistivity measurements, (2) 4-line seismic refraction (MASW), and (3) six Microtremor measurements.

3.2. Regional Geology

The oldest unit around Düzce is Precambrian metagranodiorite (PEy), which is outcropped between Efteni Lake and Çapayakbey village in the southwest Düzce plain. The Düzce fault is a boundary between this unit and Quaternary deposits.

3.2.1. Kocatöngel Formation (Oko)

Kocatöngel formation, which consists of silty mudstone with interbedded sandstone, discordantly overlies Bolu Massif base rocks between the villages of Karacaören-Gürcühüseyinağa in the north of Düzce. The formation, which has approximately 1000m thick, is thin-medium and locally massive layers. The formation's age is Ordovician.

3.2.2. Kurtköy Formation (Ok)

Kurtköy Formation, which is Ordovician aged, comprise sandstone with interbedded mudstone, siltstone, conglomerate and is surfaced around Kaynaşlı in the southeast of Düzce. The thickness of the formation is around 1500m. The formation has the characteristics of deposited in a terrestrial environment (meandered stream).

3.2.3. Ereğli Formation (ODe)

Ereğli Formation, which consists of shale-sandstone with interbedded limestone, is outcropped to the north of Kaynaşlı. The formation, which is transitive with Yılanlı formation, is between 500-700m thick (Pehlivan et al., 2002). The formation is Devonian.

3.2.4. Yılanlı Formation (Dcy)

Yılanlı Formation was observed in a minimal area around Dokuzlar village in the northwest of Çilimli, consisting of dolomitic limestone and dolomite. The formation is middle-upper Devonian-lower Carboniferous. The lower part of the formation

represents the shelf-slope, and the shelf environment means the upper part of the formation.

3.2.5. Çakraz Formation (PTrç)

Çakraz's formation was named Çakraz sandstone by Akyol et al. (1974). The formation consists of conglomerate, sandstone, and mudstone, which is in contact with the Ereğli formation in the east of Düzce. The formation thickness could vary between 750-1500m, placed on the Paleozoic units with angular conformity. The formation is covered with angular agreement by upper Cretaceous aged Yeşilçay formation at the top. The formation is Cainozoic.

3.2.6. Yemişliçay Formation (Ky)

Yemişliçay formation, which is Cretaceous-Paleocene aged, consists of volcanic sandstone, claystone, agglomerate, andesitic-basaltic lava, suffice and micritic limestone and the formation is spread out with Yılanlı formation limitedly in the northeast of Düzce. The formation includes sediments from shallow to the deep sea, consisting of a volcanic arc and volcano-sedimentary sequence.

3.2.7. Akveren Formation (KTa)

Akveren formation, which consists of silty limestone-marl interbedded claystone, siltstone, and reef limestone-marl, is outcrops between Çapayakbey and Kaynaşlı in the northeast Yukarıbayır, around Sallar and Nalbantoğlu villages, between Ketenciler-Kurtköy and in the northwest of Domuzgölü hill region. The formation has sandstone-clastic limestone in the bottom and continues clayey limestone-marl, siltstone-claystone alternation to upward. Craterous-Paleocene formation deposited in the environment ranging from shallow sea to deep sea.

3.2.8. Çaycuma Formation (Tç) and Yığılca Member (Tçy)

Çaycuma formation, which consists of sandstone-conglomerate-marl-suffice (volcanic sandstone), is observed north and west of Düzce. The widespread ebonite in the formation is separated as a Yığılca member. Yığılca member consists of primary sandstone, tuff/suffice, andesite-basaltic breccia and is observed in the south, west, and northeast of Düzce. The thickness of the formation is approximately 1000m, and it is lower-middle Eocene. The formation consists of a slope deposit.

3.2.9. Karapürçek Formation (PlQk)

Karapürçek formation, which consists of a poorly attached conglomerate, sandstone, and mudstone, is occurred in the east of Düzce, which creates a skirt flat in front of bedrocks.

3.2.10. Alluvium (Qal)

All the clastic sediments (late Pleistocene-Holocene), which filled the Düzce basin, consist of gravel-sand-silt and clay regardless of the repository. The clastic sediments were observed in alluvial and lacustrine areas other than a small number of debris or slope rubble at the basin edges. According to geophysical investigations in 3-5 km vicinity around the site, the sediments' thickness is approximately 150 - 250m. The unit is aged as Quaternary, in which the alluvial deposits consist of different interbedding of sand-clay-gravel layers that is shown in Figure 3.2.

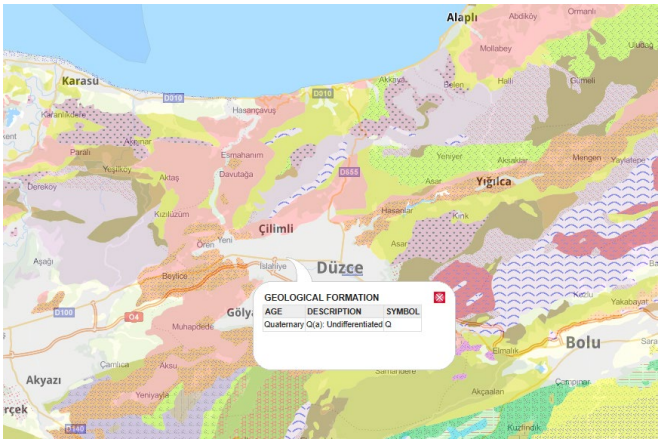

Figure 3.2 General Geological Map (http://yerbilimleri.mta.gov.tr)

The General Directorate of Mineral Research and Exploration (MTA) is a public economic institution under the Ministry of Energy and Natural Resources, established on June 14, 1935. MTA was established to research mining and quarry areas suitable for operation, to carry out research for more efficient operation of the operated mines, to conduct geological and geophysical surveys and laboratory investigations, to train expert and technical personnel and qualified workers for the mining sector. Figure 3.3 and **Hata! Başvuru kaynağı bulunamadı.** illustrate geological map and stratigraphic column section of investigation area published by MTA.

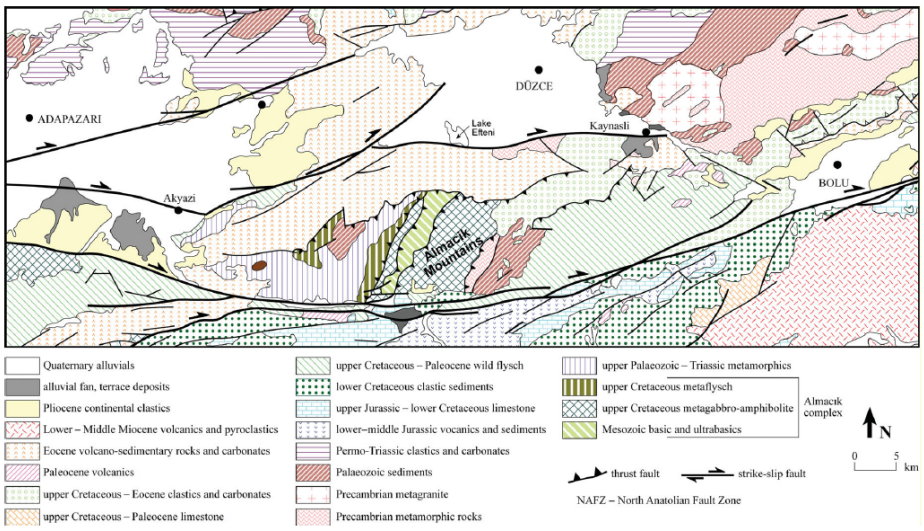

Figure 3.3 Simplified Geological Map Showing the Vicinity of Düzce (Bozkurt et al. 2013)

3.3. Existing Studies at Düzce Basin

More than surveys above, additional geophysical tests were performed at Düzce Basin by several researchers. Two of them are summarized below to have a rough estimation of the surroundings. The sample areas are almost 3.5 to 5 km away from the project site.

The first area is in the Gölyaka region to investigate the soil profile and Karadere Fault segment. Shear wave velocity (V_s) distribution throughout the depth by MASW test performed in Gölyaka District is given in Figure 3.4.

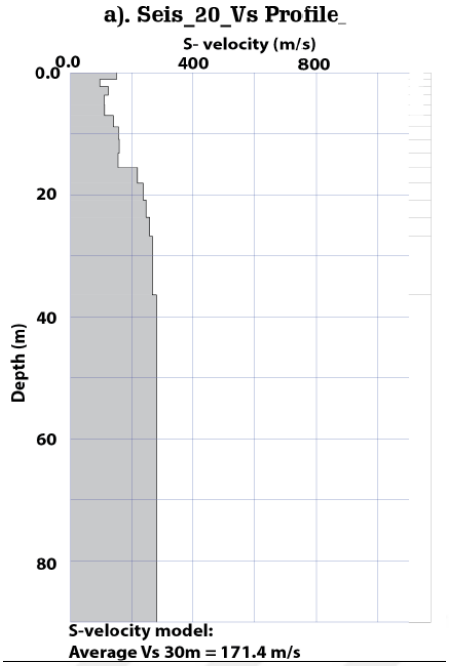

Figure 3.4 Vs Logging for Gölyaka

According to the study in Gölyaka (Yousefi-Bavil et al.,2015), shear wave velocities are around 300m/s at 100m.

The second study of the vicinity of Düzce is by Hasal et al. 2015. Twenty-three Micro-tremor monitoring was performed starting from the south to the north district of Düzce. The aim is to define the basin effect in Düzce deep alluvium basin. Figure 3.5 shows that Engineering Bedrock (Vs>760 m/s) can be determined minimum depths of 100-150 m.

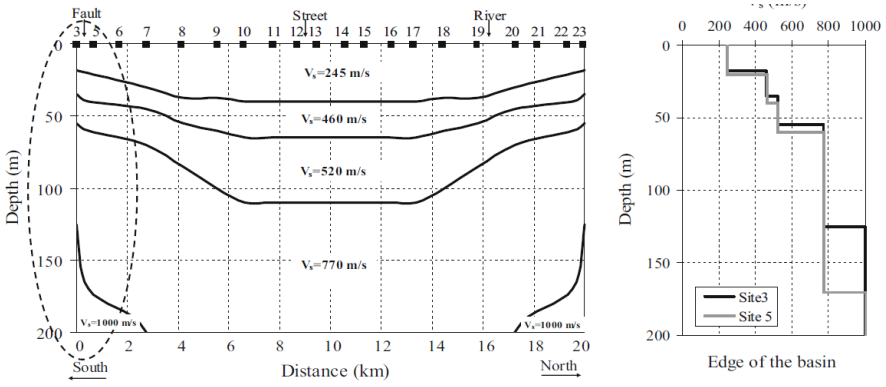

Figure 3.5 2D Shear Wave Velocity Profile of the Düzce Basin

According to the studies performed by Manou et al.,2010, Engineering Bedrock was identified at the depth of around 200 m. (Figure 3.6)

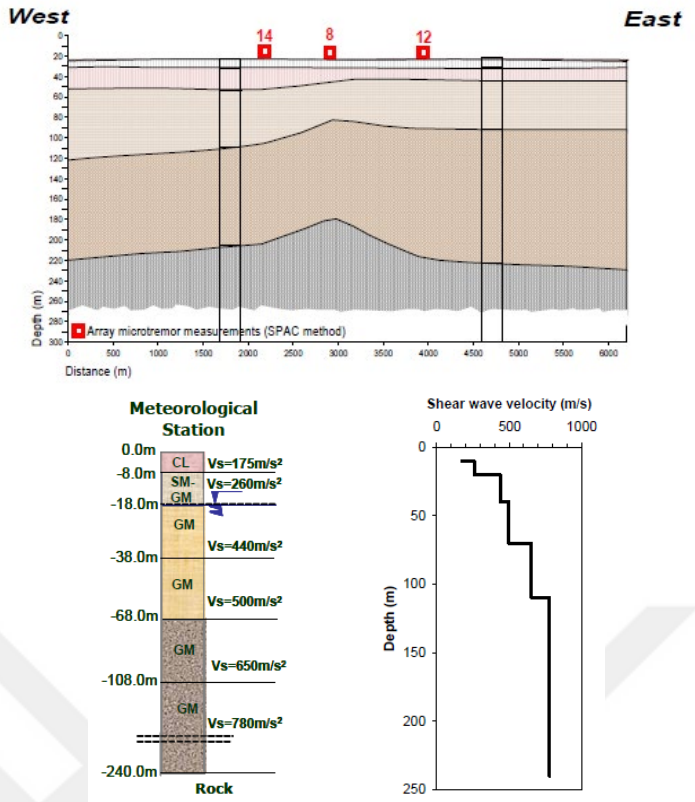

Figure 3.6 Geotechnical Cross-section in the EW Direction and Shear-wave Velocity Profile of Düzce Region (Manou et al., 2010)

Komut (2005) conducted the paleosismological studies around Düzce Fault and shared data for Düzce Fault and Geology for the area. Pucci (2007) gives an infill map for the Düzce basin. Figure 3.7 illustrates that the site has 150-200 m depth for engineering rock.

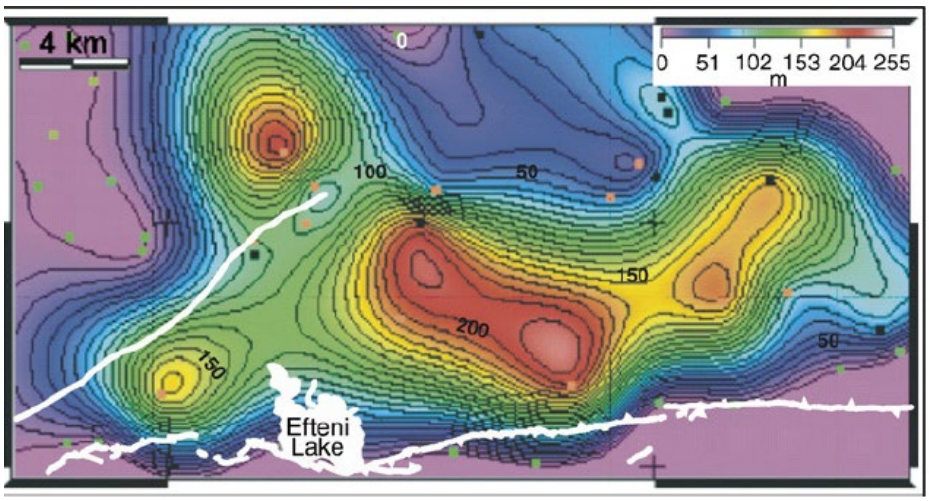

Figure 3.7 Basin Infill Thickness from Borehole Data (Pucci et al. (2007))

3.4. Soil Assessment at the Site

Before Destech, drilling and field works were carried out in the investigation area by Zemin Etüt Inc between 30.06.2017 and 10.11.2017. 4 boreholes with a total depth of 90.30m were drilled, three CPTu tests with average depths of 13m and a total length of 38.8m, four plate load tests (PLT) in the warehouse building and two profiles of MASW studies were performed.

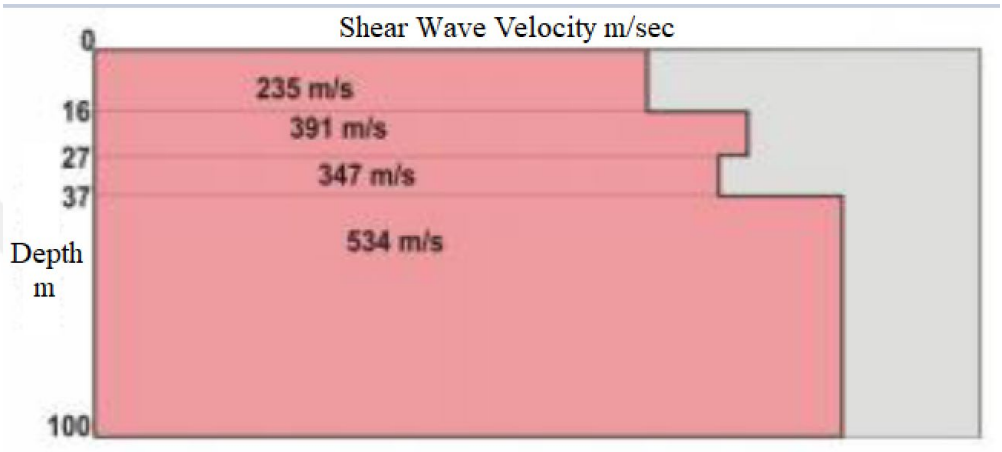

Figure 3.8 MASW Result (Zemin Etut Inc.)

Additional drilling and field works were carried out in the investigation area by Destech Consulting Engineering and Project Inc. between 14.01.2020-21.02.2020. Boreholes were drilled to investigate the geological formations and soil behavior in the area. Drilling was carried out following "Geotechnical investigation and testing - Sampling methods and groundwater measurements - Part 1: Technical principles for execution standard (TS EN ISO 22475-1). One borehole with a depth of 30m, four boreholes with a depth of 25m, and 18 boreholes with 20m were drilled.

Standard penetration tests (SPT) were performed within the boreholes, according to ASTM D1586 (2011) standard. Disturbed samples are collected during the tests. SPT-N values are corrected according to guidelines given in TBDY 2018.

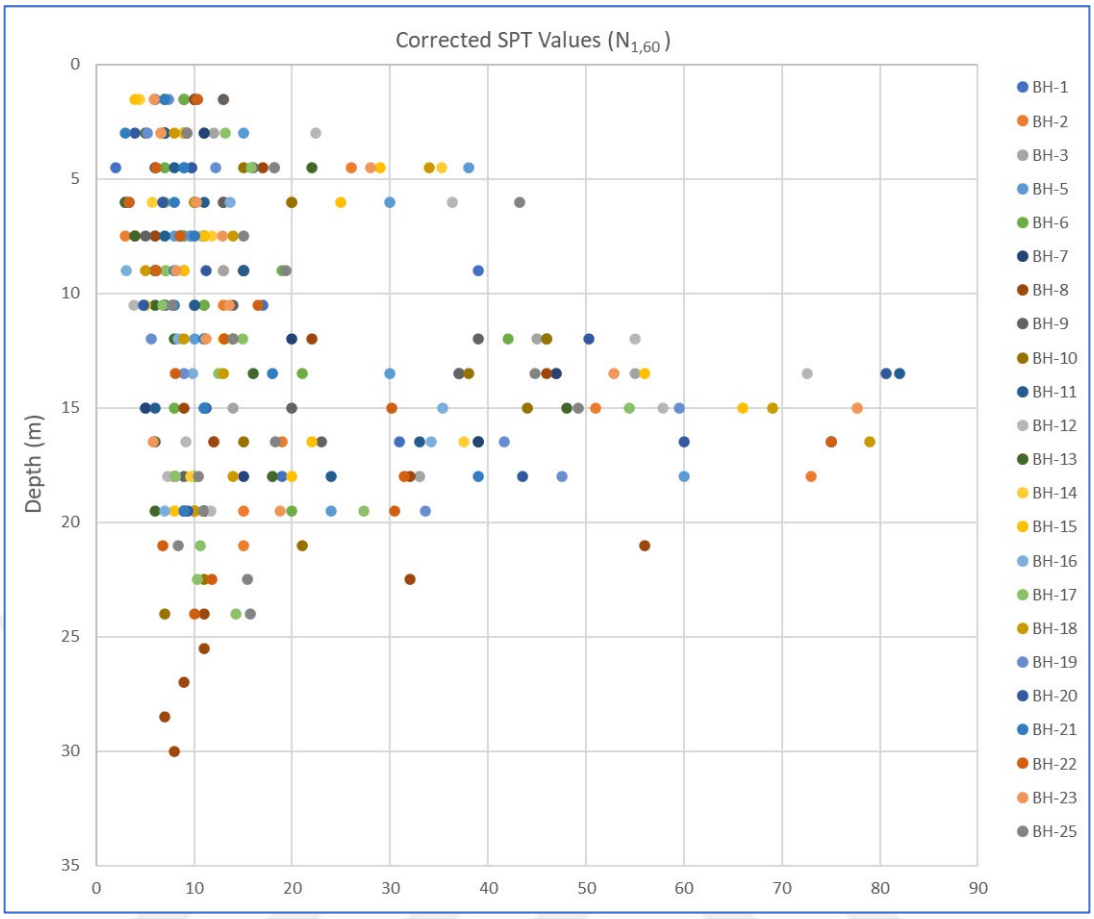

Figure 3.9 Corrected SPT Values ($N_{1,60}$) with Depth

Within the scope of site investigations, seven Cone Penetration Tests (CPT) were performed according to the "BS EN ISO 22476-12:2009- Geotechnical Investigation and Testing – Field Testing – Mechanical Cone Penetration Test (CPTM)", "ASTM D5778-95 (Reapproved 2000))", "Standard Test Method for Performing Electronic Friction Cone and Piezocone Penetration Testing of Soils" specifications. The drilling data and ground profile of CPTs based on the CPeT-IT software is given in Appendix.

Geophysical investigations were performed on the site in May 2020 by Destech. Seismic refraction, surface wave measurements (Remi, MASW), and microtremor measurements were taken to determine thickness, depth, the geometry of geological units, and calculate dynamic soil parameters. For this purpose, five Wenner electrical resistivity measurements (ASTM G57-06 (2012), 4-line seismic refraction, MASW (ASTM D5777), and six Microtremor measurements (ISO/WD 24057) were taken on the investigation area. The locations of the measurements are shown in Figure 3.10.

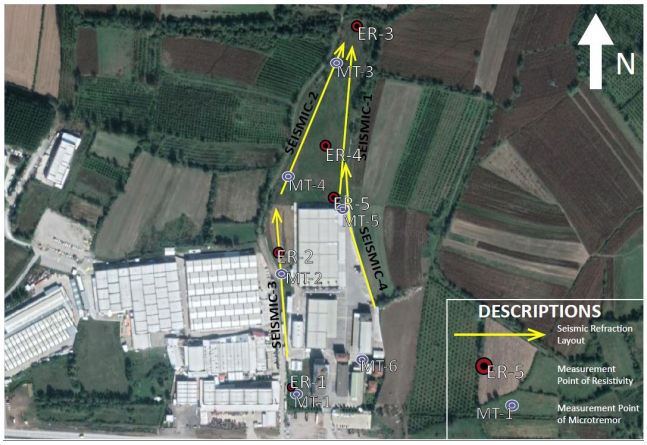

Figure 3.10 Location of the Measurements

By evaluating the measurements taken in the investigation area, seismic refraction sections and V_s values are given in Figure 3.11 a-d.

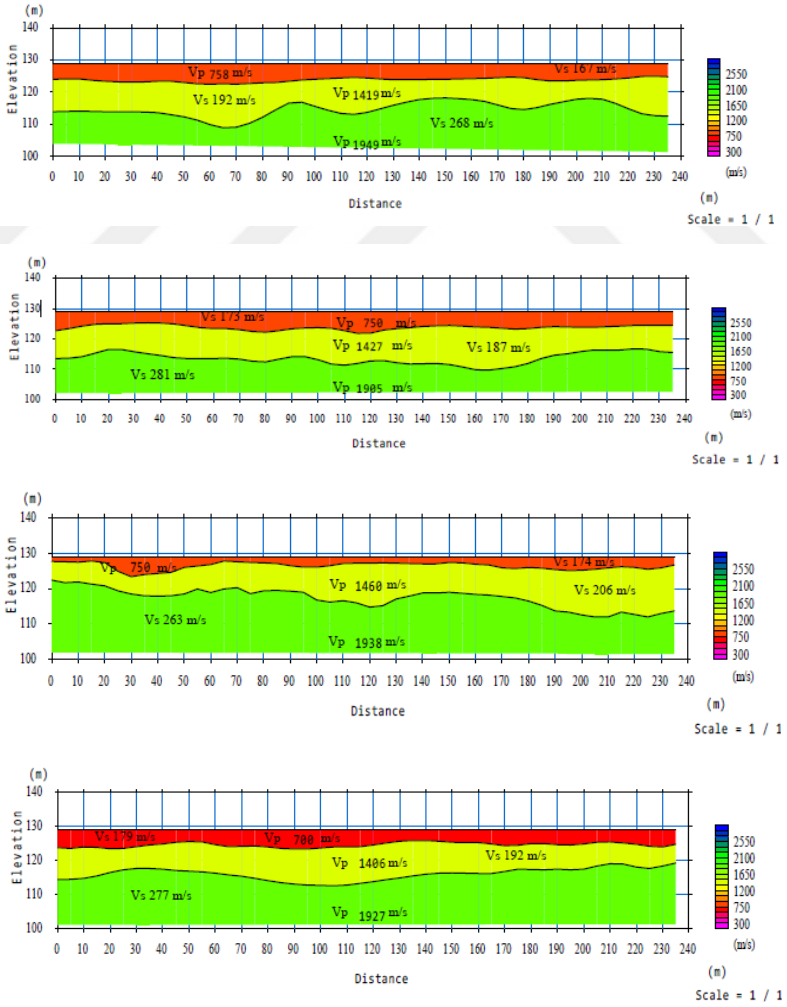

Figure 3.11 Seismic Refraction Section of (a) Seismic-1, (b) Seismic-2, (c) Seismic-3, (d) Seismic-4

The dynamic parameters (such as density, bulk-shear-elasticity modulus and Poisson ratio) produced depending on seismic velocities and summary of seismic refraction test results are presented in Table 3.1.

Dynamic elasticity modulus values are obtained by using the following equations:

Poisson Ratio $$\mu = (V_p^2 - 2V_s^2)/(2(V_p^2 - V_s^2)) \quad (3.1)$$

Dynamic shear modulus $$G = V_s^2 d \quad (3.2)$$

Young Modulus $$E = 2G(1 + \mu) \quad (3.3)$$

Bulk Modulus $$K = E/(3(1 - 2\mu)) \quad (3.4)$$

Table 3.1 Dynamic Soil Parameters at Site

Seismic Refraction Name	Level	V_p (m/s)	V_s (m/s)	Depth (m)	$Vs_{,30}$ (m/s)	Density (ρ) (kg/m³)	Bulk Modulus (K) (MPa)	Shear Modulus (G) (MPa)	Elasticity Modulus (E) (MPa)	Poisson Ratio (μ)
SEISMIC-1	1	750	167	4.6	213	1622	852	45	133	0.47
	2	1419	192	17.4		1903	3738	70	209	0.49
	3	1949	268	41.2		2060	7627	148	441	0.49
	4	-	413	-		-	-	-	-	-
SEISMIC-2	1	750	173	4.3	217	1622	848	49	143	0.47
	2	1427	187	16.7		1905	3791	67	199	0.49
	3	1903	281	41.3		2048	7217	162	482	0.49
	4	-	410	-		-	-	-	-	-
SEISMIC-3	1	750	174	4.2	224	1622	847	49	145	0.47
	2	1460	206	15.7		1916	3976	81	242	0.49
	3	1938	263	41.7		2057	7535	142	424	0.49
	4	-	413	-		-	-	-	-	-
SEISMIC-4	1	700	179	4.7	224	1595	713	51	150	0.47
	2	1406	192	15.4		1898	3659	70	209	0.49
	3	1927	277	41.1		2054	7417	158	469	0.49
	4	-	418	-		-	-	-	-	-

The soil model concerning multichannel analysis of surface waves (MASW) and spatial autocorrelation (SPAC) modeling in Düzce Basin and especially in-situ conditions is given in Figure 3.12. The first 100 m was adopted directly from MASW measurements, where it is almost the same with SPAC modeling near the site. MTA's infill thickness was used to model 760 m/s at an average depth of 205 m to 210 m. Another shear wave from

literature data is compatible with the existing conditions, and the basin effect was studied accordingly.

Depth (m)	Layer	Thickness (m)	Unit weight kN/m^3	Shear Wave Velocity m/s
1.5	L1_1	1.5	18	170
3	L1_2	1.5	18	170
4.5	L1_3	1.5	18	170
6	L2_1	1.5	18	200
7.5	L2_2	1.5	18	200
9	L2_3	1.5	18	200
10.5	L2_4	1.5	18	200
12	L2_5	1.5	18	200
13.5	L2_6	1.5	18	200
15	L2_7	1.5	18	200
16.5	L2_8	1.5	18	200
18	L2_9	1.5	18	200
19.5	L2_10	1.5	18	200
21	L2_11	1.5	18	200
22.5	L2_12	1.5	18	200
24	L3_1	2.25	19	265
26.25	L3_2	2.25	19	265
28.5	L3_3	2.25	19	265
30.75	L3_4	2.25	19	265
33	L3_5	2.25	19	265
35.25	L3_6	2.25	19	265
37.5	L3_7	2.25	19	265
39.75	L3_8	2.25	19	265
42	L3_9	2.25	19	265
44.25	L3_10	2.25	19	265
46.5	L3_11	2.25	19	265
48.75	L4_1	3.5	20	410
52.25	L4_2	3.5	20	410
55.75	L4_3	3.5	20	410
59.25	L4_4	3.5	20	410
62.75	L4_5	3.5	20	410
66.25	L4_6	3.5	20	410
69.75	L4_7	3.5	20	410
73.25	L4_8	3.5	20	410
76.75	L5_1	5	21	560
81.75	L5_2	5	21	560
86.75	L5_3	5	21	560
91.75	L5_4	5	21	560
96.75	L5_5	5	21	560
101.75	L5_6	5	21	560
106.75	L6_1	5	21	610
111.75	L6_2	5	21	610
116.75	L6_3	5	21	610
121.75	L6_4	5	21	610
126.75	L6_5	5	21	610
131.75	L6_6	5	21	610
136.75	L7_1	5	21	660
141.75	L7_2	5	21	660
146.75	L7_3	5	21	660
151.75	L7_4	5	21	660
156.75	L7_5	5	21	660
161.75	L7_6	5	21	660
166.75	L8_1	6	22	710
172.75	L8_2	6	22	710
178.75	L8_3	6	22	710
184.75	L8_4	6	22	710
190.75	L8_5	6	22	710
196.75	L9_1	6	23	735
202.75	L9_2	6	23	735
208.75	L9_3	6	23	735
210	bedrock			760

Figure 3.12 Soil Profile Concerning MASW, SPAC Modelling

Soil profile and ground model are formed in Figure 3.13 according to site investigations. According to these studies, the site contains clay, silty clay and sand, silty sand, gravelly sand, and silty layers.

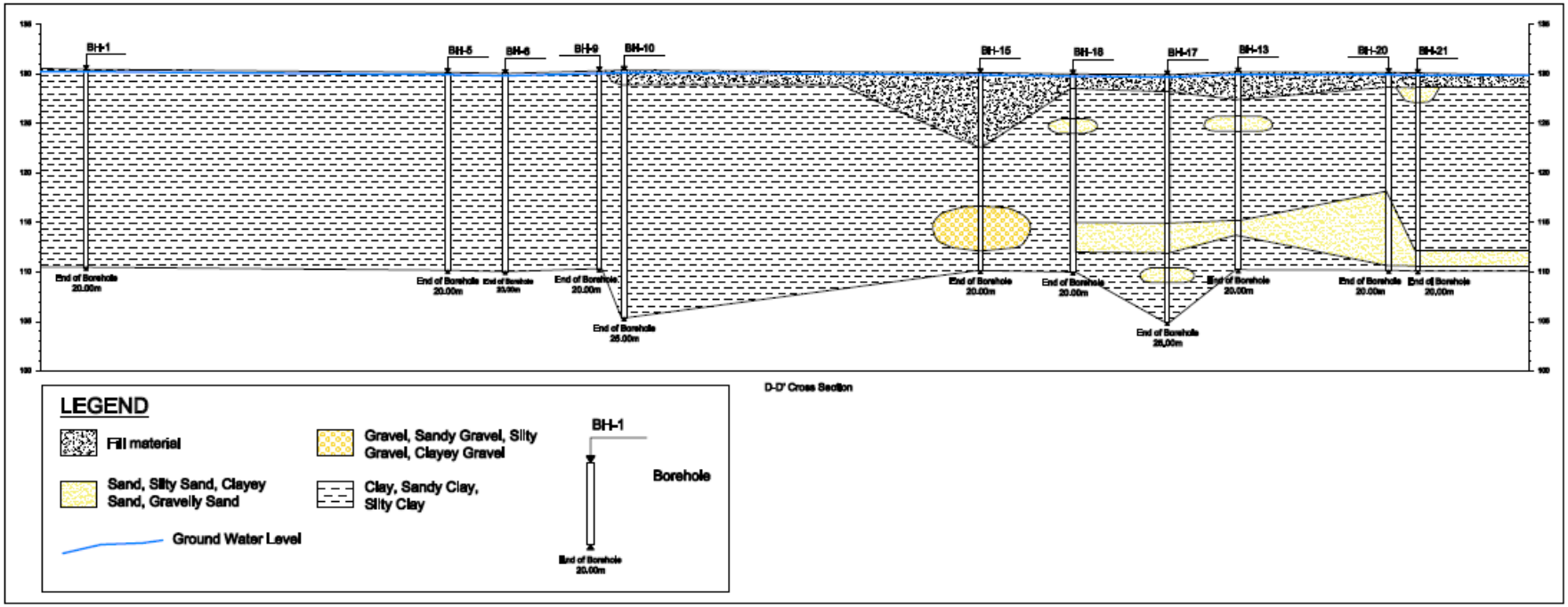

Figure 3.13 Geological Cross-section of the Study Area

CHAPTER 4

SEISMICITY OF CASE STUDY AREA

4.1. Introduction

Düzce Province has a serious earthquake potential. It is located in an area with many active faults worldwide known as Right-lateral strike-slip fault systems of North Anatolian Fault and its extensions. The seismotectonic structure (faulting mechanisms and fault characteristics) of the region, historical and instrumental earthquake records occurred in the area should be considered during the assessment of earthquake hazard in a region. Therefore, each of the factors listed above will be mentioned in the earthquake hazard assessment.

North Anatolian fault mechanism is one of the world's well-known mechanisms and is actively studied by several researchers. The literature data is well enough to define most of the faults' seismotectonic properties in the site's vicinity. In this chapter, seismotectonic units (existing fault systems), source of earthquakes and the area's seismicity with the recent earthquakes that occurred in the region are presented.

4.2. Seismotectonic Structure of the Site

North Anatolian Fault (NAF) zone is a well-known source that can create high magnitudes globally. It is a right-lateral strike-slip fault zone and has already been studied by several researchers (Şengör, 1979; McKenzie, 1972; Barka ve Kadinsky- Cade, 1988). Satellite imaging procedures monitor it; hence the propagation is clearly shown with geological studies and GPS measurements. NAF was almost totally broken with westward migrated earthquakes during the 20th Century. Kocaeli and Düzce earthquakes were the last events occurred in, August, and November 1999, respectively. Active faults modified from Şaroğlu et al., 1992 and Barka et al., 2002 and focal mechanisms reproduced from Barka, 1992; Ayhan et al., 2002 and Ayhan and Koçyiğit, 2010 are shown in Figure 4.1 and Figure 4.2.

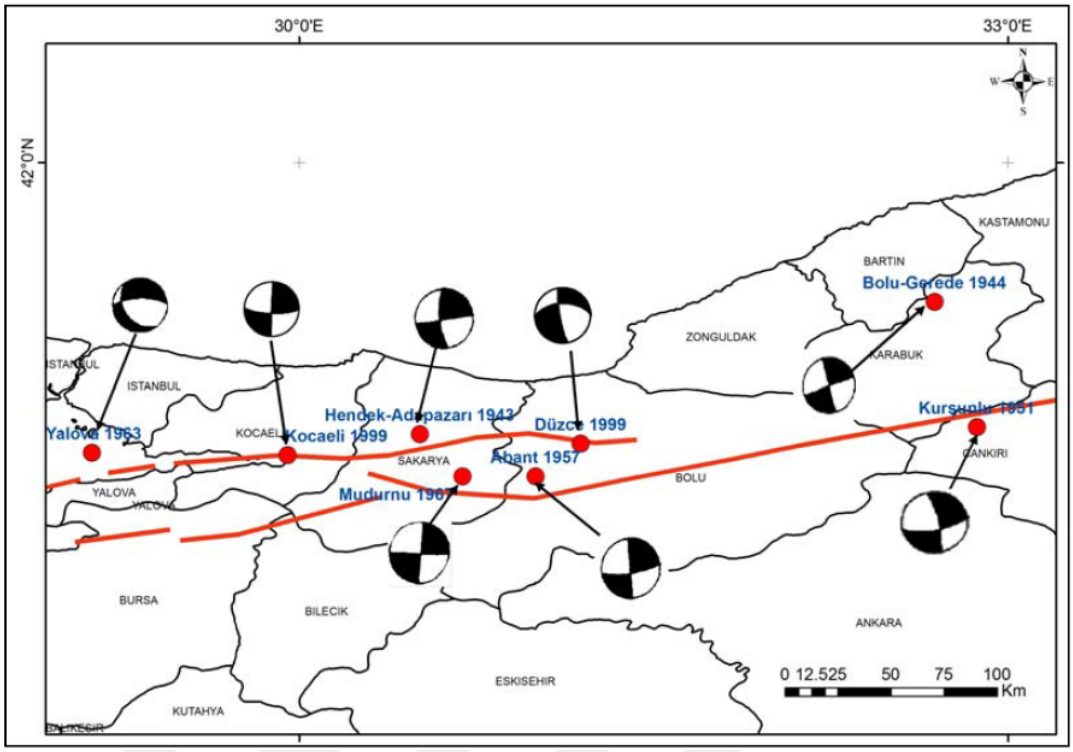

Figure 4.1 Large Earthquakes and Their Focal Mechanisms in NAF

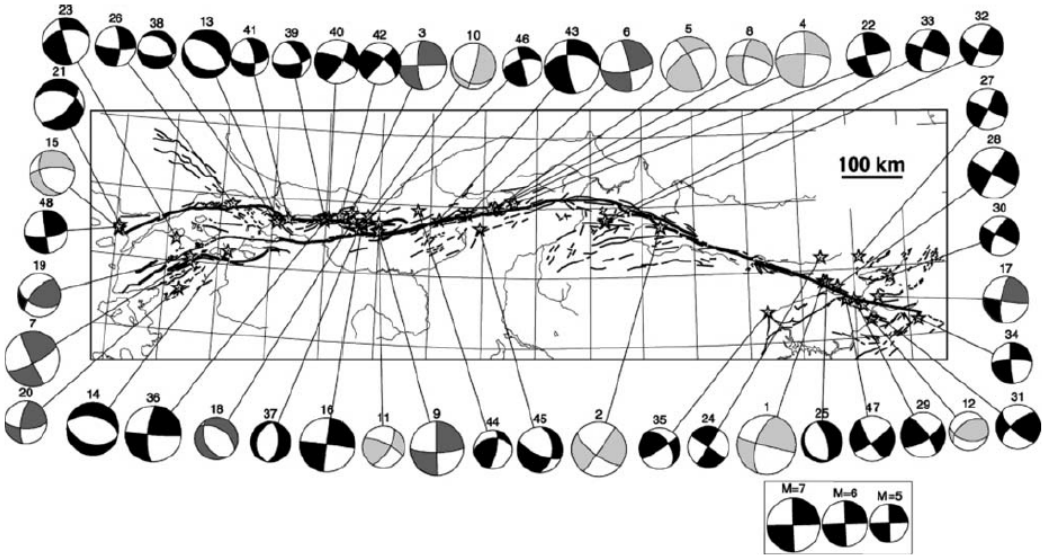

Figure 4.2 Focal Mechanism Solutions for NAF 1939-2003 (Şengör 2005)

The Düzce area segmentation for NAF has been studied for the last 70 years, and various researchers made different fault segmentation interpretations. After two devastating earthquakes in 1999 at the area, each segment was studied again intensely. The latest two earthquakes had a rupture of 145 km (Kocaeli) and 30-40 km from Düzce.

4.3. Seismicity and Active Tectonics

Düzce earthquake on November 12, 1999, is the second of the devastating 1999 earthquakes, which resulted in an average of 45 km rupture surface. Horizontal and vertical displacements of 3 m and 5 m have occurred along the rupture, respectively (Taymaz, 1999).

As one of Turkey's most critical active faults, the NAF, which extends east-west direction along the northern part of the country, starts from the Karlıova (Bingöl) region in the east passes through the Düzce basin. This fault, which is observed in a narrow zone consisting of single fractures up to the Bolu region, is bifurcated to the west of Bolu (Dokurcum Valley). It is divided into two main branches and reaches towards the Marmara Sea. Hendek faults in the Sakarya-Düzce region also join the NAF system, and the width of the fault zone reaches 40km. Earthquakes in 1944, 1957, and 1967, surface faulting, occurred between Bolu Abant and Abant Lake-Adapazarı Plain. Active faults, which are closest to the Düzce basin and have earthquake potential, are Düzce and Hendek faults' active fault characteristics that have led to this basin's formation. Çilimli fault is an active fault. Directional analysis of segments of Kocaeli and Düzce province are given in Figure 4.3 and Figure 4.4, respectively.

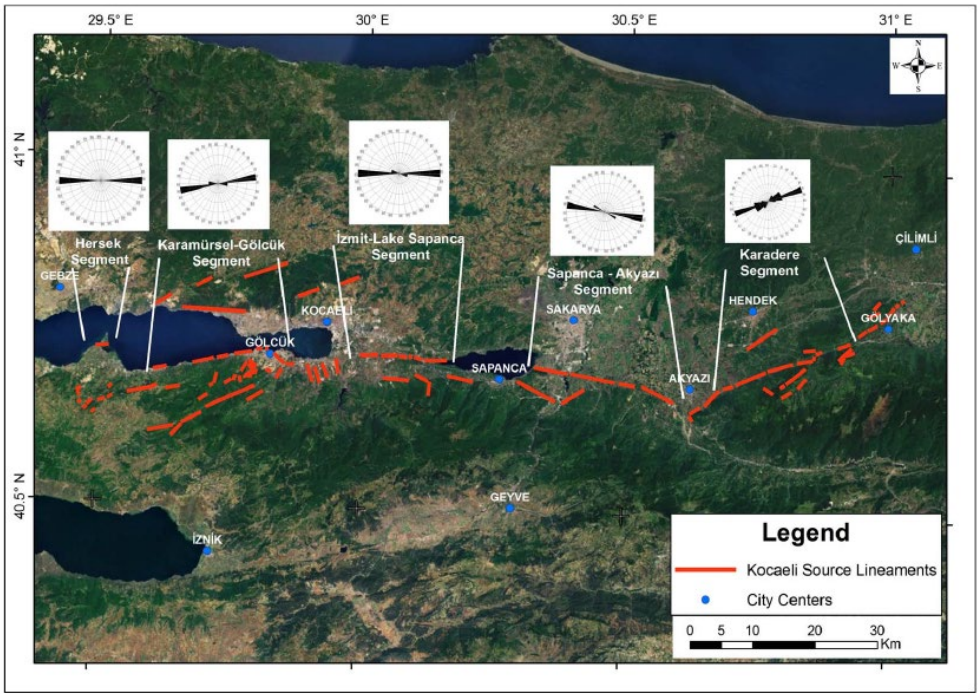

Figure 4.3 Directional Analysis of Segments of the Kocaeli Source, Cambazoğlu (2012)

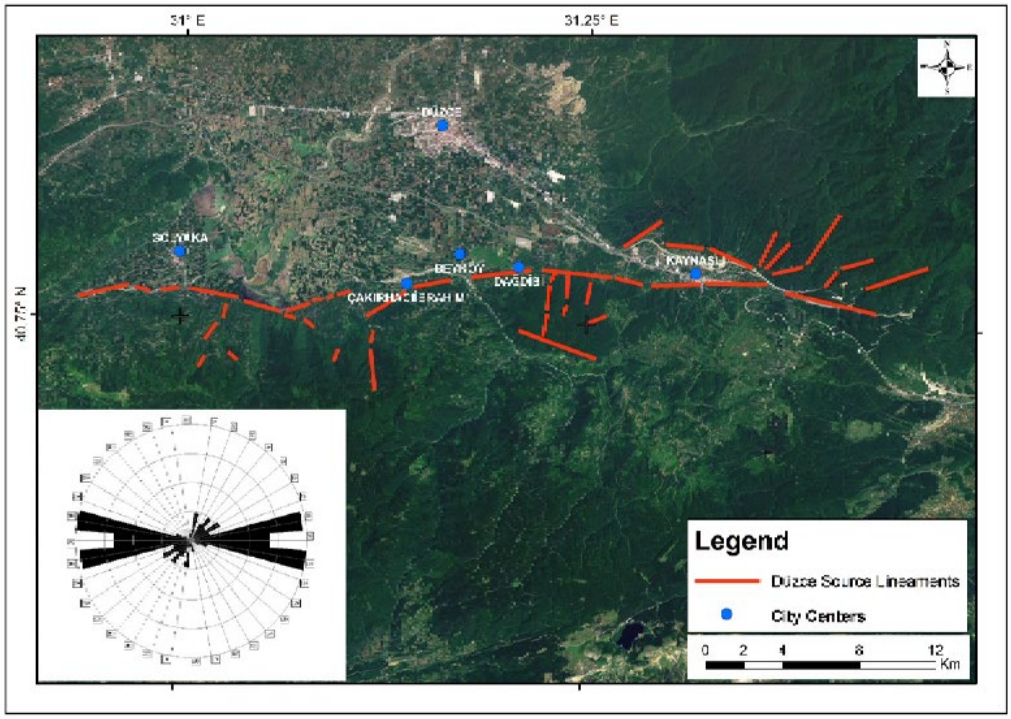

Figure 4.4 Directional Analysis of Düzce Seismic Source Lineaments Cambazoğlu (2012)

4.4. Active Faults

The fault systems enlisted below is summary of the literature survey of the existing research. The active fault map produced by MTA is given in Figure 4.5.

4.4.1. Düzce Fault:

Düzce fault, which borders the Düzce basin morphologically from the south, is 70 km long between Akyazı and Kaynasli. Düzce fault, consisting of three complementary parts that complement each other, is an active fault in the right direction. The activity of the fault also emerged with the earthquakes on August 17 and November 12, 1999. The 30km east part of the 130km long surface fracture developed in the earthquake on August 17 is located on the Düzce fault. This earthquake took place on the part of the Düzce fault up to Efteni lake. It was fractured between the Efteni Lake in the eastern part of the Düzce fault in the earthquake on November 12, 1999, and the Pyramids in the northwest of Bolu. (The length of the fault fractured in this earthquake is 45km.)

4.4.2. Hendek Fault:

Hendek fault is trending in the north-east and south-west, located in the west of the Düzce basin. This fault, which is a right-sided excursion, is approximately 50km long. The 1994 Düzce-Hendek earthquake probably occurred on this fault. A surface crevasse formed is in the northwest of Hendek on the fault. This fracture is a right-sided breakthrough. 5 km rupture has happened during the August 17, 1999, Kocaeli earthquake (MTA, 2003b).

4.4.3. Çilimli Fault:

Çilimli fault is between Cumayeri and Konuralp in the north of the Düzce basin. This fault, which is approximately 13km long, is continuing the Hendek fault in the southwest. The fault in the general direction in the north west-south east corresponds to the morphological discordance between the Odunluk Mountain in the north and the Düzce Basin base. Many resource sequences have been observed along the fault line. Considering these features, Çilimli Fault was evaluated as a possible active fault.

This fault, which is approximately 13km long, is located in continuing the Hendek fault in the southwest. The fault in the general direction in the north west-south east corresponds to the morphological discordance between the Odunluk Mountain in the north and the Düzce Basin base. Many resource sequences have been observed along the fault line. Considering these features does not appear to be modifying the subject, the probability of Çilimli Fault.

Figure 4.5 Active Fault Map (http://yerbilimleri.mta.gov.tr)

The nearest fault to the site is the Karadere Segment of Düzce Fault, and its distance to the site is 3km (Figure 4.6). The distance from the site to the North Anatolian Fault is 30 km.

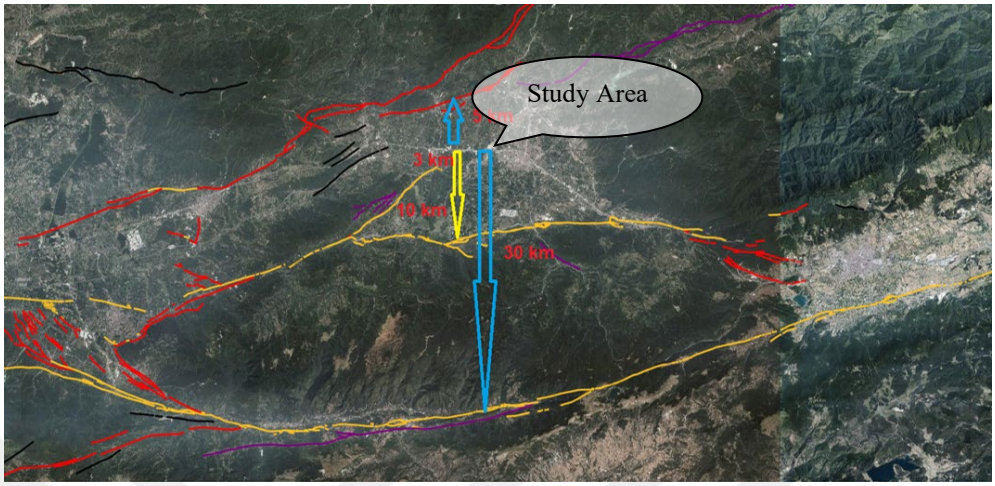

Figure 4.6 Site Distance to Nearest Active Faults

The project site is in a very high seismic zone where the area to fault distances are 3 km, 10 km, and 30 km away from North Anatolian Fault segments (Figure 4.7 and Figure 4.8). This consequence needs to be considered in the strong ground motion selection and scaling. It must also be carefully implemented in site-specific spectrum analysis.

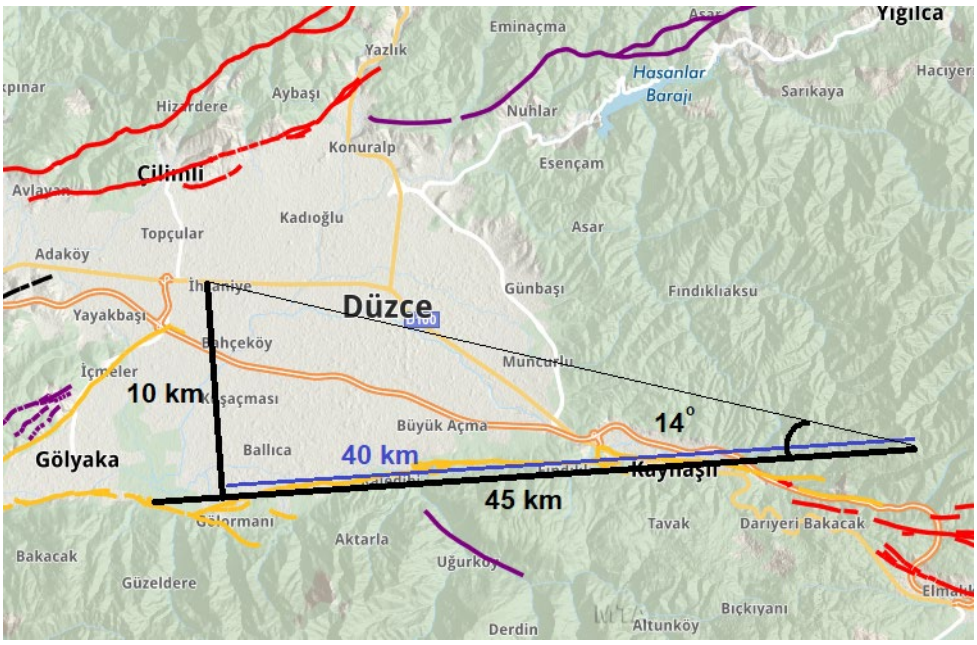

Figure 4.7 Düzce Fault and its Interference with Site

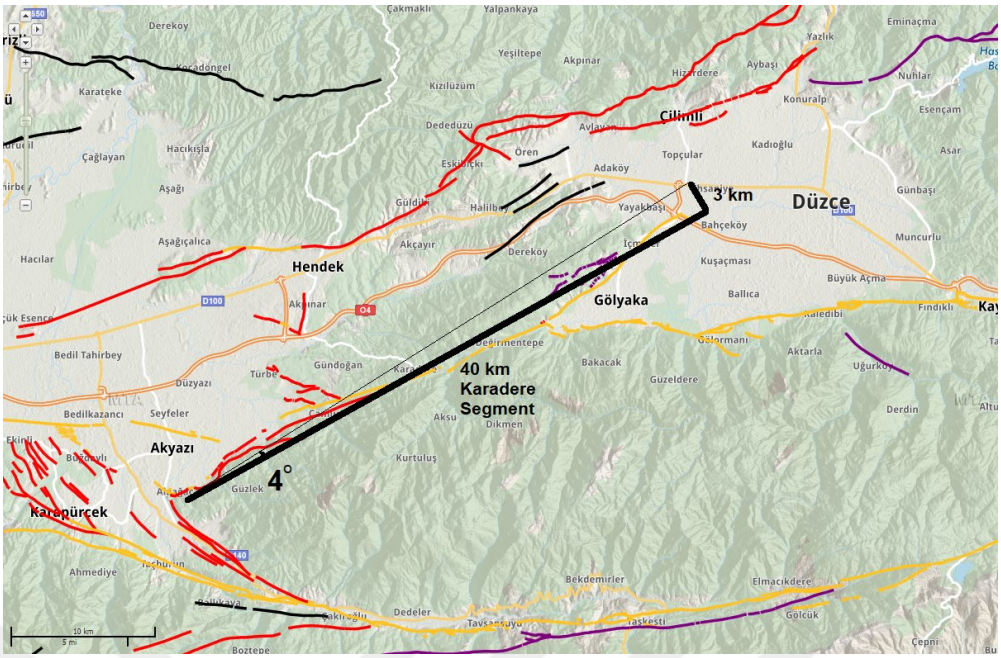

Figure 4.8 Karadere Segment and its Interference with Site

4.5. Historical Earthquakes in Düzce Province

Düzce province and its vicinity are exposed to many earthquakes throughout history. Earthquakes occurred around Izmit until 500 B.C. In the 1800s, earthquakes occurred intensively around Istanbul. Earthquakes that occurred up to 1900 are given in Table 4.1.

Table 4.1 Information about Historical Earthquakes in the Region

Year	Latitude	Longitude	Intensity	Location
69	40.00	30.00	VII	İznik, İzmit
120	40.00	30.00	VIII	İznik, İzmit
170	41.00	30.00	VIII	İzmit Region
212	41.00	29.00	VII	İstanbul
358	41.00	30.00	IX	Kocaeli,İznik,İstanbul
359	41.00	30.00	XIII	İzmit
362	41.00	30.00	VIII	İznik, İzmit, İstanbul
447	41.00	30.00	IX	İzmit Gulf, İzmit, İstanbul
488	41.00	30.00	VIII	İzmit,Karamürsel
500	41.00	30.00	VIII	İzmit
525	41.00	29.00	VI	İstanbul
1296	41.00	29.00	VIII	İstanbul
1323	41.00	29.00	VIII	İstanbul
1672	41.00	30.00	VIII	İzmit, İstanbul
1841	41.00	29.00	VII	İstanbul
1855	40.00	29.00	VI	Bursa, İstanbul
1862	40.00	30.00	VII	Söğüt, Bilecik

.cont. next page

cont. Table 4.1

Year	Latitude	Longitude	Intensity	Location
1873	41.00	29.00	VI	İstanbul
1878	41.00	29.00	V	İstanbul
1880	41.00	29.00	VI	İstanbul
1884	40.00	29.00	VI	Bursa Region
1886	41.00	29.00	VI	İstanbul
1894	41.00	29.00	X	İstanbul,Prens Island.Karamürsel
1897	40.00	29.00	V	Gemlik Region
1897	40.00	31.00	V	Beylikahır

On August 17, 1999, the most significant earthquake magnitude in the region was M_w=7.6 (Kocaeli, Gölcük). Another earthquake that affected the area that occurred on November 12, 1999, is the Düzce Earthquake (M_w=7.1). Düzce Earthquake occurred because of the Kocaeli Earthquake ruptures, which is triggered the eastern part of the Düzce Fault. The depth of the Düzce Earthquake is 11 km.

Düzce province has been exposed to many destructive earthquakes throughout its history. Almost thirty earthquakes occurred around Düzce province between 1900 and 2000, with the magnitudes varying between 5.0 and 7.0 (M_w, M_s, M_b). The depths of the earthquakes are between 6.0 km and 50 km. When the earthquake map is analyzed, it is seen that earthquakes occur mostly in the years of 1999 and 1967. No significant earthquake has affected the region since the year 2000 (Figure 4.9 and Table 4.2).

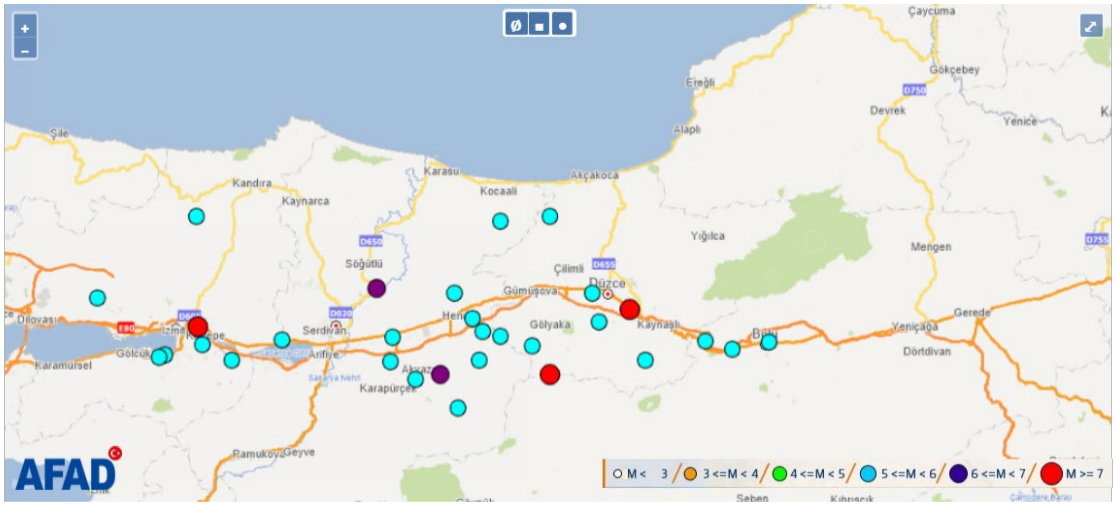

Figure 4.9 Earthquakes Occurred in the Vicinity of Construction Site (https://deprem.afad.gov.tr)

Table 4.2 Earthquakes that Occurred between 1900-2020 around the Site Area, M>5 (https://deprem.afad.gov.tr)

No	Time (UTC)	Lat.	Long.	Depth	Source No 2	Source Explanation 2	Type	Magnitude	Source No 3	Source Explanation 3	Location
8945	8/23/2000 13:41	40.787	30.781	15.3	41	EHB	Mw	5.3	10	HRVD-GCMT	-
8765	11/16/1999 17:51	40.738	31.620	10.0	41	EHB	mb	5.0	5	ISC	-
8724	11.12.1999 17:29	40.723	31.516	6.0	41	EHB	mb	5.0	5	ISC	-
8721	11.12.1999 17:17	40.780	31.139	8.4	41	EHB	mb	5.2	5	ISC	-
8716	11.12.1999 16:57	40.806	31.226	11.0	41	EHB	Mw	7.1	10	HRVD-GCMT	Düzce-Bolu
8714	11.11.1999 14:41	40.473	30.242	17.9	8	EMSC-CSEM	Mw	5.6	10	HRVD-GCMT	-
8675	9.13.1999 11:55	40.733	30.017	17.8	8	EMSC-CSEM	Mw	5.8	10	HRVD-GCMT	-
8634	8.31.1999 08:10	40.706	29.894	20.0	8	EMSC-CSEM	Mw	5.1	10	HRVD-GCMT	-
8548	8/17/1999 00:16	40.711	29.911	10.0	41	EHB	mb	5.0	5	ISC	-
8546	8/17/1999 00:01	40.770	30.004	15.0	41	EHB	Mw	7.6	10	HRVD-GCMT	Gölcük-Kocaeli
2375	7/30/1967 01:31	40.697	30.550	14.7	41	EHB	mb	5.4	5	ISC	-
2344	7/22/1967 18:09	40.748	30.555	37.3	41	EHB	mb	5.1	5	ISC	-
2340	7/22/1967 17:48	40.660	30.620	26.0	1	Ayhan et al. 1981	MS	5.1	1	Ayhan et al. 1981	-
2337	7/22/1967 17:14	40.700	30.800	6.0	5	ISC	mb	5.2	5	ISC	-
2336	7/22/1967 16:56	40.670	30.690	33.0	1	Ayhan et al. 1981	MS	6.8	1	Ayhan et al. 1981	Akyazı-Sakarya
1677	12/26/1957 15:01	40.830	29.720	10.0	1	Ayhan et al. 1982	MS	5.2	1	Ayhan et al. 1982	-
1657	6.01.1957 05:26	40.750	30.860	50.0	1	Ayhan et al. 1983	MS	5.0	1	Ayhan et al. 1983	-
1678	5/27/1957 11:01	40.730	30.950	50.0	1	Ayhan et al. 1984	MS	5.8	1	Ayhan et al. 1984	-
1644	5/26/1957 09:36	40.760	30.810	10.0	1	Ayhan et al. 1985	MS	5.9	1	Ayhan et al. 1985	-

.cont. next page

cont. Table 4.2

No	Time (UTC)	Lat.	Long.	Depth	Source No 2	Source Explanation 2	Type	Magnitude	Source No 3	Source Explanation 3	Location
1641	5/26/1957 08:54	40.600	30.740	40.0	1	Ayhan et al. 1986	MS	5.4	1	Ayhan et al. 1986	-
1640	5/26/1957 06:33	40.670	31.000	10.0	3	Ayhan et al. 1987	MS	7.1	3	Ayhan et al. 1987	Düzce-Bolu
1232	4.05.1944 04:40	40.840	31.120	10.0	1	Ayhan et al. 1988	MS	5.5	1	Ayhan et al. 1988	-
1227	2.02.1944 03:33	40.740	31.440	40.0	1	Ayhan et al. 1989	MS	5.1	1	Ayhan et al. 1989	-
1225	2.01.1944 06:08	40.700	31.270	10.0	1	Ayhan et al. 1990	MS	5.0	1	Ayhan et al. 1990	-
1209	6/20/1943 16:47	40.840	30.730	10.0	1	Ayhan et al. 1991	MS	5.5	1	Ayhan et al. 1991	-
1208	6/20/1943 15:32	40.850	30.510	10.0	3	Ayhan et al. 1992	MS	6.6	3	Ayhan et al. 1992	Sakarya
780	1/24/1928 07:36	40.990	30.860	10.0	1	Ayhan et al. 1993	MS	5.3	1	Ayhan et al. 1993	-
632	5/29/1923 11:34	41.000	30.000	25.0	1	Ayhan et al. 1994	MS	5.5	1	Ayhan et al. 1994	-
280	8/21/1907 00:00	40.700	30.100	15.0	1	Ayhan et al. 1995	MS	5.5	1	Ayhan et al. 1995	-
232	10/22/1905 03:42	41.000	31.000	27.0	1	Ayhan et al. 1996	MS	5.2	1	Ayhan et al. 1996	-

4.6. DÜZCE Earthquake – 12/11/1999

An earthquake of moment magnitude (M_w) 7.1 has taken place to the nearest south of the Düzce, a town of 80,000 (1999) in Bolu province. The earthquake took place along the Düzce Fault at the section showed on the map (marked with the red color green rectangle Figure 4.10) prepared by Aykut Barka and his colleagues.

The preliminary report by KOERI (2000) states that a fault rupture of about 30km with predominantly right-lateral offsets. The offsets were reported to be about 1.5 m. at Düzce (west end) reach up to 3m towards Bolu (east end).

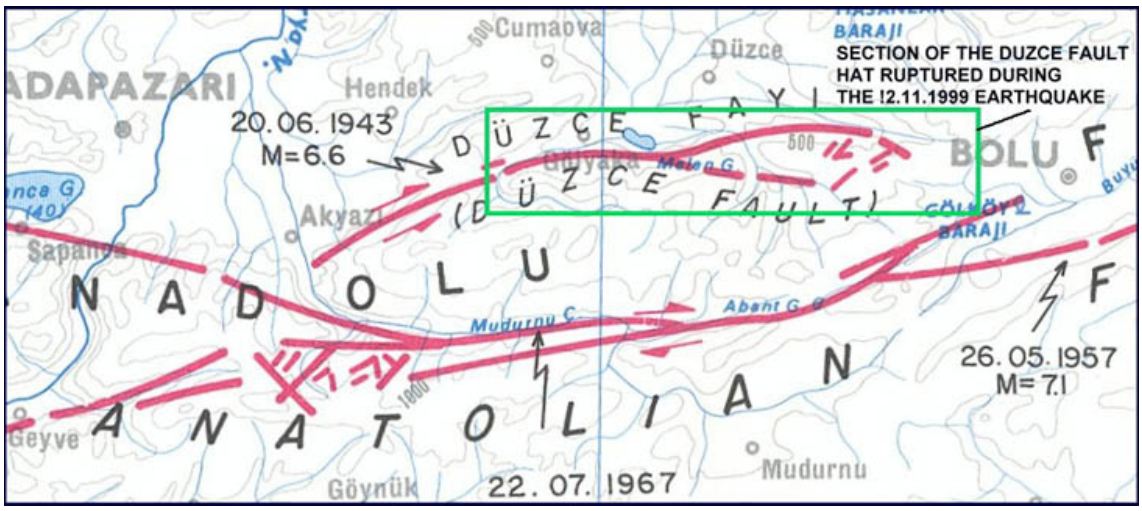

Figure 4.10 1999 Düzce Earthquake Rupture Zone (www.koeri.boun.edu.tr)

There are few strong ground motion stations operated by the General Directory of Disaster Affairs near the earthquake-affected area. The peak ground accelerations recorded are 24 mg at Sakarya (Adapazarı) and 804 mg at Bolu.

The rupture trend is reported to be in the E-W direction (Çakır et al., 2003; Umutlu et al., 2004; Duman et al., 2005). Directional analysis of the extracted lineaments yielded the same result, with trends ranging between N80°E and N100°E. The faulting characteristics of the Düzce rupture changes throughout the surface rupture area. Although the main rupture zone is dominated by right-lateral strike-slip motion (Akyüz et al., 2002), there are normal (near Gölkaya), and thrust (at Düzce rupture zone) features present (Akyüz et al., 2002; Pucci et al., 2007).

4.7. Turkish Code Elastic Spectrum for Different Levels of Earthquakes

Elastic spectrum for vertical and horizontal spectra for DD1 and DD-2 is created for all soil profiles using AFAD Seismic Hazard Maps.

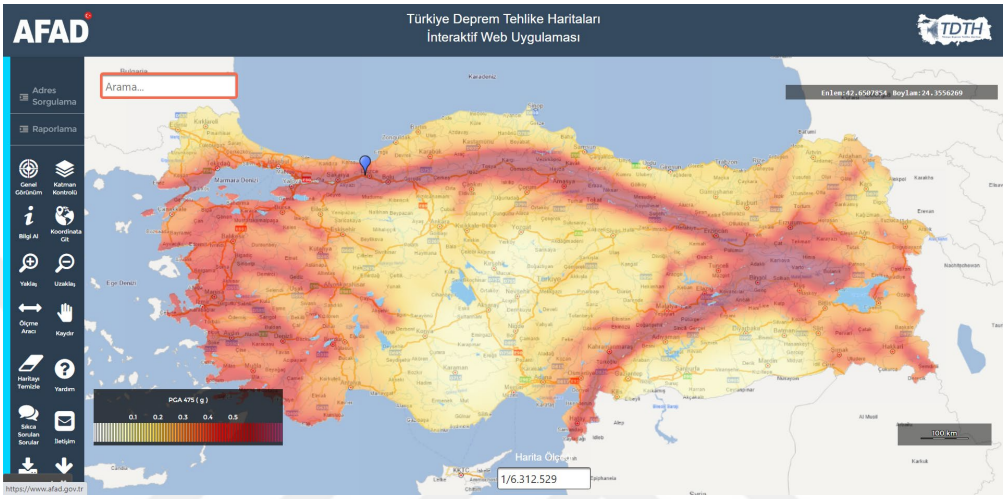

Figure 4.11 Earthquake Hazard Map (https://tdth.afad.gov.tr)

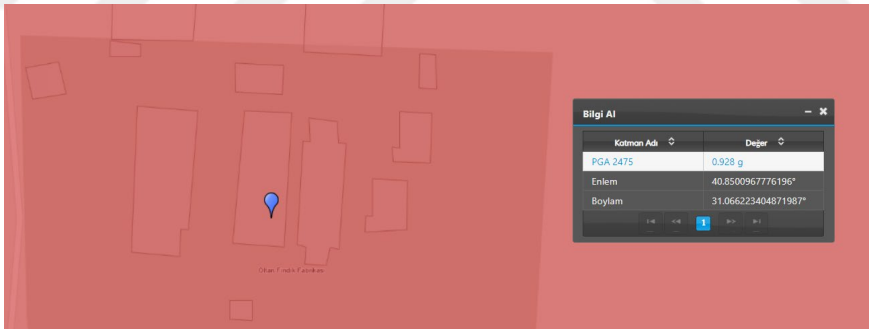

Figure 4.12 PGA value for DD-1 (https://tdth.afad.gov.tr)

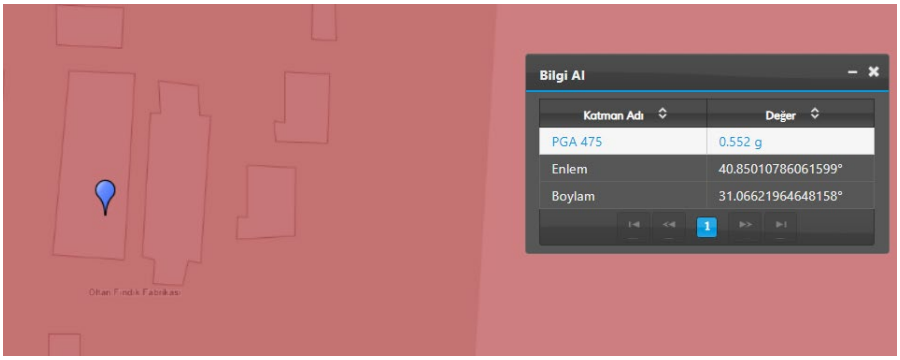

Figure 4.13 PGA value for DD-2 (https://tdth.afad.gov.tr)

Site independent earthquake spectra according to TBDY 2018 Maps for DD-1 and DD-2 earthquake levels are given in the form of horizontal elastic spectrum (Figure 4.14 and Figure 4.16) and vertical elastic spectrum (Figure 4.15 and Figure 4.17).

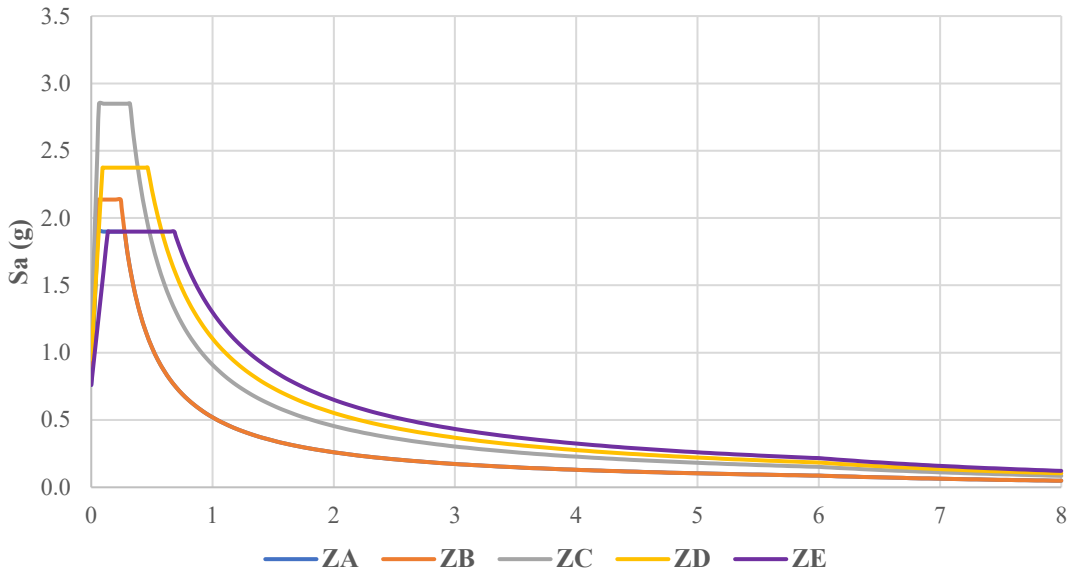

Figure 4.14 DD-1 Horizontal Elastic Spectrum

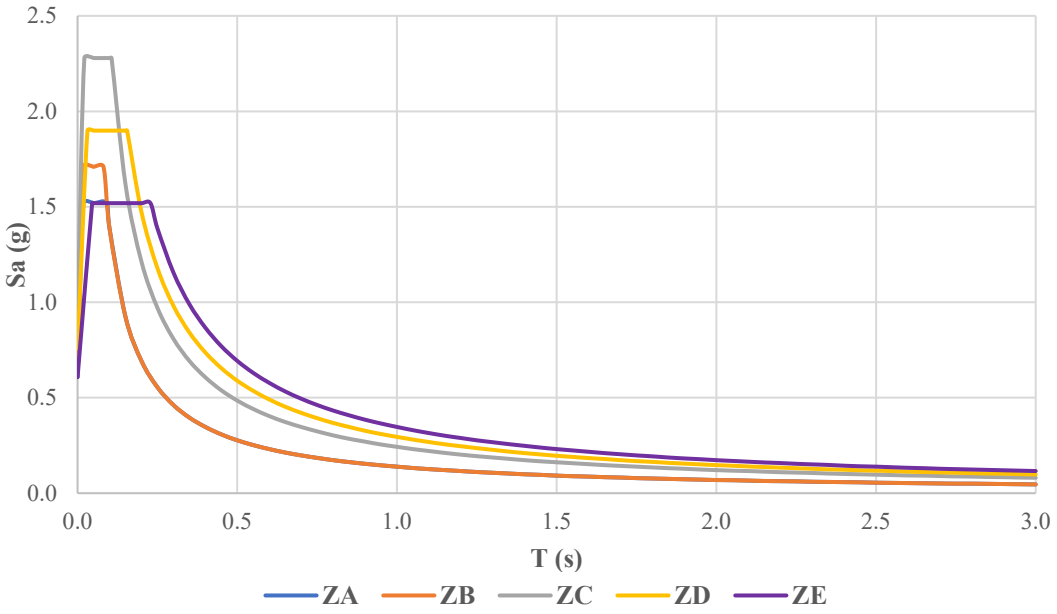

Figure 4.15 DD-1 Vertical Elastic Spectrum

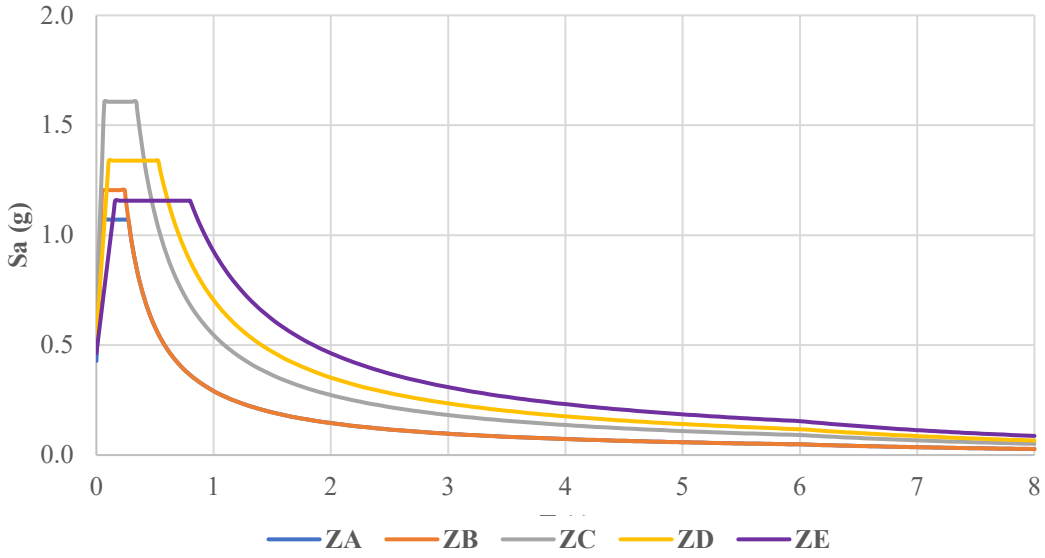

Figure 4.16 DD-2 Horizontal Elastic Spectrum

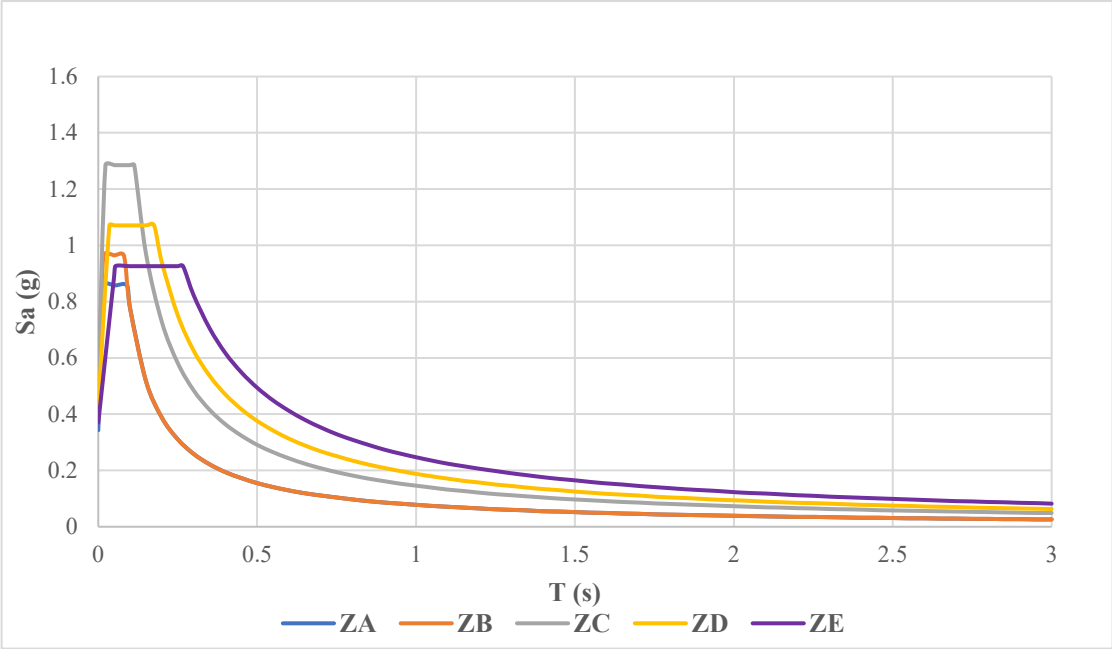

Figure 4.17 DD-2 Vertical Elastic Spectrum

CHAPTER 5

LIQUEFACTION ANALYSIS OF UNDERLYING SOILS AND SELECTION OF SOIL IMPROVEMENT

5.1. Introduction

According to TBDY 2018, soil liquefaction is defined as a significant decrease in shear strength and stiffness, and the increase in pore water pressure of the cohesionless or low cohesive (PI <12%) soils during the earthquake loading at the first 20 m depth of soil layers. A decrease in effective stress causes strength loss of these soils. There will be bearing resistance and settlement problems because of the strength loss.

Liquefaction analysis methodology and calculations for the site by using in-situ test results are given in this chapter.

5.2. Liquefaction Analysis According to SPT and Laboratory Results

According to TBDY 2018, liquefaction potential safety condition is:

$$\frac{\tau_R}{\tau_{earthquake}} \geq 1.10 \tag{5.1}$$

where, τ_R and $\tau_{earthquake}$ are cyclic resistance stress and cyclic shear stress, respectively.

5.2.1. Calculation of Cyclic Resistance Stress

Cyclic resistance ratio is calculated by using the formula is given below according to TBDY-2018

$$\tau_R = CRR_{m7.5} \times C_M \times \sigma'_{v0} \tag{5.2}$$

τ_R: Cyclic Resistance Stress σ'_{V0}: Effective overburden stress

C_M: Magnitude scaling factor depending on the design earthquake magnitude will be calculated with the formula in Equation 5.3.

$$C_M = \frac{10^{2.24}}{M_W^{2.56}} \tag{5.3}$$

$CRR_{M7.5}$: Cyclic resistance ratio for magnitude 7.5 earthquakes

5.2.2. Calculation of cyclic resistance ratio

The cyclic resistance ratio is calculated according to the equation proposed by TBDY 2018.

$$CRR_{M7.5} = \frac{1}{34-N_{1,60f}} + \frac{N_{1,60f}}{135} + \frac{50}{(10N_{1,60f}+45)^2} - \frac{1}{200} \tag{5.4}$$

$N_{1,60f}$: corrected SPT-N values for fine grain size

5.2.3. Calculation of Cyclic Shear Stress

The Cyclic Shear Stress on the ground is calculated by the following formula.

$$\tau_{earthquake} = 0.65\ \sigma_{V0}(0.4\ S_{DS})r_d \tag{5.5}$$

where;

S_{DS}: Short term design spectral acceleration coefficient r_d: Depth Reduction Factor

$$r_d = 1.0 - 0.00765z \qquad z \leq 9.15m \tag{5.6}$$

$$r_d = 1.174 - 0.0267z \qquad 9.15m < z < 23m \tag{5.7}$$

$$r_d = 0.744 - 0.008z \qquad 23m \leq z \leq 30m \tag{5.8}$$

$$r_d = 0.5 \qquad z > 30m \tag{5.9}$$

Liquefaction analysis results using SPT are given in Figure 5.1. According to the analysis results, it is seen that soils in topmost 20 meters have liquefaction potential.

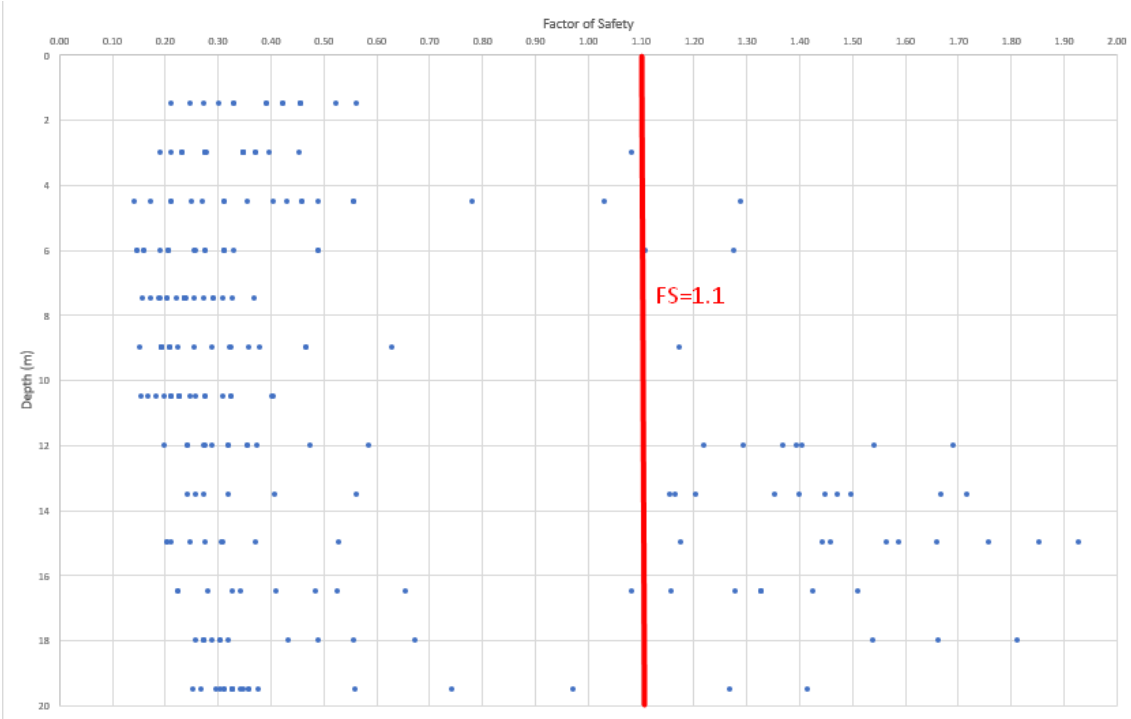

Figure 5.1 Liquefaction Analysis Results using SPT

For clayey and silty soils, the chart given by Seed et al. (2003) was used, which is developed by studies on fine-grained soil liquefaction cases obtained from Kocaeli and Chi earthquakes. Studies were developed on non-plastic silt layers after observing silt and clay soils liquefied in the 1999 Adapazarı earthquakes.

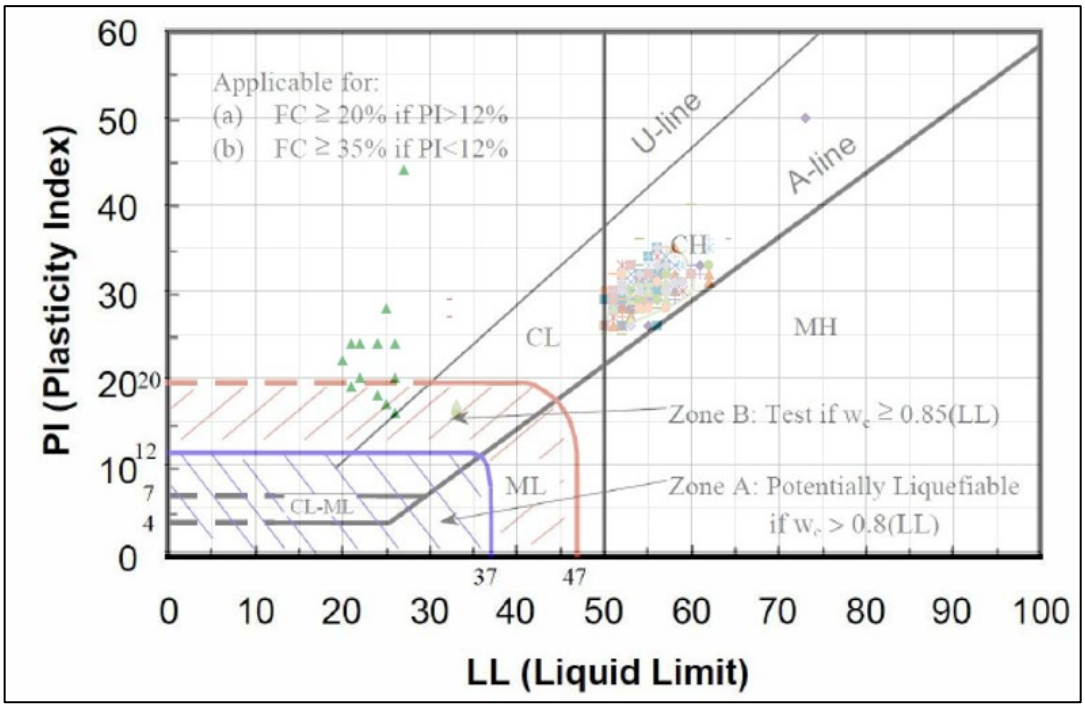

Figure 5.2 Liquefaction Potential of Fine-grained Soils

5.3. Liquefaction Analysis According to CPT Results

Cliq software uses the method developed by Boulanger and Idriss (2014) to calculate liquefaction potential. The formulation of the process is given in Figure 5.3.

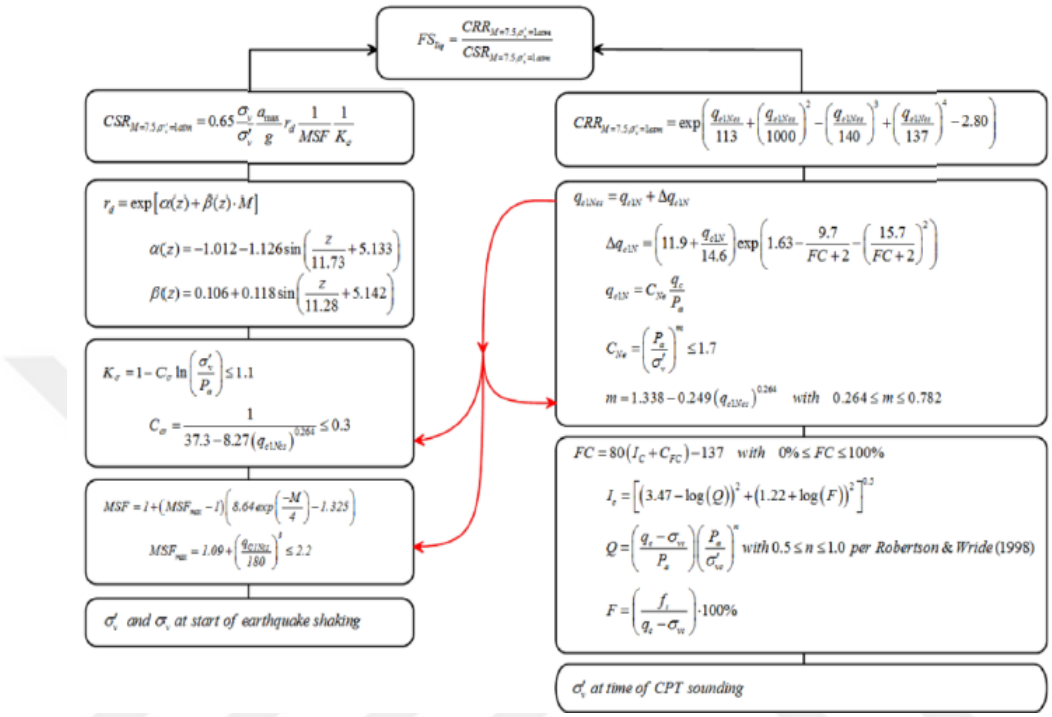

Figure 5.3 Liquefaction Method Scheme

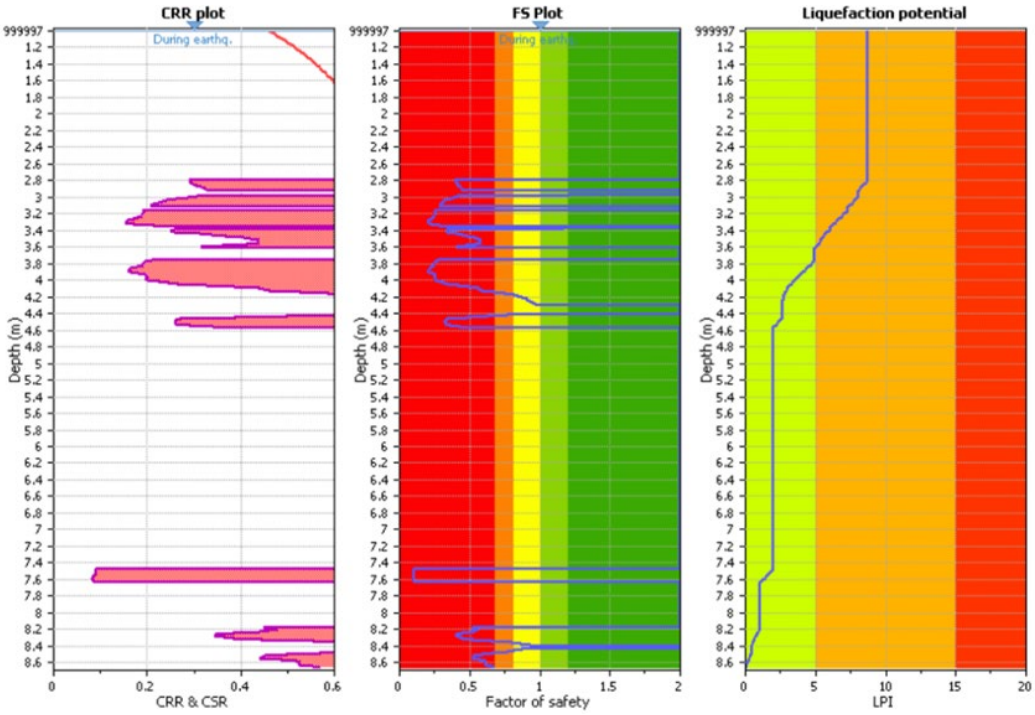

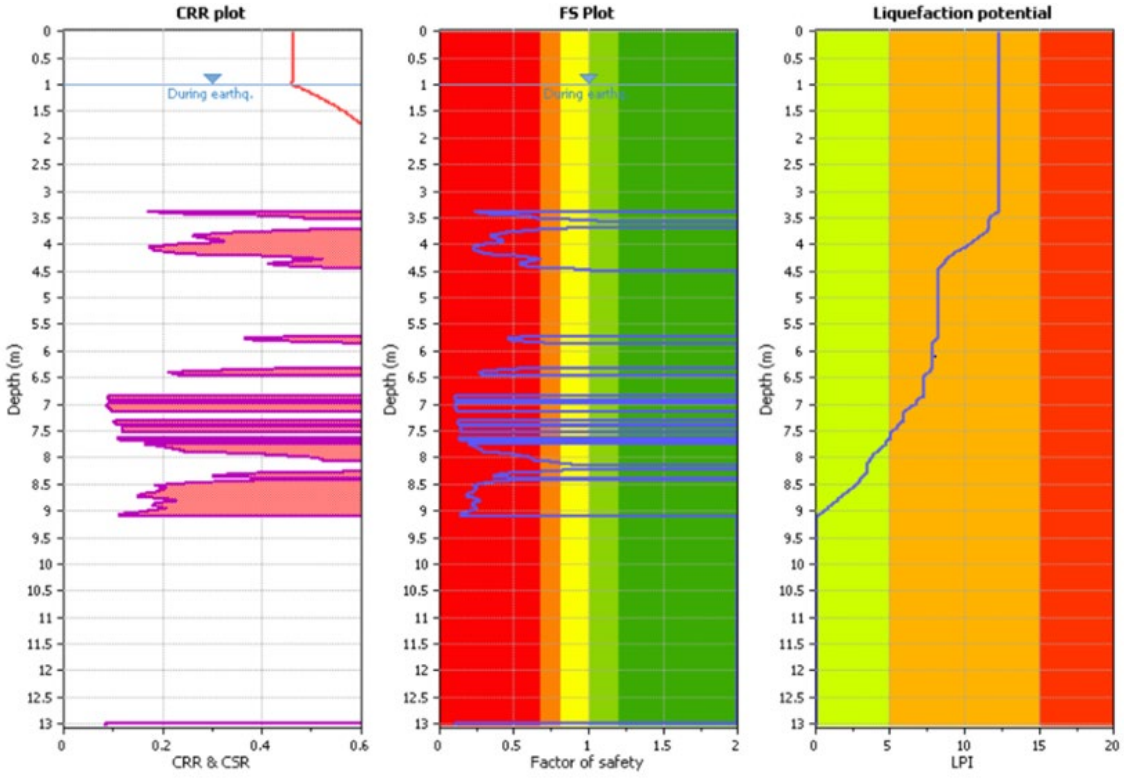
CRR plot
During earthq.
Depth (m)
CRR & CSR
FS Plot
During earthq.
Depth (m)
Factor of safety
Liquefaction potential
Depth (m)
LPI

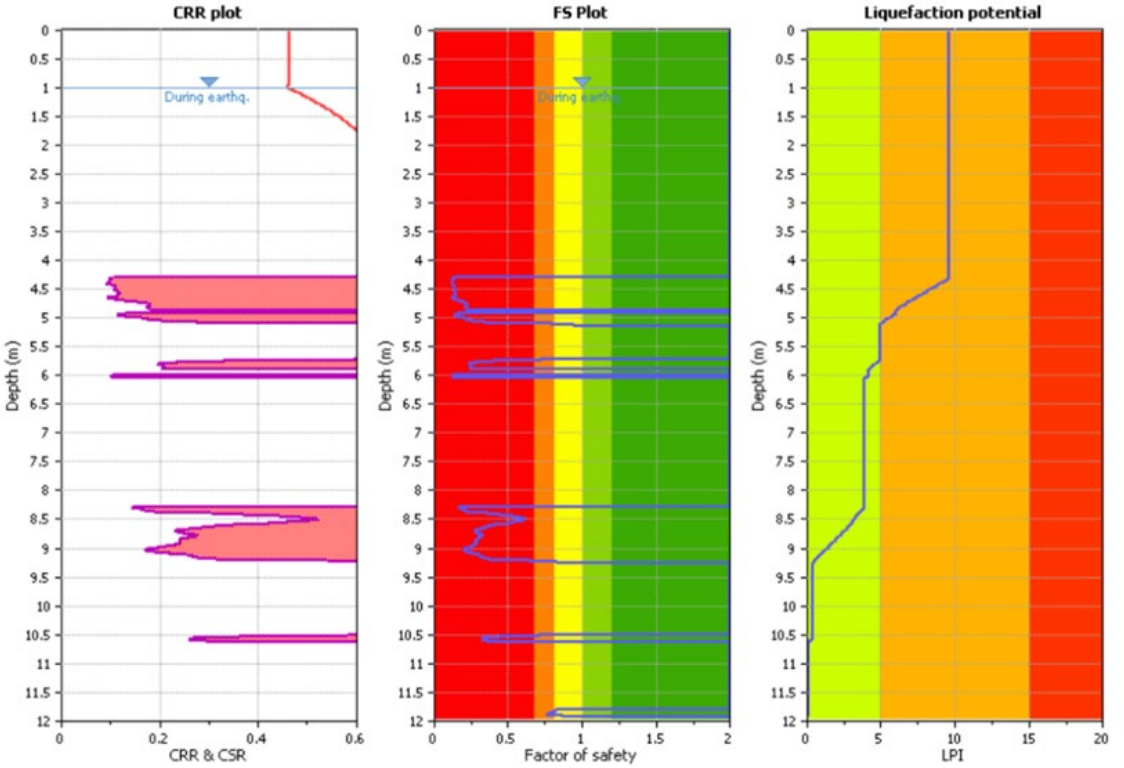
CRR plot
During earthq.
Depth (m)
CRR & CSR
FS Plot
During earthq.
Depth (m)
Factor of safety
Liquefaction potential
Depth (m)
LPI

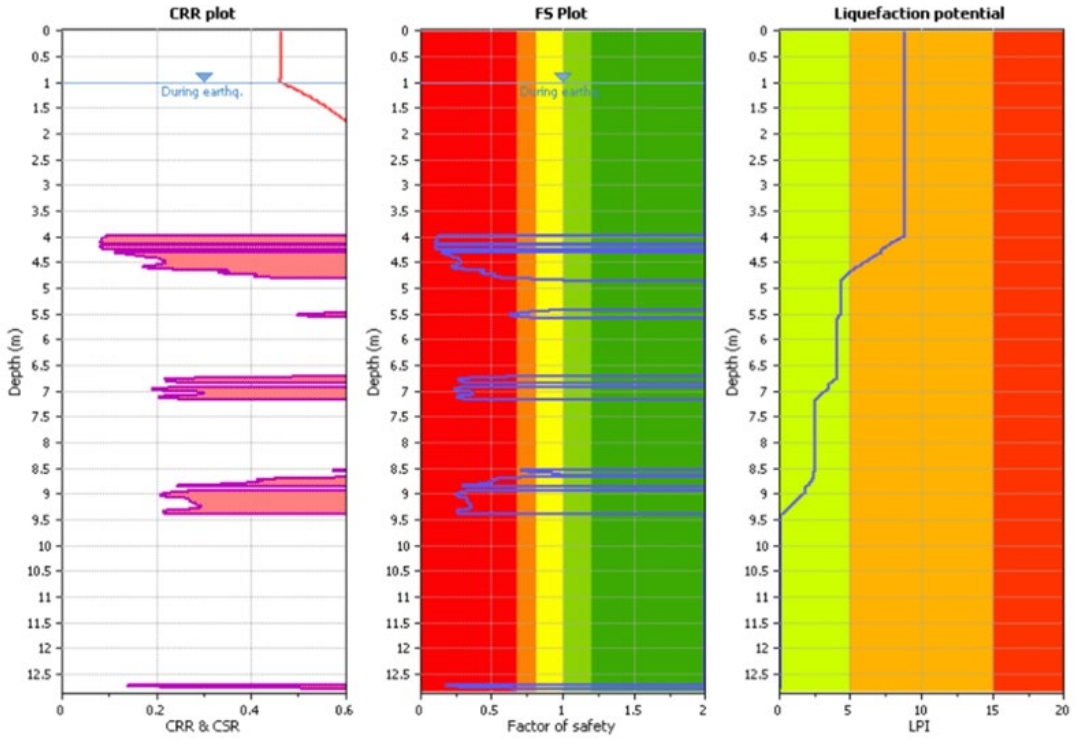
CRR plot
During earthq.
Depth (m)
CRR & CSR
FS Plot
During earthq.
Depth (m)
Factor of safety
Liquefaction potential
Depth (m)
LPI

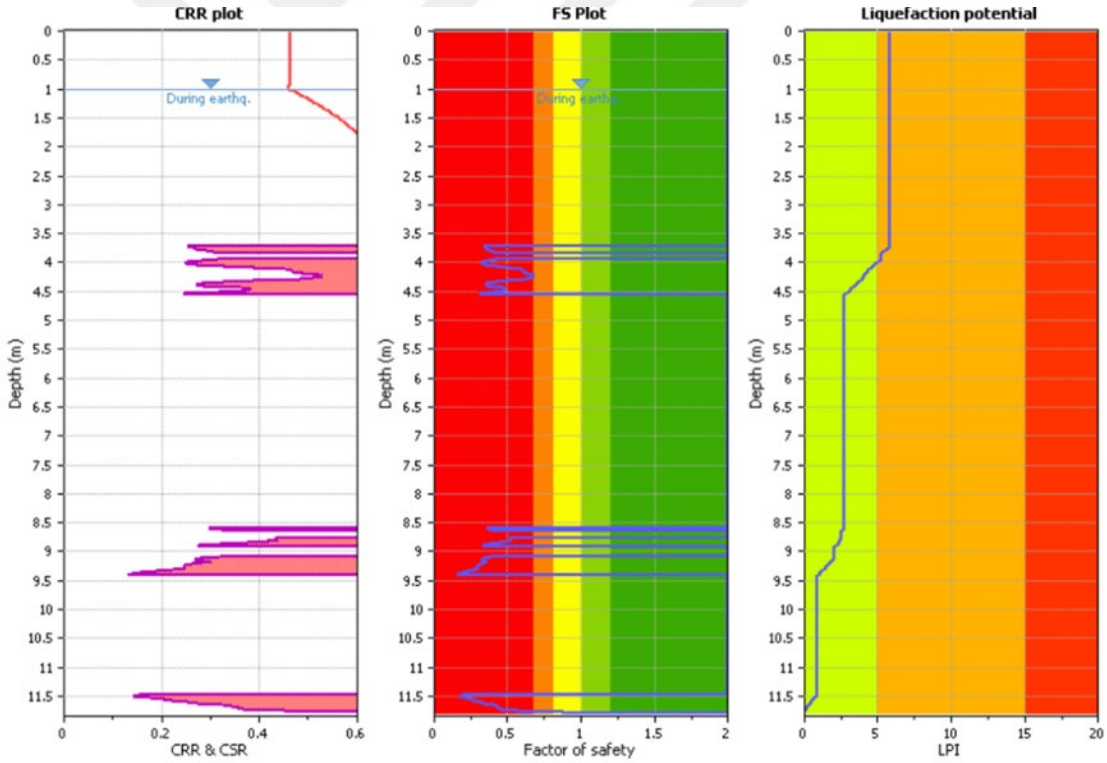
CRR plot
During earthq.
Depth (m)
CRR & CSR
FS Plot
During earthq.
Depth (m)
Factor of safety
Liquefaction potential
Depth (m)
LPI

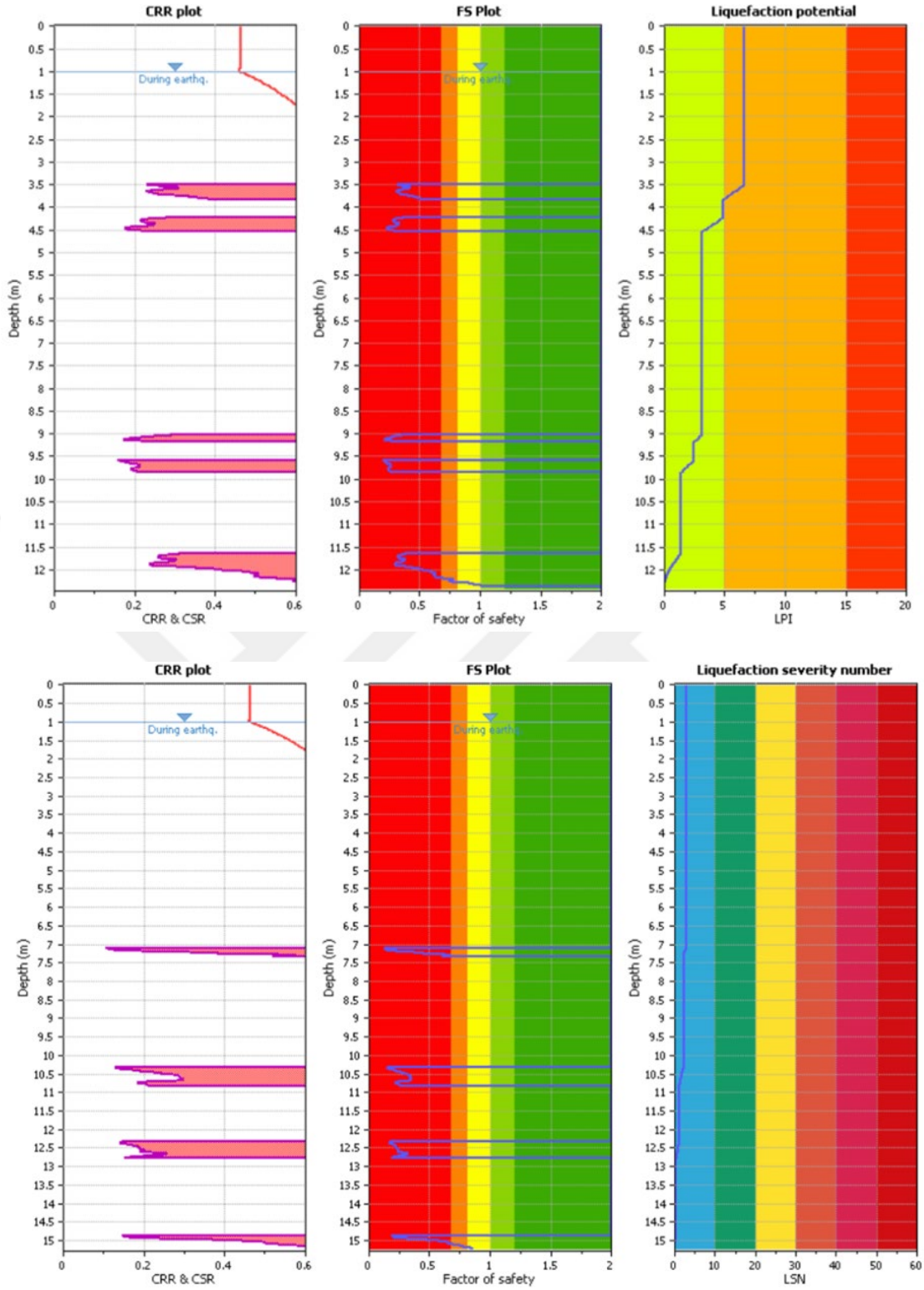

Figure 5.4 Liquefaction Potential and Safety Factors for (a) CPT-1, (b) CPT-2, (c) CPT-3, (d) CPT-4, (e) CPT-5, (f) CPT-6, (g) CPT-7

According to the liquefaction analysis made using the CPT results, liquefaction between 3m and 15 m is expected in silty sands.

5.4. Liquefaction and Lateral Spreading Assessment

According to the Turkish Earthquake Code (2018), liquefaction analyses are performed based on SPT values for each borehole and CPT results. Since the average SPT $N_{1,60}$ values of the first 30 m of completed boreholes between BH-1 to BH-25 are less than 15, the site class is designated as ZF (Table 5.1). However, analysis results of BH-11, BH-12, BH-13, BH-15, BH-16, and BH-21, indicate that the first 6 m of the soil is liquefiable. Also, there is liquefiable soil in deeper layers, as stated in analyses of BH-17, BH-20, and BH-23. Hence, the soil class in the site area is designated as ZF (Liquefiable soils) according to the Turkish Earthquake Code.

The safety factor against liquefaction is proposed as 1.1, according to the TBDY-2018. The points where the factor of safety is lower than 1.1 have liquefaction potential. According to the CPT results, liquefaction is expected to occur in sand-silty sand and silty sand-sandy silt layers with variable depths.

Table 5.1 Soil Classification (TBDY 2018)

Soil Class	**Soil Type**	**Average at the top 30 meters**		
		$(V_s)_{30}$ (m/s)	**$(N_{60})_{30}$ (blow/30 cm)**	**$(c_u)_{30}$ (kPa)**
ZA	Hard rocks	>1500	-	-
ZB	Little weathered medium-strong rocks	760 - 1500	-	-
ZC	Very dense sand, gravel, and hard clay layers or very weak jointed weak rocks	360 - 760	>50	>250
ZD	Medium dense - dense sand, gravel or very hard clay layers	180 - 360	15 - 50	70 - 250
ZE	Loose sand, gravel or soft - stiff clay layers or profiles with a soft clay layer (cu < 25 kPa) thicker than 3 m in total providing PI > 20 and w > % 40 conditions	<180	<15	<70
ZF	Soils requiring site-specific research and evaluation; 1) Soils with a risk of collapse and potential collapse failure under earthquake effect (Liquefiable soils, highly sensitive clays, collapsible weak cemented soils, etc.) 2) Total thickness is more than 3 meters peat or high content of organic material clays. 3) High plasticity clays (PI >50) with a total thickness of more than 8 meters. 4) Very thick (>35 m) soft or medium stiff clays.			

The soil group of the site is designated as ZF when in-situ tests and laboratory results. According to TBDY-2018, site-specific soil behavior analysis is required to determine the effect of earthquake ground motion for the ZF soil class.

The general geotechnical design principle of the Turkish Building Earthquake Code (2018) is as follows:

To determine the site-specific earthquake spectrum at the surface does not appear to be modifying the subject, the ratio of the ground surface spectral acceleration to the base rock spectral acceleration for each spectral period. If these coefficients are multiplied by the corresponding baseline spectrum, the site-specific earthquake spectrum at the ground surface would be determined. According to TBDY-2018, the non-linear analysis shall be done in the time domain on the liquefaction potential.

5.5. Evaluations of Soil Improvement

According to liquefaction analyses, liquefaction was observed in silty and sandy soil layers. Deep mixing columns applications are recommended as a soil improvement method in order to mitigate liquefaction.

Discrete columns or grids obtained by mixing the soil in place using cement or lime, usually with the help of augers or bladed mixers with holes in the middle, in fine grained and soft soils (usually soft clays) is defined as deep soil mixing method (DSM) (Ergün, 2009:28). This method, which has been applied in many countries since 1960s, was added to Turkish Standards in 2006 with the ID of TS-EN14679. It is aimed to create high modulus columns in the soil with this method (Kılıç, Onur, A. Tuncan ve M. Tuncan, 2016:195).

Deep soil mixing is the process of mixing the soil with materials such as cement, lime, etc. in place. While vibration processes are used for the improvement of cohesionless soils (coarse-grained materials); they cannot be used on cohesive soils (fine grained materials) due to the effect of water content. The most appropriate soil improvement method should be chosen by determining the properties of the soil. Soil improvement methods are used to increase the shear strength of the soil, increase the bearing capacity of the foundations, decrease the amount of settlement, decrease the

shrinkage/swelling and liquefaction potential of the soil and increase the stability of the slopes.

The deep soil mixing method is the process of boring the soil layers appropriately and mixing it with additives such as cement and lime. It is a very common method due to applying fast and construct easily in the field. In addition to the main purposes of using this method, it can be used for purposes such as providing impermeability, meeting lateral soil pressure. The equipment used in the application of deep soil mixing process is cement tank, mixer, and pump.

5.5.1. Liquefaction Analysis After Improvement

Two studies were (Rayamajhi et. al., 2014; Nguyen et. al., 2013) conducted by Boulanger and the working group have developed practical calculation methods regarding liquefaction- improvement rates with DSM and stone columns. The studies were performed for discrete columns (square type) and grid type columns, and it was observed that grid type tangent columns were more effective against liquefaction.

According to the liquefaction analyses prepared by Destech Consulting Engineering and Project Inc., the minimum safety factor was calculated as FS=0.62.

The design steps for stone columns and deep soil mixing are given below. The shear stress reduction factor method developed by Rayamajhi et.al. (2014) is given below.

$$R_{rd} = \frac{1}{(G_r \times A_r \times C_g \times \gamma_r) + (1 - A_r)} \leq 1.0 \quad (5.10)$$

where,

R_{rd}: The shear stress reduction factor

G_r: Shear modulus ratio = G_{DSM}/G_S

A_r: Area ratio= A_{DSM}/A_{total}

For system of grid:

C_g: Equivalent Shear Factor = $1\text{-}0.5\times (1\text{-}A_r)^{0.5}$

γ_r: Shear strain ratio = $1\text{-}(1\text{-}A_r)^{1.3}\times ((G_r\text{-}1)/185)^{0.4}$)

For system of discrete:

C_g: Equivalent Shear Factor = 1.0

γ_r: Shear strain ratio = (1.04 × Gr-0.65) -0.04

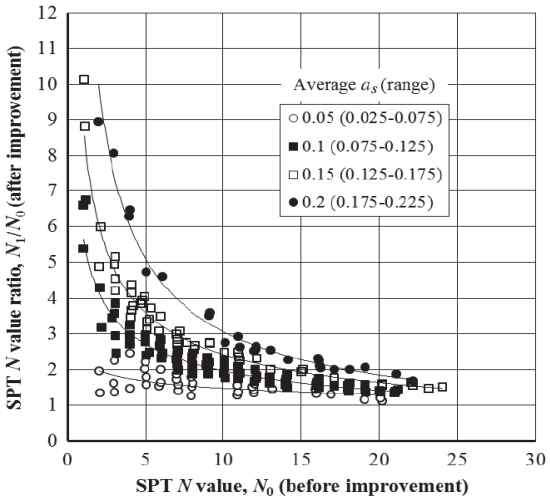

Figure 5.5 Improvement Ratio of SPT-N1,60 According to Area Ratio (Han, 2016)

For the purpose of liquefaction mitigation, deep soil mixing columns and stone columns are designed as 20 m of length and 80 cm of diameter.

Deep Soil Mixing Columns are designed with 7.50 m×7.50 m of grid systems and 2.5 m×2.5 m of discrete system. Details of soil improvement with deep mixing columns are shown in Table 5.2.

Table 5.2 Soil Improvement Analysis with DSM

Soil Ipmrovement Ratio Calculation With DSM	DESTECH	
*The compaction of the surrounding soil and the distribution of shear stress are not considered.		
DSM Design Parameters		
Diameter Of DSM , m	D	0.8
Area Ratio	Ar	0.20
Before Improvement SPT, N1_60	PreSpt	12.00
Before Improvement GS	PreGS	0.620
Density, t/m3	Ps	1.60
DSM Shear Modulus, MPa	Gc	576.00
PostSPT/PreSPT	SPTRatios	2.56
Densification Calculation		
After Improvement SPT (Baez, 1995)	PostSpt	30.74
Pre-CRR (Based on NCEER, 1997 Formula)	PreCRR	0.13
Post-CRR (Based on NCEER, 1997 Formula)	PostCRR	0.29
Improved Safety Factor	ImpDens	2.20
Calculation of shear stress		
Shear Wave Velocity (Hasancebi & Ulusay, 2007), m/s	Vs	255.37
Share Modulus Of Soil (Ps*Vs^2), kPa	Gs	104.34
Shear Modulus Ratio, Gc/Gs	Gr	5.52
Shear Deformation Ratio (Rayamajhi et. al., 2014)	SSRat	0.83
Equivalent Shear Factor (Rayamajhi et al., 2014)	Cg	0.55
Shear Stress Reduction Factor (Rayamajhi et. al., 2014)	Rrd	0.76
Safety Factor Improved By Shear Stress	ImpShe	1.31
Safety Factor After Improvement		
PreFS*ImpDens*ImpShe	PostFS	**1.79**

CHAPTER 6

PROBABILISTIC SEISMIC HAZARD ASSESSMENT OF THE SITE

6.1. Introduction

Earthquake hazard is basically defined as the determination of the ground motion caused by an earthquake that can cause damage and loss of life in a certain place and within a certain time period. The purpose of seismic hazard analysis is to calculate the parameters (acceleration, velocity, displacement) related to seismic ground motion required for the calculation of the earthquake loading conditions that the soil and the engineering structure will be exposed to in the future. There are two seismic hazard analysis. These are probabilistic and deterministic seismic hazard analyses. In the deterministic approach, the level of ground motion to be created by the largest earthquake in the region is determined regardless of the time dimension. In the probabilistic approach, the possibility of occurrence of damaging ground motion at a certain place and within a certain time period is investigated.

This chapter presents the general methodology to assess seismic hazard in a probabilistic way, accounting for a full description of the seismogenic sources' geometry that is also characterized by using instrumental information in terms of their seismic activity. Results at the national level for Düzce are presented in terms of hazard curves for different spectral ordinates that allow calculating probabilistic seismic hazard (PSH) maps for several return periods and spectral ordinates besides the classical uniform hazard spectra. The main objective of a PSH analysis is to quantify the rate of exceedance for different ground motion levels in one or several sites of interest, considering the participation of all possible earthquakes. Earthquakes, on the other hand, can, at the same time, be generated in different seismogenic sources.

6.2. Proposed Earthquake Effect for Project

The site-specific seismic hazard analysis within the project's scope is performed for earthquake ground motion levels described according to the Turkish Earthquake Code (2018). For DD-1 and DD-2 earthquake levels, peak ground acceleration, horizontal and vertical spectral acceleration values in the range of 0.01 sec-8.0 sec will be determined using the probabilistic seismic hazard analysis steps.

Two different earthquake ground motion levels were considered for the design of structural systems under earthquake effect.

(1) DD-2 Earthquake Ground Motion Level (Design Earthquake Ground Motion)

(2) DD-1 Earthquake Ground Motion Level (Maximum Earthquake Ground Motion)

6.3. Earthquake Catalogue

In this study, a catalog of seismic parameters was compiled with data from the Disaster and Emergency Management Authority Earthquake Department Directorate Earthquake Catalogue (AFAD) and Kandilli Earthquake Research Institute. 7240 events were collected from 20.09.1900 to 30.01.2020.

6.3.1. Homogenization of Catalogue

Empirical correlations given in UDAP-Ç-13-06 (2014) document were used to transform the instrumental period earthquake catalog containing different magnitude types (Surface-wave magnitude (M_s), Body-wave magnitude (M_b), Richter magnitude (M_l), Duration magnitude (M_d)) into a single magnitude type (moment magnitude, M_w). Empirical relations to find the Mw magnitude from different magnitude types are given below.

$$M_w=1.0319(\pm0.025) \times M_b+0.0223(\pm0.117197) \quad 3.9\leq M_b\leq 5.8 \quad (6.1)$$

$$M_w=0.5716(\pm0.024927) \times M_s+2.4980(\pm0.117197) \quad 3.4\leq M_s\leq 5.4 \quad (6.2)$$

$$M_w=0.8126(\pm0.034602) \times M_s+1.1723(\pm0.208173) \quad M_s\geq 5.5 \quad (6.3)$$

$$M_w=0.7947(\pm0.033) \times M_d+1.3420(\pm0.163) \quad 3.5\leq M_b\leq 5.0 \quad (6.4)$$

$$M_w=0.7947(\pm0.031) \times M_l+1.3003(\pm0.154) \quad 3.3\leq M_d\leq 5.3 \quad (6.5)$$

Using the above equations, the earthquake catalog is homogenized in terms of Mw magnitude.

6.3.2. De-Clustering of Catalogue

Since aftershocks and foreshocks are temporally and spatially dependent on the main shock, de-clustering was performed using ZMap software to remove these dependent events from the catalog. Before de-clustering, there were 7240 earthquakes in the catalog. After the de-clustering process, 5879 earthquakes remained. Earthquake catalog before and after de-clustering is given in Figure 6.1 and Figure 6.2, respectively.

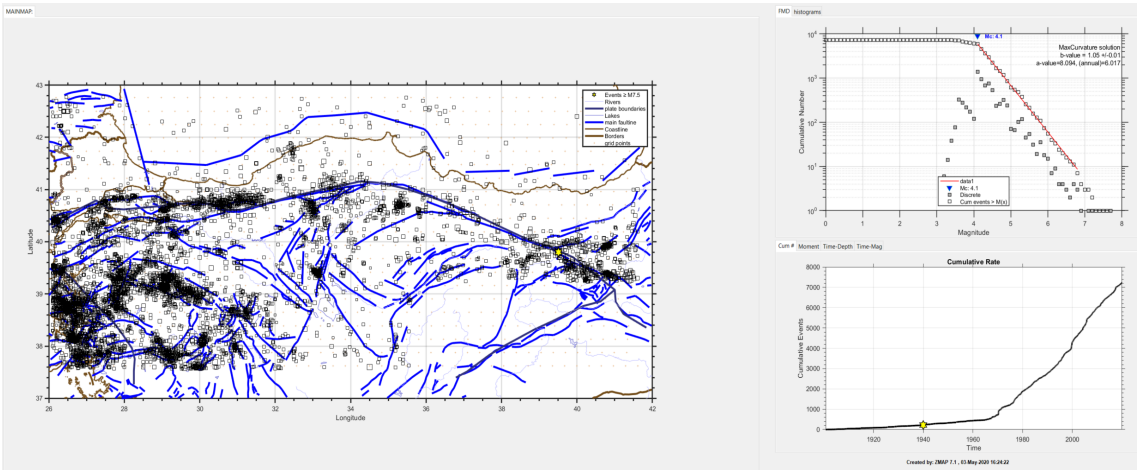

Figure 6.1 Earthquake Catalog without De-clustering (09.20.1900-01.30.2020)

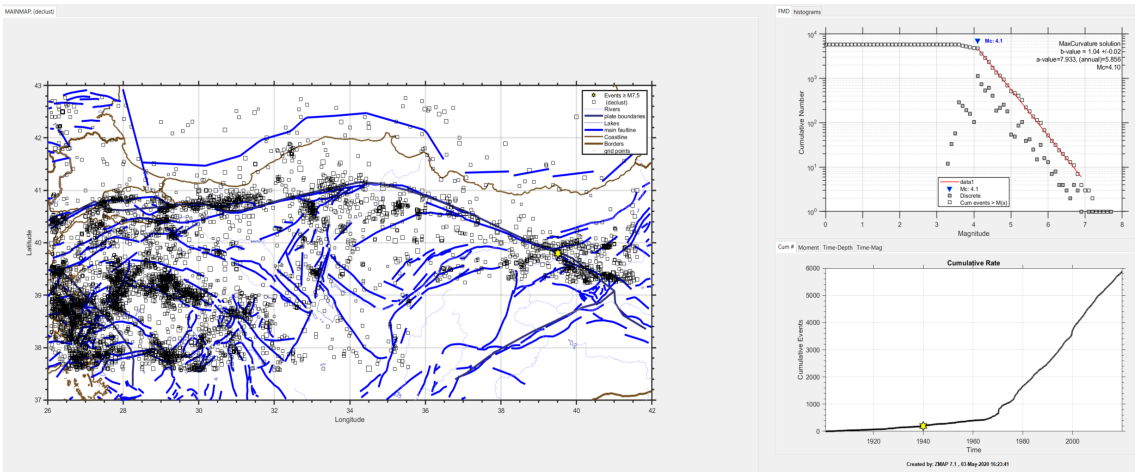

Figure 6.2 Earthquake Catalog with De-clustering (09.20.1900-01.30.2020)

6.3.3. Completeness Analysis of Earthquake Catalogue

Completeness analysis process included computing the time window for which the catalog could be considered as completed. The period of completeness is assumed to begin at the earliest time when a straight line can reasonably approximate the slope of the cumulative fitting curve for a given magnitude class. Magnitude completeness values (M_c) were calculated by using ZMap software and shown in Table 6.2. In this study, the Maximum Curvature Method developed by Wiemer and Wyss (2000) was used in the calculation of area source parameters (a, b, and M_c values).

6.4. Earthquake Source Models

The analysis was carried out within the project's scope by considering a 250 km diameter circle, with the project coordinates in the center. In this study, two different seismic source models were used for probabilistic earthquake hazard assessment.

Line sources and area sources were used as earthquake source models. Active faults in the region were modeled as line sources. Line sources were created based on the UDAP-Ç-13-06 document (2014) and SHARE Project. Parameters of the line sources were determined depending on the relevant fault characteristic. Line source models are given in Figure 6.3. Parameters of line sources are shown in Table 6.1.

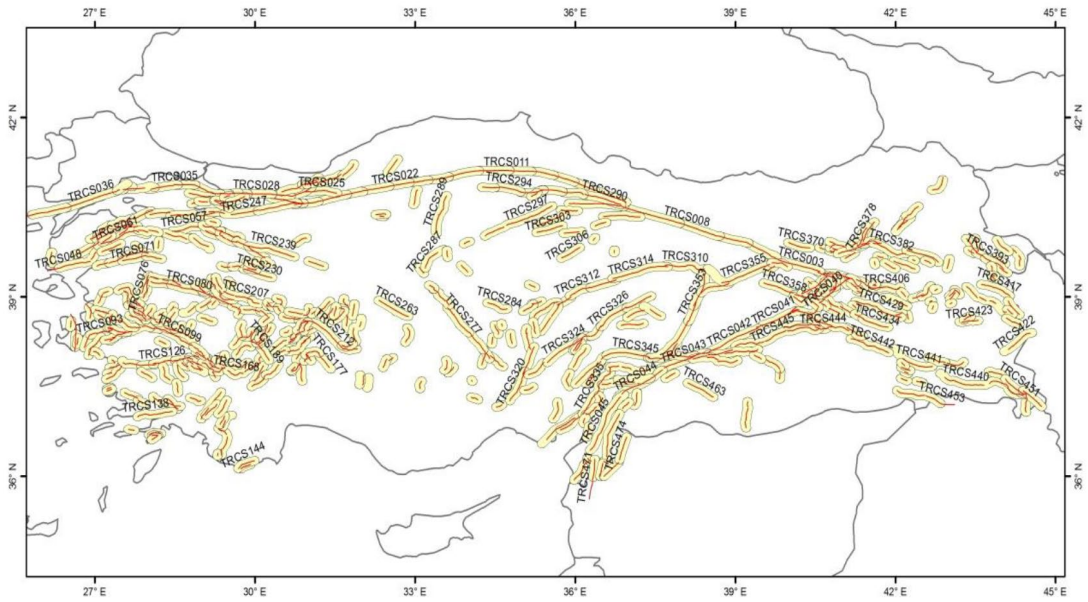

Figure 6.3 Line Sources (UDAP-Ç-13-06)

Area sources were also created based on the UDAP-Ç-13-06 document (2014) and SHARE Project. Geometry and locations of area sources are given in Figure 6.5. The calculated parameters of area sources are shown in Table 6.2. Both line and area sources are defined by considering earthquakes in the region.

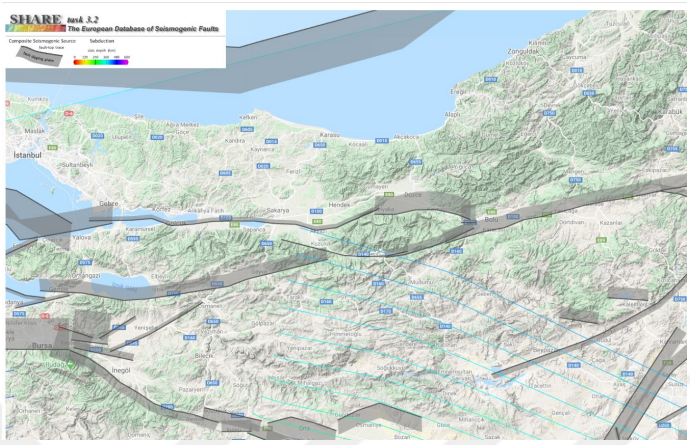

Figure 6.4 Line Sources (SHARE Project)

Table 6.1 Parameters of Line Sources (the slip rate data is from SHARE Project)

Fault ID	Slip Rate	Fault Type	MinDepth	MaxDepth	DipMin	DipMax	MinM$_w$	MaxM$_w$	Area Source
#	mm/y	#	m	m	°	°	-	-	#
TRCS004	3	Strike Slip	0	15	85	85	7.37	7.63	TRBG045
TRCS006	25.8	Strike Slip	0	18	73	73	7.73	8.06	TRBG045
TRCS007	24.22	Strike Slip	0	16	70	70	7.44	7.67	TRBG045
TRCS008	12	Strike Slip	0	18	78	78	6.79	6.95	TRBG045
TRCS009	13.19	Strike Slip	0	18	89	89	6.99	7.12	TRBG045
TRCS010	26.41	Strike Slip	0	18	64	64	6.81	7.02	TRBG045
TRCS011	12.15	Strike Slip	0	18	64	64	5.55	6.16	TRBG045
TRCS012	20.05	Strike Slip	0	18	83	85	7.39	7.6	TRBG045
TRCS013	27.9	Strike-Slip	0.5	15	35	78	7.26	7.47	TRBG045
TRCS014	10.13	Strike Slip	0	18	58	66	6.98	7.18	TRBG045
TRCS015	5.29	Strike Slip	0	18	80	90	7.01	7.15	TRBG045
TRCS022	8	Strike Slip	0	18	65	85	7.4	7.63	TRBG101
TRCS023	5.39	Strike Slip	0	18	85	85	7.22	7.38	TRBG101
TRCS024	3	Strike Slip	0	18	49	85	6.71	6.96	TRBG101
TRCS025	3	Strike Slip	0	18	85	85	6.78	6.94	TRBG101
TRCS026	3	Strike Slip	0	18	85	85	5.93	6.36	TRBG101
TRCS028	3.4	Strike Slip	0	18	85	85	6.86	7.01	TRBG101
TRCS029	4.04	Normal	0	18	50	50	6.7	6.9	TRBG101
TRCS030	4.9	Normal	0	18	40	40	7.03	7.2	TRBG101
TRCS031	4.13	Strike Slip	0	18	60	76	7.06	7.24	TRBG101
TRCS038	5.3	Strike Slip	0	18	85	85	6.45	6.71	TRBG101
TRCS039	3.4	Strike Slip	0	18	85	85	6.27	6.59	TRBG101
TRCS040	3.4	Strike Slip	0	18	85	85	6.62	6.83	TRBG101
TRCS041	4.1937	Normal	0	18	50	50	6.26	6.61	TRBG101
TRCS042	4.19	Normal	0	18	50	50	6.23	6.6	TRBG101

.cont. next page

cont. Table 6.1

Fault ID	Slip Rate	Fault Type	MinDepth	MaxDepth	DipMin	DipMax	$MinM_w$	$MaxM_w$	Area Source
#	mm/y	#	m	m	°	°	-	-	#
TRCS044	3.1672	Strike Slip	0	18	80	80	6.51	6.76	TRBG101
TRCS138	2.08	Strike Slip	0	15	60	60	6.94	6.98	TRBG108
TRCS148	2.0101	Strike Slip	0	15	84	84	6.12	6.34	TRBG108
TRCS191	3.04	Strike Slip	0	16	80	80	6.89	6.95	TRBG102
TRCS192	3.1832	Strike Slip	0	10	70	70	6.43	6.52	TRBG102
TRCS193	3.05	Strike Slip	0	16	70	70	6.93	6.97	TRBG102
TRCS194	3	Strike Slip	0	16	80	80	6.89	6.95	TRBG102
TRCS195	3.18	Strike Slip	0	15	70	70	6.88	6.94	TRBG102
TRCS196	3.18	Strike Slip	0	15	70	70	6.88	6.94	TRBG102
TRCS197	3.18	Strike Slip	0	15	60	70	6.82	6.84	TRBG102
TRCS198	3.2334	Strike Slip	0	15	56	56	6.6	7.06	TRBG102
TRCS199	3.18	Strike Slip	0	15	70	70	6.79	6.92	TRBG102
TRCS200	3.18	Strike Slip	0	15	70	70	6.5	6.92	TRBG102
TRCS201	3.18	Strike Slip	0	15	70	70	6.06	6.92	TRBG102
TRCS202	3.17	Strike Slip	0	13	70	75	6.73	6.85	TRBG102
TRCS203	4.8574	Normal	0	15	40	40	7.21	7.31	TRBG103
TRCS204	4.8574	Normal	0	15	40	40	6.75	6.87	TRBG103
TRCS205	3.97	Normal	0	15	54	54	6.53	6.64	TRBG103
TRCS206	3.89	Strike Slip	0	15	50	50	6.8	7.15	TRBG104
TRCS207	3.89	Strike Slip	0	15	50	50	6.52	7.15	TRBG104
TRCS208	4.82	Normal	0	15	52	52	6.74	7.16	TRBG104
TRCS209	4.82	Normal	0	15	56	56	6.69	6.96	TRBG104
TRCS210	5.02	Normal	0	15	50	50	6.61	6.77	TRBG104
TRCS211	1.31	Normal	0	15	50	50	6.48	6.63	TRBG103
TRCS212	1.3092	Normal	0	10	50	50	6.47	6.5	TRBG103
TRCS213	1.3054	Normal	0	10	50	50	6.69	6.86	TRBG103
TRCS215	1.3054	Normal	0	10	50	50	6.41	6.42	TRBG103
TRCS216	1.31	Normal	0	10	50	50	6.47	6.5	TRBG103
TRCS217	1.31	Normal	0	10	50	50	6.67	6.83	TRBG103
TRCS218	1.4	Normal	0	10	50	50	6.04	6.19	TRBG103
TRCS219	1.4	Normal	0	8	50	50	6.27	6.33	TRBG103
TRCS221	1.3054	Normal	0	10	50	50	5.66	5.97	TRBG103
TRCS222	1.3054	Normal	0	10	50	50	5.9	6.11	TRBG103
TRCS223	4.3528	Normal	0	12	50	50	6.59	6.6	TRBG103
TRCS224	4.3528	Normal	0	12	50	50	6.09	6.3	TRBG103
TRCS225	1.3054	Normal	0	8	50	50	5.63	6.19	TRBG103
TRCS226	1.3979	Normal	0	10	50	50	6.4	6.7	TRBG104
TRCS227	1.3979	Normal	0	8	50	50	6.19	6.41	TRBG104
TRCS228	1.3979	Normal	0	8	50	50	5.92	6.19	TRBG104
TRCS229	1.31	Normal	0	8	50	50	5.5	6.19	TRBG104
TRCS230	1.63	Normal	0	10	40	40	5.72	6.56	TRBG104
TRCS231	1.56	Normal	0	10	40	40	6.52	6.6	TRBG104
TRCS232	3.1832	Strike Slip	0	15	70	70	6.84	6.94	TRBG105
TRCS233	2	Strike Slip	0	15	70	70	6.84	6.94	TRBG105
TRCS235	1.5844	Normal	0	12	40	40	7.02	7.15	TRBG103
TRCS236	1.0074	Strike Slip	0	12	55	55	6.8	6.9	TRBG108
TRCS237	1	Strike Slip	0	12	60	60	6.75	6.86	TRBG122
TRCS238	1.13	Strike Slip	0	15	70	70	6.88	6.94	TRBG122
TRCS239	1.13	Strike Slip	0	15	70	70	6.88	6.94	TRBG122
TRCS240	1	Strike Slip	0	15	80	80	6.83	6.92	TRBG122

cont. Table 6.1

Fault ID	Slip Rate	Fault Type	MinDepth	MaxDepth	DipMin	DipMax	$MinM_w$	$MaxM_w$	Area Source
#	mm/y	#	m	m	°	°	-	-	#
TRCS241	1.13	Strike Slip	0	15	70	70	6.31	6.48	TRBG122
TRCS242	1.13	Strike Slip	0	15	70	70	6.28	6.46	TRBG122
TRCS243	2.01	Strike Slip	0	12	84	90	6.63	6.76	TRBG122
TRCS244	1	Strike Slip	0	12	77	77	6.57	6.65	TRBG122
TRCS245	1.13	Strike Slip	0	15	70	70	6.88	6.94	TRBG108
TRCS246	1.13	Strike Slip	0	15	70	70	6.88	6.94	TRBG108
TRCS247	2.02	Strike Slip	0	15	87	87	6.82	6.92	TRBG120
TRCS248	1.0056	Strike Slip	0	12	70	80	5.78	6.05	TRBG120
TRCS249	1.14	Strike Slip	0	15	66	66	6.18	6.42	TRBG108
TRCS250	1.0056	Strike Slip	0	15	70	70	6.88	6.94	TRBG108
TRCS251	2.01	Strike Slip	0	15	66	66	6.26	6.46	TRBG108
TRCS252	1	Strike Slip	0	15	87	87	6.56	6.6	TRBG108
TRCS253	1.01	Strike Slip	0	12	87	87	6.63	6.76	TRBG108
TRCS254	1	Strike Slip	0	12	80	80	6.41	6.43	TRBG122
TRCS255	2.61	Normal	0	15	50	50	7.06	7.19	TRBG121
TRCS262	2.61	Normal	0	15	50	50	6.27	6.51	TRBG121
TRCS277	5.2216	Normal	0	14	50	50	6.7	6.89	TRBG124
TRCS278	5.22	Normal	0	14	50	50	6.67	6.77	TRBG124
TRCS280	2.61	Normal	0	8	50	50	6.19	6.73	TRBG124
TRCS281	2.61	Normal	0	15	50	50	6.65	6.73	TRBG104
TRCS283	1.31	Normal	0	5	50	50	6.1	6.39	TRBG104
TRCS290	3.9277	Normal	0	14	50	50	7	7.14	TRBG121
TRCS292	1.32	Normal	0	8	50	50	6.51	6.73	TRBG121
TRCS297	1.3054	Normal	0	15	50	50	5.74	6.19	TRBG104
TRCS298	1.3054	Normal	0	8	50	50	5.85	5.98	TRBG104
TRCS299	1.3054	Normal	0	14	50	50	6.21	6.44	TRBG104
TRCS300	1.3054	Normal	0	14	50	50	5.58	6.06	TRBG104
TRCS301	1.31	Normal	0	4	50	50	5.59	5.69	TRBG104
TRCS306	1.31	Normal	0	14	50	50	6.25	6.7	TRBG124
TRCS310	2.68	Normal	0	15	64	64	6.62	7.07	TRBG103
TRCS311	2.68	Normal	0	15	64	64	6.62	7.07	TRBG103
TRCS312	1.3054	Normal	0	4	50	50	5.55	6.27	TRBG103
TRCS313	1.3054	Normal	0	14	50	50	6.7	6.8	TRBG103
TRCS314	1.3054	Normal	0	15	50	50	6.7	6.77	TRBG103
TRCS373	3	Strike Slip	0	18	85	90	6.91	7.06	TRBG045
TRCS374	3	Strike Slip	0	18	85	85	6.85	7	TRBG045
TRCS375	2.2655	Strike Slip	0	18	70	70	5.92	6.38	TRBG045
TRCS376	3	Strike Slip	0	18	70	85	6.91	7.07	TRBG045
TRCS377	5.17	Normal	0	18	39	39	6.44	6.82	TRBG045
TRCS378	3	Strike Slip	0	18	80	80	6.92	7.07	TRBG045
TRCS379	3.0004	Strike Slip	0	18	80	80	6.94	7.09	TRBG045
TRCS407	2	Reverse	1.5	16	30	38	7.14	7.4	TRBG043
TRCS418	1	Strike Slip	0	16	85	85	6.84	6.95	TRBG043
TRCS434	5	Strike Slip	0	20	85	85	5.59	6.18	TRBG045
TRCS435	4	Normal	0	10	60	60	5.7	5.94	TRBG045
TRCS436	3	Strike Slip	0	18	85	85	5.57	6.12	TRBG045
TRCS437	2	Strike Slip	0	15	85	85	6.83	6.92	TRBG120
TRCS438	1.39	Normal	0	6	46	46	5.98	6.36	TRBG104
TRCS996	28.89	Strike Slip	0	19	55	90	7.7	8.08	TRBG045

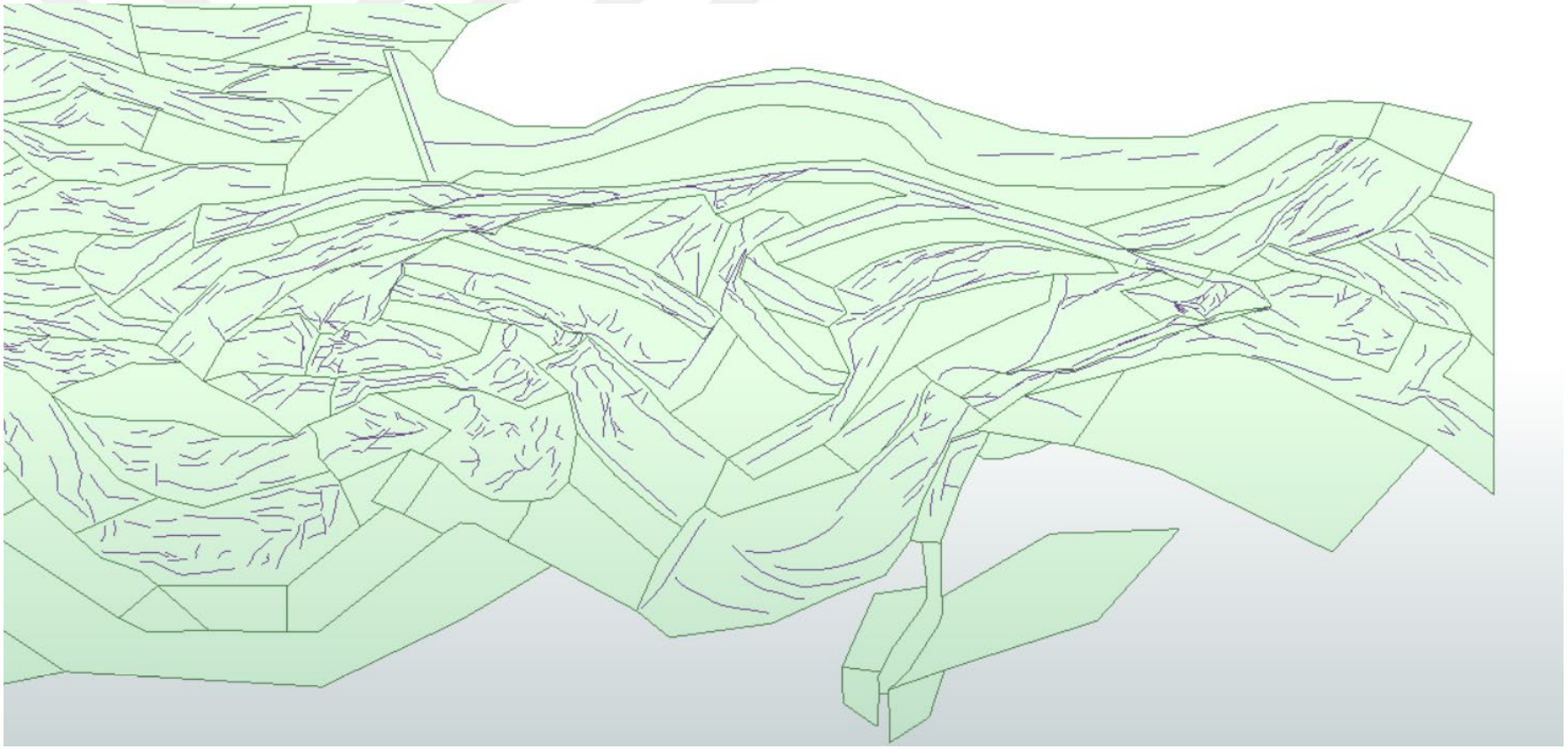

Figure 6.5 Area Sources (SHARE Project)

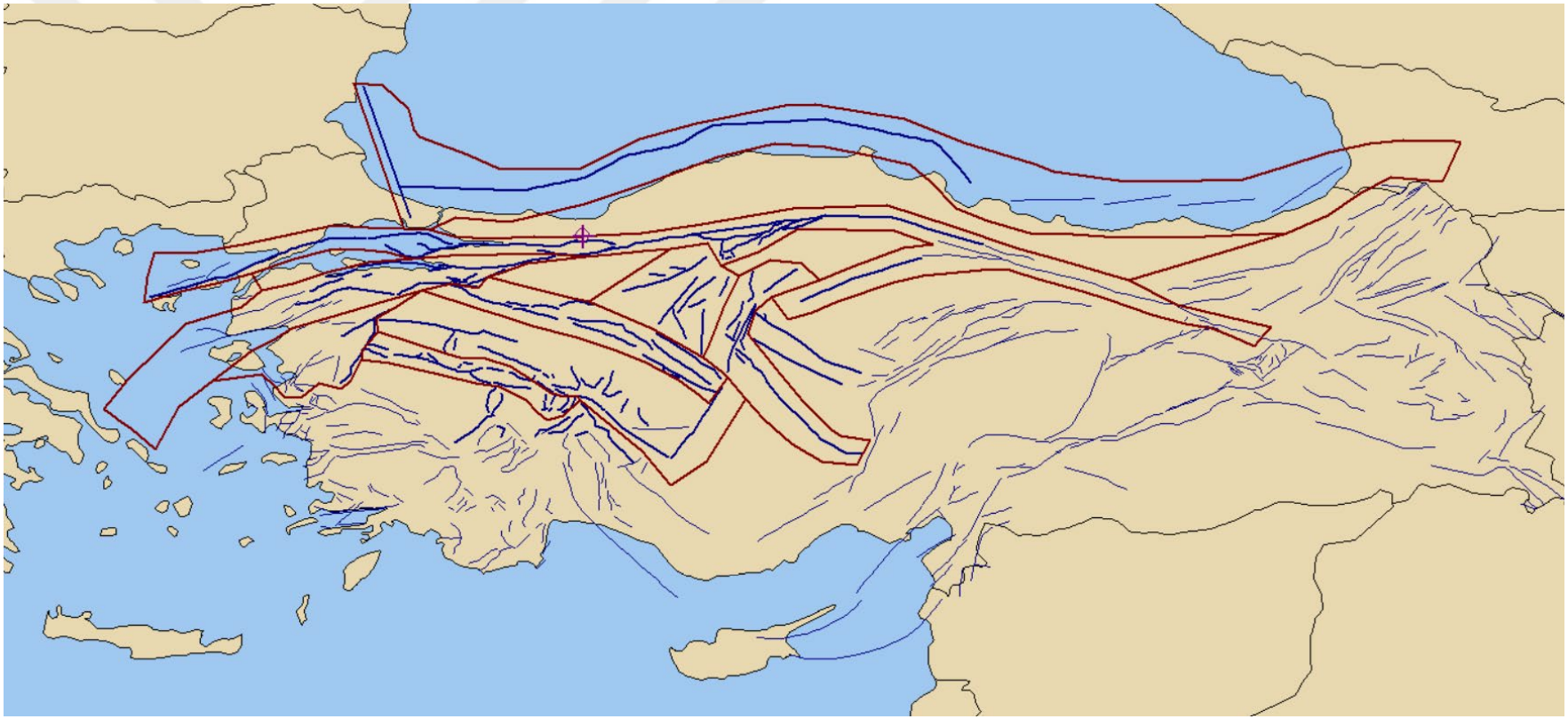

Figure 6.6 Area Sources Used in PSHA

Table 6.2 Statistical Parameters Calculated for Area Sources

Source Area	a value	b value	M_c	M_{max}	Number of events	β	Lambda(M_0)
TRBG 101	6.89	1.06	4.1	6.8	471	2.441	4.830
TRBG 122	7.99	1.51	4.1	5.3	71	3.478	6.134
TRBG 108	7.82	1.37	4.1	5.8	168	3.155	5.860
TRBG 105	8.42	1.40	4.1	6.7	662	3.224	6.354
TRBG 104	6.85	1.01	4.1	6.0	608	2.326	4.870
TRBG 103	6.68	0.98	4.1	6.2	631	2.257	4.604
TRBG 102	5.18	0.80	4.1	6.2	103	1.842	3.117
TRBG 045	6.71	0.91	4.1	7.7	1096	2.096	4.647
TRBG 043	6.44	1.08	4.3	6.0	89	2.487	4.401
TRAS 755	6.26	1.09	4.1	6.2	96	2.510	4.332
TRAS 754	6.85	1.14	4.1	5.9	169	2.625	4.849
TRAS 753	8.12	1.47	4.1	5.8	139	3.380	6.240
TRAS 746	5.77	0.86	4.1	6.8	199	1.981	3.720

6.5. Strong ground motion attenuation relationships

Once the activity rate of each seismogenic source has been defined through the seismicity parameters, it is necessary to evaluate the effects of seismic physical intensities generated at any point of interest. It is required to know the intensity that could occur in the site of analysis; in this stage, at the bedrock level, if in the seismogenic source, an earthquake occurs with known magnitude and distance.

The selection of the GMPEs to be used in the analysis constitutes a fundamental step in the PSHA. It is through them that the physical parameters of seismic hazard are quantified. Usually, the relative position between the source and the analysis site is specified using the focal distance, which is the distance between the rupture area and the analysis site. In this study, it is assumed that the relevant seismic intensities are the spectral ordinates of the response spectra. These quantities are approximately proportional to the lateral inertial forces generated on the structures during the earthquakes.

Attenuation relationships used in the seismic hazard analysis and these equations are given below:

Abrahamson and Silva (2008) NGA

$$lnSa(g) = f_1(M, R_{rup}) + a_{12}F_{RV} + a_{13}F_{NM} + a_{15}F_{AS} + f_5(PGA_{1100}, V_{s30}) + F_{HW}f_4(R_{jb}, R_{rup}, R_x, W, \delta, Z_{TOR}, M) + f_6(Z_{TOR}) + f_8(R_{rup}, M) + f_{10}(Z_{1.0}, V_{s30}) \quad (6.6)$$

where;

M: moment magnitude, R_{rup}: Rupture distance (km),

R_{jb}: Joyner-Boore distance (km), Z_{TOR}: Depth to top of rupture (km),

R_x: horizontal dist. (km) from top edge of rupture,

F_{RV}: flag for reverse faulting earthquakes, F_{AS}: flag for aftershocks,

F_{NM}: flag for normal faulting earthquakes,

F_{HW}: flag for hanging wall sites, δ: fault dip in degrees,

$Z_{1.0}$: depth to Vs=1.0 km/s, W: down-dip rupture width (km)

PGA_{1100}: median peak acceleration (g) for $V_{s,30}$=1100 m/s

Boore-Atkinson (2008) NGA

$$lnY = F_M(M) + F_D\left(R_{jb}, M\right) + F_S\left(V_{s30}, R_{jb}, M\right) + \varepsilon\sigma_T \tag{6.7}$$

Campbell-Bozorgnia (2008) NGA

$$lnY = f_{mag} + f_{dis} + f_{flt} + f_{hng} + f_{site} + f_{sed} \tag{6.8}$$

where;

f_{mag}: dependence on magnitude

f_{dis}: dependence on source-to-site distance

f_{flt}: dependence on style of faulting

f_{hng}: dependence on hanging-wall effect

f_{site}: dependence on shallow linear and nonlinear site condition

f_{sed}: dependence on shallow sediment effects and 3D basin effects

Chiu and Youngs (2008) NGA

$$\ln\left(y_{ref_{ij}}\right) = c_1 + \left(c_{1a}F_{RVi} + c_{1b}F_{NMi} + c7(Z_{TORi} - 4)\right)(1 - AS_i) + (c_{10} + c_{7a}\,(Z_{TORi} - 4)AS_i + c_2(M_i - 6) + \frac{c_2 - c_3}{c_n}\ln\left(1 + e^{c_n(c_M - M_i)}\right) + c_4\ln\left(R_{rupij} + c_5\cosh(\max(M_i - c_{HM}, 0))\right) + (c_{4a} - c_4)\ln\sqrt{R_{RUPij}^2 + c_{RB}^2} + \left(c_{\gamma 1} + \frac{c_{\gamma 2}}{\cosh(\max(M_i - c_{HM}, 0))}\right)R_{RUPij} + c_9F_{HWij}\tanh\left(\frac{R_{xij}\cos^2\delta_i}{c_{9a}}\right)\left(1 - \frac{\sqrt{R_{JBij}^2 + Z_{TORi}^2}}{R_{RUPij} + 0.001}\right) \tag{6.9}$$

6.6. Results of Probabilistic Seismic Hazard Analysis Using EZ-Frisk

In seismic hazard analysis, to include each seismic source's effects separately, EZ-Frisk software was used. New Generation Attenuation Relationships (NGA) was utilized for DD-1, DD-2, DD-3, DD-4 earthquake levels, with a 5 % damping ratio in the period of 0.01sec to 8 sec for shear wave velocity of 760 m/s.

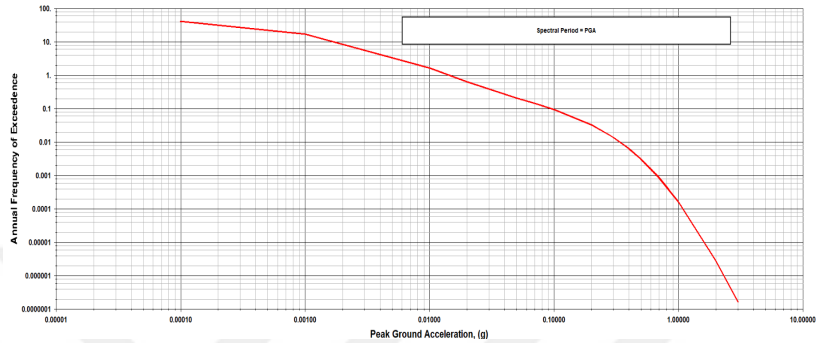

Figure 6.7 Annual Frequency of Exceedance to PGA

For the DD-1 earthquake level (return period of 2475 years), spectral acceleration values calculated using four different attenuation relationships given in Table 6.3. The mean values also given in the table. Geometric mean values of probabilistic seismic hazard analysis results for earthquake levels with a return period of 2475, 475, 72, 43 years are given in Table 6.4.

Table 6.3 Spectral Acceleration Values for DD-1 (2475 year)

Period	Mean	Abrahamson and Silva (2008) NGA	Boore and Atkinson (2008) NGA	Chiou and Youngs (2008) NGA	Campbell and Bozorgnia (2008) NGA
PGA	0.823	0.838	0.738	0.636	0.969
0.05	1.113	1.035	0.943	0.936	1.364
0.10	1.695	1.576	1.385	1.484	2.107
0.20	2.071	2.227	1.719	1.748	2.302
0.30	1.971	2.285	1.598	1.428	2.078
0.40	1.623	1.947	1.392	1.204	1.675
0.50	1.332	1.537	1.169	1.059	1.383
0.75	0.906	0.988	0.858	0.740	0.974
1.00	0.671	0.681	0.659	0.571	0.742
1.25	0.529	0.500	0.561	0.459	0.580
1.50	0.439	0.375	0.496	0.385	0.478
1.75	0.368	0.305	0.427	0.329	0.391
2.00	0.316	0.241	0.377	0.288	0.328
2.25	0.275	0.207	0.331	0.255	0.282
2.50	0.244	0.179	0.297	0.229	0.247

.cont. next page

cont. Table 6.3

Period	Mean	Abrahamson and Silva (2008) NGA	Boore and Atkinson (2008) NGA	Chiou and Youngs (2008) NGA	Campbell and Bozorgnia (2008) NGA
2.75	0.220	0.156	0.268	0.209	0.219
3.00	0.201	0.139	0.245	0.192	0.198
3.25	0.184	0.125	0.227	0.178	0.179
3.50	0.170	0.115	0.212	0.167	0.164
3.75	0.158	0.105	0.199	0.158	0.151
4.00	0.149	0.097	0.186	0.149	0.140
4.25	0.142	0.089	0.178	0.146	0.129
4.50	0.135	0.082	0.170	0.142	0.120
4.75	0.130	0.076	0.164	0.139	0.112
5.00	0.125	0.072	0.158	0.137	0.105
5.25	0.119	0.068	0.150	0.130	0.097
5.50	0.113	0.065	0.143	0.123	0.090
5.75	0.108	0.062	0.137	0.118	0.083
6.00	0.103	0.059	0.132	0.113	0.078
7.00	0.087	0.050	0.114	0.097	0.061
8.00	0.073	0.041	0.094	0.085	0.048
9.00	0.062	0.034	0.074	0.077	0.038
10.00	0.053	0.029	0.060	0.071	0.031

Table 6.4 Calculated Horizontal Probabilistic PGA and spectral acceleration values (GM)

Design Earthquake	Probability of Exceedance	Geometric Mean		
		PGA	S_s(T=0.2 sec)	S_1(T=1 sec)
DD-1	%2 in 50 years	0.82	2.07	0.67
DD-2	%10 in 50 years	0.55	1.31	0.44
DD-3	%50 in 50 years	0.30	0.69	0.23
DD-4	%68 in 50 years	0.24	0.54	0.18

Horizontal earthquake hazard spectrum plots are shown in Figure 6.8 in terms of the geometric mean.

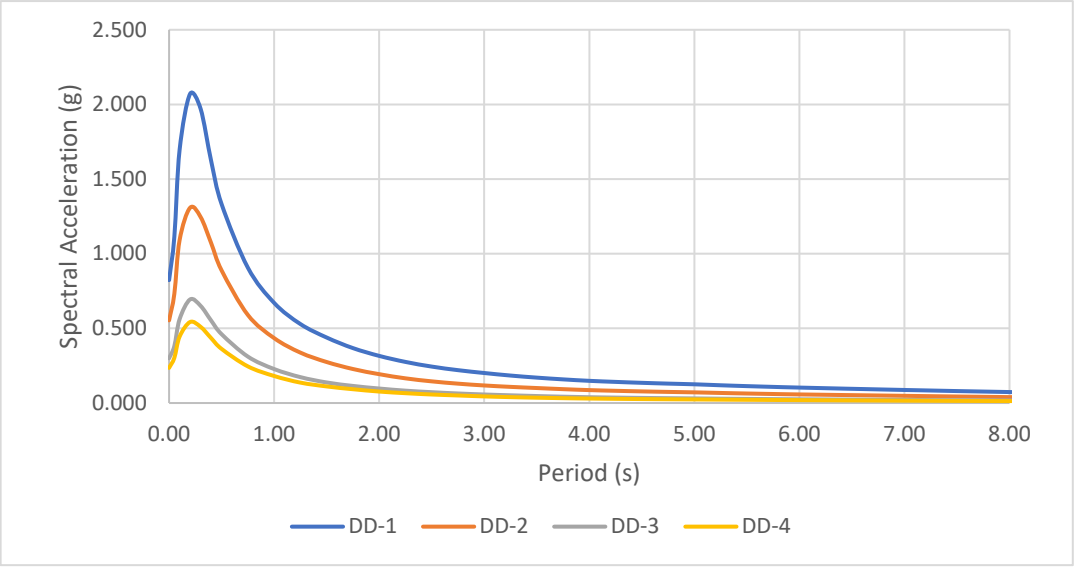

Figure 6.8 Horizontal Earthquake Design Spectra (Vs=760 m/sec, GM)

Maximum direction spectral acceleration values are given in Table 6.5. Horizontal earthquake hazard spectrum plots are shown in Figure 6.9 in terms of maximum direction.

Table 6.5 Calculated Horizontal Probabilistic PGA and Spectral Acceleration Values (max direction)

Design Earthquake	Probability of Exceedance	Maximum Direction		
		PGA	S_s(T=0.2 sec)	S_1(T=1 sec)
DD-1	%2 in 50 years	0.91	2.28	0.87
DD-2	%10 in 50 years	0.61	1.44	0.57
DD-3	%50 in 50 years	0.33	0.76	0.30
DD-4	%68 in 50 years	0.26	0.60	0.24

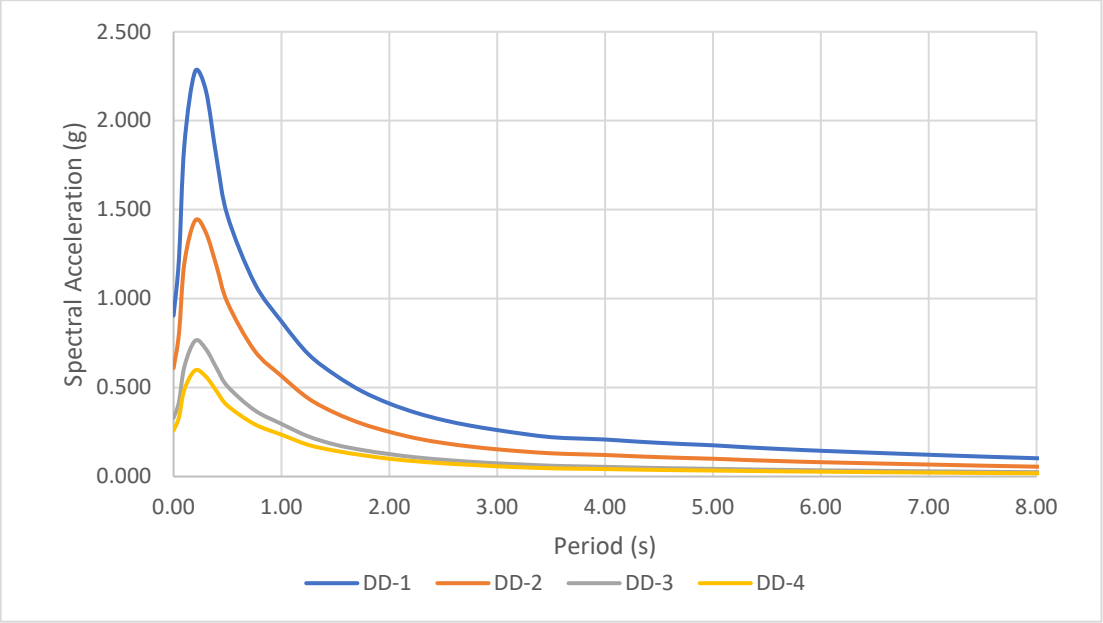

Figure 6.9 Horizontal Earthquake Design Spectra (Maximum Direction)

Probabilistic Vertical Spectral Acceleration values are given in Table 6.6. Vertical earthquake hazard spectrum plots are shown in Figure 6.10.

Table 6.6 Calculated Vertical Probabilistic PGA and Spectral Acceleration Values

Design Earthquake	Probability of Exceedance	Vertical Component		
		PGA	S_s(T=0.2 sec)	S_1(T=1 sec)
DD-1	%2 in 50 years	0.79	1.21	0.38
DD-2	%10 in 50 years	0.47	0.72	0.25
DD-3	%50 in 50 years	0.22	0.35	0.13
DD-4	%68 in 50 years	0.16	0.27	0.11

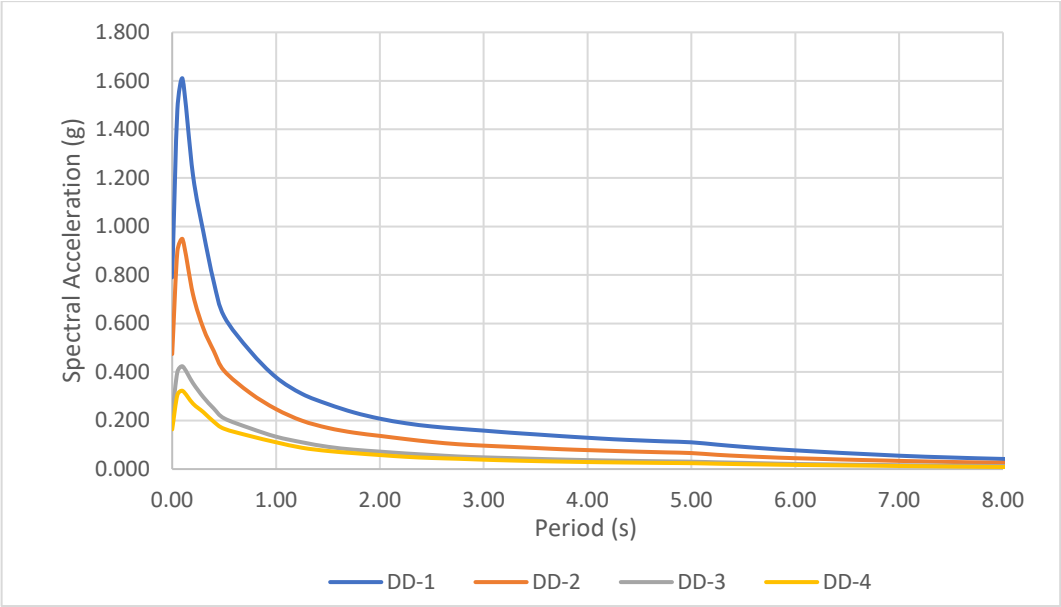

Figure 6.10 Vertical Earthquake Design Spectra

Average hazard spectrum, fault normal hazard spectrum, fault parallel hazard spectrum is calculated based on Somerville et al. (1997) and Abrahamson (2000). Near field hazard spectrums are given in Figure 6.11, Figure 6.12, and Figure 6.13.

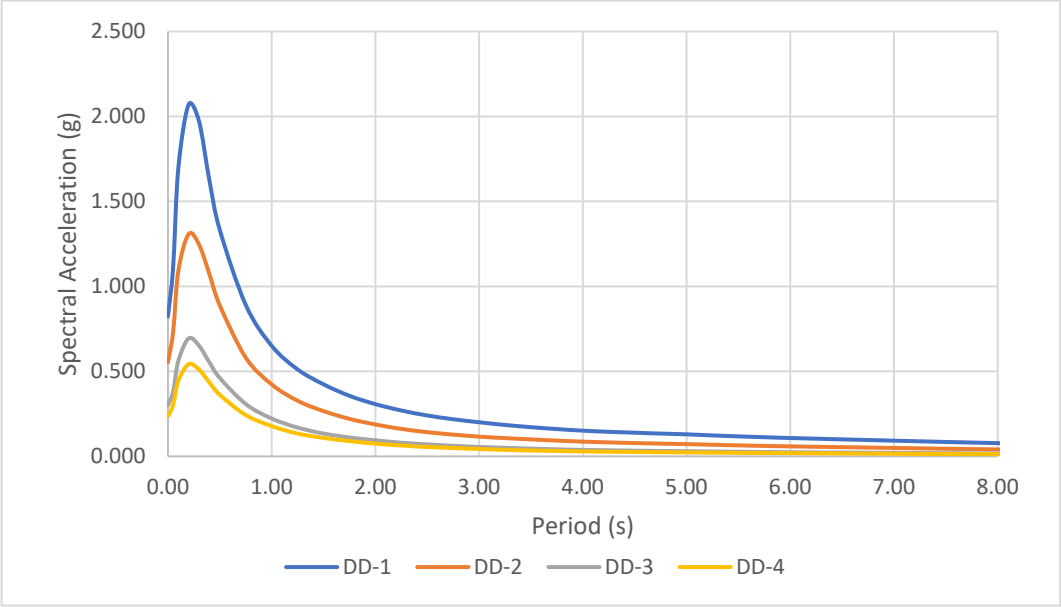

Figure 6.11 Near Field Average Hazard Spectrum (Directivity)

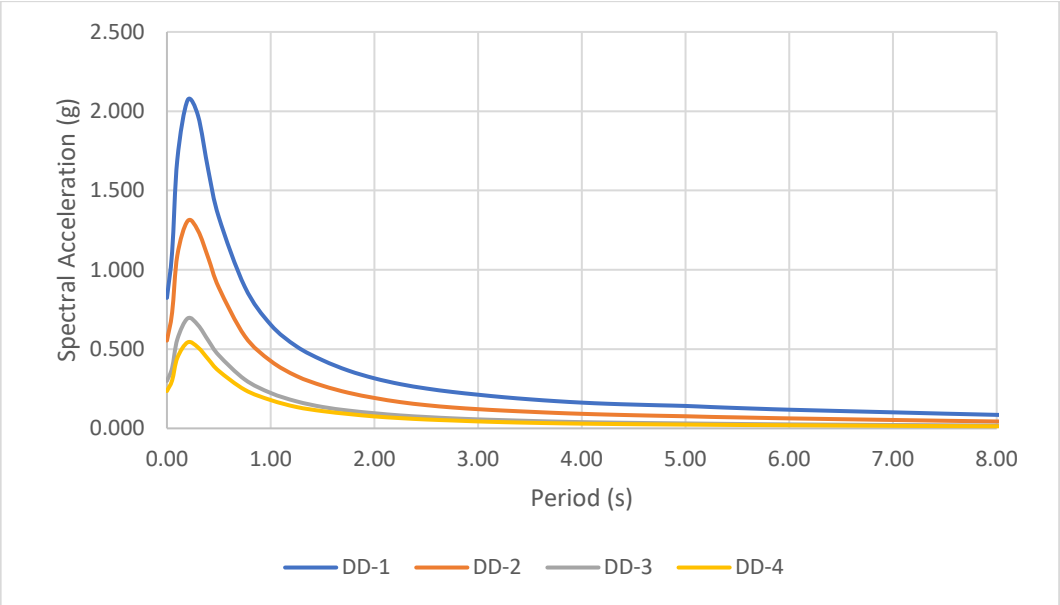

Figure 6.12 Near Field Fault Normal Hazard Spectrum

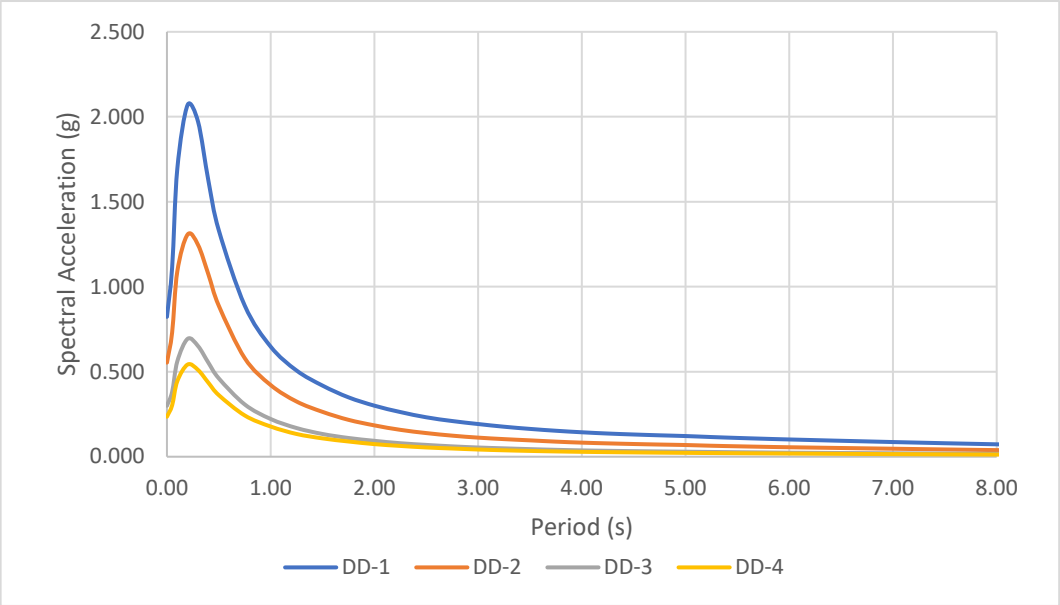

Figure 6.13 Near Field Fault Parallel Hazard Spectrum

6.7. Results of Probabilistic Seismic Hazard Analysis Using R-CRISIS

Additionally, seismic hazard analysis was performed using R-CRISIS software. Analysis results are given in Figure 6.14 and Figure 6.15. Line sources and area sources were also created based on the UDAP-Ç-13-06 document (2014) and SHARE Project. A comparison of EZ-Frisk and R-CRISIS analysis results are given in Figure 6.16.

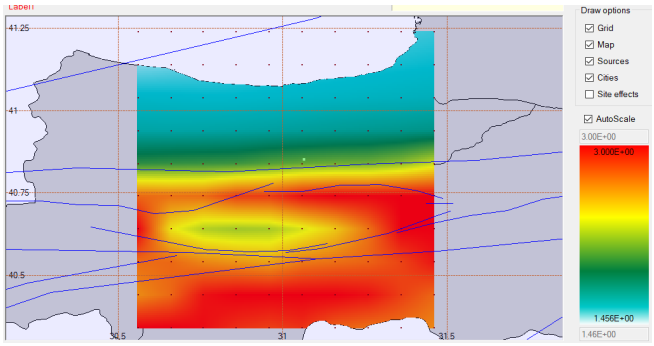

Figure 6.14 Seismic Hazard Map for T=0.2 sec

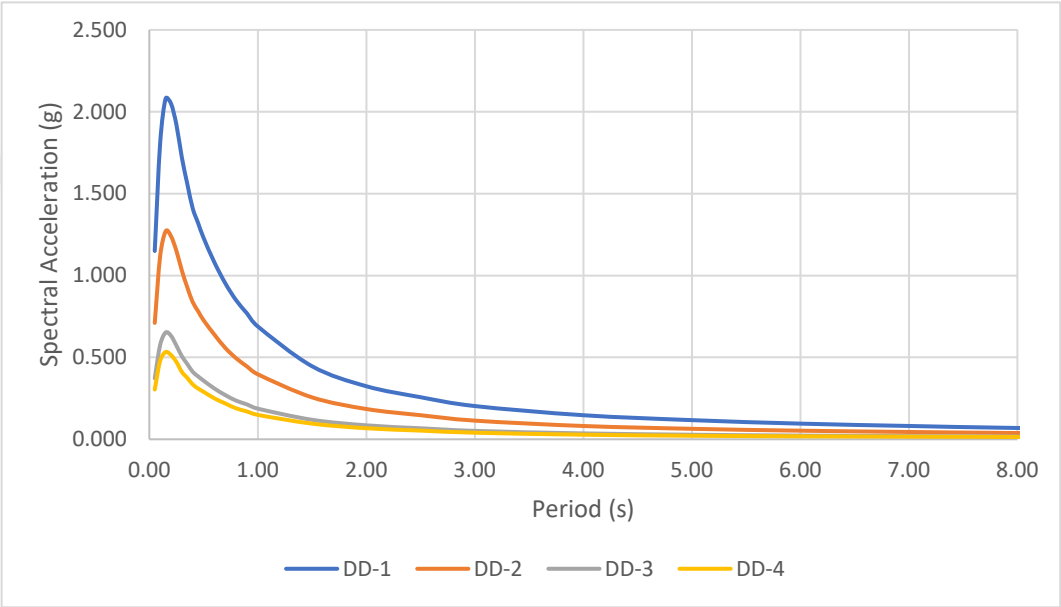

Figure 6.15 Horizontal Design Spectra using R-CRISIS

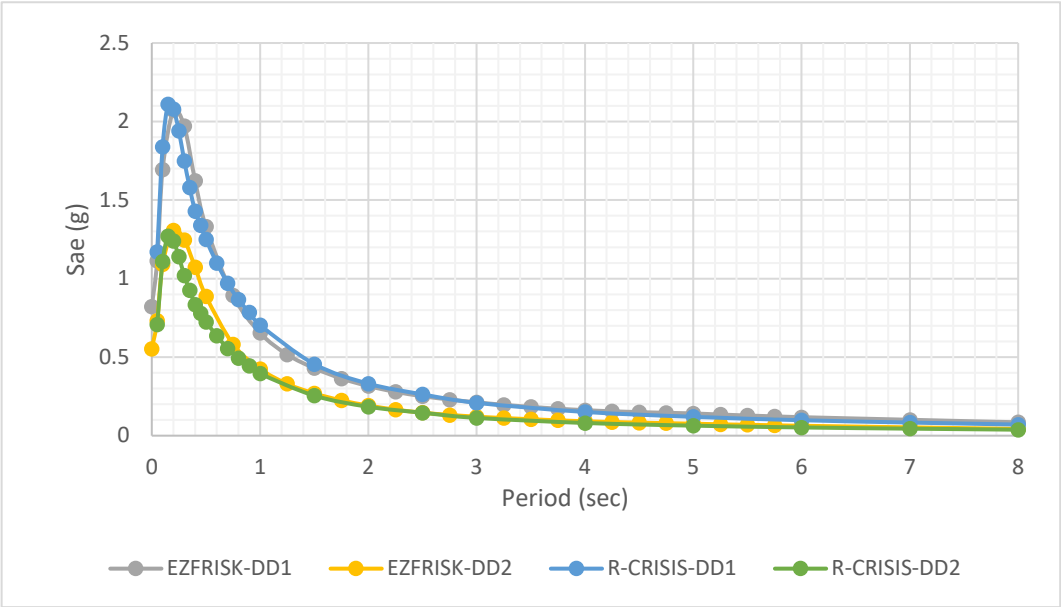

Figure 6.16 Comparison of EZ-Frisk and R-CRISIS results

6.8. De-aggregation of Probabilistic Seismic Hazard Analysis Results and Deterministic Earthquake Hazard

As a result of the de-aggregation of probabilistic earthquake hazard analysis results, it was observed that earthquakes occurred 0-50 km from the project site that cumulated between 5.50-6.0 and 7.0-7.5 magnitudes. De-aggregation analysis results are shown in Figure 6.17.

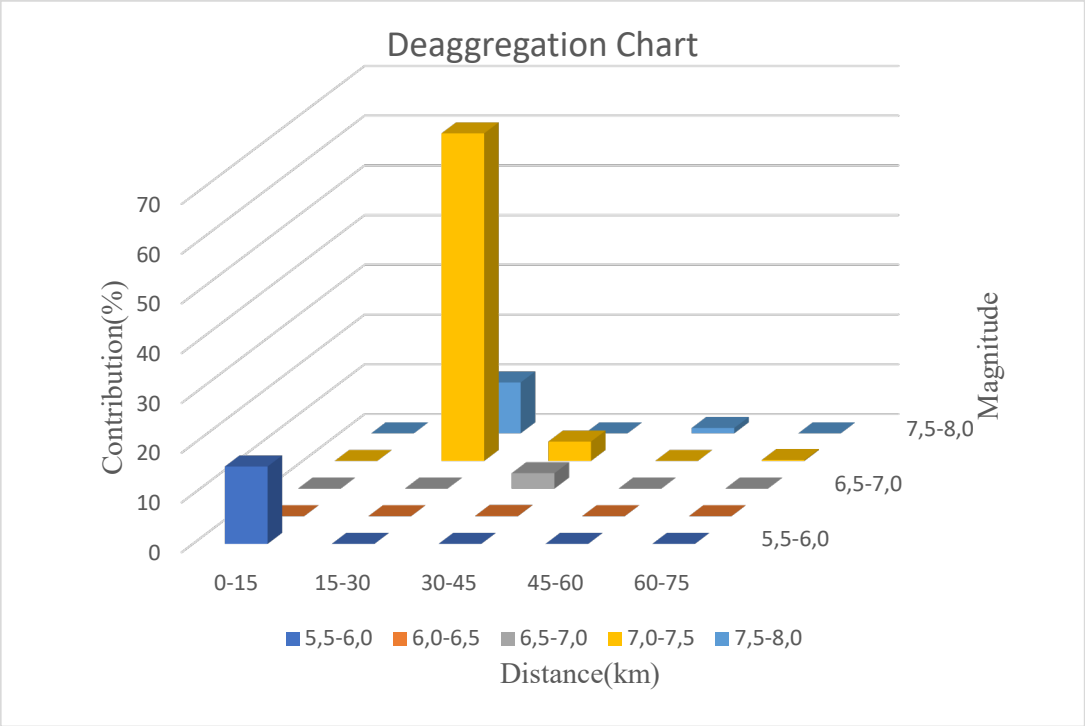

Figure 6.17 De-aggregation Analysis Results

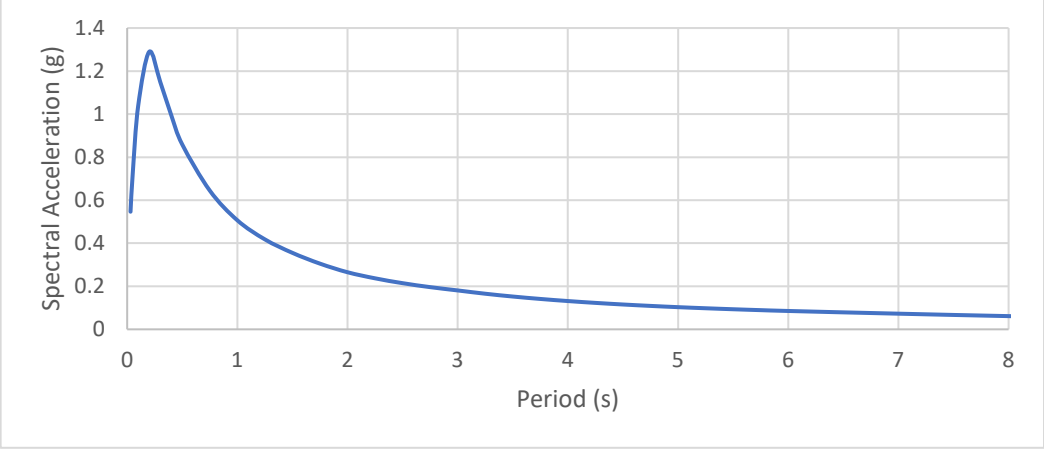

Figure 6.18 Deterministic Seismic Hazard Analysis Results

CHAPTER 7

SELECTION AND SCALING OF SITE-SPECIFIC EARTHQUAKE GROUND MOTIONS

7.1. Introduction:

In TBDY-2018, at least eleven earthquake ground motion sets are required to be selected for analysis in the time history. In this study, according to TBDY 2018, the following items were considered in the selection of 11 ground motion sets compatible with DD-1 and DD-2 spectra:

For the structural systems, the selection of the earthquake records to be used in the earthquake calculation to be made in the time history will be made by considering the earthquake magnitudes compatible with the earthquake ground motion level, fault distances, source mechanisms and local ground conditions. If there are historical earthquake records compatible with the earthquake ground motion level in the area where the building is located, these records will be used.

The number of earthquake records to be selected for one- or two-dimensional calculation and earthquake record sets to be selected for three-dimensional calculation will be at least eleven. The number of recording or recording sets to be selected from the same earthquake shall not exceed three.

The amplitudes of the earthquake ground motion components shall be scaled according to the rule that the amplitudes of the resultant spectrum between the periods of 0.2Tp and 1.5Tp (Tp = the dominant natural vibration period of the building) should not be less than 1.3 times the amplitude of the earthquake design spectrum in the same period interval. Scaling of both components will be done in the same proportions. In the time history field of earthquake insulated buildings, $0.5T_M$ instead of 0.2Tp will be used instead of 0.2Tp and $1.25T_M$ will be used instead of 1.5Tp. T_M represents the effective vibration period calculated with the upper limit values of the earthquake insulated building.

7.2. Selection of Earthquake Ground Motion

Eleven acceleration records were selected and presented in detail with the help of the Pacific Earthquake Engineering Research Centre (PEER) Ground Motion Database (https://ngawest2.berkeley.edu/) considering the near field fault normal and fault parallel hazard spectrum obtained from probabilistic seismic hazard analysis. Earthquake records, earthquake magnitudes, fault type, fault distance, $V_{s,30}$ values, measurement source mechanisms, and scaling factors were considered when selecting earthquake records. The target spectrum for DD-1 and DD-2 earthquake levels is given in Figure 7.1 and Figure 7.2.

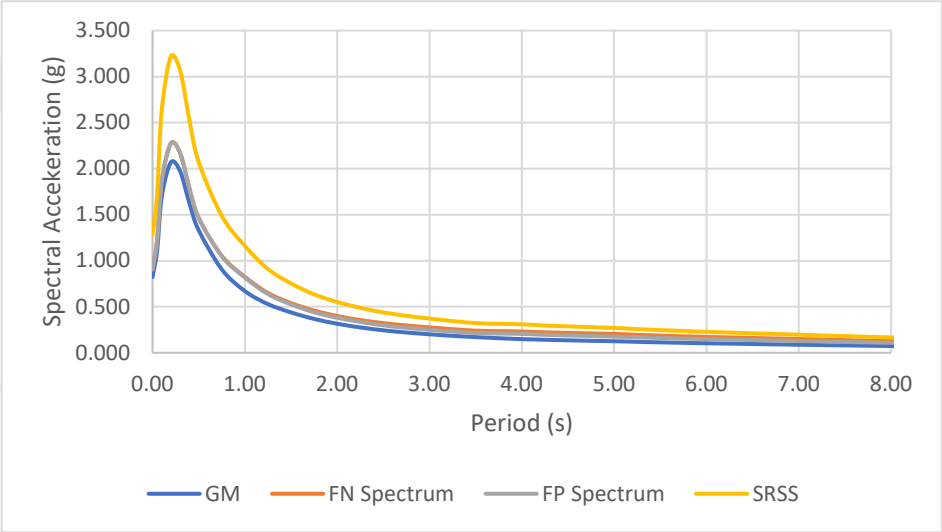

Figure 7.1 DD-1 Level Target Spectrum

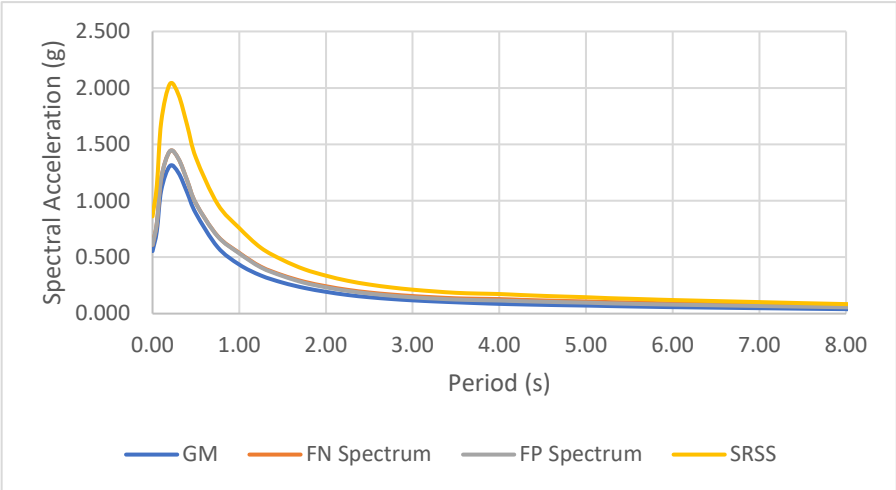

Figure 7.2 DD-2 Level Target Spectrum

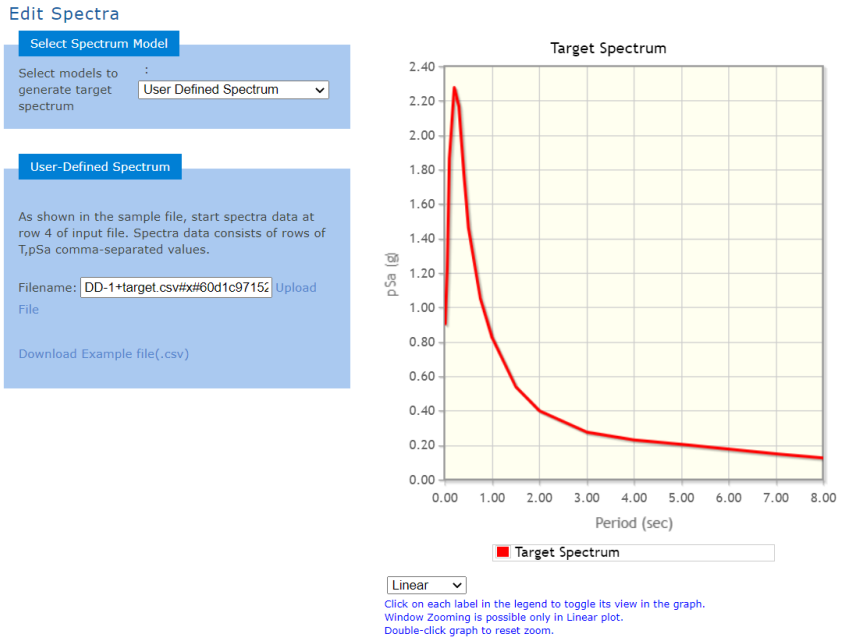

Figure 7.3 User Defined Spectrum screen for NGAWest2 database

The main seismic source in the vicinity is strike-slip faults. These parameters are used while selecting ground motion data. Since the distance to a fault has a high impact on ground motion attenuation, the selection was made considering these input data.

The input compatible with site data is as follows and is used to select earthquake ground motion data.

Fault type: All Types Magnitude: 6-9 R_{JB}(km): 0-40

R_{rup}(km): 0-40 Vs_{30} (m/s): 600-1000 D5-95 (sec): 10, 60

The SRSS method is used as described in the Turkish Seismic Code. Initial scale factor is determined as 0.25-4.0 for DD-1 level 0.5-2.0 for DD-2 level.

The natural period of structure for the base-isolated part is 2.9-4.4 seconds, as given below. The fixed base structures have 0.4 seconds. When conditions given in TBDY 2018 is considered, the minimum period points were taken as 0.15 sec – 6 sec for DD1 ground motion selection.

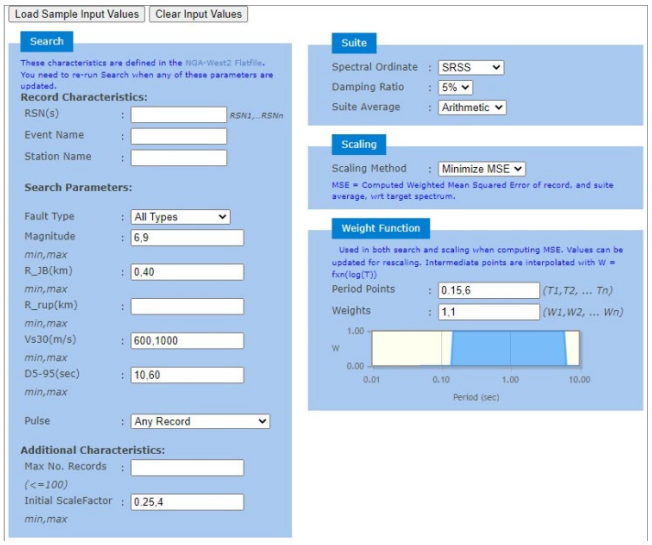

Figure 7.4 Input Screen for NGAWest2 Database, https://ngawest2.berkeley.edu/

The list of ground motions used for scaling in the case study is given in Table 7.1.

Table 7.1 Earthquake Record Information

	Spectral Ordinate	Record Sequence Number	Eartquake Name	D5-95(s)	Arias Intensity (m/s)	Year	Station	Magnitude	Mechanism	Rjb(km)	Rrup(km)	Vs30(m/s)	Scale Factor-DD-1	Scale Factor-DD-2
1	SRSS	285	Irpinia, Italy-01	19.6	0.4	1980	Bagnoli Irpinio	6.9	Normal	8.14	8.18	649.67	2.9883	1.8693
2	SRSS	1111	Kobe, Japan	11.2	3.4	1995	Nishi-Akashi	6.9	strike slip	7.08	7.08	609	1.4678	0.9181
3	SRSS	1165	Kocaeli, Turkey	15.1	0.8	1999	Izmit	7.51	strike slip	3.62	7.21	811	2.3514	1.4709
4	SRSS	1633	Manjil, Iran	29.1	7.5	1990	Abbar	7.37	strike slip	12.55	12.55	723.95	1.0424	0.652
5	SRSS	1787	Hector Mine	11.7	1.9	1999	Hector	7.13	strike slip	10.35	11.66	726	1.9317	1.2083
6	SRSS	4841	Chuetsu-oki, Japan	15.8	0.7	2007	Joetsu Yasuzukaku Yasuzuka	6.8	Reverse	20.65	25.52	655.45	3.176	1.9867
7	SRSS	4858	Chuetsu-oki, Japan	17	0.5	2007	Tokamachi Chitosecho	6.8	Reverse	25.35	30.65	640.14	2.8752	1.7985
8	SRSS	4864	Chuetsu-oki, Japan	15.8	1.9	2007	Yoitamachi Yoita Nagaoka	6.8	Reverse	4.69	16.1	655.45	1.9082	1.1936
9	SRSS	5806	Iwate, Japan	17.4	0.7	2008	Yuzawa Town	6.9	Reverse	22.41	25.56	655.45	2.4551	1.5357
10	SRSS	5810	Iwate, Japan	27.3	0.5	2008	Machimukai Town	6.9	Reverse	21.07	24.1	655.45	2.8296	1.7699
11	SRSS	6928	Darfield, New Zealand	12.9	0.7	2010	LPCC	7	strike slip	25.21	25.67	649.67	2.6328	1.6469

7.3. Spectral Matching

Acceleration records were examined separately with SeismoSignal software, and necessary records were corrected with Baseline Correction. Spectral matches were performed by using the SeismoMatch software. For DD-1 Plots of mean spectral acceleration, velocity spectra, displacement spectra are given in Figure 7.5 to Figure 7.10. For DD-2 Plots of mean spectral acceleration, velocity spectra, displacement spectra are given in Figure 7.11 to Figure 7.16. Original and matched earthquake records are given in the Appendix.

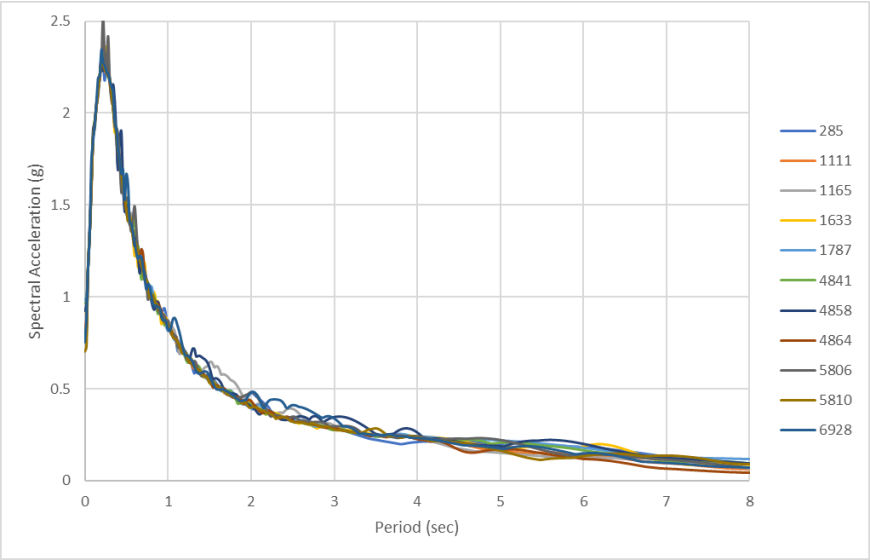

Figure 7.5 Spectral Acceleration of Matched Earthquakes FN Direction-DD1

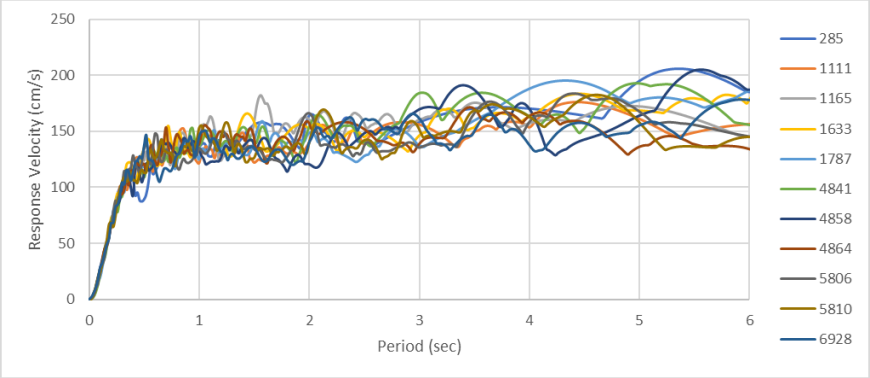

Figure 7.6 Velocity Spectra of Matched Earthquakes FN Direction-DD1

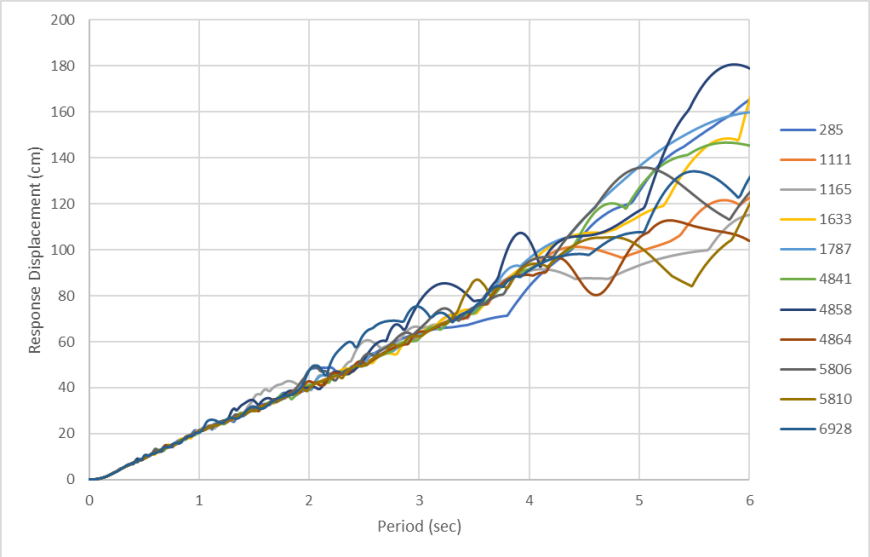

Figure 7.7 Displacement Spectra of Matched Earthquakes FN Direction-DD1

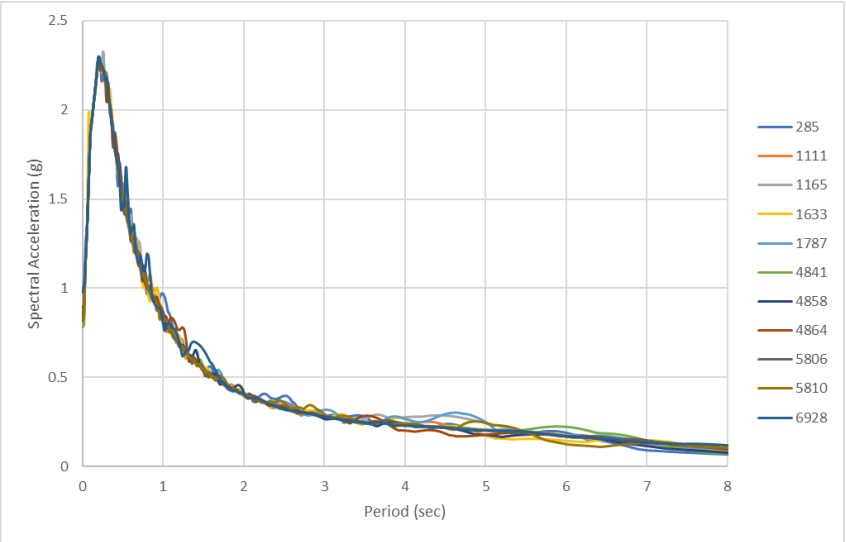

Figure 7.8 Spectral Acceleration of Matched Earthquakes FP Direction-DD1

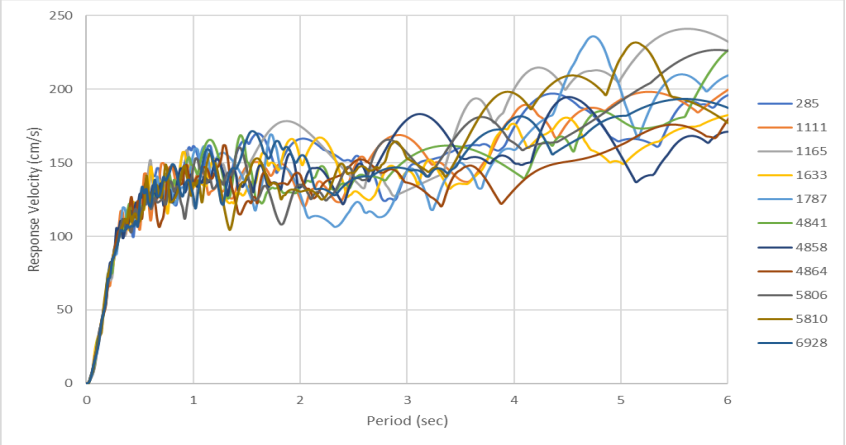

Figure 7.9 Velocity Spectra of Matched Earthquakes FP Direction-DD1

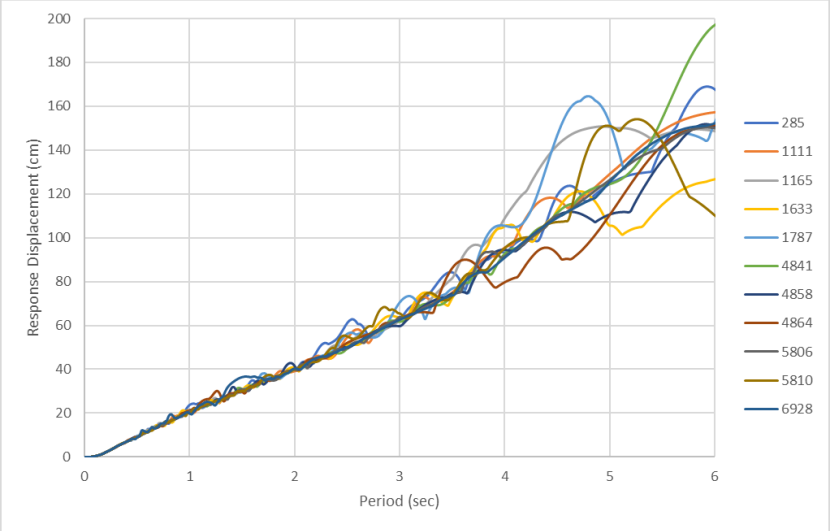

Figure 7.10 Displacement Spectra of Matched Earthquakes FP Direction-DD1

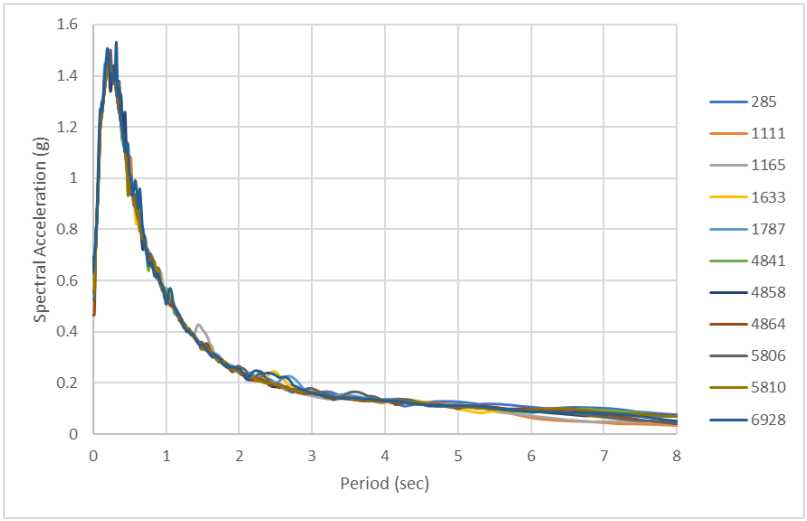

Figure 7.11 Spectral Acceleration of Matched Earthquakes FN Direction-DD2

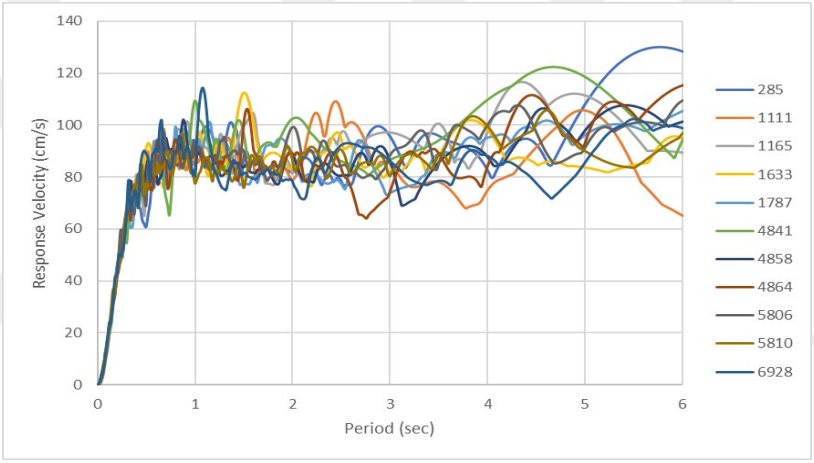

Figure 7.12 Velocity Spectra of Matched Earthquakes FN Direction-DD2

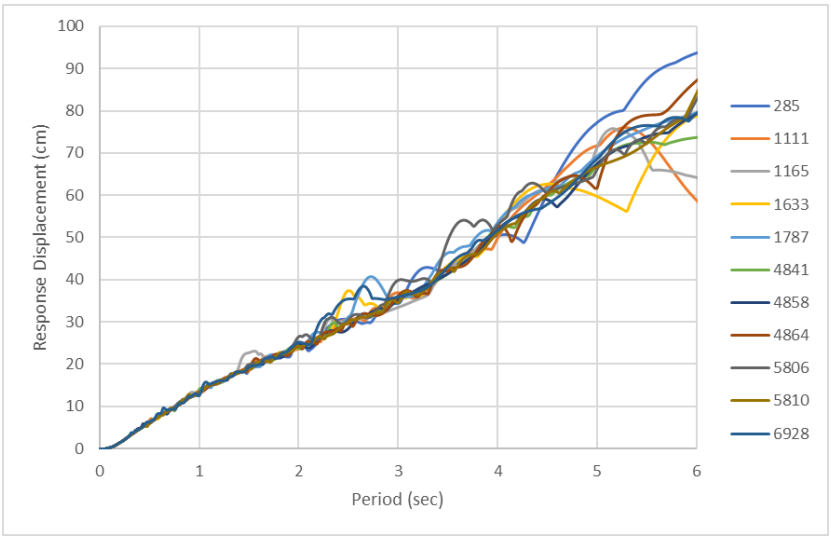

Figure 7.13 Displacement Spectra of Matched Earthquakes FN Direction-DD2

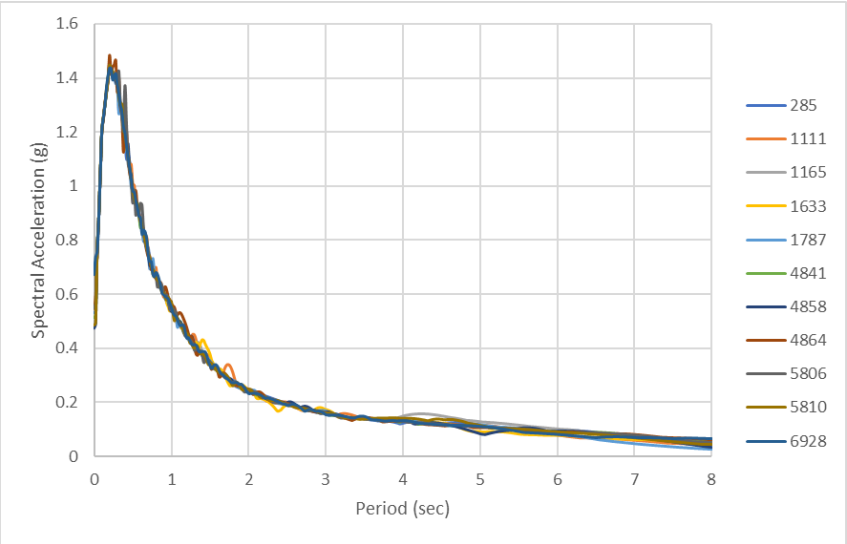

Figure 7.14 Spectral Acceleration of Matched Earthquakes FP Direction-DD2

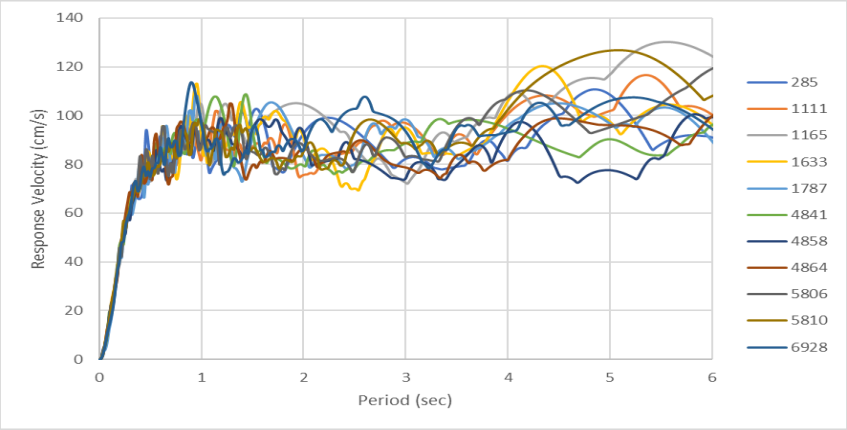

Figure 7.15 Velocity Spectra of Matched Earthquakes FP Direction-DD2

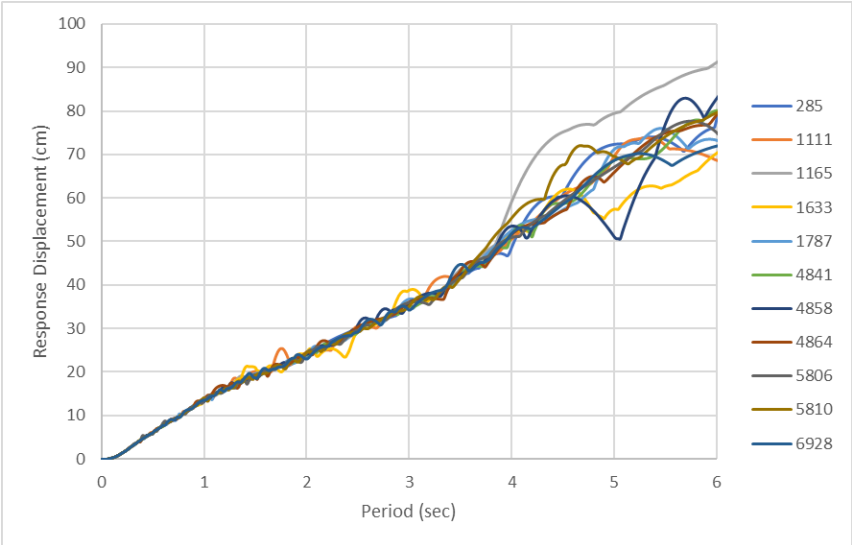

Figure 7.16 Displacement Spectra of Matched Earthquakes FP Direction-DD2

CHAPTER 8

SITE-SPECIFIC RESPONSE ANALYSIS

8.1. Introduction

To determine the site-specific earthquake spectrum at the ground surface, the ratio of the ground surface spectral acceleration to the bedrock spectral acceleration for each spectral period. Then the average of these ratios for 11 records was defined as the local soil effect coefficient for the relevant period. These coefficients were multiplied by the corresponding baseline spectrum. After that, the site-specific response spectrum at the ground surface was determined. According to TBDY-2018, the non-linear analysis was performed in the time domain on the liquefaction potential.

In this chapter site-specific response analyses were performed by DeepSoil v7 (Nonlinear and Equivalent Linear Seismic Site Response of One-Dimensional Soil Columns-University of Illinois) software with eleven earthquake records. First, not improved then improved spectrum were represented.

8.2. Site-Specific Response Analyses

Due to different soil layers the ground motion changes as the earthquakes move from the bedrock to the surface. The change of seismic waves in terms of amplitude, duration, and frequency content at any depth can be determined by ground motion analysis. Local soil stratigraphy, material properties, area topography, groundwater depth, and earthquake characteristics significantly impact ground motion analysis modeling.

The site-specific spectrum analysis was performed with DeepSoil v7 in one-dimension to transfer the earthquakes that occurred in the bedrock to the ground. The spectral accelerations transmitted from the ZB soil to the surface were determined using the General Quadratic/Hyperbolic Model (GQ/H) for the soil models and Rigid Half-Space Model (If a rigid half-space is being used, no input parameters are required) for the bedrock model.

Darendeli (2001) study constructed a shear strength-shear strain curve based on experimental data. At small strains, the resonance column test is used to collect data, and for medium shear strain levels, the torsional shear test results are used. This value is extrapolated at large strain levels. This extrapolation method may underestimate or overestimate the shear strength under large strains. Therefore, the shear strength must be corrected to account for the correct shear strength at large strains (Phillips and Hashash 2009). The general quadratic/hyperbolic model proposed by Groholski et al. 2016 has a curve fitting scheme that can automatically correct the reference curve according to the specified large strain shear strength (for example, Darendeli (2001)).

The general quadratic/hyperbolic shear model is a simple soil model, which defines the backbone curve of the nonlinear shear strain-shear stress relationship, as described by Groholski et al. This model is attractive because it defines a smooth transition between linear elastic shear stiffness and shear strength. Linear elastic shear stiffness directly comes from Young's modulus and Poisson's ratio. For a given hydrostatic pressure, the shear strength can be calculated from the cohesion and friction angle of the Mohr-Coulomb parameters:

$$G_{max} = \frac{E}{2(1-\mu)} \tag{8.1}$$

$$\tau_{max} = c + \sigma \, tan\emptyset \tag{8.2}$$

Linear elastic shear stiffness and shear strength define the asymptote of the general quadratic/hyperbolic shear model. The shear strain value defines the intersection of the asymptotes and is defined by the following formula:

$$\gamma_r = \frac{\tau_{max}}{G_{max}} \tag{8.3}$$

The smooth transition curve between linear elastic shear stiffness and shear strength is defined by the second-order relationship between shear strain and shear stress, where the fitting parameters can be defined between zero and one:

$$\frac{\tau}{\tau_{max}} = \frac{1+\frac{\gamma}{\gamma_r}-\sqrt{\left(1+\frac{\gamma}{\gamma_r}\right)^2-4\theta_\tau\frac{\gamma}{\gamma_r}}}{2\theta_\tau} \tag{8.4}$$

Figure 8.1 shows the asymptotes and backbone curves for G_{max} = 5000 kPa and τ_{max} = 10 kPa when the fitting parameters θ_τ= 0.1 and θ_τ = 0.9.

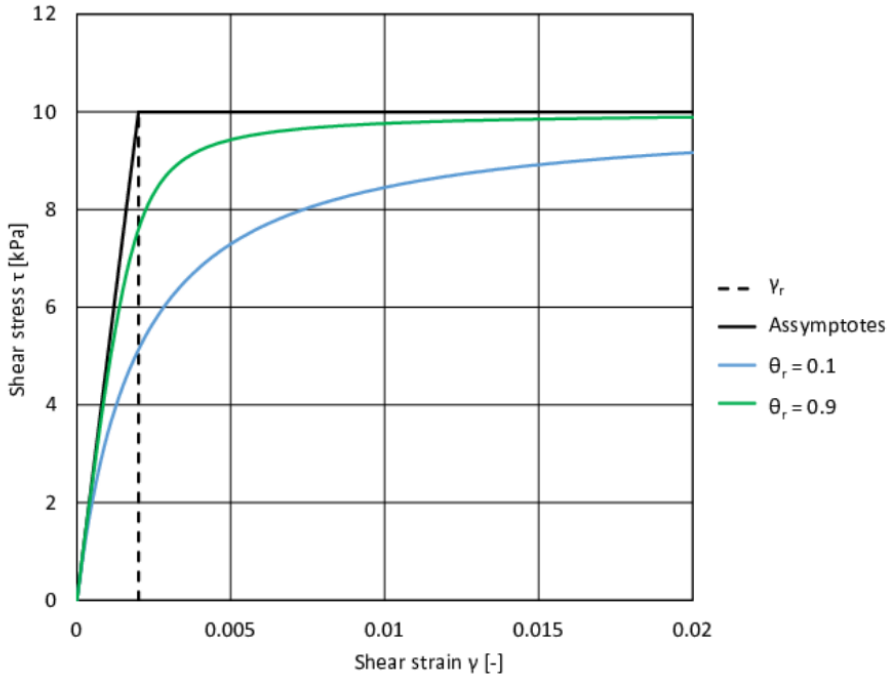

Figure 8.1 General Quadratic/Hyperbolic Shear Model

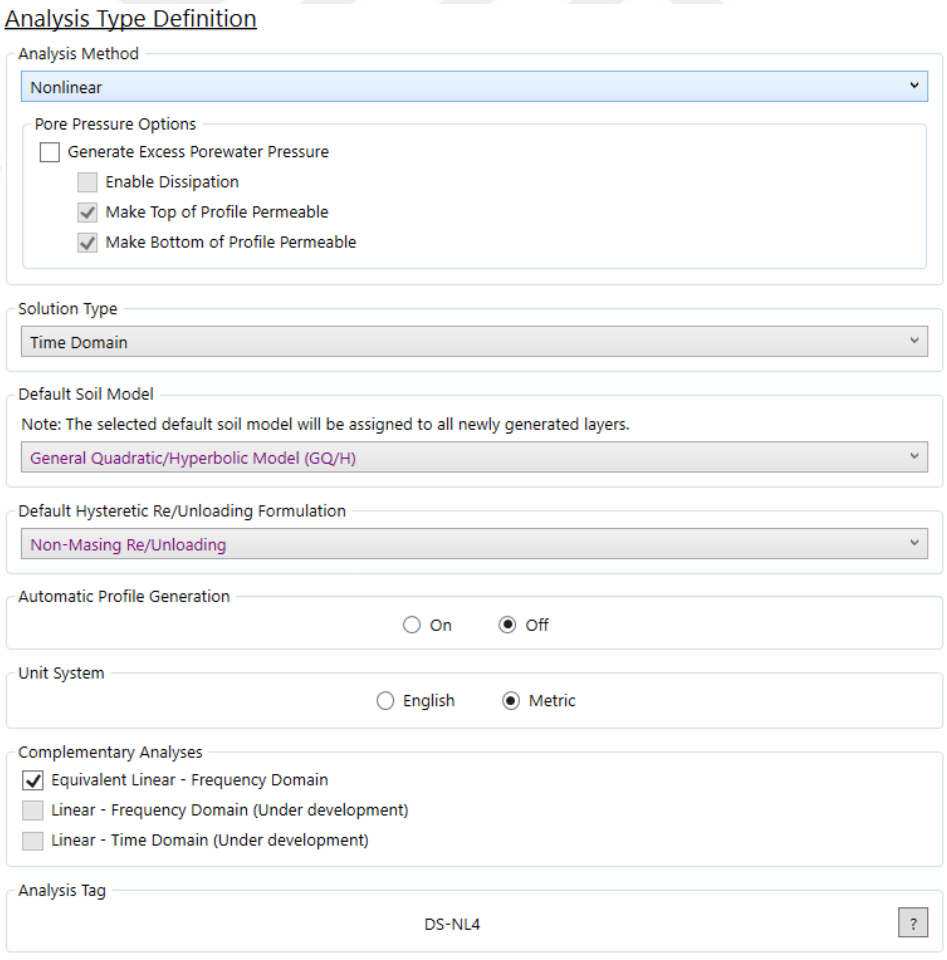

Figure 8.2 Analysis Method Definition

For clay and sand layers, Darendeli (2001) was used while creating material models with Deep-Soil software. The use of the GQ/H model requires the input of the shear strength of the soil layer to represent the large strain behavior of the soil. The target shear strength of the nonlinear shear modulus reduction (G/Gmax) is calculated using the Mohr-Coulomb equation as:

$$\tau_{target} = C_{Vs} + \sigma_v' \times tan\emptyset \tag{8.5}$$

$$c_{vs} = \rho \times V_s^2 \times 0.8 \times 0.1\% \tag{8.6}$$

Using modulus reduction and damping curve fitting (MRDF) with UIUC reduction coefficient to capture non-Masing behavior, and considering the modulus reduction curve, the GQ/H model is suitable for up to 0.05% if the following conditions are met the shear strain range: when the shear strain is 10%, the shear stress reaches 95% of the target shear strength. The fitting modulus reduction and damping curve and the fitting range of the 57th layer is shown in Figure 8.3 and Figure 8.4.

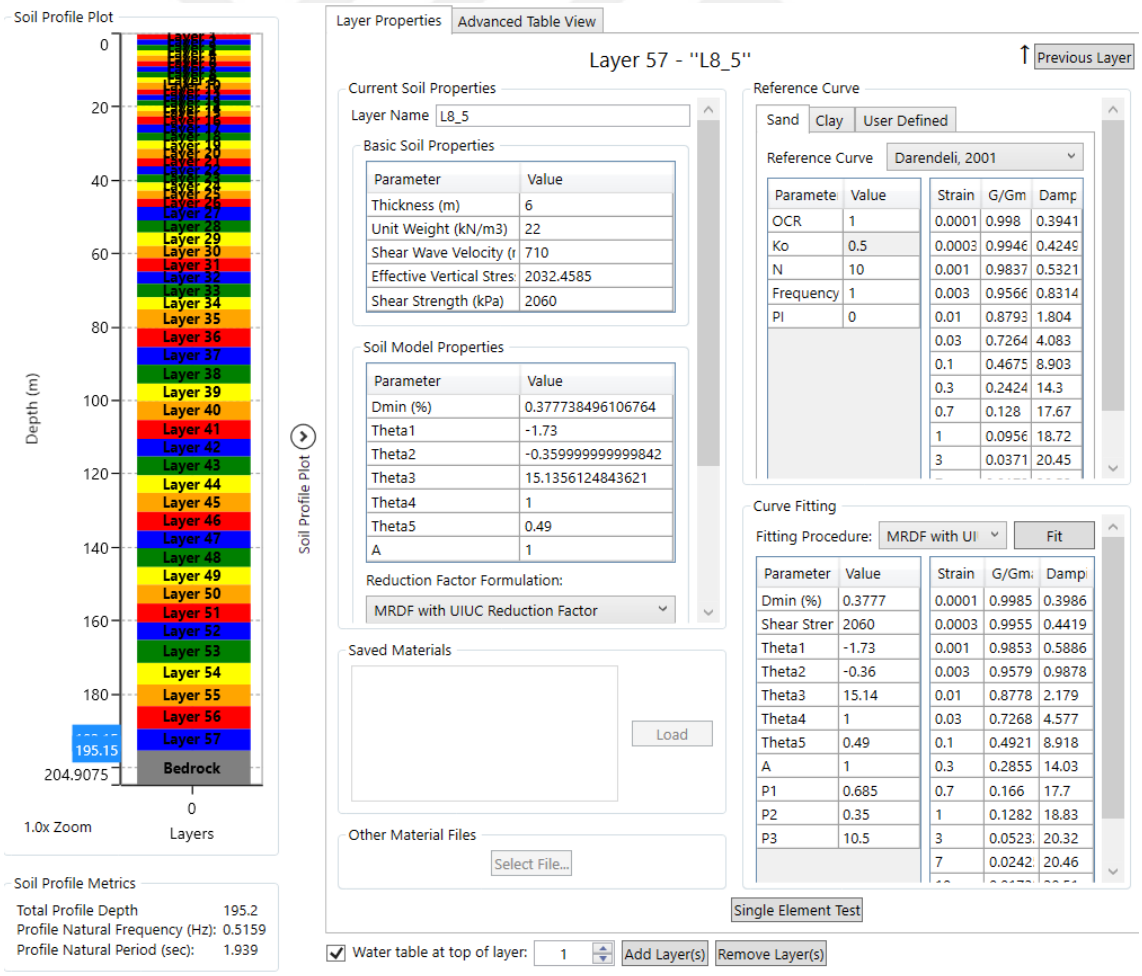

Figure 8.3 Definition of Darendeli (2001) Parameters

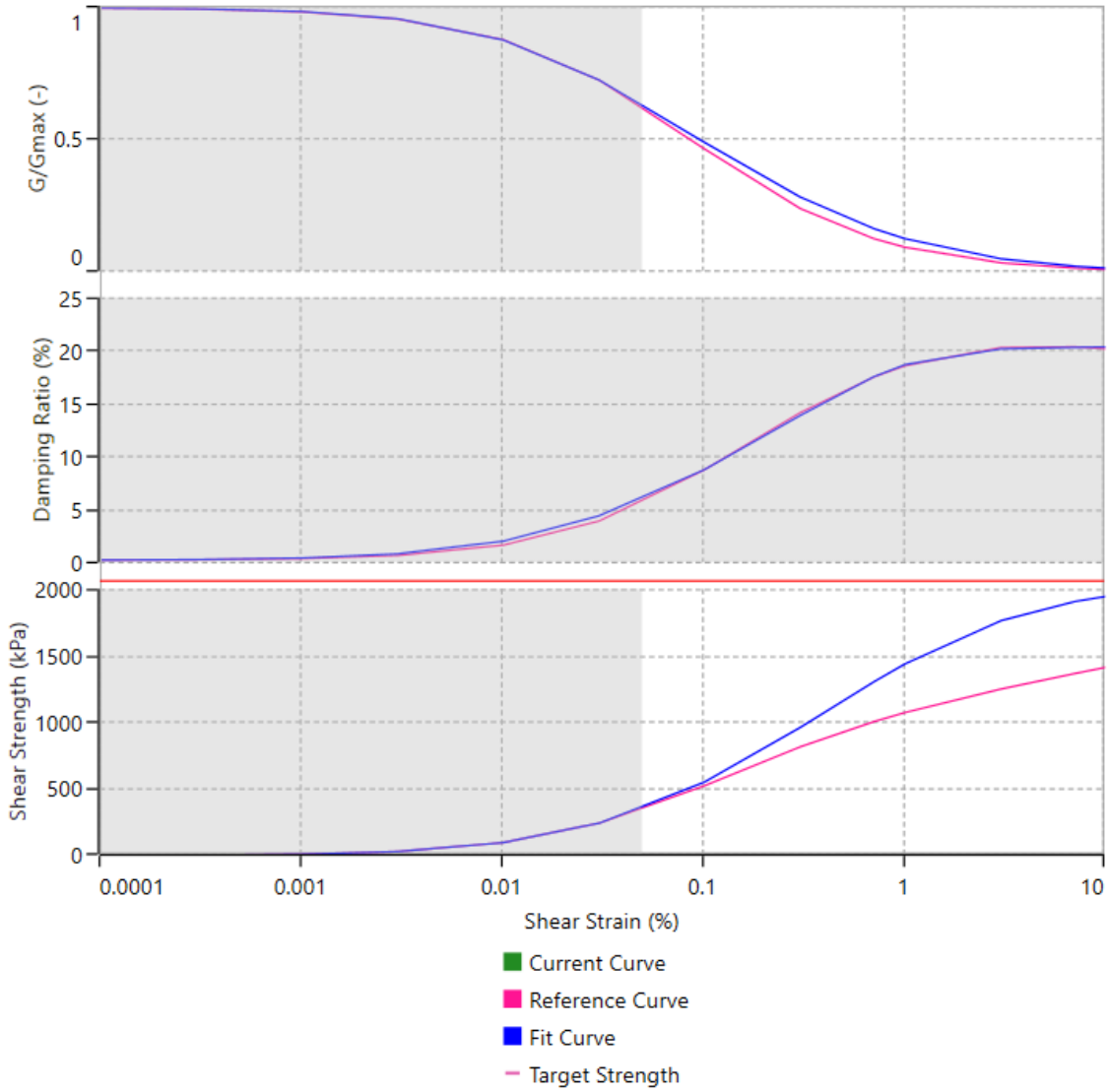

Figure 8.4 Darendeli (2001) Dynamic Curve of the 57th layer

The maximum frequency is the highest frequency that the layer can propagate, and its calculation formula is: $f_{max} = V_S/4H$, where V_S is the shear wave velocity of the layer and H is the thickness of the layer. In order to increase f_{max}, the thickness of the layer should be reduced. This is only checked for time domain analysis. It is recommended that the maximum frequency of each layer is the same throughout the soil profile, although this is not required. For all layers, the maximum frequency should generally be at least 30 Hz. Dynamic material parameters determined for soil behavior analysis are given in Figure 8.5.

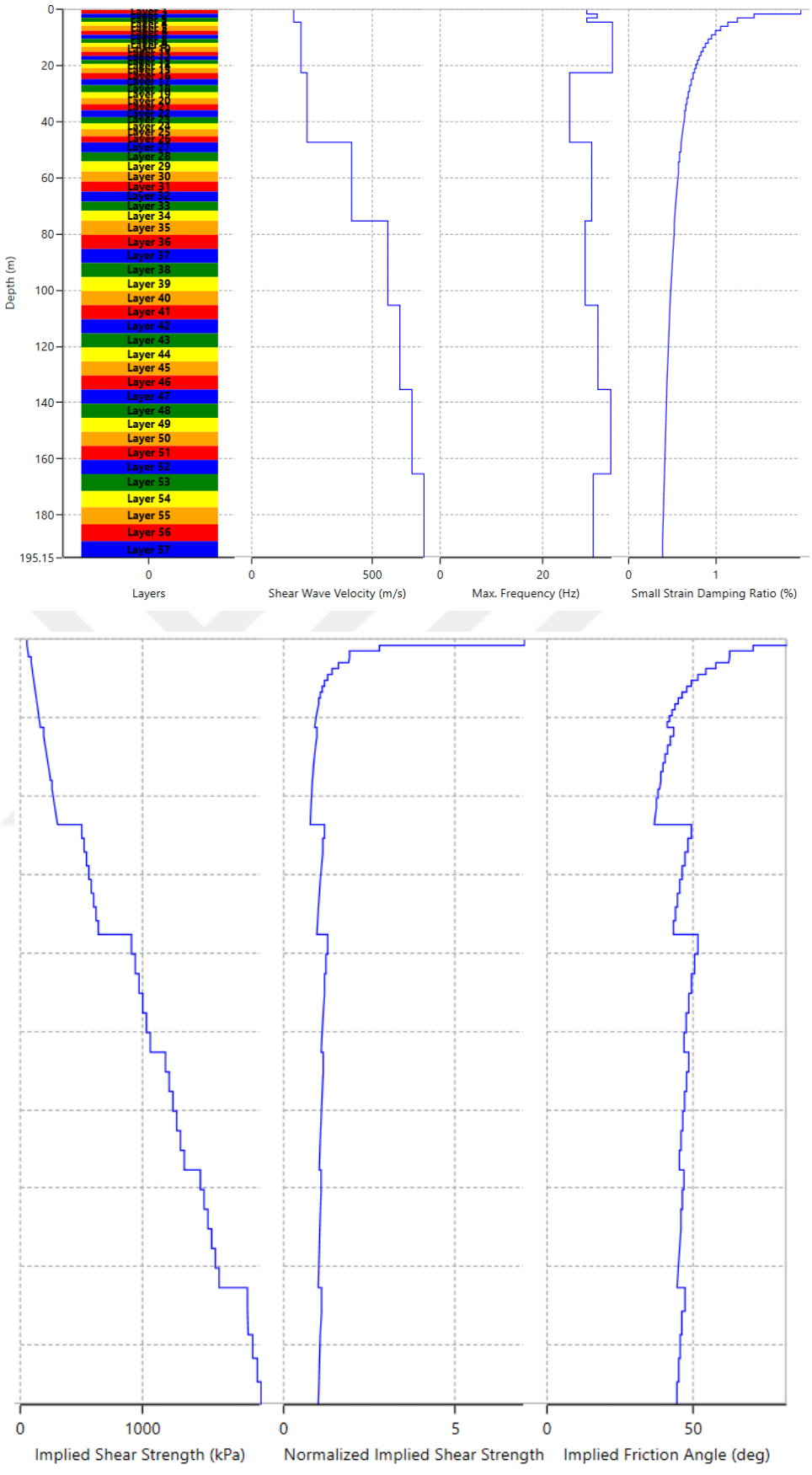

Figure 8.5 Soil Profile and Parameters

Parameters for nonlinear analysis are assigned as:

For frequency-domain analysis:

- Number of iterations: 15
- Effective Shear Strain Ratio (SSR): 0.65
- Complex Shear Modulus Formulation: Frequency-Independent

For nonlinear (time-domain) analysis:

- Step Control: Flexible
- Maximum Strain Increment: 0.005 %
- Time History Interpolation Method: Linear in time domain

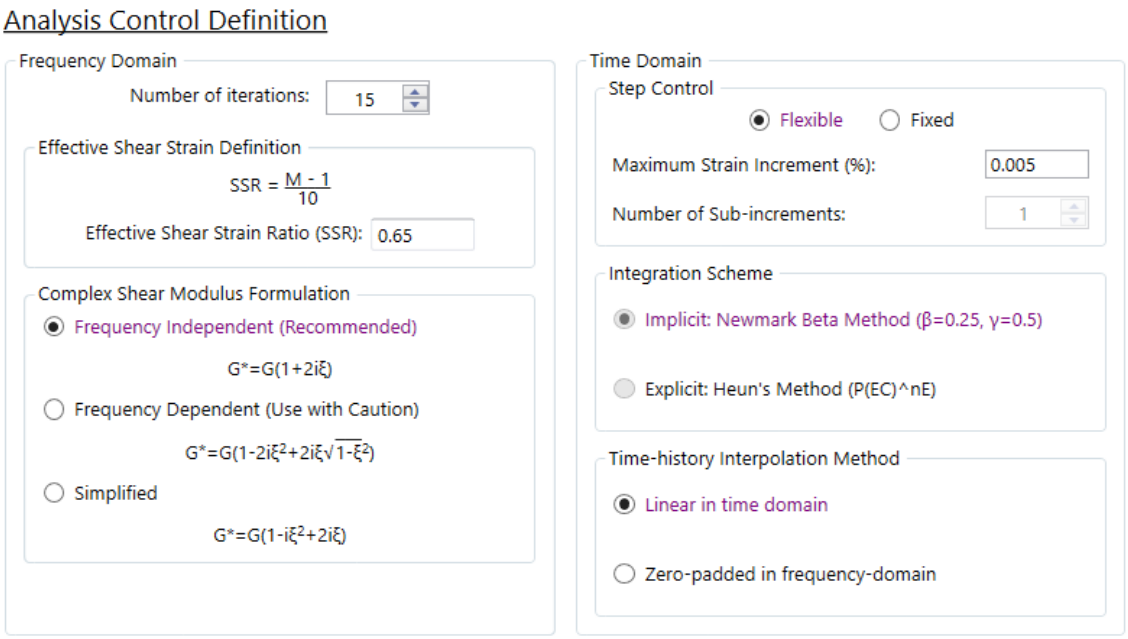

Figure 8.6 Analysis Control Definition

According to site specific response analysis results, the spectral acceleration parameters on the ground surface were obtained to use in structural dynamic analysis are given in Figure 8.7 to Figure 8.13.

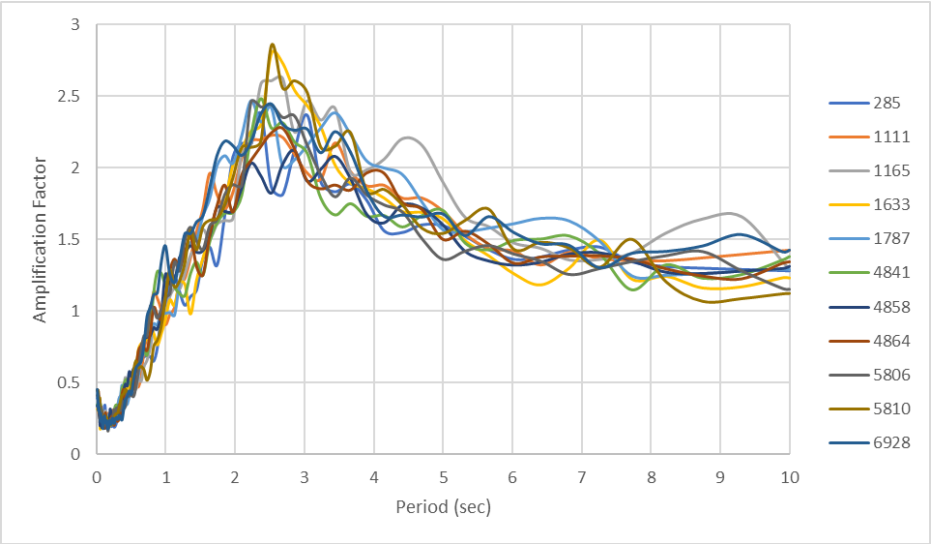

Figure 8.7 Amplification Factor of Non-Improved Soil for DD-1 Level

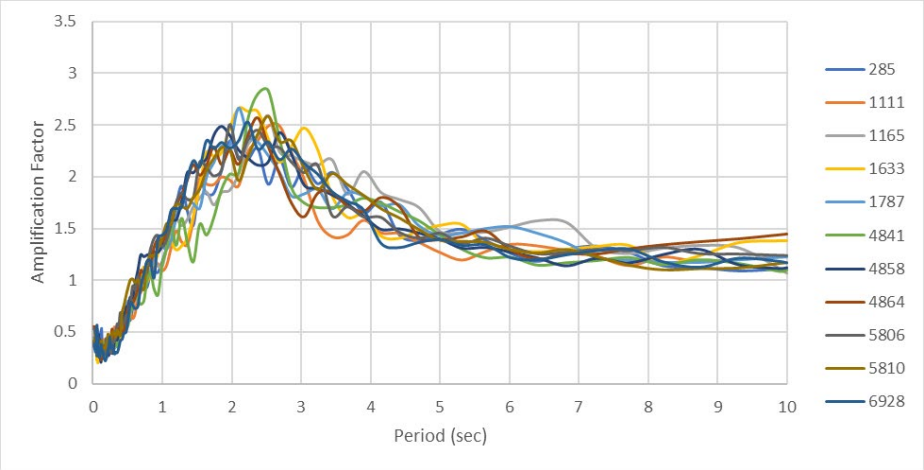

Figure 8.8 Amplification Factor of Non-Improved Soil for DD-2 Level

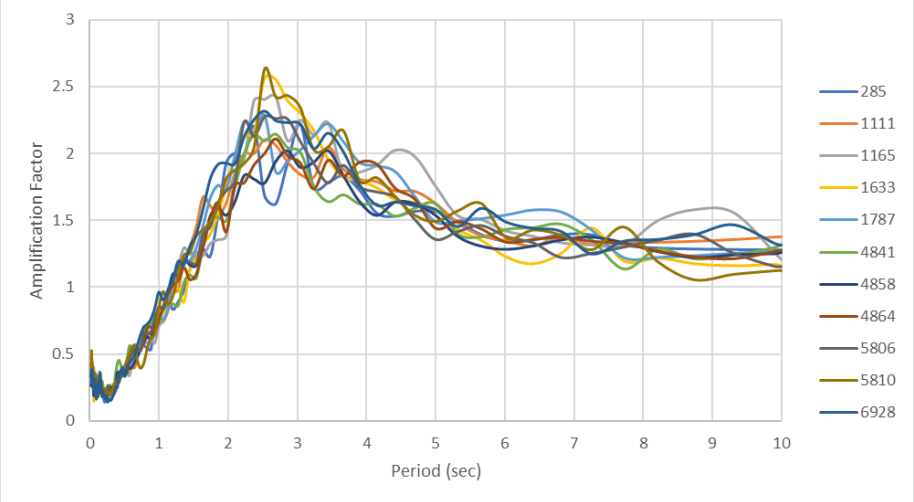

Figure 8.9 Amplification Factor of Improved Soil for DD-1 Level

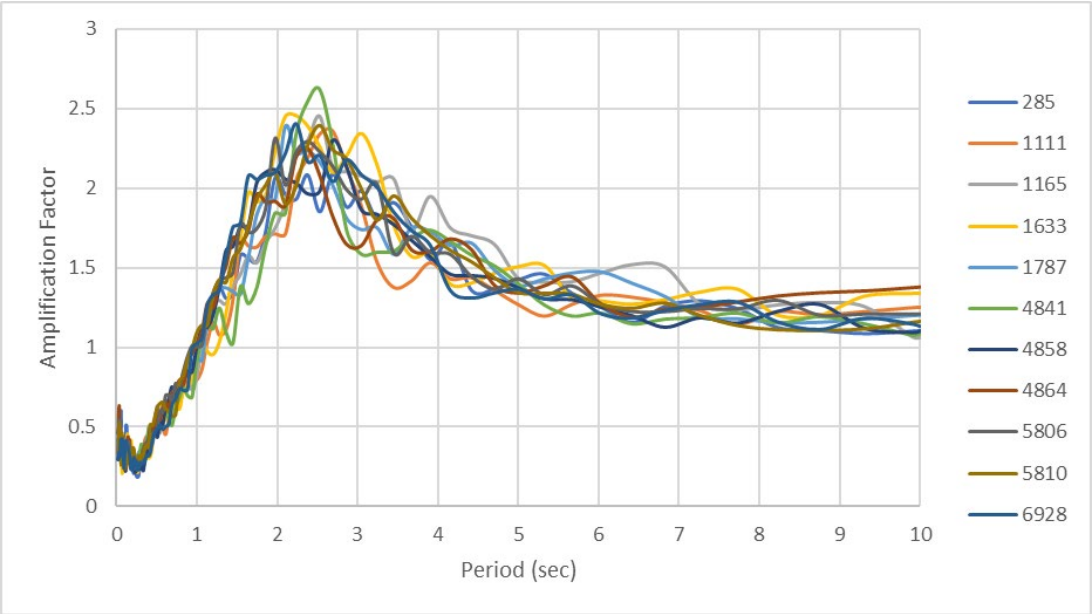

Figure 8.10 Amplification Factor of Improved Soil for DD-2 Level

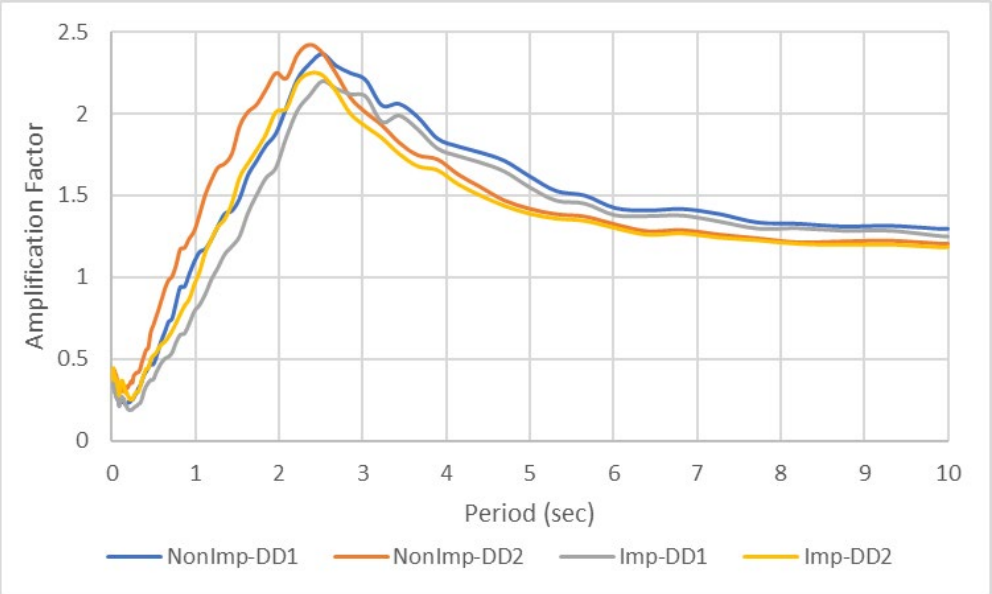

Figure 8.11 Mean Amplification Factor of Non-Improved and Improved Soil

The natural period of the soil strata is between 1.7-2.2 seconds. The mean amplifications were obtained at around 2.2 seconds where it is at the edge of natural period of the soil. The main results indicate a linear amplification factor in displacement zone (after 6 seconds) of the spectrum. The other result is that the amplification is lower than unity between 0.1 to 1 seconds which decreases the outcrop motion spectrum at this zone. Improvement affects the spectrum with lowering the spectral accelerations for the 20 m/200 m thickness in this study.

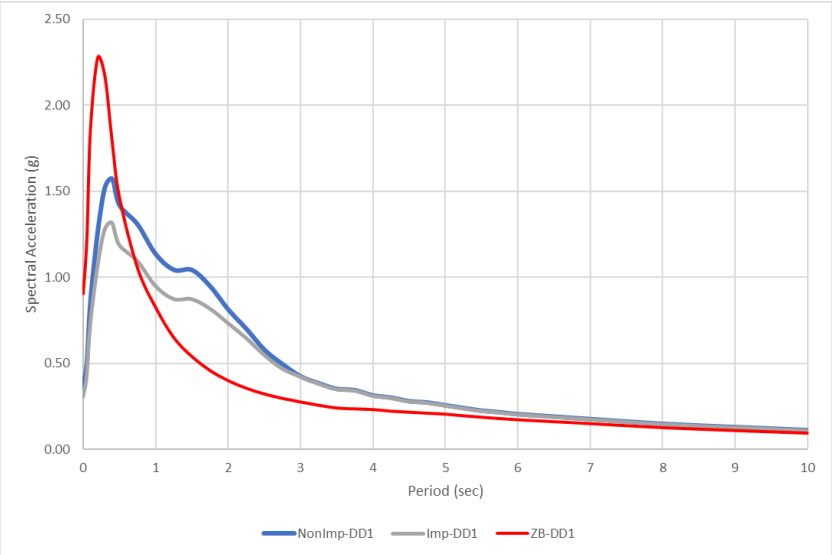

Figure 8.12 Horizontal Elastic Response Spectrum of Non-Improved and Improved Soil for DD-1 Level

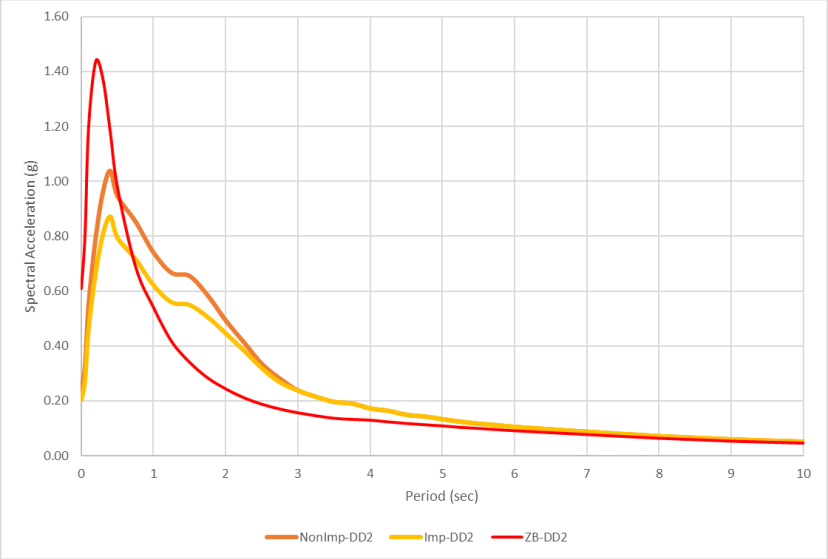

Figure 8.13 Horizontal Elastic Response Spectrum of Non-Improved and Improved Soil for DD-2 Level

It is noted that the improvement process has an influence on the spectral accelerations where the periods are up to 2.5 seconds. Basically, it can be discussed that improvement has no effect on the structures those demands higher displacements such as base-isolated structures. The second argument is that the acceleration part of the spectrum is almost two thirds of the spectrum on the outcrop (engineering rock formation V_s>760 m/s). this result is important that the thick soil strata has lower bound impact on the lower period structures where it has upper bound effect on higher period structures.

CHAPTER 9

CONCLUSION

This thesis aims to present an assessment on dynamic soil behavior and foundation system based on local geology, in-situ tests, seismic risks, liquefaction potential, seismic hazard assessment, selecting and scaling earthquake records the base-isolated factory planned in the Çilimli district, Düzce, Turkey.

Liquefaction analyses are conducted based on the in-situ test results. According to calculations, liquefaction potential is identified. Since there are liquefiable layers, the soil group is designated as ZF. According to the 2018 Turkish Building Earthquake Code, if the soil group underlying the site is defined as ZF, site-specific hazard assessment is required to determine the ground motion effect at the surface exerted by an earthquake.

In the definition of earthquake impact, first, methods of analyses in national and international regulations were investigated, then the earthquake levels suggested for the project were explained. Evaluation of the current earthquake hazard in the area where the project site is located; the general geology, tectonic features, soil conditions and engineering geology of the region and the seismotectonic units (existing fault systems) that may be the source of earthquakes that may affect the region, historical earthquakes that impact the region in general and the seismicity of the region with the last earthquakes in the region were examined. Probabilistic hazard analysis (PSHA) of the project site was carried out considering the local soil conditions and available data. PSHA calculations were performed for DD-1, DD-2, DD-3, and DD-4 seismic hazard levels considering V_s=760 m/sec. TBDY (2018) principles were considered in determining the earthquake design spectra and spectrum compatible ground motions. According to TBDY-2018, the non-linear analyses was performed in the time domain in order to assess the liquefaction potential.

A database of near-fault ground motion records including the effects of forward directivity is evaluated. The recorded near-fault motion is represented by a simplified velocity time history, which consists of a series of half-period sinusoidal pulses. This database is used to develop the attenuation relationship between pulse period and

amplitude. The influence of local site conditions on these parameters is evaluated, and the relationship between the pulse period on the rock and the pulse period on the soil is proposed.

Different soil improvement methods to increase the bearing capacity and decrease the settlement potential and against the liquefaction risks can be applied depending on many factors such as the existing ground structures, geological environment, groundwater condition, availability of the materials, equipment, and workforce, cost of improvement, environmental impact, and construction schedule. Methods aim to improve the soil conditions by compacting with mechanical methods, reducing the void ratio, or injecting various mixtures to achieve the solution of the problems. With the application of soil improvement methods, liquefaction potential, swelling and shrinkage potential, and compressibility decrease, along with the significant increase of strength. Application of deep soil mixing (grid system) is recommended as a soil improvement method.

The most important conclusions are summarized as below:

- The improvement process would affect the spectral acceleration, during which the spectral acceleration is at most 2.5 seconds. Basically, it can be discussed that the improvement has no effect on those structures that require greater displacement.
- The acceleration part of the spectrum is almost two-thirds of the outcrop spectrum.
- A thicker soil layer has a lower impact on the structure of a lower period, and a higher impact on the structure of a higher period.
- The linear amplification factor is in the displacement zone of the spectrum.
- The amplification is lower than the unit between 0.1 and 1 second, which reduces the outcrop motion spectrum.

REFERENCES

Abrahamson, N.A., 2000. Effects of rupture directivity on probabilistic seismic hazard analysis. Proceedings of the 6th International Conference on Seismic Zonation, Palm Springs, Earthquake Engineering Research Institute

Abrahamson. N.A. and W.J. Silva, 1997. Empirical response spectral attenuation relations for shallow crustal earthquakes. Seismological Research Letters, 68: 94-127.

Akkar S, Gülkan P., (2001). "Near-Field Earthquakes and Their Implications on Seismic Design Codes," Earthquake Engineering and Research Center, Report 2001-01, Department of Civil Engineering, Middle East Technical University, Ankara, Turkey.

Akkar S, Kale Ö, Ansari A, Durgaryan R, Askan Gündoğan A, Hamzehloo H, Harmandar E, Tsereteli N, Waseem M, Yazjeen T, Yılmaz MT (2014a) EMME strong-motion database serving for predictive model selection to EMME ground-motion logic-tree applications. In: Second European conference on earthquake engineering and seismology, İstanbul, Turkey, Abstract No. 3220

Akkar, S., and Cagnan, Z., 2010. A local ground-motion predictive model for Turkey and its comparison with other regional and global ground-motion models. Bulletin of the Seismological Society of America 100, 2978-2995.

Akkar, S., Çağnan, Z., Yenier, E., Erdoğan, Ö., Sandıkkaya, A., Gülkan, P., 2010. The recently compiled Turkish strong motion database: preliminary investigation for seismological parameters. Journal of Seismology 14, 457– 479.

Alavi, B., and H. Krawinkler, 2000. Design considerations for near-fault ground motions. Proceedings of the U.S. – Japan Workshop on the Effects of Near-Fault Earthquake Shaking, San Francisco, March 20-21.

Alavi, B., and Krawinkler, H. (2000). "Consideration of near-fault ground motion effects in seismic design." Proceedings, 12th World Conference on Earthquake Engineering, New Zealand.

Ambraseys, N. N. (2002), The Marmara Sea region's seismic activity over the last 2000 years, Bull. Seismol. Soc. Am., 92(1), 1– 18.

Ambraseys, N. N., and C. F. Finkel (1995), The Seismicity of Turkey and Adjacent Areas: A Historical Review, 1500–1800, 240 pp., Muhittin Salih Eren, Istanbul

Anderson, J.G., and J.N. Brune (1999). Probabilistic hazard analysis without the ergodic assumption, Seism. Res. Lett. 70, 19-23.

ASCE/SEI 7-16 2017. Minimum Design Loads for Buildings and Other Structures American Soc. Civil Eng.

Ayhan, M. E., and Koçyiğit, A., 2010, Displacements and Kinematics of February 1, 1944, Gerede Earthquake (North Anatolian Fault System, Turkey): Geodetic and Geological Constraints, Turkish J. Earth Sci., 19, 285–311.

Ayhan, M.E., Demir, C., Lenk, O., Kiliçoğlu, A., Altiner, Y., Barka, A., Ergintav, S. & Özener, H. 2002. Inter-seismic strain accumulation in the Marmara Sea Region. Bulletin of Seismological Society of America 92, 216–229.

Ayhan, Mehmet & Koçyiğit, A. (2010). Displacements and Kinematics of February 1, 1944, Gerede Earthquake (North Anatolian Fault System, Turkey): Geodetic and Geological Constraints. Turkish Journal of Earth Sciences. 19. 284-311. 10.3906/yer-0901-17.

Baker, J.W. & Cornell, C.A. 2006. Spectral shape, epsilon, and record selection. Earthquake engineering and structural dynamics, 35, 1077-1095.

Baker, J.W. & Jayaram, N. 2008. Correlation of spectral acceleration values from NGA ground-motion models. Earthquake Spectra 24, 299-317.

Baker, J.W. (2011). Conditional mean spectrum: Tool for ground motion selection. Journal of Structural Engineering. 137:3, 322-331.

Barka, A. & Kadinsky-Cade, K.(1988). Strike-slip fault geometry in Turkey and its influence on earthquake activity. Tectonics, 7, 663-684.

Barka, A., 1992, The North Anatolian Fault Zone, Ann. Tecton., 6 (1), 64–95

Basili R., Kastelic V., Demircioglu M. B., Garcia Moreno D., Nemser E. S., Petricca P., Sboras S. P., Besana-Ostman G. M., Cabral J., Camelbeeck T., Caputo R., Danciu L., Domac H., Fonseca J., García-Mayordomo J., Giardini D., Glavatovic B., Gulen L., Ince Y., Pavlides S., Sesetyan K., Tarabusi G., Tiberti M. M., Utkucu M., Valensise G., Vanneste K., Vilanova S., Wössner J. (2013). The European Database of Seismogenic

Faults (EDSF) compiled in the framework of the Project SHARE. http://diss.rm.ingv.it/share-edsf/,

Beyer, K., and J. J. Bommer (2006). Relationships between median values and between aleatory variabilities for different definitions of the horizontal component of motion, Bull. Seismol. Soc. Am. 96, no. 4A, 1512–1522.

Bommer JJ, Acevedo AB. (, 2004). The use of real earthquake accelerograms as input to dynamic analysis. Journal of Earthquake Engineering. 8 : (Special Issue 1),43–91.

Boore, D. M. (2010). Orientation-independent, nongeometric-mean measures of seismic intensity from two horizontal components of motion, Bull. Seismol. Soc. Am. 100, no. 4, 1830–1835.

Boore, D. M., Watson-Lamprey, J., and Abrahamson, N. A., 2006. GMRotD and GMRotI: Orientation-independent measures of ground motion, Bull. Seismol. Soc. Am. 96, 1202–1511.

Bozkurt, E., Winchester, J., Satır, M., Crowley, Q., & Ottley, C. (2013). The Almacık mafic-ultramafic complex: Exhumed Sakarya subcrustal mantle adjacent to the İstanbul Zone, NW Turkey. Geological Magazine, 150(2), 254-282. DOI:10.1017/S0016756812000556

Bozorgnia Y., Niazi M., and Campbell K.W.; 1995: Characteristics of free field vertical ground motion during the Northridge earthquake. Earthquake Spectra, 11, 515-525

Building Seismic Safety Council (BSSC) (2009). NEHRP Recommended Seismic Provisions for New Buildings and Other Structures (FEMA P-750), Federal Emergency Management Agency, Washington, D.C., 404 pp.

Cambazoglu S (2012) Preparation of a source model for the EasternMarmara Region along with the North Anatolian fault segments and probabilistic seismic hazard assessment of Düzce Province. Middle East Technical University, MS Thesis Dissertation

Cambazoglu S., Akgün H., Koçkar MK (2012) Preparation of a line source model for probabilistic seismic hazard analyses of Düzce Province, Turkey. In: Proceedings of 15th world conference on earthquake engineering, Paper# 3472, Lisbon, Portugal

Champion C. and Liel A.; 2012: The effect of near-fault directivity on building seismic collapse risk. Earthq. Eng.

Cornell, C.A. (1968). Engineering seismic risk analysis, Bull. Seism. Soc. Am., 58, 1583-1606. SSHAC (Senior Seismic Hazard Analysis Committee). Recommendations for Probabilistic

Danciu L, Kale Ö, Akkar S (2016) The 2014 Earthquake Model of the Middle East: ground motion model and uncertainties. Bull Earthq Eng (2016). DOI:10.1007/s10518-016-9989-1

Danciu L, Şeşetyan K, Demircioglu M, Gülen L, Zare M, Basili R, et al. (2017) The 2014 Earthquake Model of the Middle East: seismogenic sources, Bulletin of Earthquake Engineering, DOI:10.1007/s10518-017-0096-8

Demircioglu, Mine & Sesetyan, Karin & Duman, Tamer & Can, Tolga & Tekin, Senem & Ergintav, Semih. (2017) "A probabilistic seismic hazard assessment for the Turkish territory—part II: fault source and background seismicity model," Bulletin of Earthquake Engineering. 1-40.

Di Sarno L., Elnashai A.S. and Manfredi G.; 2010: Seismic response of RC members subjected to the 2009 L'Aquila (Italy) near-field earthquake ground motions. Report No.01-2010. Mid-America Earthquake Center, the University of Illinois at Urbana-Champaign, U.S.A.

Dikbaş, A. (2009), "Kuzey Anadolu Fay Zonunun İzmit-Gölyaka (Düzce) Arasindaki Segmentlerinin Paleosismolojisi ve Morfolojik Özellikleri", PhD Thesis, ITU

EC8, "Eurocode 8: Design of Structures for Earthquake Resistance Part 1: General Rules, Seismic Actions and Rules for Buildings" European Standard prEN 1998-1, 2003

Elgamal A. and He L.C.; 2004: Vertical earthquake ground motion records: An overview. J. Earthq. Eng., 8, 663-697

EPRI (1993). Guidelines for Determining Design Basis Ground Motions. Electric Power Research Institute, EPRI TR-012293s, Palo Alto, CA

Fahjan, Y., "Selection and Scaling of Real Earthquake Accelerograms to Fit the Turkish Design Spectra," Teknik Dergi, 19:3, pp.4423-4444, 2008.

Fahjan, Y.M. (2010). Selection, Scaling and Simulation of Input Ground Motion for Time History Analysis of Structures, Seminar, and Lunch on Earthquake Engineering and Historic Masonry

Fahjan, Y.M., Ozdemir, Z. ve Keypour, H. (2007). Procedures for Real Earthquake Time Histories Scaling and Application to Fit Iranian Design Spectra, 5th International Conference on Seismology and Earthquake Engineering (SEE5), May 14-16, Tahran, Iran

Fahjan, Y & Kara, F & Mert, A. (2017). Selection and Scaling Time History Records for Performance-Based Design. 10.4018/978-1-5225-2089-4.ch001.

Garini E. and Gazetas G.; 2013: Damage potential of near-fault records: sliding displacement against conventional "Intensity Measures." Bull. Earth. Eng., 11, 455-480. Struct. Dyn., 41, 1391-1409.

Grimaz, S., Malisan, M., 2014. "Near field domain effects and their consideration in the international and Italian seismic codes," Bollettino di Geofisica Teorica ed Applicata, 55, 4, 717-738

Gülen L, Şeşetyan K, Adamia S, Sadradze N, Gvencadze A, Karakhanyan A et al. (2014) Earthquake model of the Middle East (EMME) project: active faults and seismic sources second European conference on earthquake engineering and seismology, 2ECEES, 24–29 Aug 2014, Istanbul, Turkey, Abstract No. 3216

Gülerce Z. And Ocak, S. "Probabilistic seismic hazard assessment of Eastern Marmara Region," Bulletin of Earthquake Engineering, vol.11, pp.1259-1277, 2013

Gülerce, Z., and Akyüz, E., 2013. NGA-W1 Vertical-to-Horizontal Spectral Acceleration Ratio Prediction Equations Adjusted for Turkey, Seismological Research Letters 84, 678 - 688.

Gulerce, Z., Abrahamson, N. A., 2011. Site-Specific Design Spectra for Vertical Ground Motion. Earthquake Spectra, Volume 27, No. 4, pages 1023–1047, November 2011

Gülerce, Z., Kargıoğlu, B., and Akyüz E., 2012. Comparison of the NGA-W1 vertical-to-horizontal spectral acceleration ratio prediction equations with Turkish strong ground motion database, Proceedings of 15th World Conference on Earthquake Engineering (15th WCEE), 24-28 September 2012, Lisbon.

Hasal, M.E.; Iyisan, R.; Khanbabazadeh, H.; Bayin, A.; Cevikbilen, G.; Kepceoglu, O.: A preliminary seismic microzonation study based on microtremor measurements. In: International Conference: Skopje Earthquake-50 years of European Earthquake Engineering, Skopje (2013)

Hasal, Murat Emre, et al. “Basin Edge Effect on Seismic Ground Response: A Parametric Study for Düzce Basin Case, Turkey.” Arabian Journal for Science and Engineering, vol. 43, no. 4, 2017, pp. 2069–2081.

Hashash, Y.M.A., Musgrove, M.I., Harmon, J.A., Okan, I., Groholski, D.R., Phillips, C.A., and Park, D. (2017) “DEEPSOIL 7.0, User Manual

Hayden, C. P., Bray, J. D., and Abrahamson, N. A., 2014. Selection of near-fault pulse motions, Journal of Geotechnical and Geoenvironmental Engineering 140

Huang, Y.N., Whittaker A.S., Luco, N., 2008. Maximum Spectral Demands in the Near-Fault Region. Earthquake Spectra, Volume 24, No. 1, pages 319–341, February 2008

Joyner, W. B., Boore, D. M. (1982). "Prediction of earthquake response spectra." USGS Open-File Report 82-977.

Kalkan E. and Kunnath S.K.; 2006: Effects of fling step and forward directivity on buildings' seismic response. Earthquake Spectra, 22, 367-390.

Kalkan, E. ve Chopra, A.K. (2010). Practical Guidelines to Select and Scale Earthquake Records for Nonlinear Response History Analysis of Structures. U.S. Geological Survey Open-File Report

Kayhan, A.H. (2011). Eurocode-8 ile Uyumlu Ölçeklendirilmemiş İvme Kaydı Setlerinin Armoni Araştırması Tekniği ile Elde Edilmesi, Türkiye Deprem Mühendisliği ve Sismoloji Konferansı, 11-14 Ekim, ODTÜ, Ankara.

Kayhan, A.H., Korkmaz, K.A. ve Irfanoglu, A. (2011). Selecting and scaling real ground motion records using harmony search algorithm, Soil Dynamics and Earthquake Engineering, 31, 941-953.

Kim S.J., Holub C.J., and Elnashai A.S.; 2011: Analytical assessment of vertical earthquake motion effect on RC bridge piers. J. Struct. Eng., 137, 252-260.

Komut, T., (2005) “Paleoseismological studies on Düzce fault and geological data on the seismogenic sources in the vicinity of Düzce area” Ph.D. Thesis Boğaziçi University

Kramer, S. L. (1996). "Geotechnical Earthquake Engineering." Prentice-Hall, Upper Saddle River, New Jersey.

Krawinkler H., Alavi B., Zareian F. (2005) Impact of Near-Fault Pulses on Engineering Design. In: Gülkan P., Anderson J.G. (eds) Directions in Strong Motion Instrumentation. Nato Science Series: IV: Earth and Environmental Sciences, vol 58. Springer, Dordrecht

Li S. and Xie L.-L.; 2007: Progress and trend on near-field problems in civil engineering. Acta Seismologica Sinica English edition, 20, 105-114.

McKenzie, D.P. (1972). Active tectonics of the Mediterranean region, Geophys. J.R.Astron. Soc., 30, 109-185.

Mert, A., Fahjan, Y., Pınar, A. ve Hutchings, L. (2014). Prens adaları fayında kuvvetli yer hareketi benzeşimleri. İMO Teknik Dergi, 6775-6804.

Moustafa A. and Takewaki I.; 2010: Characterization and modeling of near-fault pulse-like strong ground motion via damage-based critical excitation method. Struct. Eng. and Mechanics, 34, 755-778.

Özdemir, Z. ve Fahjan, Y.M. (2007). Gerçek deprem kayıtlarının tasarım spektrumlarına uygun olarak zaman ve frekans tanım alanlarında ölçekleme yöntemlerinin karşılaştırılması. Altıncı Ulusal Deprem Mühendisliği Konferansı, 16-20 Ekim, İstanbul.

Papazoglou A.J. and Elnashai A.S.; 1996: Analytical and field evidence of the damaging effect of vertical earthquake ground motion. Earthq. Eng. Struct. Dyn., 25, 1109-1137.

Pucci, S., Pantosti, D., Barchi, M., & Palyvos, N. (2007). A complex seismogenic shear zone: The Düzce segment of North Anatolian Fault (Turkey). Earth and Planetary Science Letters, 262(1-2), 185-203. DOI: 10.1016/j.epsl.2007.07.038

Risk Engineering, EZ-FRISK-Software for Ground Motion Estimation, Risk Engineering Inc., Boulder, Colorado, v7.52

Şaroğlu, F., Emre, Ö., Kuşçu, İ., 1992. Active Fault Map of Turkey, General Directorate of the Mineral Research and Exploration, Ankara, Turkey, 2 sheets, 1.2.000.000 scale.

Seismic Hazard Analysis: Guidance on Uncertainty and Use of Experts, US Nuclear Regulatory Commission report CR-6372, Washington DC.

Şengör, A.M.C. (1979). The North Anatolian transform fault: its age, offset, and tectonic significance. Journal of the Geological Society of London 136, 269-282.

Şeşetyan K, Danciu L, Demircioğlu M, Giardini D, Erdik M, Akkar S, Gülen L, Zare M et al. (2018) The 2014 Earthquake Model of the Middle East: overview and results. Bulletin of Earthquake Engineering (2018): 1-32. https://doi.org/10.1007/s10518-018-0346-4

Şeşetyan, K., Demircioglu, M.B., Duman, T.Y. vd.,(2016) “A probabilistic seismic hazard assessment for the Turkish territory—part I: the area source model,” Bulletin of Earthquake Engineering.

Shabestari K.T. and Yamazaki F.; 2003: Near-fault spatial variation in strong ground motion due to rupture directivity and hanging wall effects from the Chi-Chi, Taiwan earthquake. Earthq. Eng. Struct. Dyn., 32, 2197- 2219.

Somerville, P. G. (1997). "Engineering characteristics of near-fault ground motion." SMIP 97, Seminar on Utilization of Strong Motion Data: Los Angeles, CA.

Somerville, P. G. (1998). "Development of an improved ground motion representation for near-fault ground motions." SMIP 98, Seminar on Utilization of Strong Motion Data: Oakland, CA.

Somerville, P.G. (2001). Magnitude scaling of the near-fault rupture directivity pulse. Proceedings of the International Workshop on the Quantitative Prediction of Strong-Motion and the Physics of Earthquake Sources, October 23-25, 2000, Tsukuba, Japan

Somerville, P.G. (2003). Magnitude scaling of the near-fault rupture directivity pulse. Physics of the Earth and Planetary Interiors, 137, 201-212.

Somerville, P.G., 2000. “Seismic hazard evaluation,” Bull. New Zealand Soc. Earthq. Eng., 33, 371-386

Somerville, P.G., N.F. Smith, R.W. Graves, and N.A. Abrahamson (1997). Modification of empirical strong ground motion attenuation relations includes the amplitude and duration effects of rupture directivity, Seismological Research Letters 68, 199-222.

TBDY, “Türkiye Bina Deprem Yönetmeliği,” Çevre Ve Şehircilik Bakanlığı, Mart 2018.

Yağcı, B. ve Ansal, A. (2008). Mikrobölgeleme için yapay ve gerçek ivme kayıtlarının kullanımı. İTÜ Dergisi/d 7:2, 3-14.

Yousefi-Bavil K, Koçkar MK, Akgün H (2015)” Near Field Seismic Site Response Analysis of Alluvial Basin: A Case Study for the Gölyaka, Düzce, Turkey,” 4. Uluslararası Deprem Mühendisliği ve Sismoloji Konferansı 11 - 13 Ekim 2017– Anadolu Üniversitesi – Eskişehir

Zare M, Amini H, Yazdi P, Sesetyan K, Demircioglu MB et al. (2014) Recent developments of the Middle East catalog. J Seismol 18(4):749–772

Zhao, G., Xu, L., Gardoni, P., & Xie, L. (2019). A new method of deriving the acceleration and displacement design spectra of pulse-like ground motions based on the wavelet multi-resolution analysis. Soil Dynamics and Earthquake Engineering, 119, 1-10.

http://www.koeri.boun.edu.tr/depremmuh/eqspecials/Düzce/Düzce4.htm

http://diss.rm.ingv.it/share-edsf/sharedata/SHARE_WP3.2_Map.html

http://peer.berkeley.edu/nga/index.ht

APPENDIX A

SOIL INVESTIGATION

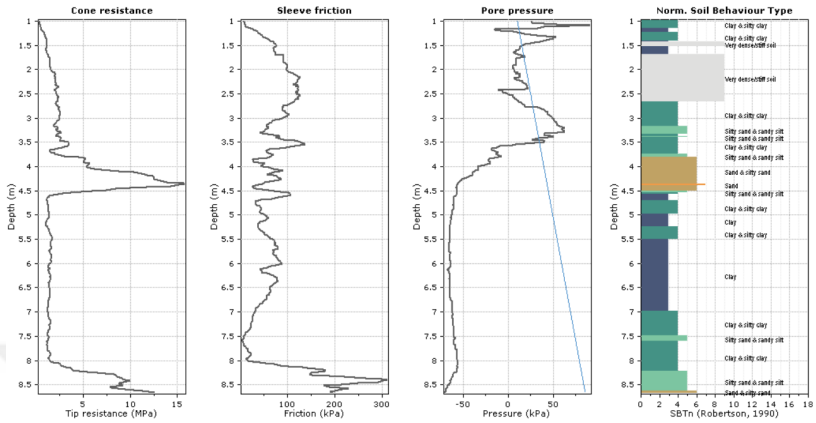

CPT-1 Values and Soil Profile by the CPeT-IT Software

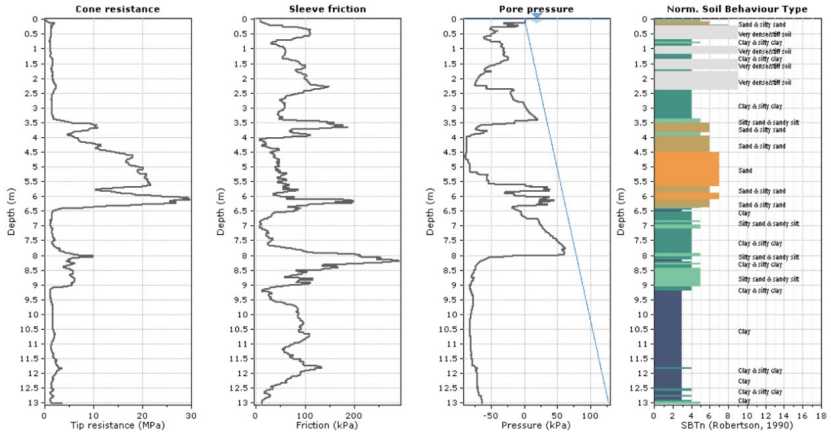

CPT-2 Values and Soil Profile by the CPeT-IT Software

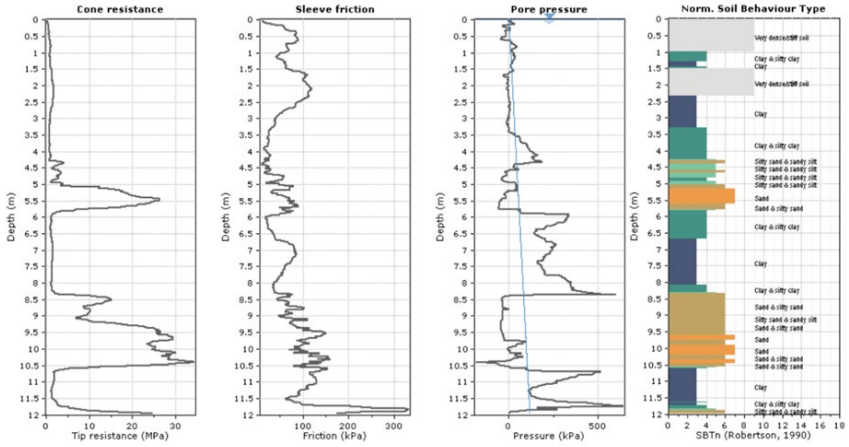

CPT-3 Values and Soil Profile by The CPeT-IT Software

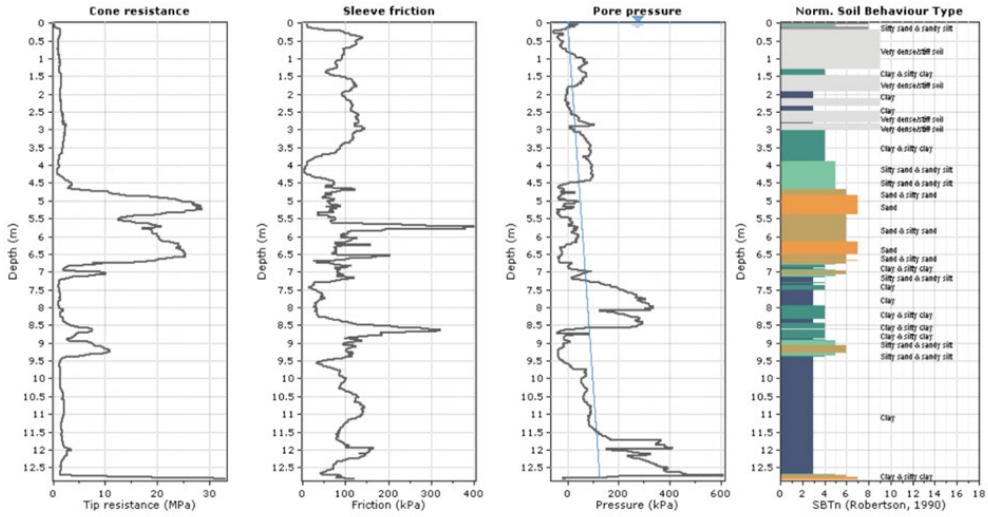

CPT-4 Values and Soil Profile by The CPeT-IT Software

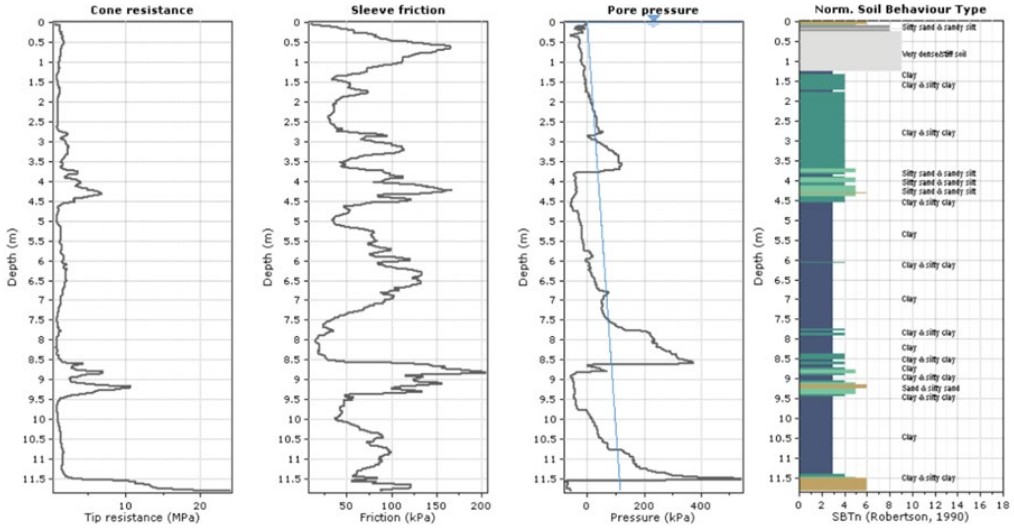

CPT-5 Values and Soil Profile by The CPeT-IT Software

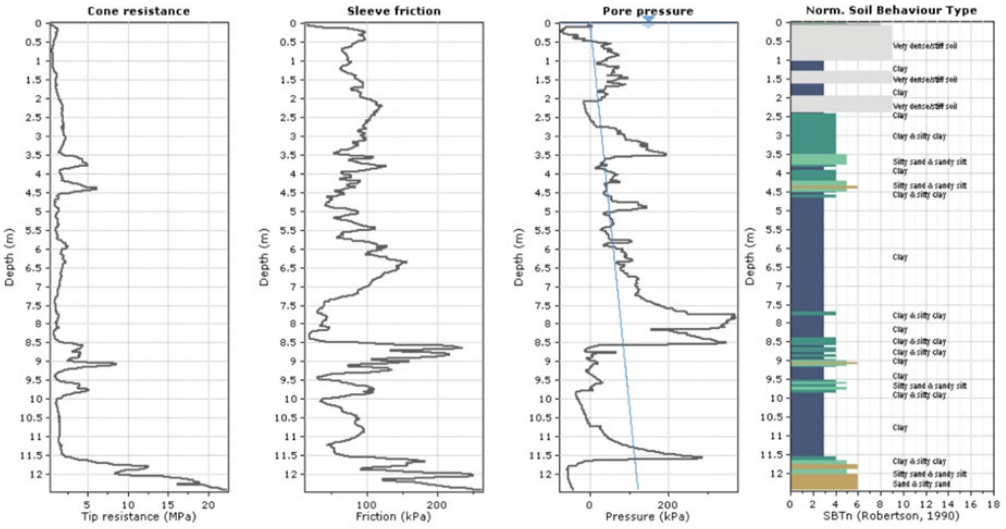

CPT-6 Values and Soil Profile by The CPeT-IT Software

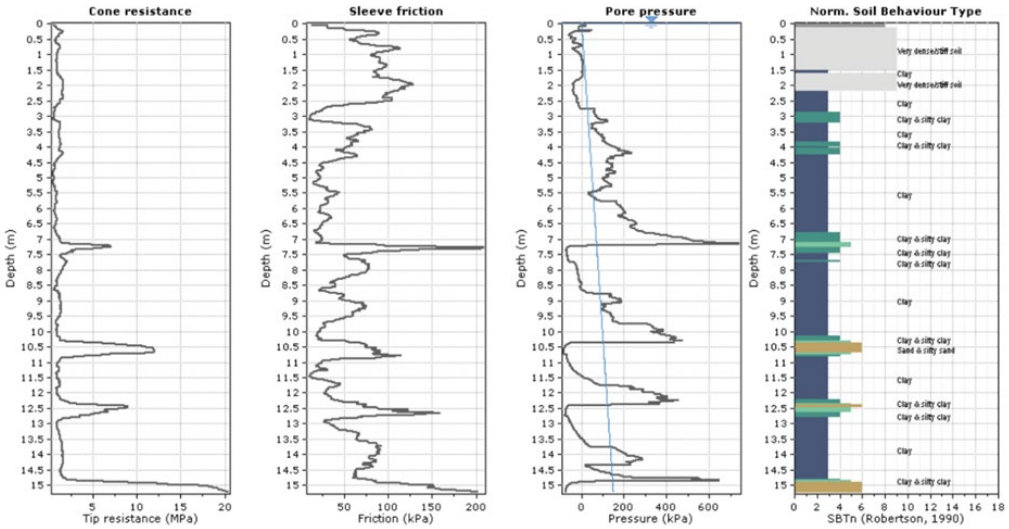

CPT-7 Values and Soil Profile by The CPeT-IT Software

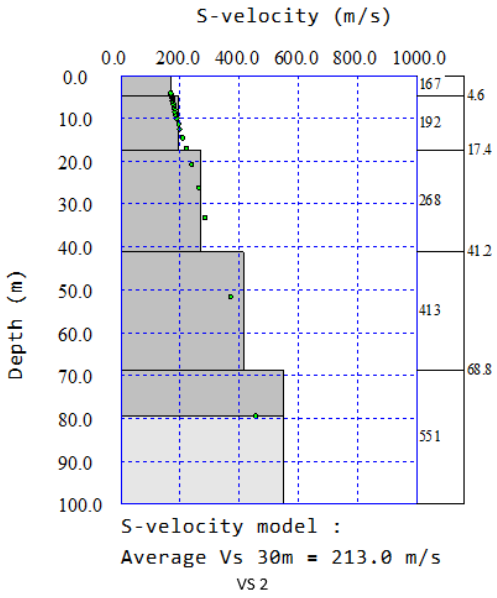

Values of Seismic-1

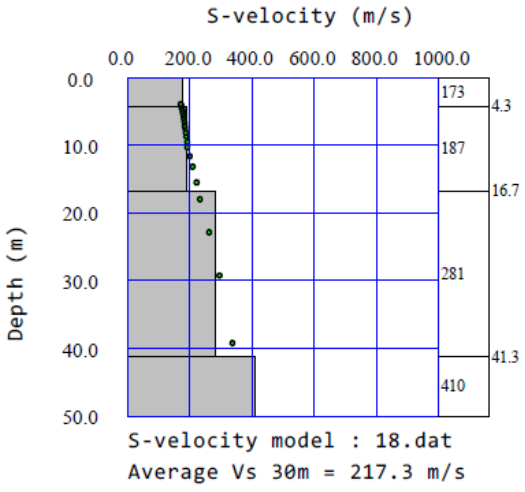

Values of Seismic-2

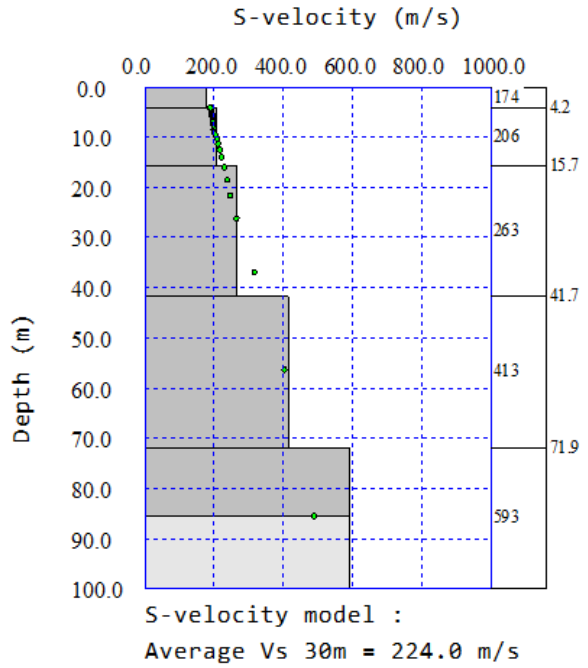

Values of Seismic-3

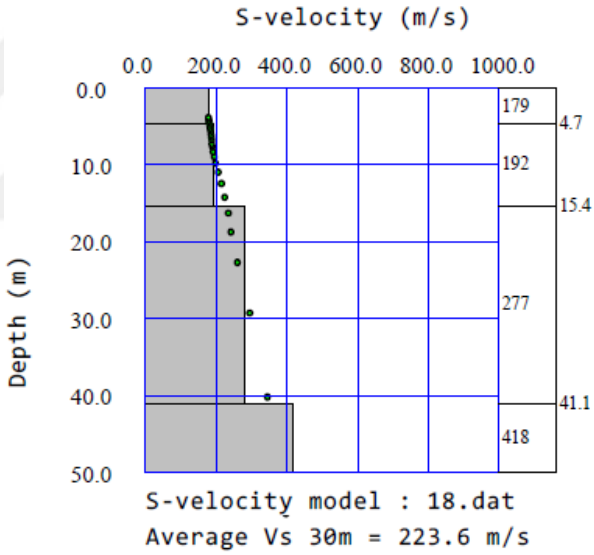

V_s Values of Seismic-4

APPENDIX B

ZMAP OUTPUT

- **TRAS754**

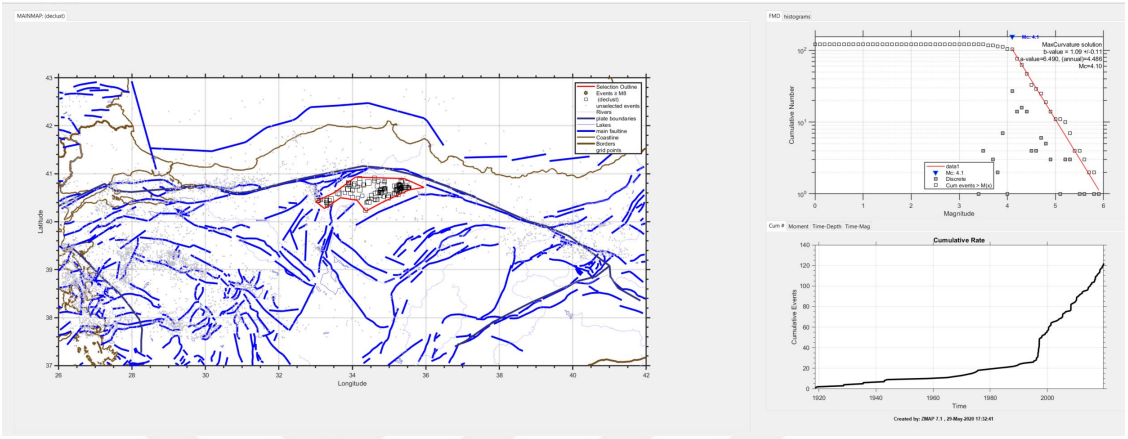

- **TRAS755**

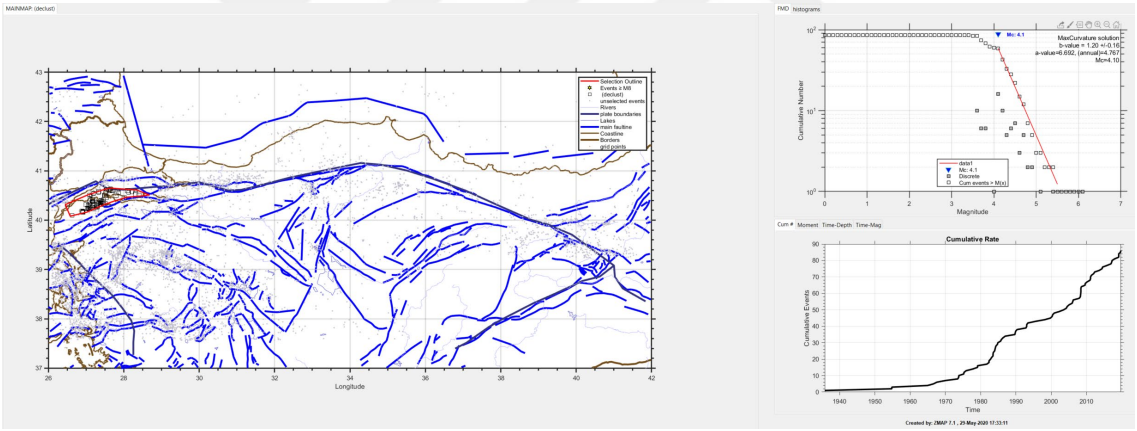

- **TRBG043**

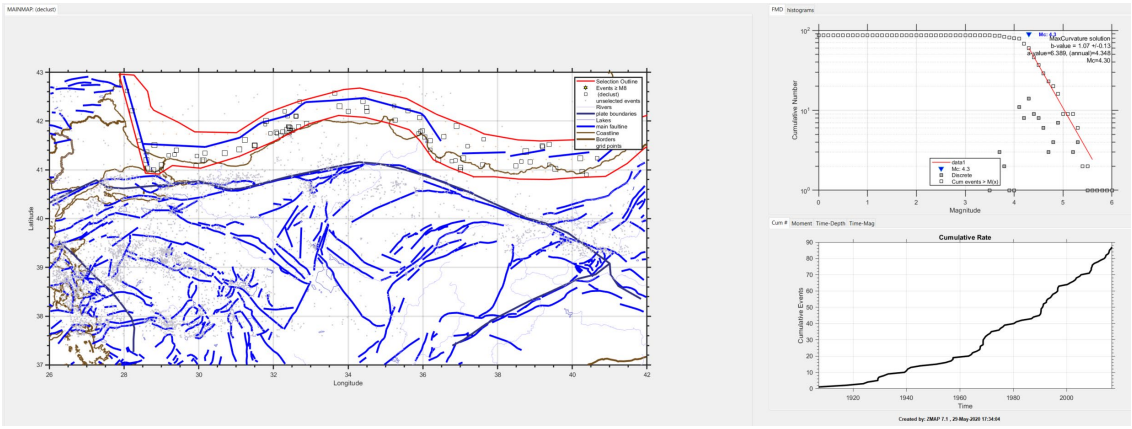

- **TRBG045**

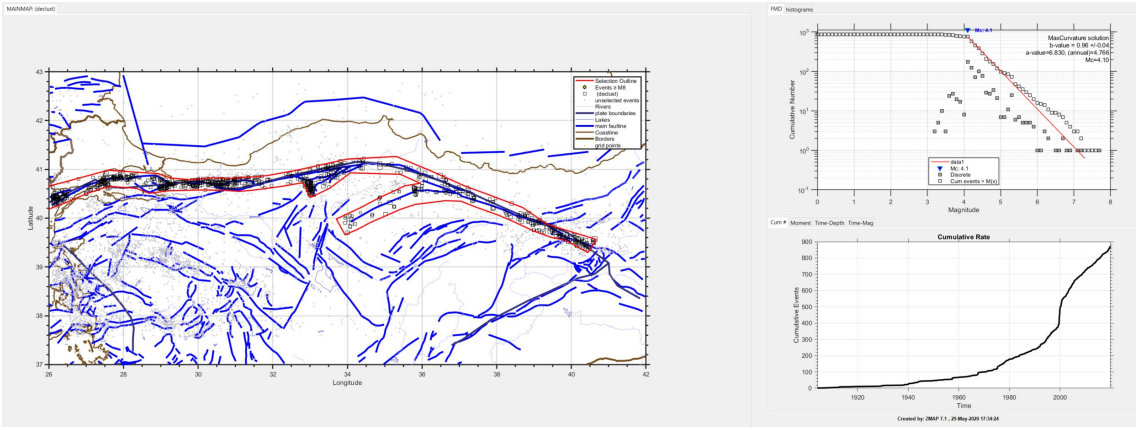

- **TRBG101**

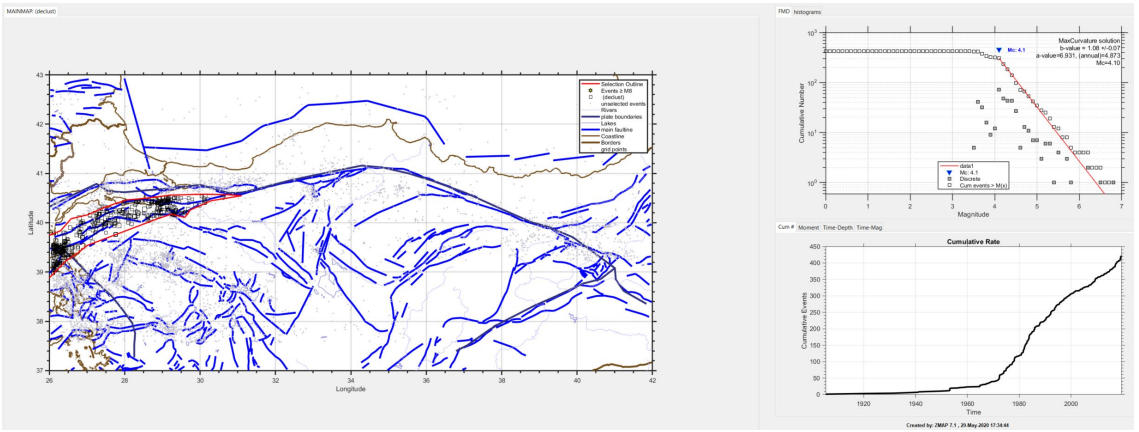

- **TRBG102**

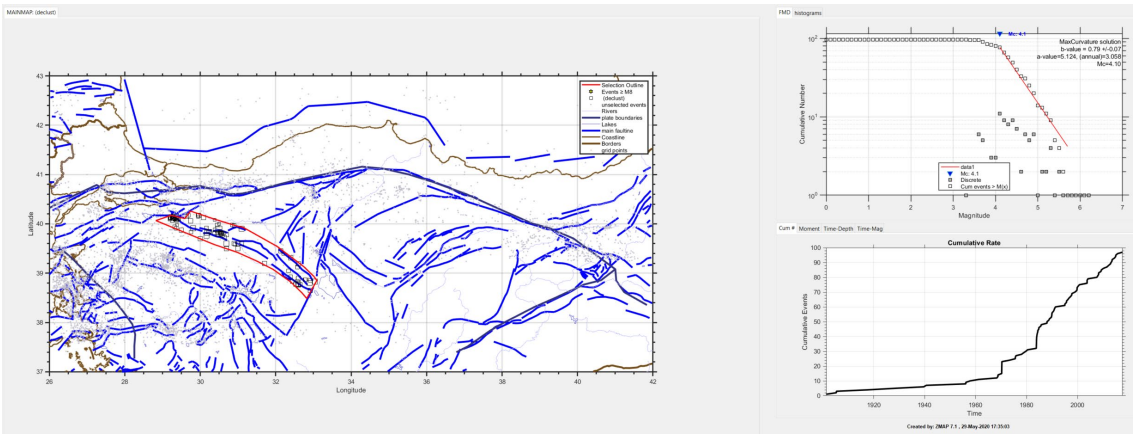

- **TRBG103**

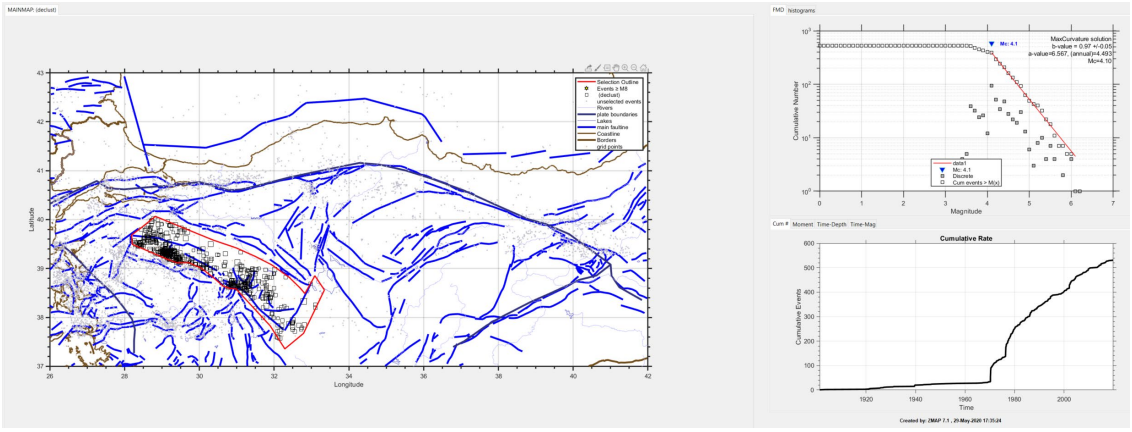

- **TRBG104**

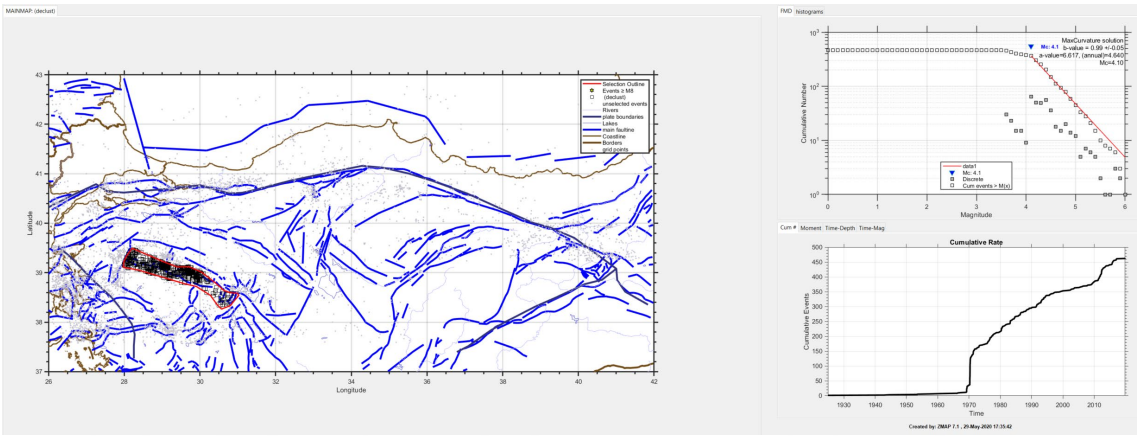

- **TRBG105**

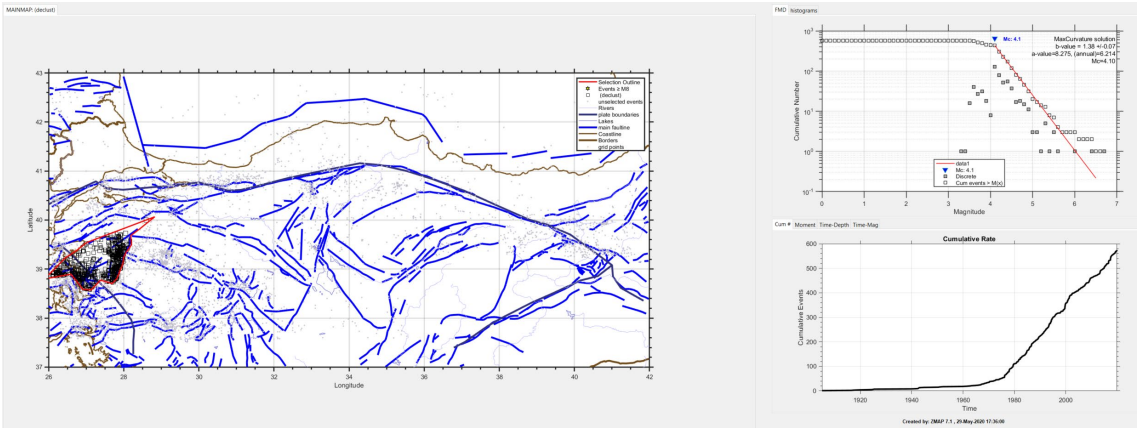

- **TRBG108**

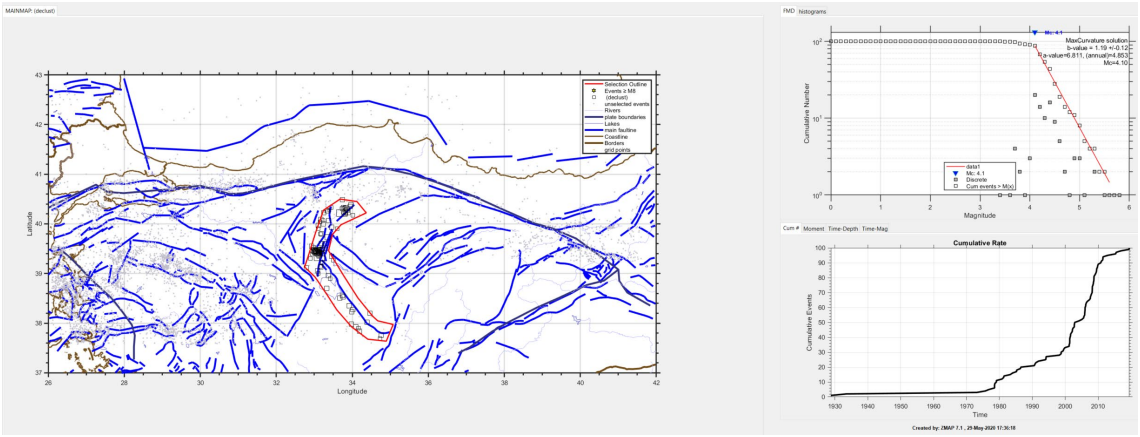

- **TRBG122**

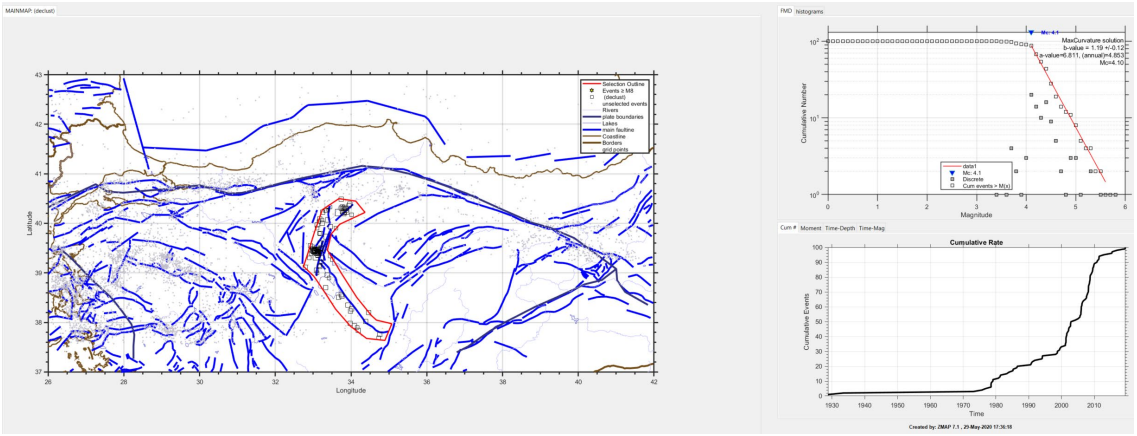

- **TURAS034**

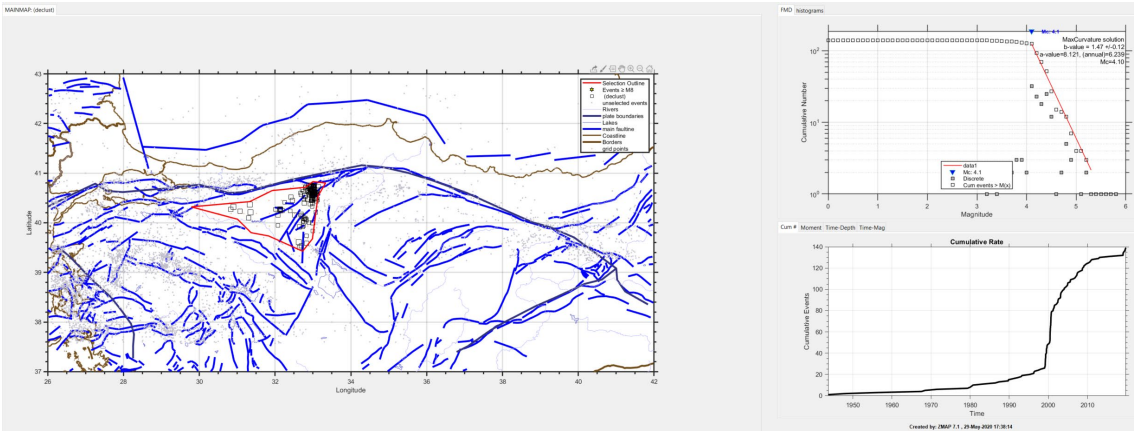

APPENDIX C

EARTHQUAKE RECORDS

- **DD-1 EARTHQUAKES**

IRPINIA 285-FN

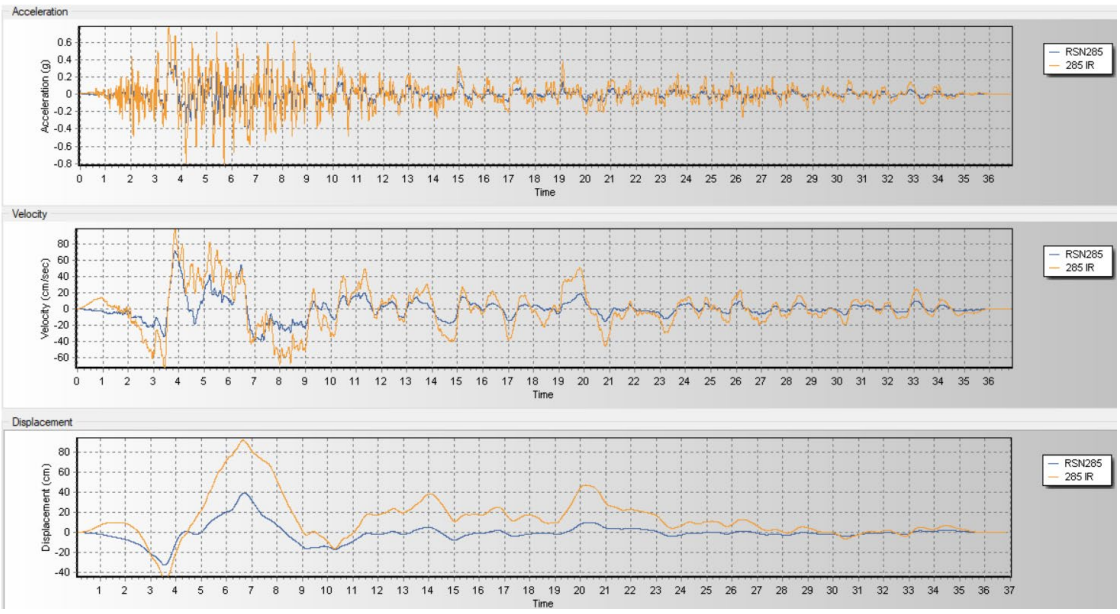

IRPINIA 285-FP

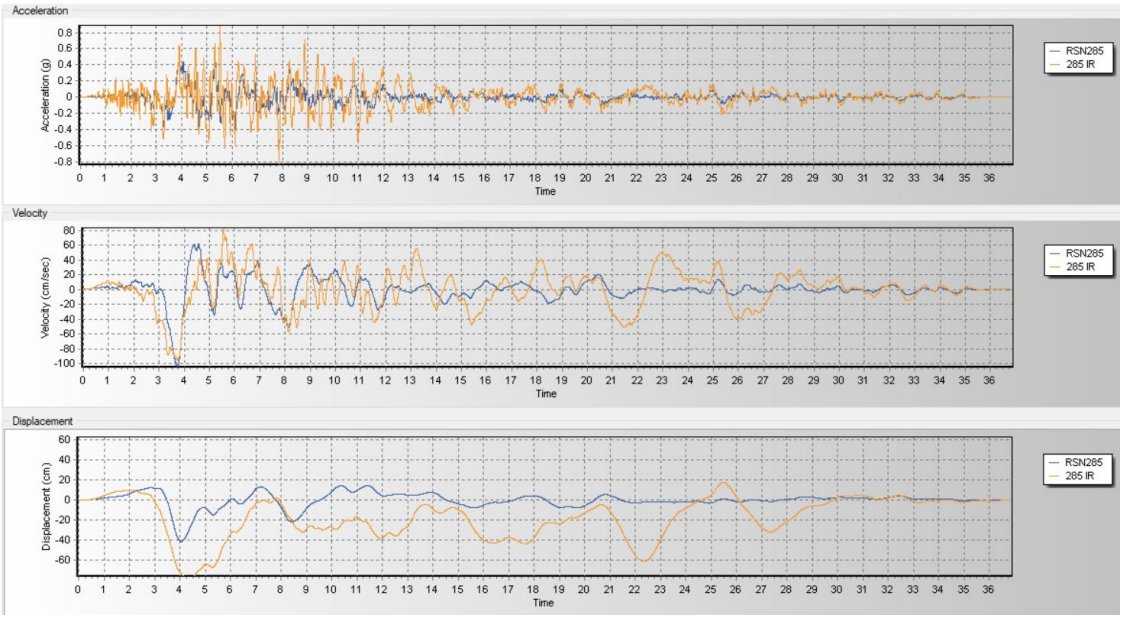

KOBE 1111-FN

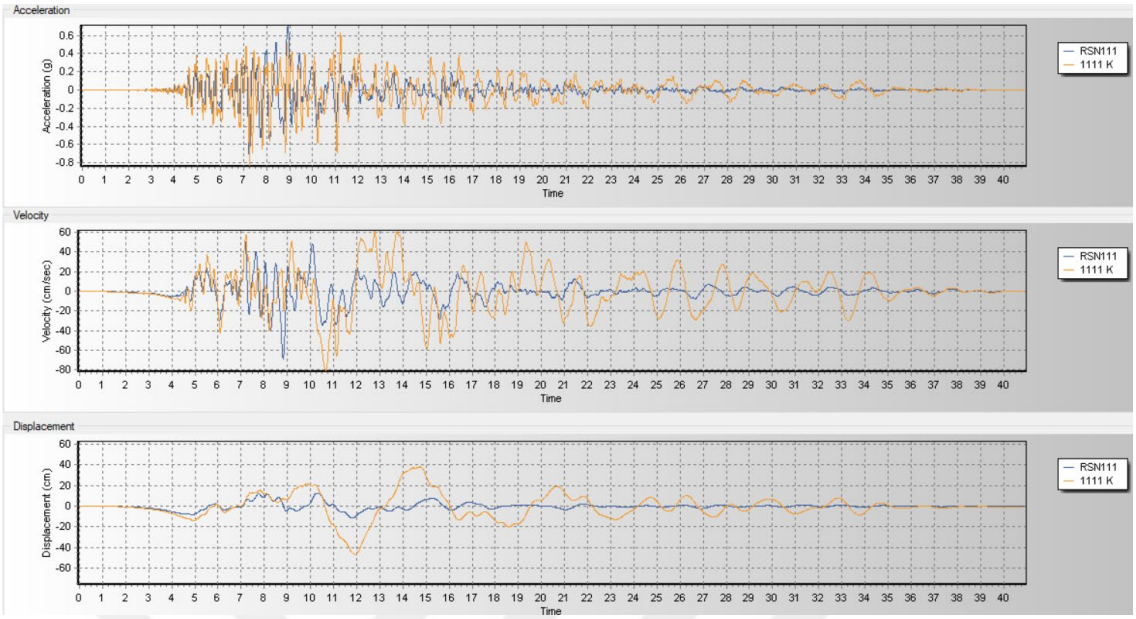

KOBE 1111-FP

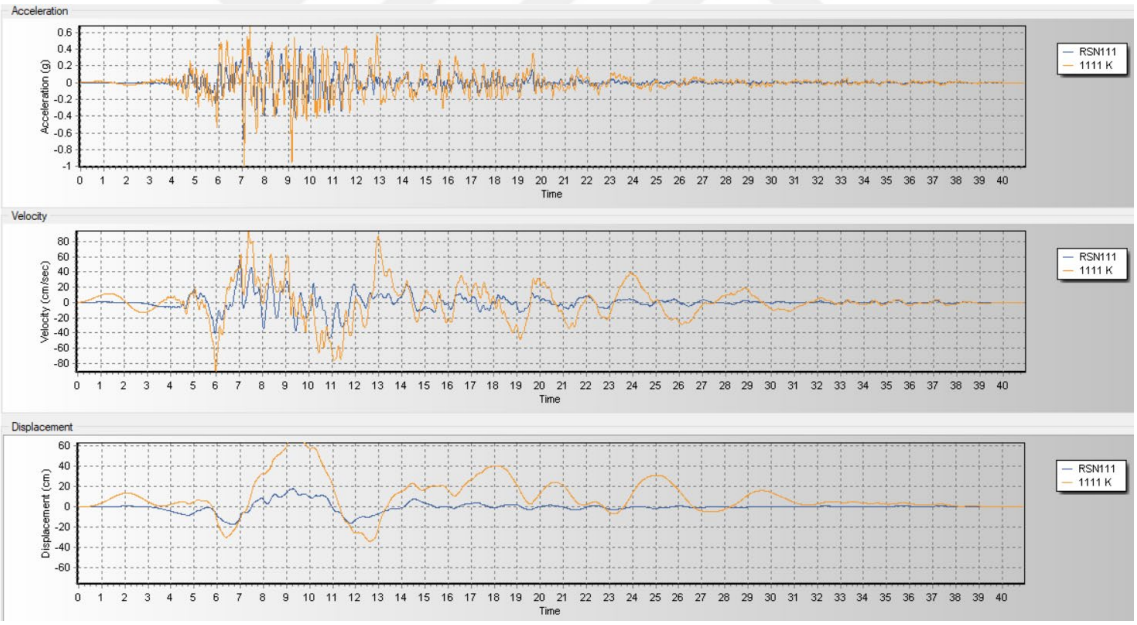

KOCAELI 1165-FN

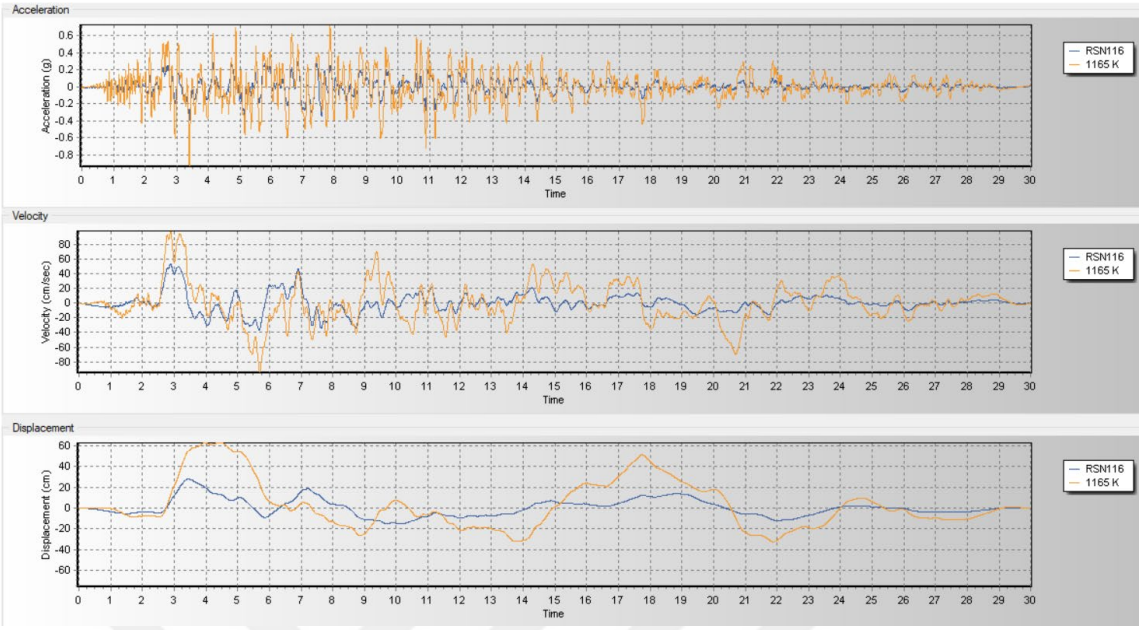

KOCAELI 1165-FP

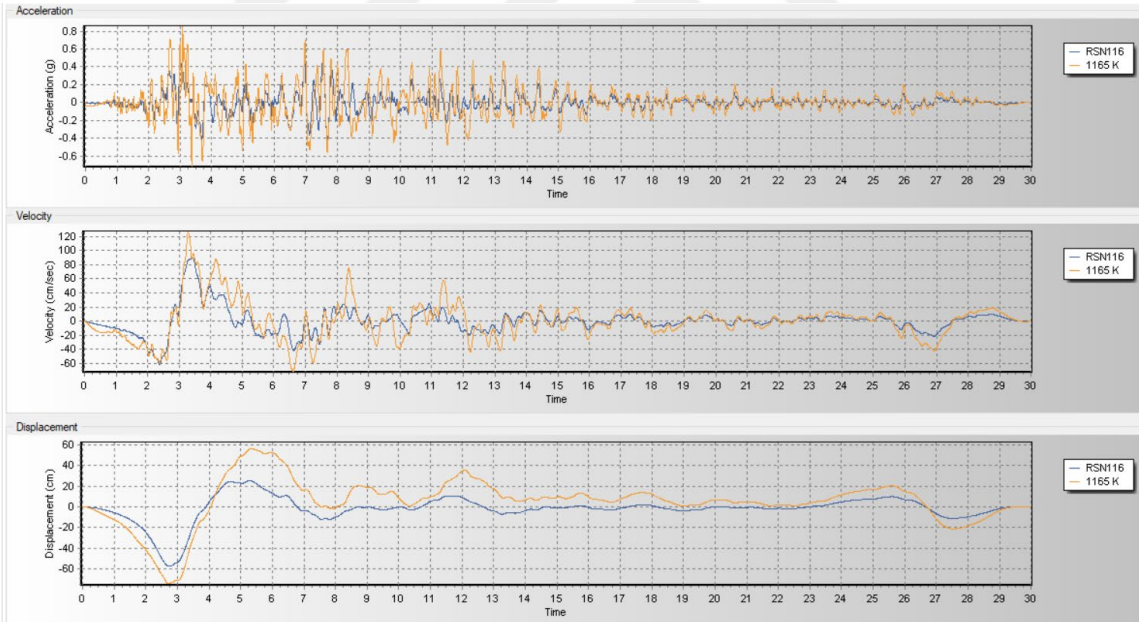

MANJIL 1633-FN

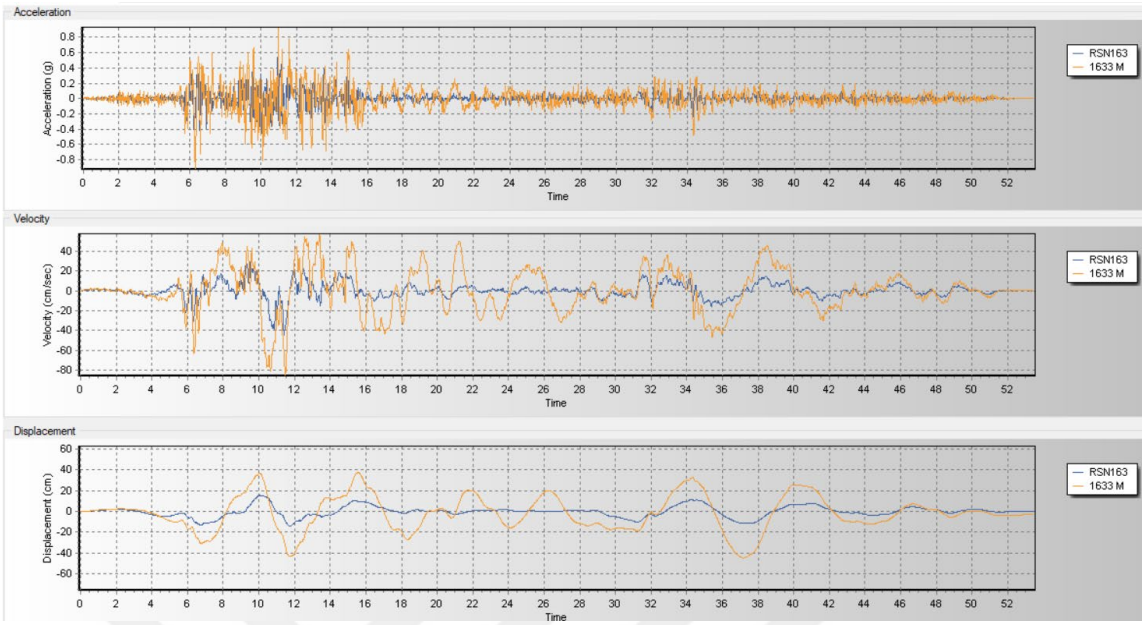

MANJIL 1633-FP

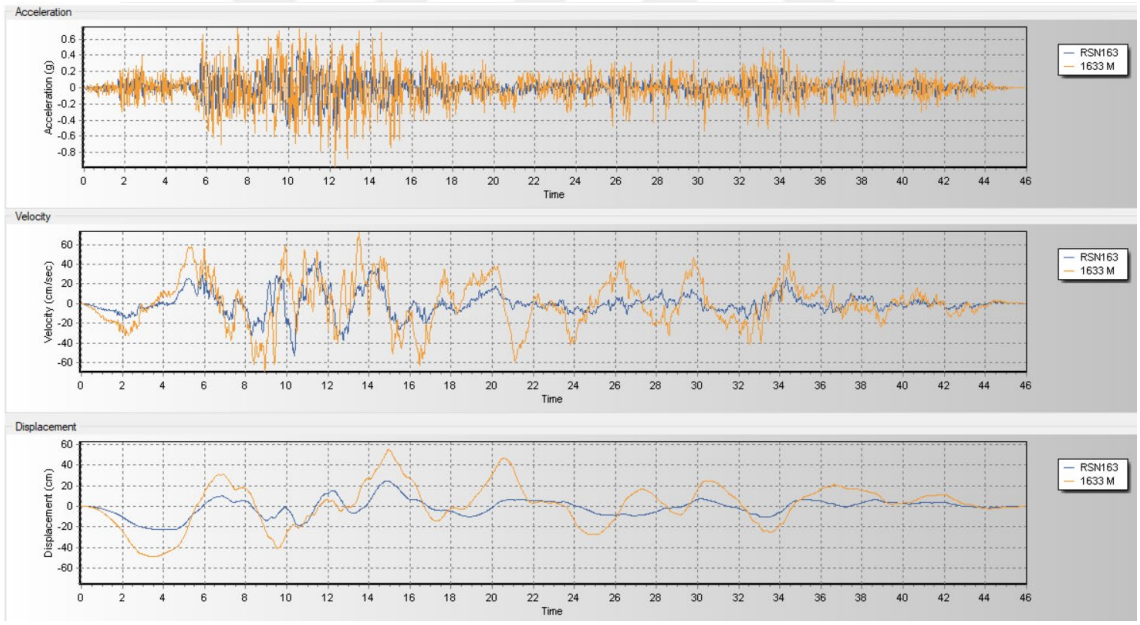

HECTOR 1787-FN

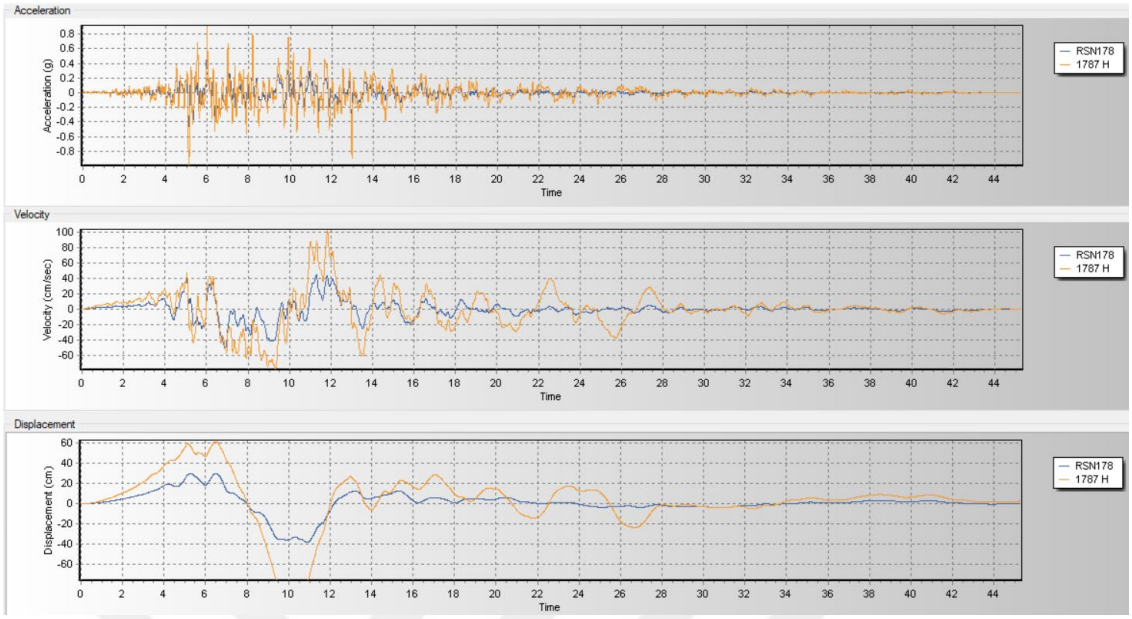

HECTOR 1787-FP

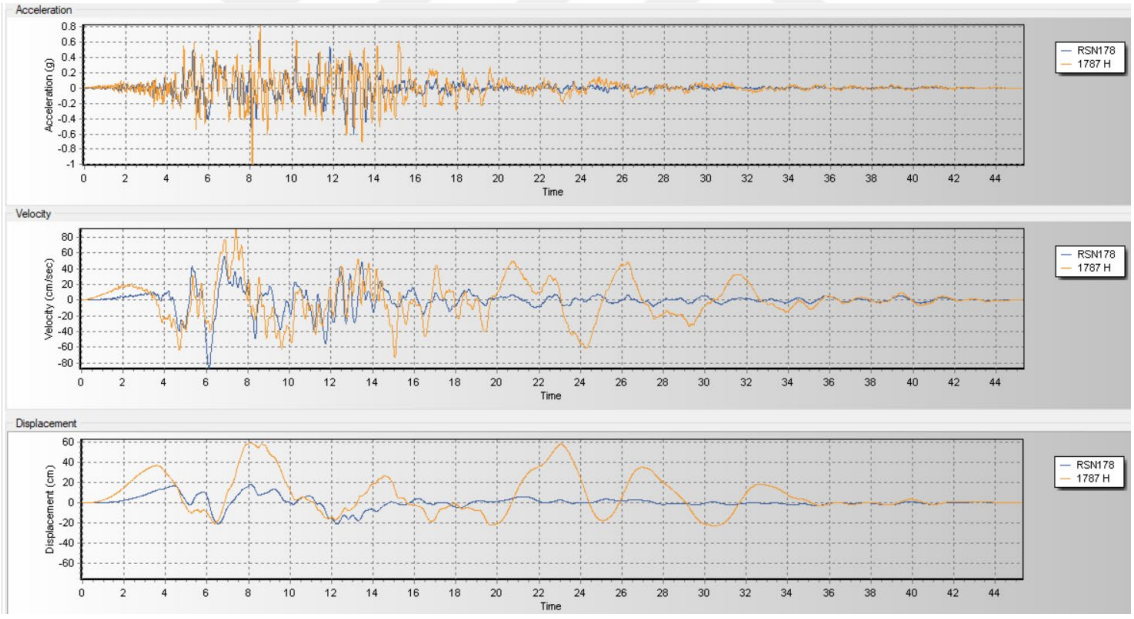

CHUETSU-OKI 4841-FN

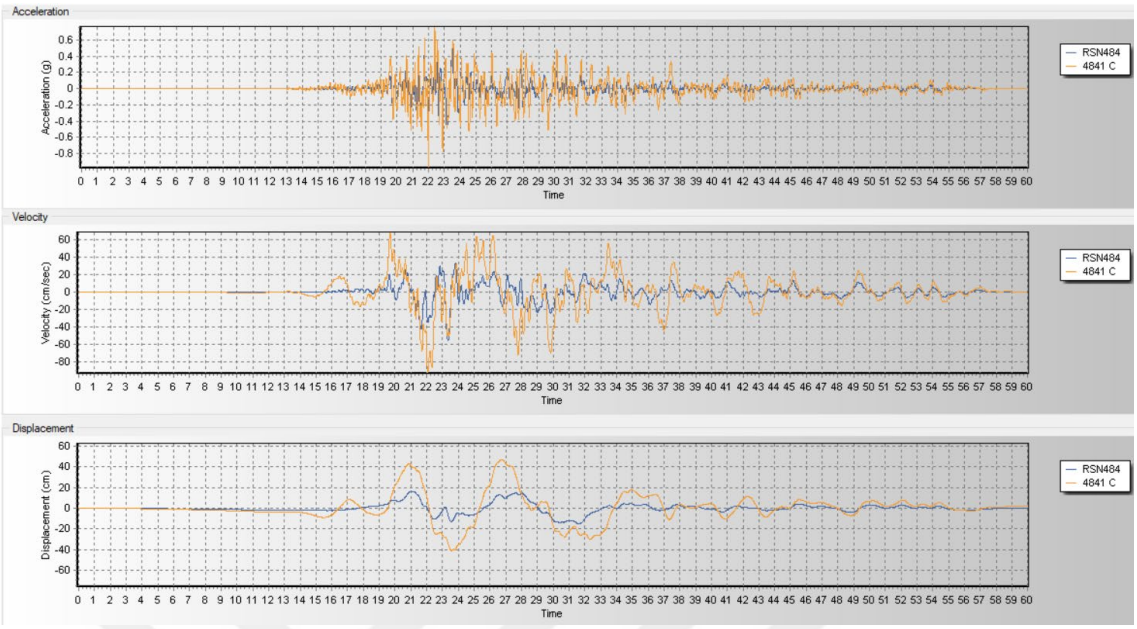

CHUETSU-OKI 4841-FP

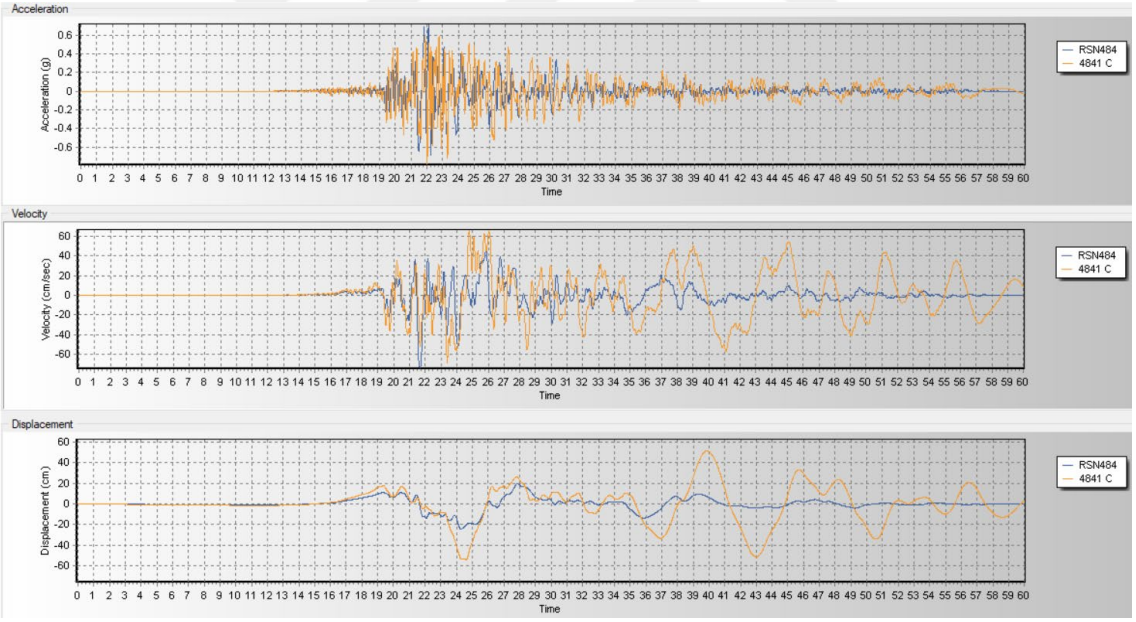

CHUETSU-OKI 4858-FN

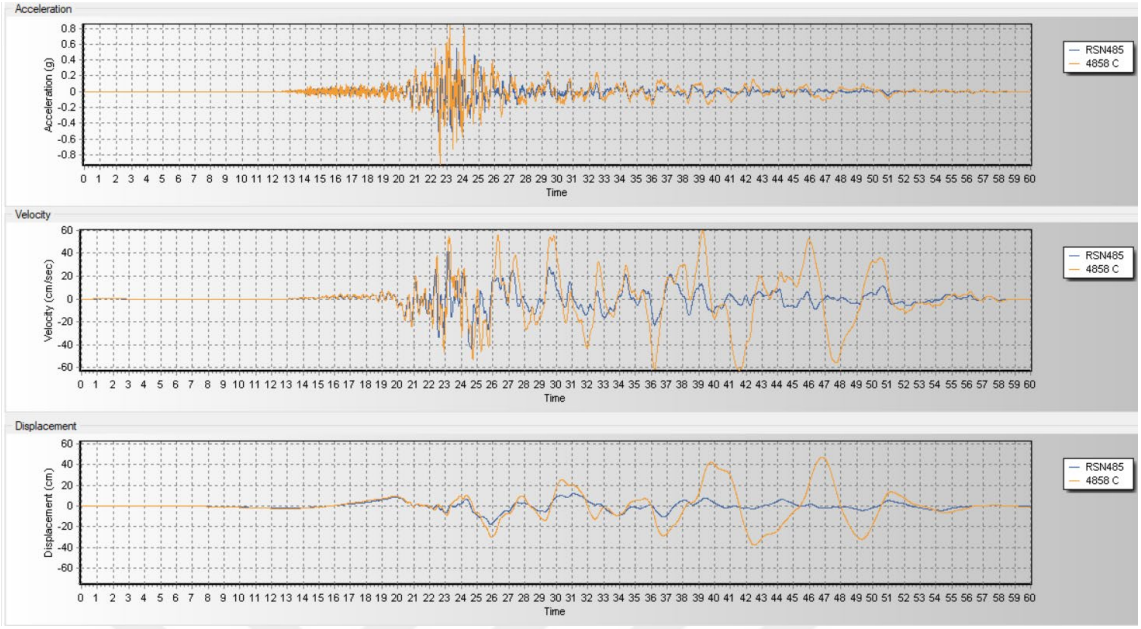

CHUETSU-OKI 4858-FP

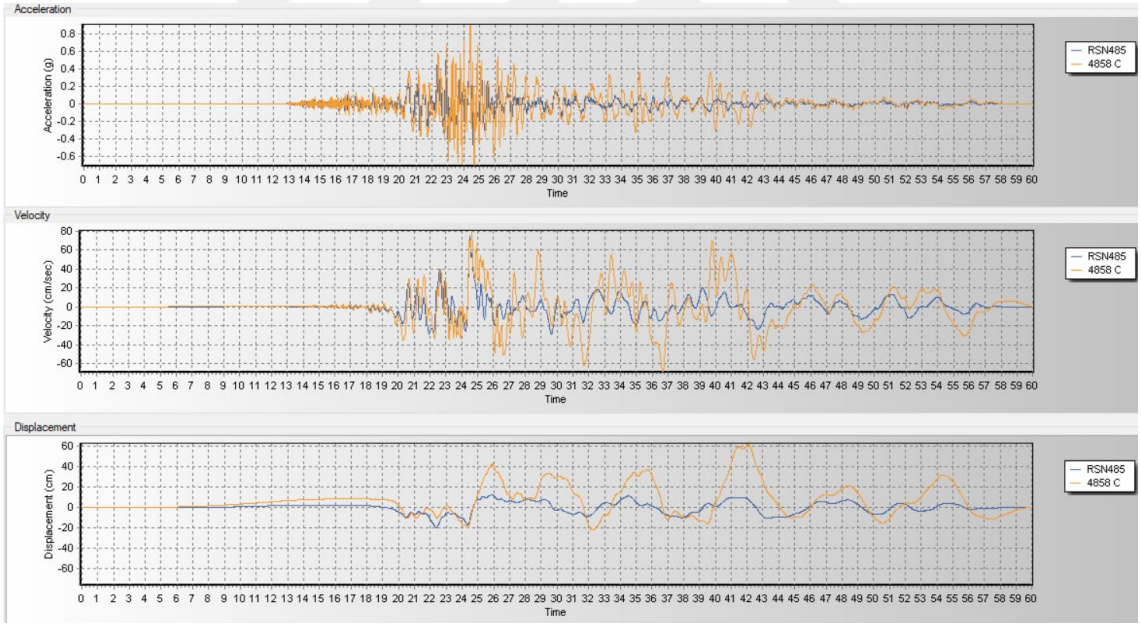

CHUETSU-OKI 4864-FN

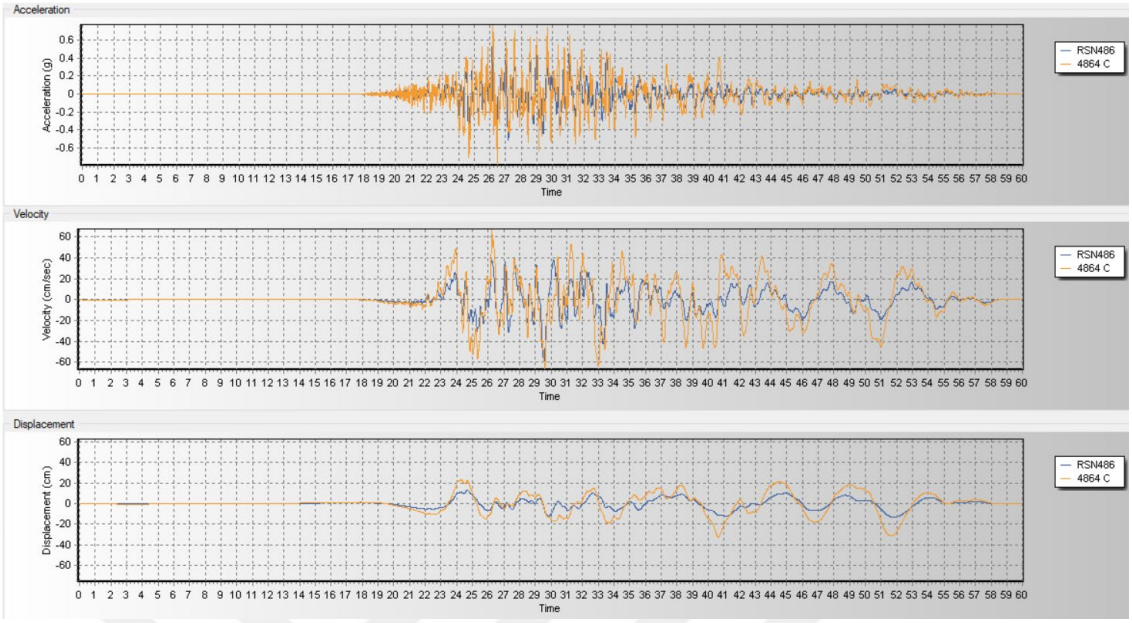

CHUETSU-OKI 4864-FP

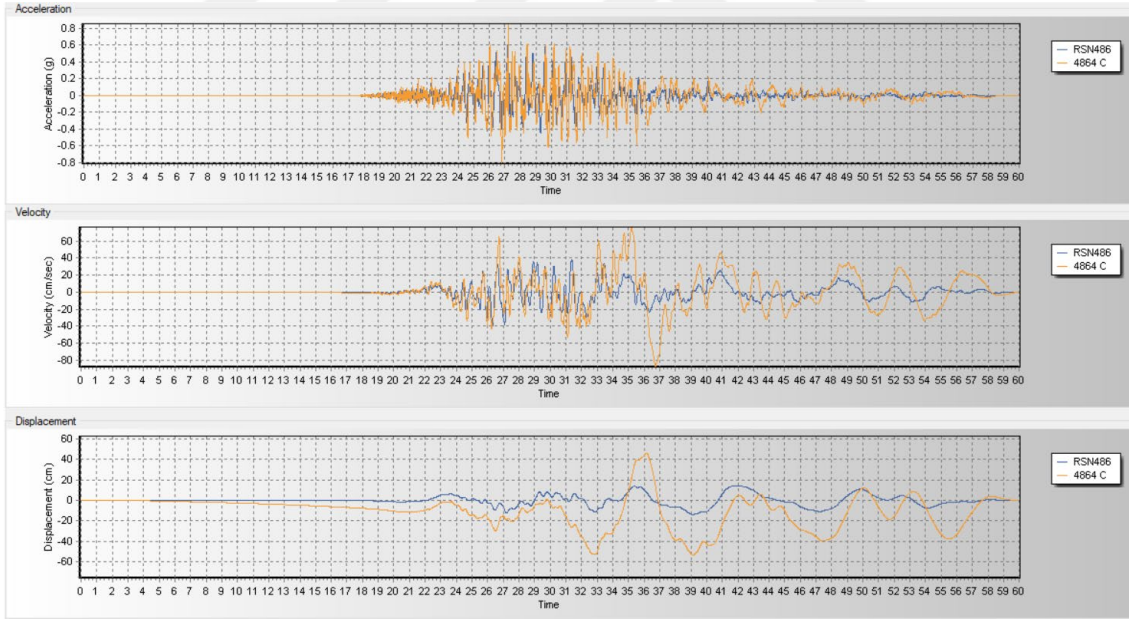

IWATE 5806-FN

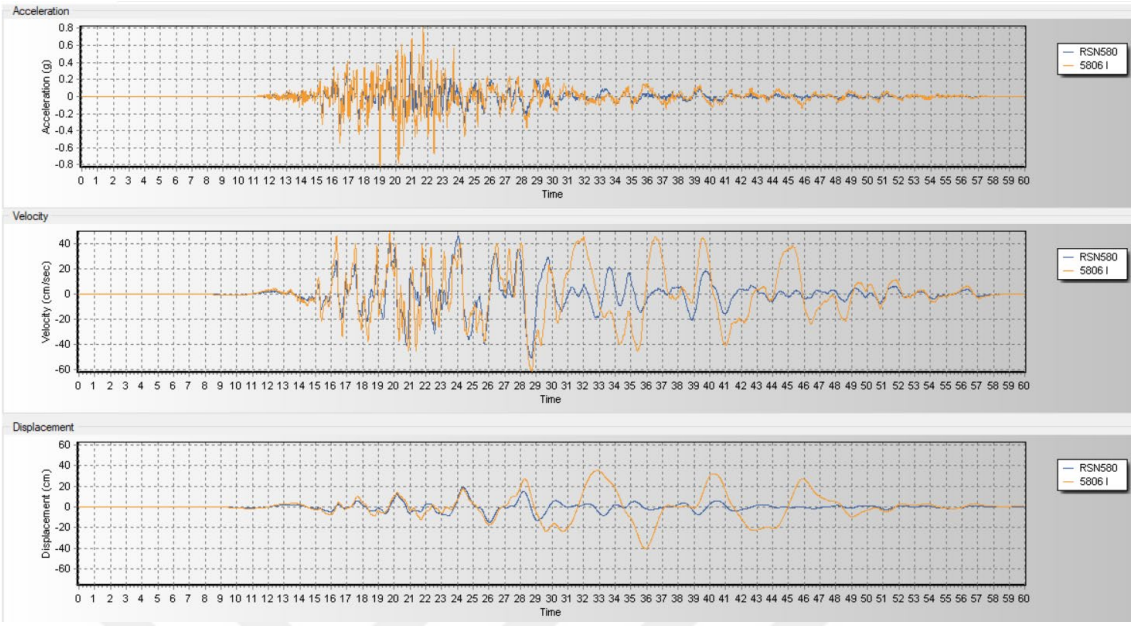

IWATE 5806-FP

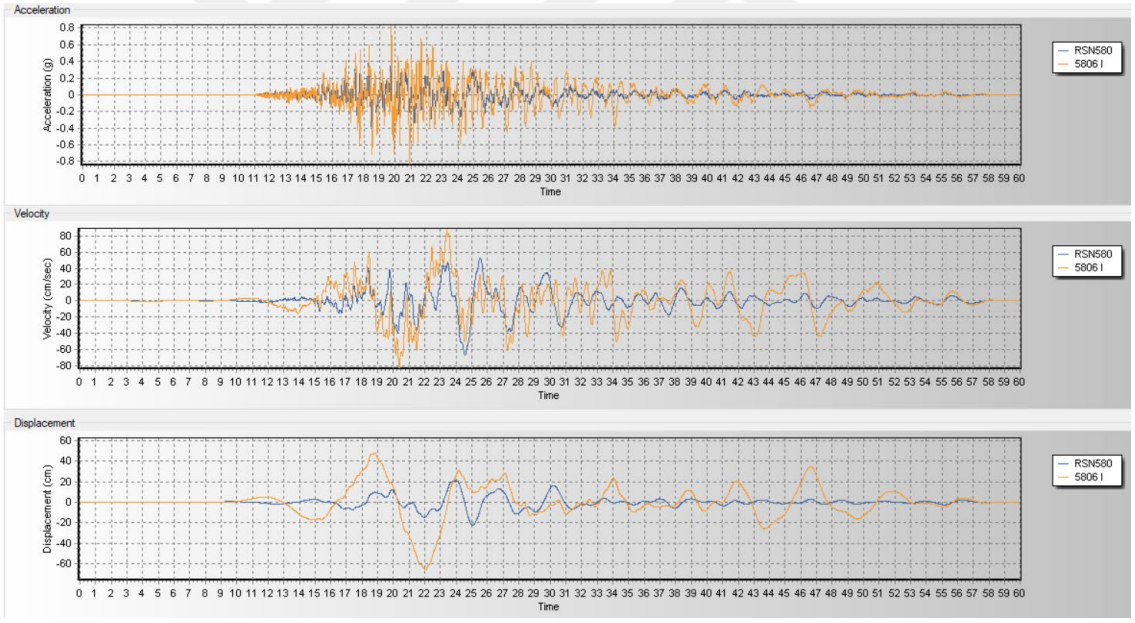

IWATE 5810-FN

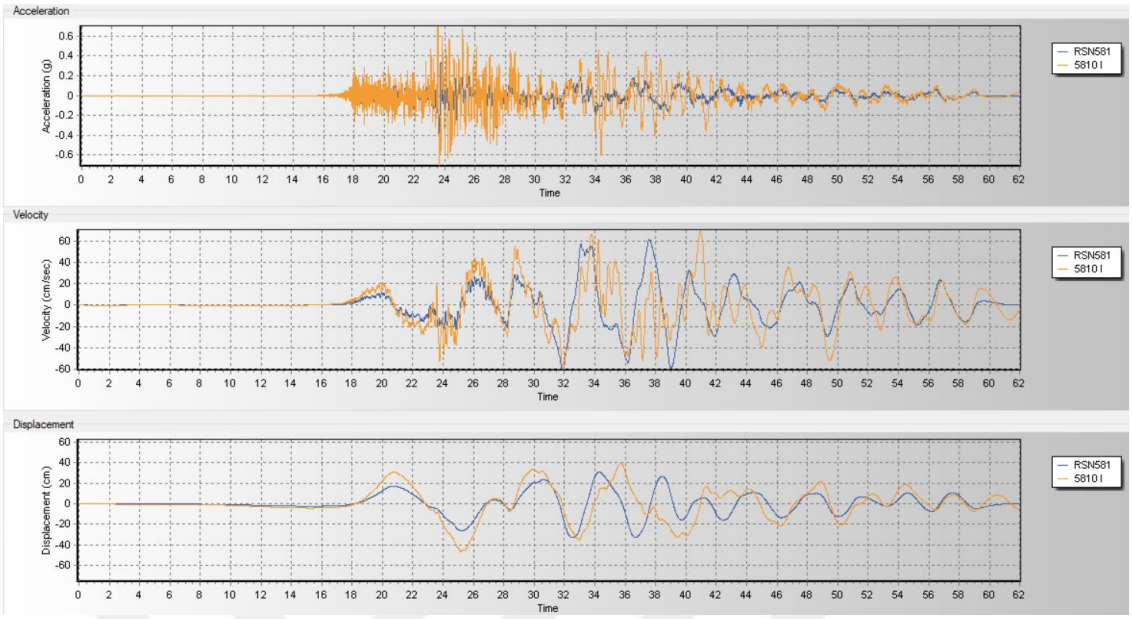

IWATE 5810-FP

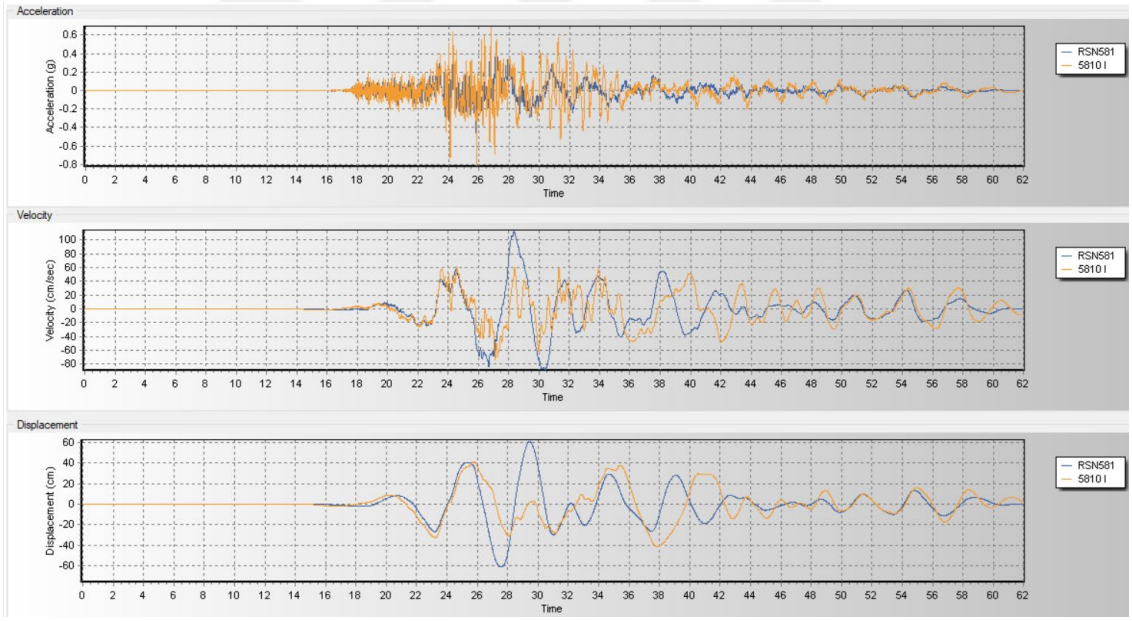

DARFIELD 6928-FN

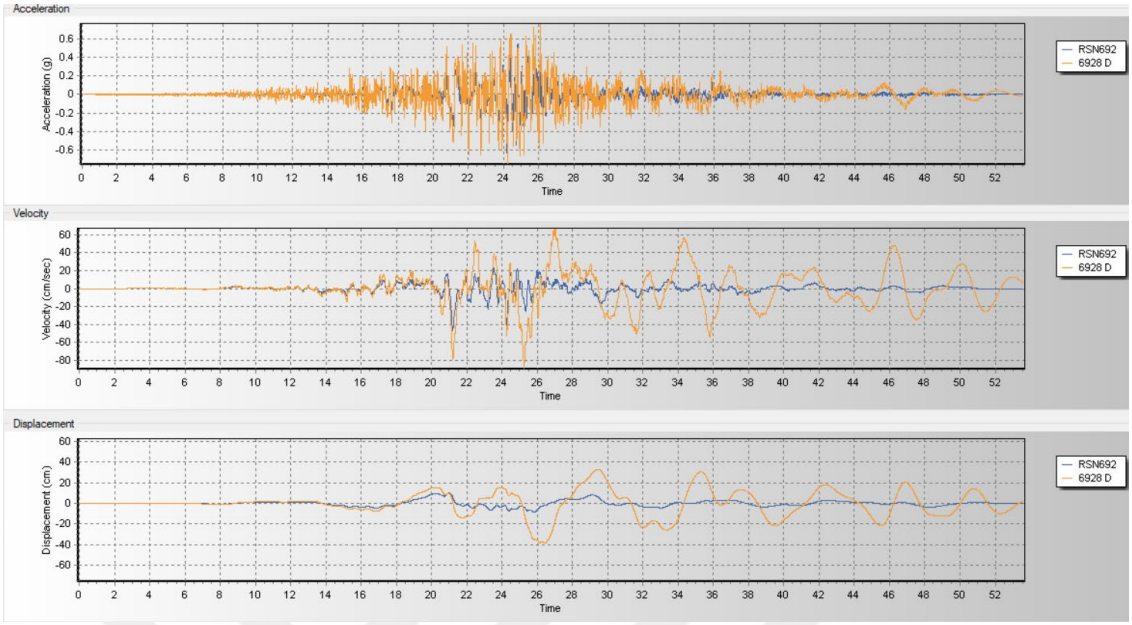

DARFIELD 6928-FP

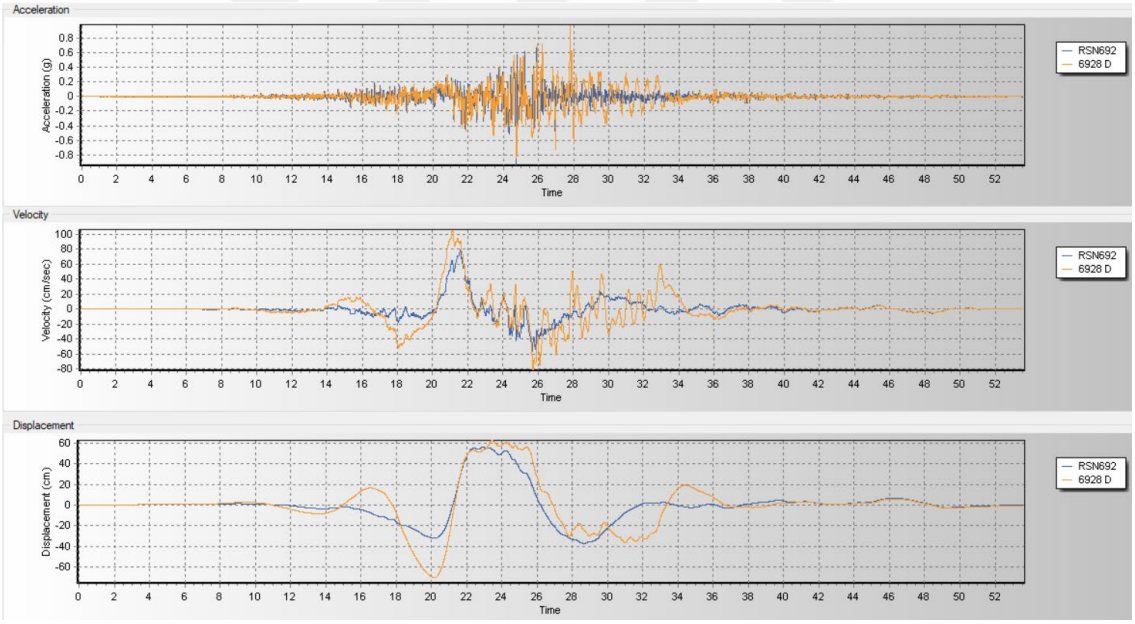

- **DD-2 EARTHQUAKES**

IRPINIA 285-FN

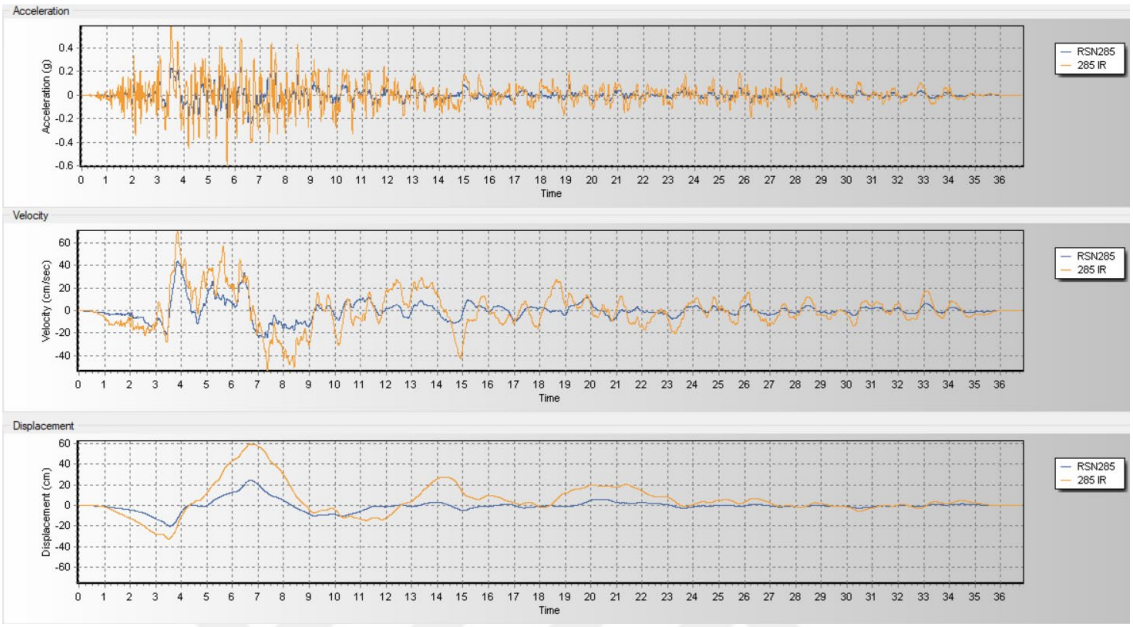

IRPINIA 285-FP

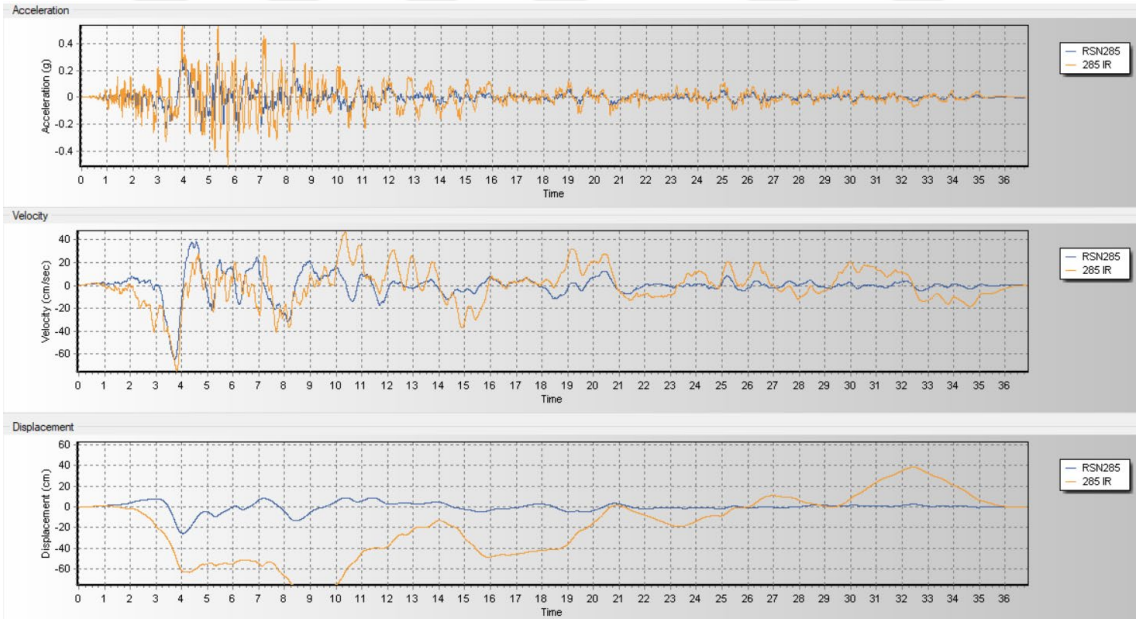

KOBE 1111-FN

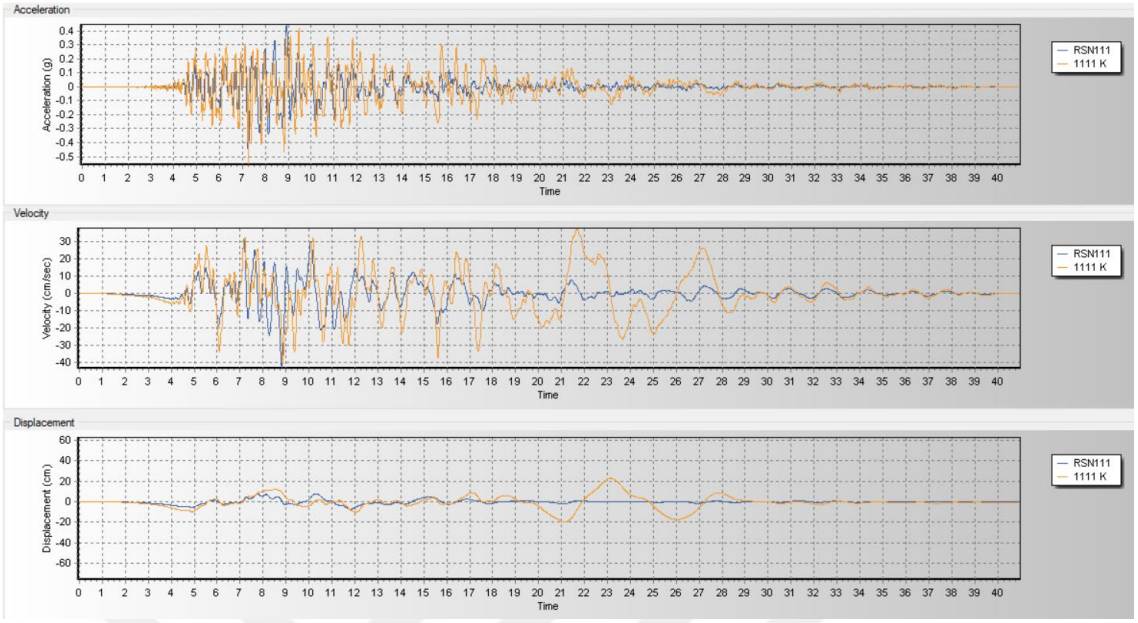

KOBE 1111-FP

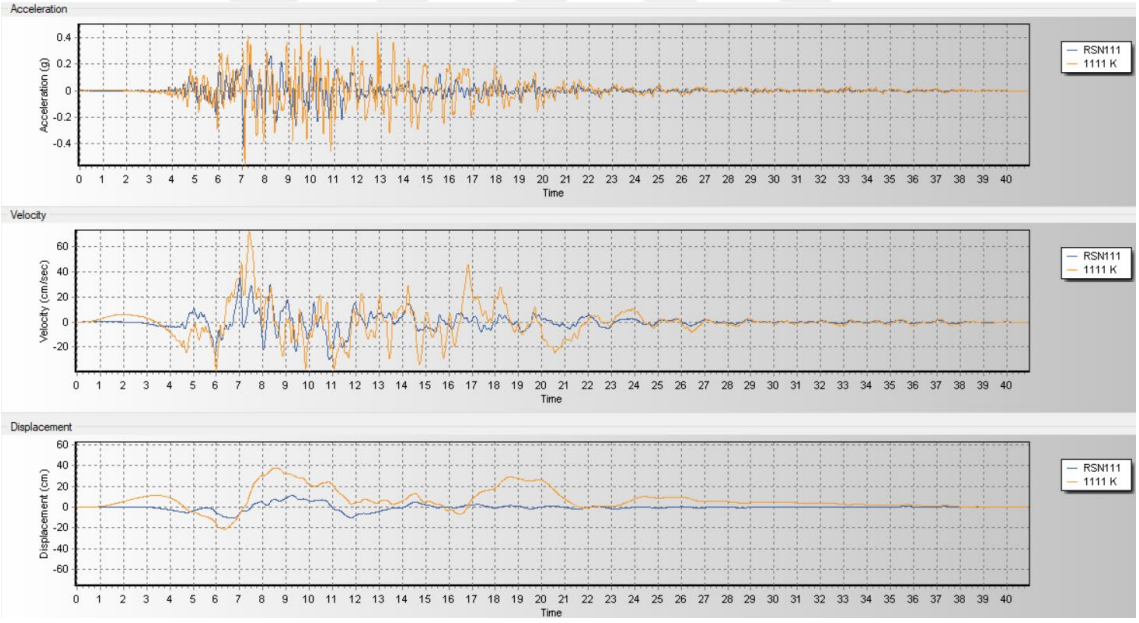

KOCAELI 1165-FN

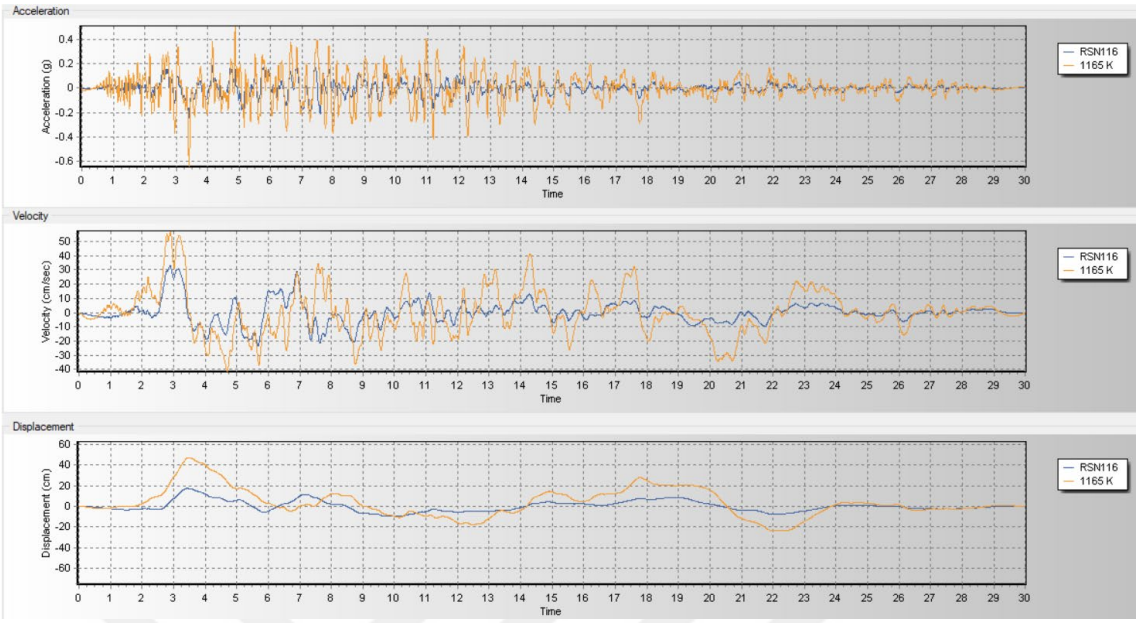

KOCAELI 1165-FP

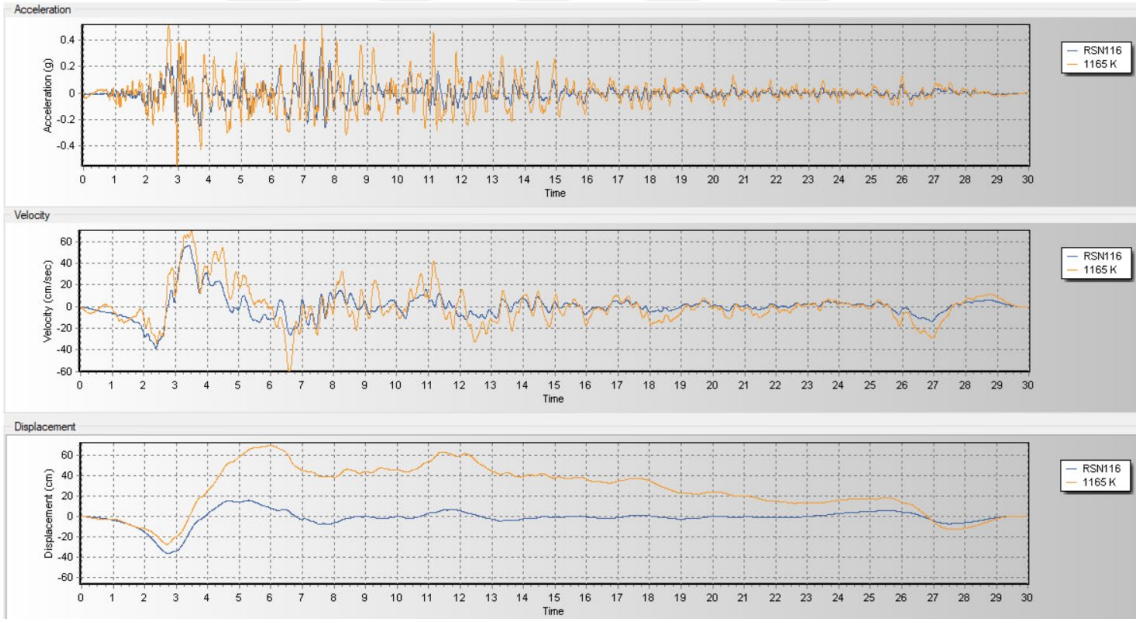

MANJIL 1633-FN

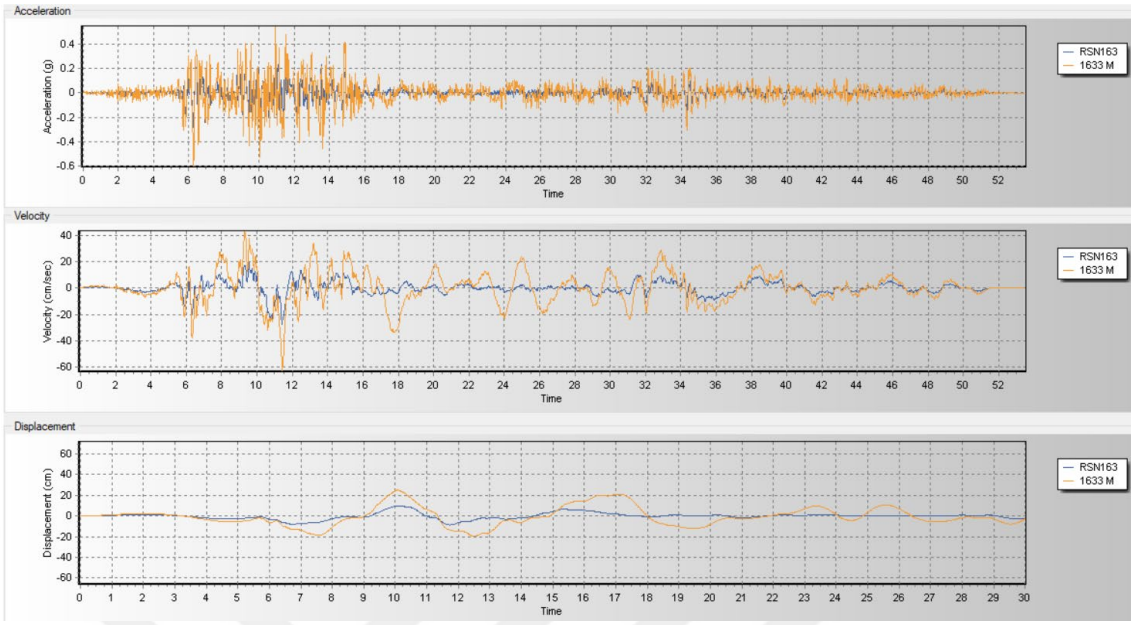

MANJIL 1633-FP

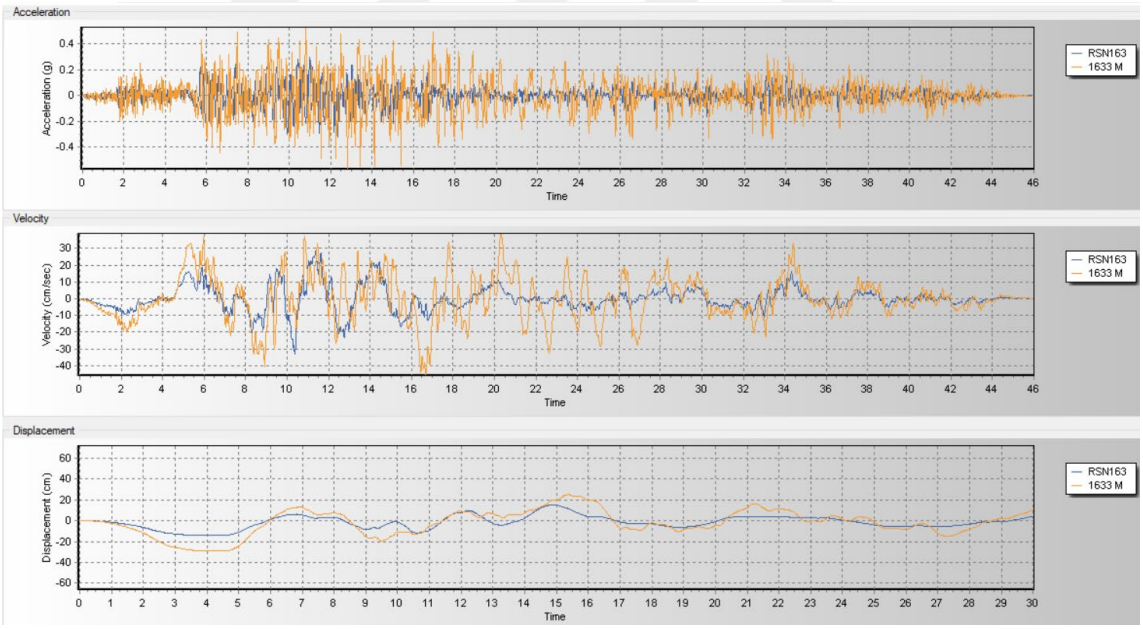

HECTOR 1787-FN

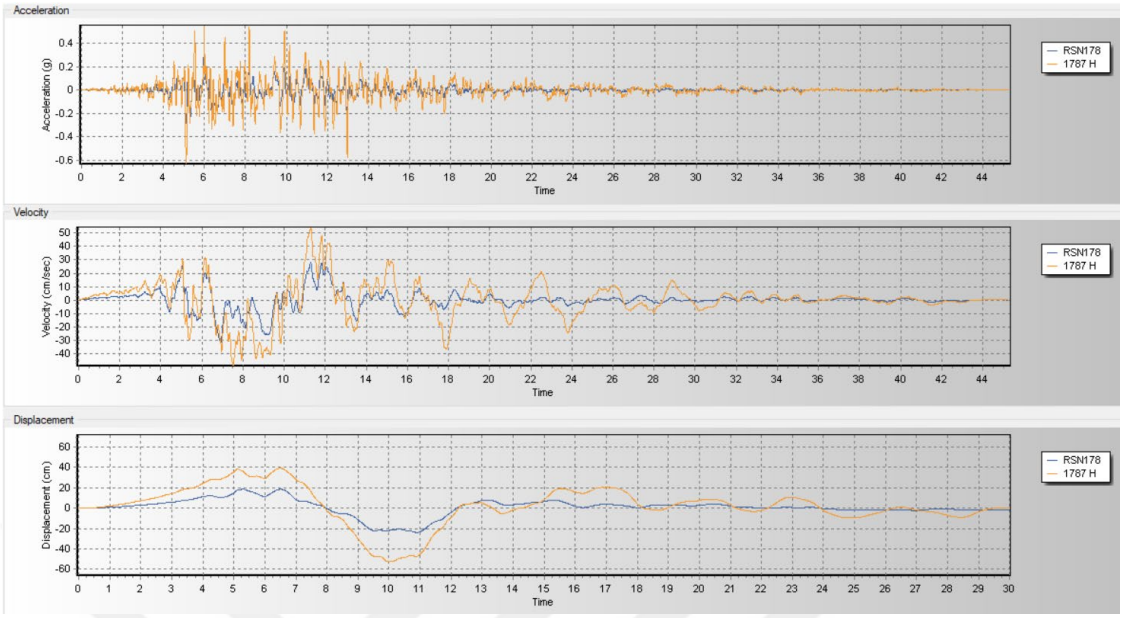

HECTOR 1787-FP

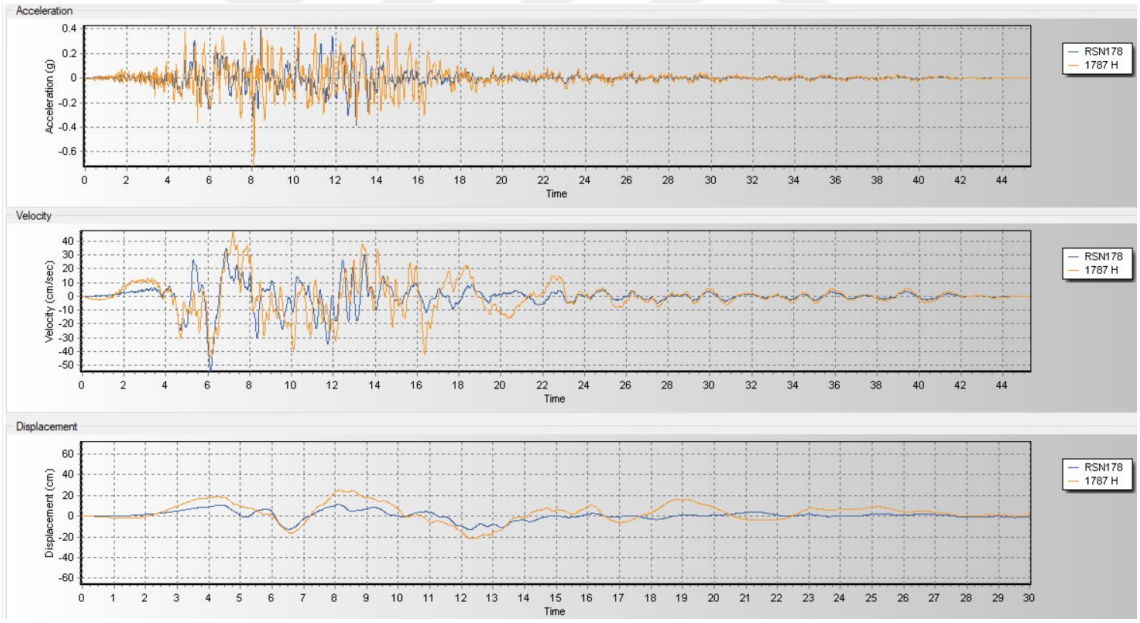

CHUETSU-OKI 4841-FN

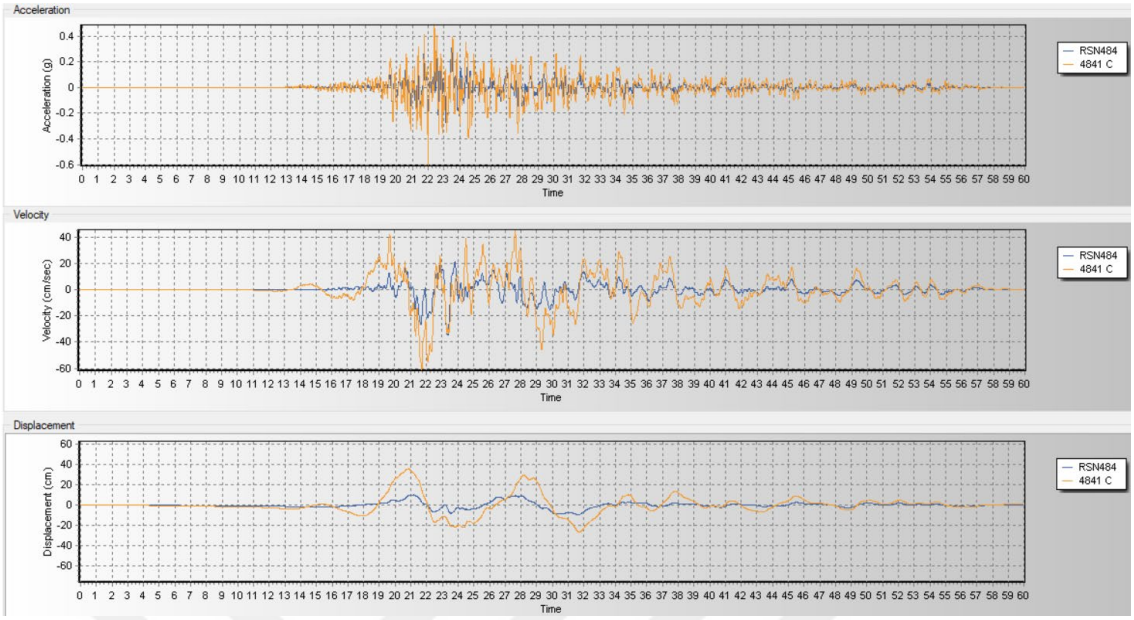

CHUETSU-OKI 4841-FP

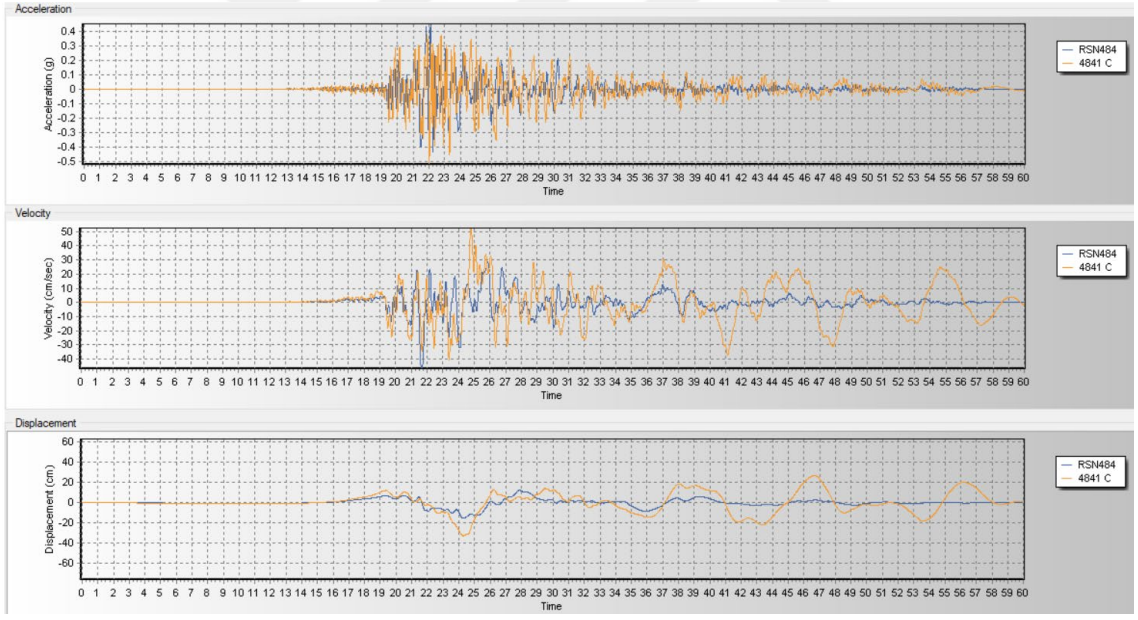

CHUETSU-OKI 4858-FN

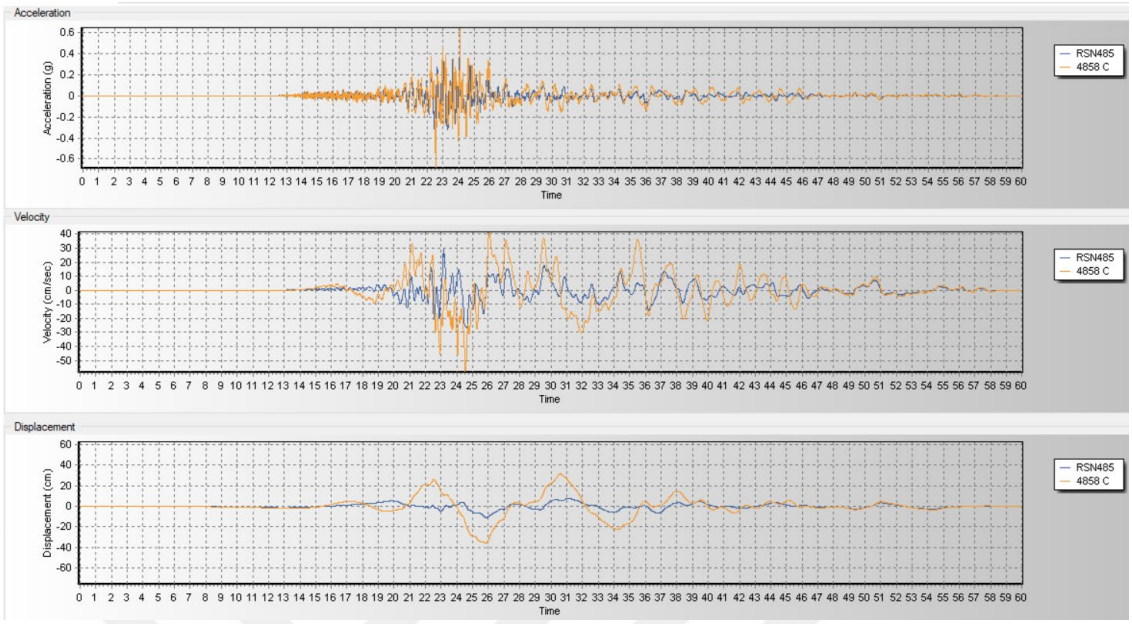

CHUETSU-OKI 4858-FP

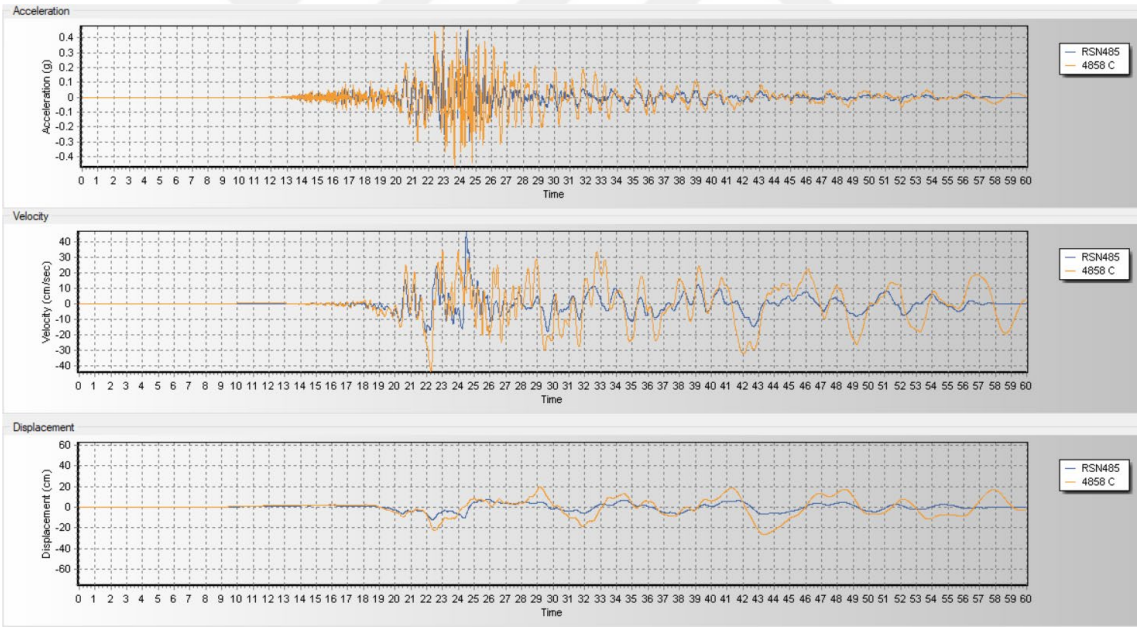

CHUETSU-OKI 4864-FN

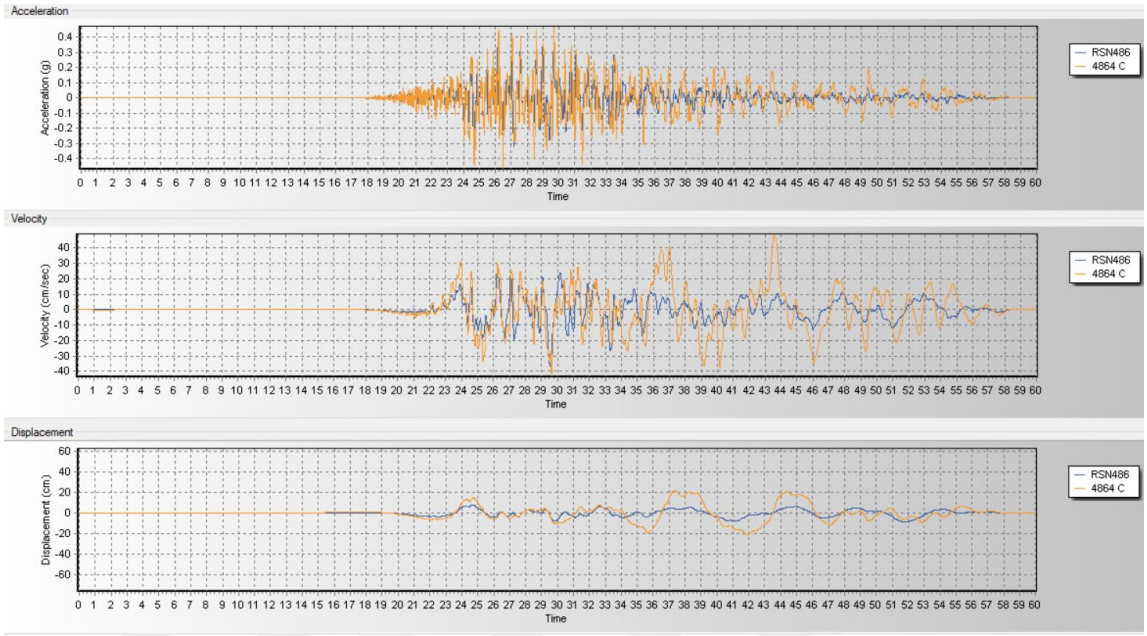

CHUETSU-OKI 4864-FP

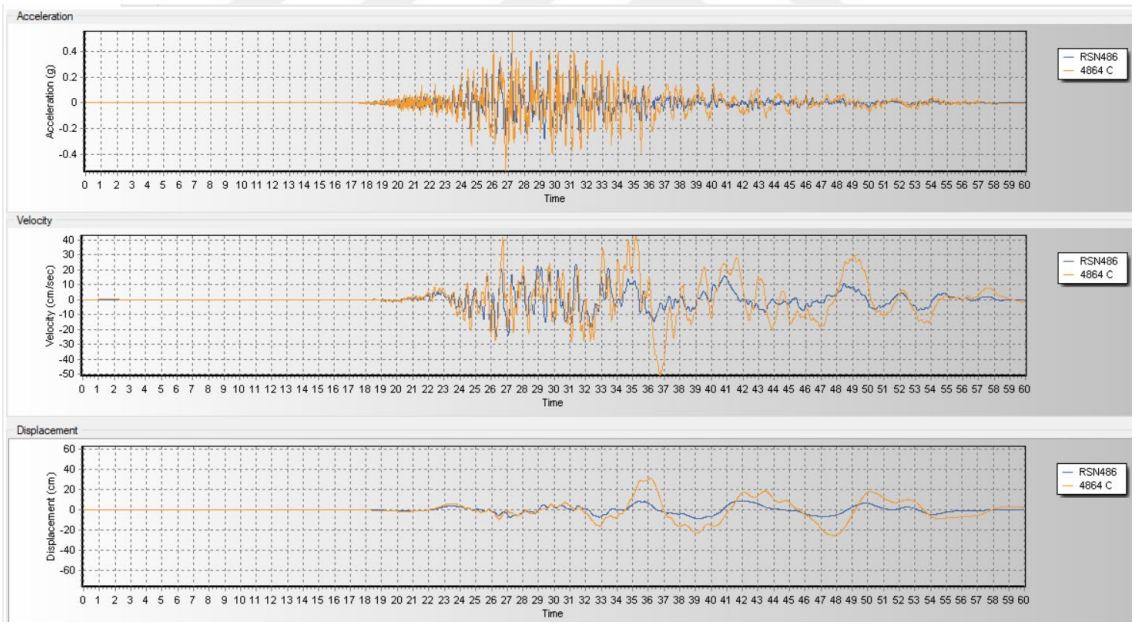

IWATE 5806-FN

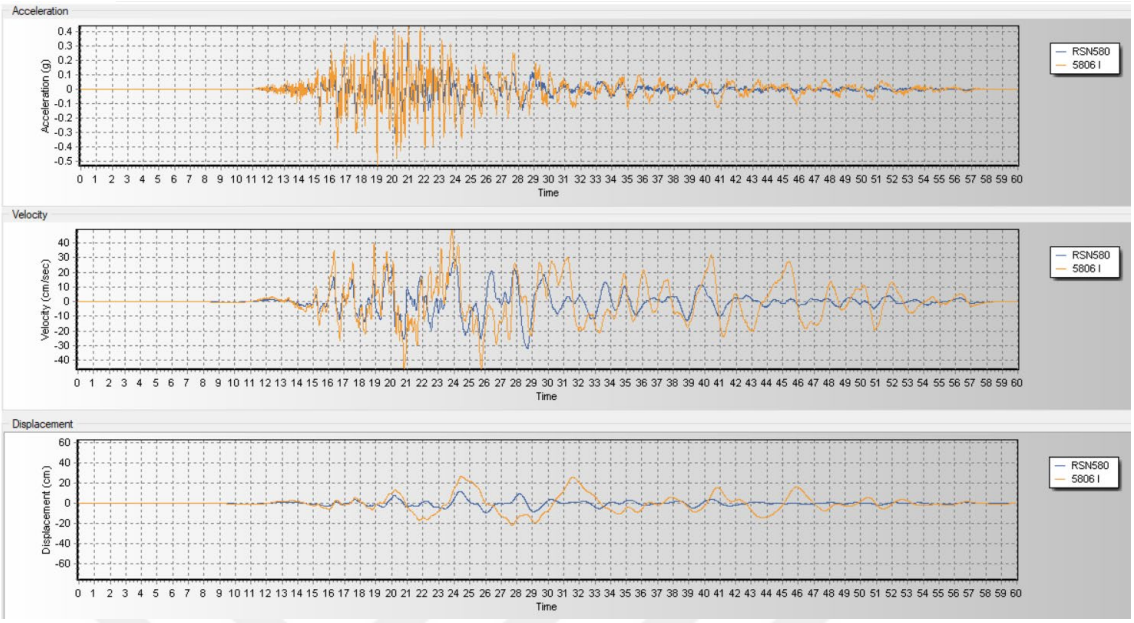

IWATE 5806-FP

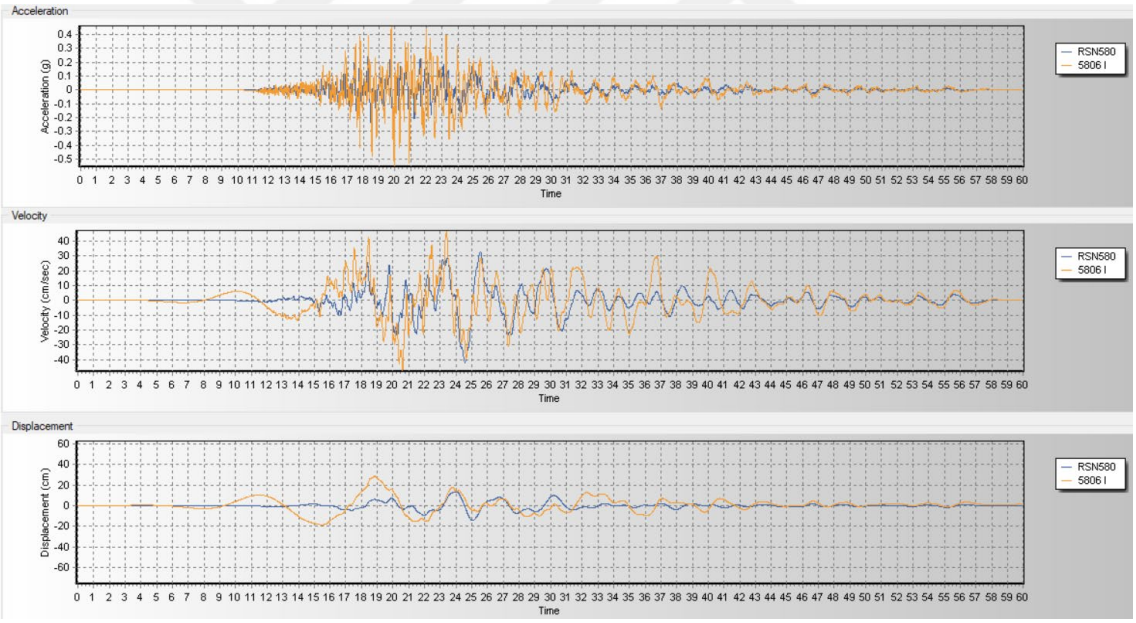

IWATE 5810-FN

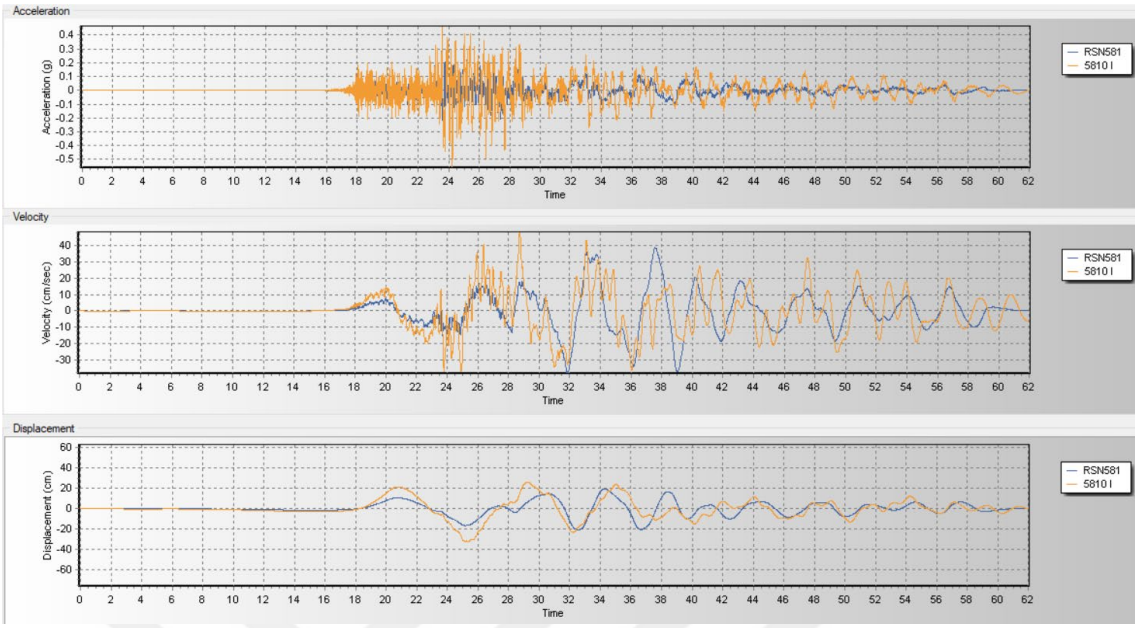

IWATE 5810-FP

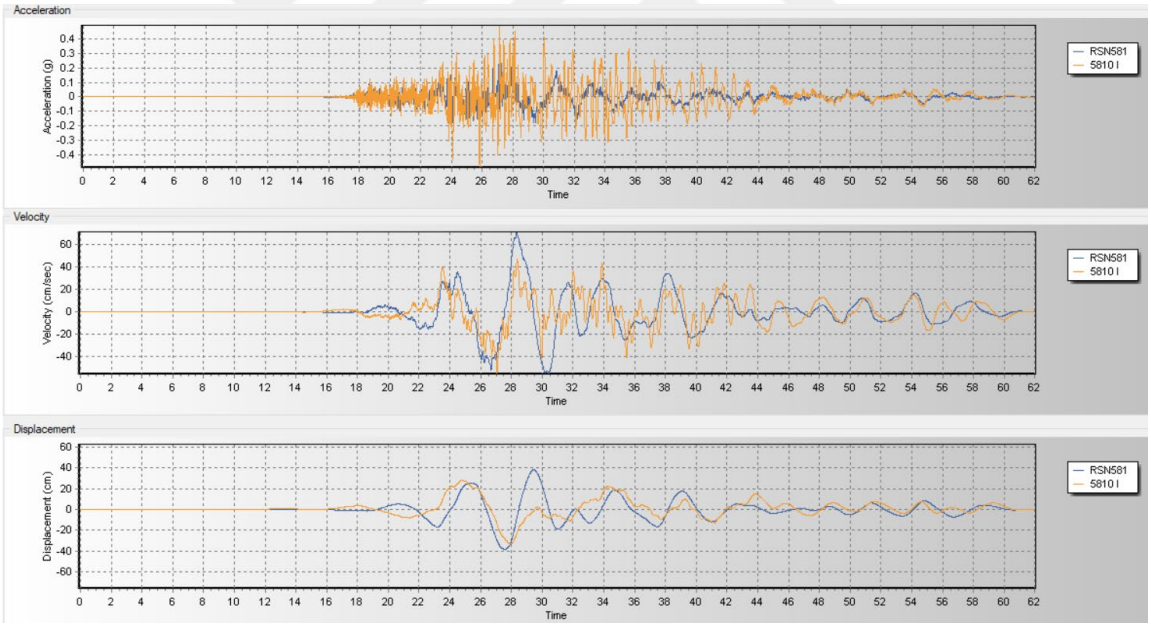

DARFIELD 6928-FN

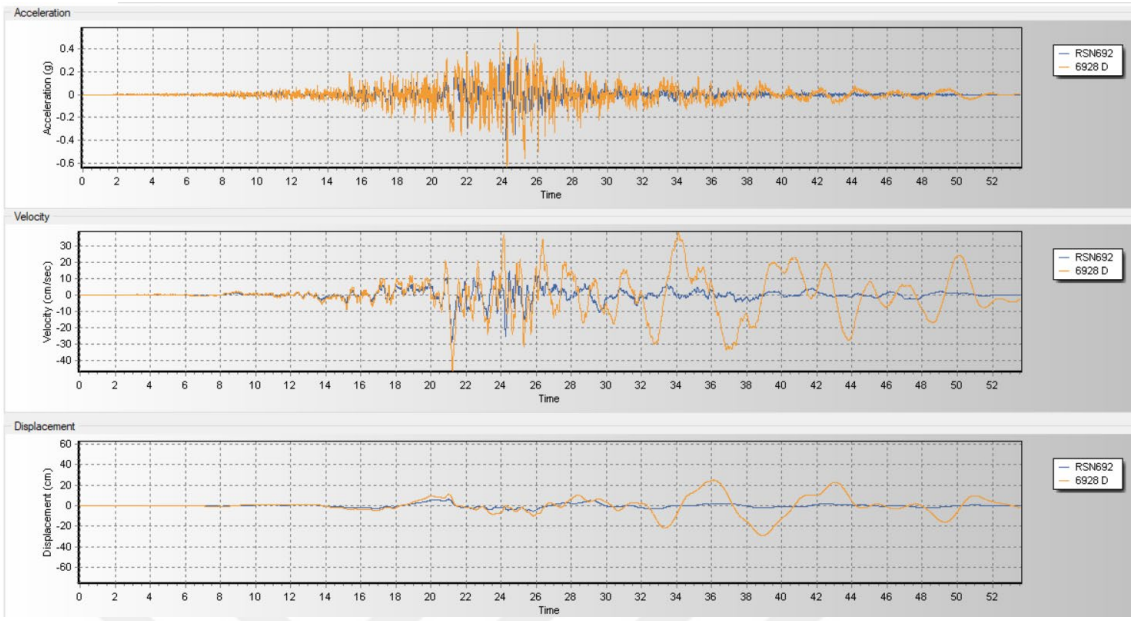

DARFIELD 6928-FP